Naval Surface Warfare Center
Carderock Division
West Bethesda, Maryland 20817- 5700

NSWCCD-50-TR-2008/025 August 2008
Hydromechanics Department Report

Formation of Large-Amplitude Wave Groups in an Experimental Model Basin

By

Christopher C. Bassler
Gerritt E. Lang
Sang Soo Lee
Jason B. Carneal
Joel T. Park
Martin J. Dipper, Jr.

NSWCCD-50-TR-2008/025 Formation of Large-Amplitude Wave Groups in an Experimental Model Basin

REPORT DOCUMENTATION PAGE

Form Approved
OMB No. 0704-0188

1. REPORT DATE *(DD/MM/YYYY)*	2. REPORT TYPE	3. DATES COVERED *(From - To)*
15-08-2008	Final	1-July-2007 - 30-June-2008

4. TITLE AND SUBTITLE
Formation of Large-Amplitude Wave Groups in an Experimental Model Basin

5a. CONTRACT NUMBER

5b. GRANT NUMBER

5c. PROGRAM ELEMENT NUMBER
0602123N

6. AUTHOR(S)
Christopher C. Bassler, Gerritt E. Lang, Sang Soo Lee, Jason B. Carneal, Joel T. Park, and Martin J. Dipper, Jr.

5d. PROJECT NUMBER

5e. TASK NUMBER

5f. WORK UNIT NUMBER
07-1-5600-179, 08-1-5600-216

7. PERFORMING ORGANIZATION NAME(S) AND ADDRESS(ES) AND ADDRESS(ES)
Naval Surface Warfare Center
Carderock Division
9500 Macarthur Boulevard
West Bethesda, MD 20817-5700

8. PERFORMING ORGANIZATION REPORT NUMBER
NSWCCD-50-TR-2008/025

9. SPONSORING / MONITORING AGENCY NAME(S) AND ADDRESS(ES)
Dr. L. Patrick Purtell
Office of Naval Research, ONR
Ballston Centre Tower One
800 North Quincy Street
Arlington, VA 22217-5660

10. SPONSOR/MONITOR'S ACRONYM(S)
ONR

11. SPONSOR/MONITOR'S REPORT NUMBER(S)

12. DISTRIBUTION / AVAILABILITY STATEMENT
Approved for public release; distribution is unlimited.

13. SUPPLEMENTARY NOTES

14. ABSTRACT
Experiments were performed to develop the capability to generate groups of large-amplitude waves in irregular seas in a model basin. Secondary objectives included demonstrating the ability to generate single extreme waves and also the application of experimental measurement techniques to produce point and wave-field topology data. The process was intended to be deterministic in nature, such that a large wave group or single large wave will occur in the model basin at a predictable and repeatable location and time. Proving the feasibility of generating asymmetric large-amplitude wave groups in an experimental basin is the first step in the development of an experimental test technique that ensures a model will be exposed to multiple realistic extreme wave events during a test run. This technique will remove the "randomness" associated with model experiments in irregular waves from the process to evaluate ship performance in severe sea conditions. (continued)

15. SUBJECT TERMS
Extreme Waves, Wave Groups, Dynamic Stability, Deterministic Model Testing, Wave-packets, Irregular Seas, Capsize, Rogue Waves

16. SECURITY CLASSIFICATION OF:			17. LIMITATION OF ABSTRACT	18. NUMBER OF PAGES	19a. NAME OF RESPONSIBLE PERSON
a. REPORT	b. ABSTRACT	c. THIS PAGE			Christopher C. Bassler
UNCLASSIFIED	UNCLASSIFIED	UNCLASSIFIED	UL	190	19b. TELEPHONE NUMBER *(include area code)* (301) 227-5926

14. ABSTRACT (cont.)

It will also reduce time in the basin and more accurately represent a full-scale seaway where ship may be at risk.

To investigate the feasibility of producing grouped extreme waves in an experimental basin, experiments were conducted in August and November 2007 in the Maneuvering and Seakeeping (MASK) basin at the Naval Surface Warfare Center, Carderock Division (NSWCCD). The first experiment (Phase I) consisted of producing several combinations of finite regular waves with varying parameters, including amplitude, frequency, and signal duration. Superposition of these finite regular waves produced repeatable wave groups at a specific location in the MASK. The second experiment (Phase II) consisted of two parts. The first part applied the wave-packet method to produce single large-amplitude waves, based on the technique developed by Clauss and Bergmann (1986) and Clauss and Kuehnlein (1994, 1995). The second part employed the achievements from Phase I to embed grouped extreme waves, obtained through finite regular wave superposition in two scaled irregular seaways: a Bretschneider sea state 8 spectrum and a Hurricane Camille spectrum.

The maximum calibrated attained wave height, normalized by a typical ship model length (h/L) was 0.205, compared to 0.1 for the typical largest regular wave height to ship model length ratio used for testing, or double the maximum wave height normally achieved in the MASK. The maximum wave steepness (h/λ) observed was approximately 1/7, approaching the theoretical limit for a non-breaking wave, compared to a 1/10 wave steepness which is typically the maximum for regular wave testing. The largest estimated full-scale wave height observed was 37.5 m (123 ft.) at a scale ratio of 46.6. Producing repeatable wave groups with the desired characteristics at a fixed location is a non-trivial task, however, this study demonstrated the feasibility of producing groups of asymmetric extreme waves in the MASK. Future work is also discussed.

Contents

Figures

Tables

This page intentionally left blank

Abstract

Experiments were performed to develop the capability to generate groups of large-amplitude waves in irregular seas in a model basin. Secondary objectives included demonstrating the ability to generate single extreme waves and also the application of experimental measurement techniques to produce point and wave-field topology data. The process was intended to be deterministic in nature, such that a large wave group or single large wave will occur in the model basin at a predictable and repeatable location and time. Proving the feasibility of generating asymmetric large-amplitude wave groups in an experimental basin is the first step in the development of an experimental test technique that ensures a model will be exposed to multiple realistic extreme wave events during a test run. This technique will remove the "randomness" associated with model experiments in irregular waves from the process to evaluate ship performance in severe sea conditions. It will also reduce time in the basin and more accurately represent a full-scale seaway where a ship may be at risk.

To investigate the feasibility of producing grouped extreme waves in an experimental basin, experiments were conducted in August and November 2007 in the Maneuvering and Seakeeping (MASK) basin at the Naval Surface Warfare Center, Carderock Division (NSWCCD). The first experiment (Phase I) consisted of producing several combinations of finite regular waves with varying parameters, including amplitude, frequency, and signal duration. Superposition of these finite regular waves produced repeatable wave groups at a specific location in the MASK. The second experiment (Phase II) consisted of two parts. The first part applied the wave-packet method to produce single large-amplitude waves, based on the technique developed by Clauss and Bergmann (1986) and Clauss and Kuehnlein (1994, 1995). The second part employed the achievements from Phase I to embed grouped extreme waves, obtained through finite regular wave superposition in two sealed irregular seaways: a Bretschneider sea state 8 spectrum and a Hurricane Camille spectrum.

The maximum calibrated attained wave height, normalized by a typical ship model length (h/L) was 0.205, compared to 0.1 for the typical largest regular wave height to ship model length ratio used for testing, or double the maximum wave height normally achieved in the MASK. The maximum wave steepness (h/λ) observed was approximately 1/7, approaching the theoretical limit for a non-breaking wave, compared to a 1/10 wave steepness which is typically the maximum for regular wave testing. The largest estimated full-scale wave height observed was 37.5 m (123 ft.) at a scale ratio of 46.6. Producing repeatable wave groups with the desired characteristics at a fixed location is a non-trivial task, however, this study demonstrated the feasibility of producing groups of asymmetric extreme waves in the MASK. Future work is also discussed.

Administrative Information

The work described in this report was performed by the Seakeeping Division (Code 5500) of the Hydromechanics Department at the Naval Surface Warfare Center, Carderock Division (NSWCCD). The work was funded by the Office of Naval Research, Code 331, as part of the Definition of Towing Basin Environment Task, Surface Ship Dynamics: Motions and Maneuvering Program (Program Element 0602123N), in FY07 (Work Unit 07-1-5600-179) and FY08 (Work Unit 08-1-5600-216).

Acknowledgements

The authors would like to thank Dan Hayden for guidance and discussion of his previous work on capsize model test techniques and Dr. John O'Dea for helpful discussions on waves and extreme event statistics. The authors would like to thank Bob Sarbacker, Lloyd McCoy, and Neal Faulkner for their assistance with wave generation in the MASK and Lawrence Snyder, for his valuable help with the Phase I testing. The authors also greatly appreciate the helpful discussions and comments on the content of this report from Dr. Arthur Reed, Prof. Leigh McCue, and Dr. Vadim Belenky.

Nomenclature

h	wave height
H_s	significant wave height
h_{fs}	estimated full-scale wave height for notional model
L	notional scale model length
λ	wavelength
T	wave period
k	wave number
s	wave steepness
c_G	group velocity
f	frequency
σ	Rayleigh distribution scale parameter
x_a	concentration position
t_a	concentration time
$\hat{s}_n$	normalized spectrum
H_n	amplitude of wave-maker piston motion
Cyc_n	number of cycles in finite regular wave
u_a	Type A standard uncertainty
U	expanded uncertainty
k_f	coverage factor
r	correlation coefficient

Introduction and Background

This teehnieal report details progress made in FY07 and FY08 for a sub-task of the Surfaee Ship Dynamies: Motions and Maneuvering projeet, sponsored by the Offiee of Naval Researeh. The sub-task, Definition of Towing Basin Environment, is part of a eombined effort at NSWCCD to improve predietions and measurement of ship motions in waves and assess the dynamie stability and seakeeping performanee of naval ships.

The advent of novel hull form geometries has demonstrated a need for improved simulation eapabilities and experimental teehniques. These are neeessary to assess stability performanee, to inerease understanding of the prineiple physics governing dynamie stability events, and to provide eorrelation data for the development of simulation tools.

Beeause of the potential risk to oeean-going vessels and platforms eaused by extreme seas, an inerease in the understanding of the eharaeteristies and oeeurrenee of large waves is important. Large amplitude waves, either singularly or in groups, ean present a serious stability risk to a ship, leading to payload and hull damage, personnel injury, or in the worst-ease seenario, eapsize and loss of life and the vessel.

Large-amplitude waves have been the subjeet of eye-witness aeeounts at sea. A report by Admiral Robert Fitz-Roy, published in 1839, reeounted the HMS *Thetis* traveling between two waves, believed to be greater than 18.3 m (60 ft) wave height, beeause the wave erests were taller than her masts and the sails were slaek despite heavy winds. Other large waves believed to be reliably reported inelude a 34 m (112 ft) wave reported by the USS *Rampo* in the North Paeifie, in 1933, and a 27.5-30.5 m (90-100 ft) wave that struek an oil rig, near Vaneouver island, in 1968. Additional reports have been made of ships sailing into "holes in the sea," made by the troughs of large waves (Draper, 1971; Buckley 2005).

These large waves are known eommonly by several names, sueh as freak, rogue, or extreme waves. For the purpose of this investigation, they will be referred to as extreme waves. They typieally are non-linear and asymmetrie, featuring deep troughs, either preeeding or following steep wave erests.

Researeh has indieated the relatively common oeeurrenee of these extreme waves, much more often than was predieted by eonventional Rayleigh distribution predietion models (Rosenthal and Lehner 2008). A European Union eollaboration projeet, MaxWave (Rosenthal and Lehner, 2004, 2008), began to investigate extreme waves in 2000. During a three-week period in 2001, European Spaee Ageney (ESA) satellites reeorded data from an imaged area of 1.5 million square kilometers. Wave heights of 25 m, or larger, were observed at an equivalent rate of one in 150,000 square kilometers in the three week period.

Approaehes for estimation of the probability of oeeurrenee of single extreme waves in an

experimental basin or ocean environment, at either a fixed point or within a wave-field, have also been investigated (Lopatoukhin, et al. 2004; Fedele, 2006a, 2006b). Guedes Soares and Pascoal (2005) and Petrova, et al. (2007) showed the inadequacy of design wave models based on linear assumptions and the difficulty of second-order hydrodynamic models to describe accurately large ocean wave characteristics, as determined from field measurements.

Extreme waves are typically characterized by wave heights of at least two times the significant wave height. Although this criteria is widely used, it is not a universally accepted definition. A more general definition, proposed by Johannessen and Swan (2003) states that an extreme wave can be characterized as a wave with a crest elevation significantly larger than considered by the statistics of the underlying frequency spectrum. These waves of large-amplitude, either single or grouped, have been reported in all the oceans of the world (Rosenthal and Lehner, 2008).

Measurements were also made over a six-year period, from 1998–2003, on a platform in the southern Indian Ocean (Liu and MacHutchon, 2008). This region, off the east coast of South Africa, is a major shipping route and is known to produce extreme waves because of the mix of the Agulhas Current and storm waves (Sverdrup, et al., 2003). These measurements have provided a preliminary data set for a possible class of extreme waves, characterized by wave heights of at least four times the developed significant wave height (Liu and MacHutchon 2008).

Extreme waves have been shown to occur in all sea states (Bitner-Gregersen and Hagen 2004), although they are of greater concern to ship safety in higher sea states. Some research has indicated the possibility that extreme waves may be more likely to form in seas dominated by swell, than in a locally wind generated sea (Gibson and Swan, 2007). Due to the complex interaction of swell and wind-generated waves, the exact environmental mechanisms for producing extreme waves are still not well understood. Possible causes of extreme waves forming singularly or in groups include well-developed storm systems, intersection of wave systems from different storm centers, and storm situations where the storm and wave group velocities are similar (Rosenthal and Lehner 2008).

The research to date has focused primarily on detection, observation, measurement, and reproduction, either experimentally or numerically, of single extreme waves. The existence of these singular large-amplitude waves, has only been confirmed by measurements within the last two decades, such as the famous "New Year's Wave" recorded from the Draupner platform in the North Sea (Figure 1). In 2000, in the Rockall Trough, west of Scotland, a British oceanographic research vessel recorded waves with a significant wave height of 18.5 m (61 ft) and individual waves up to 29.1 m (95 ft). These waves are the largest ever measured in the open ocean (Holliday, et al., 2006).

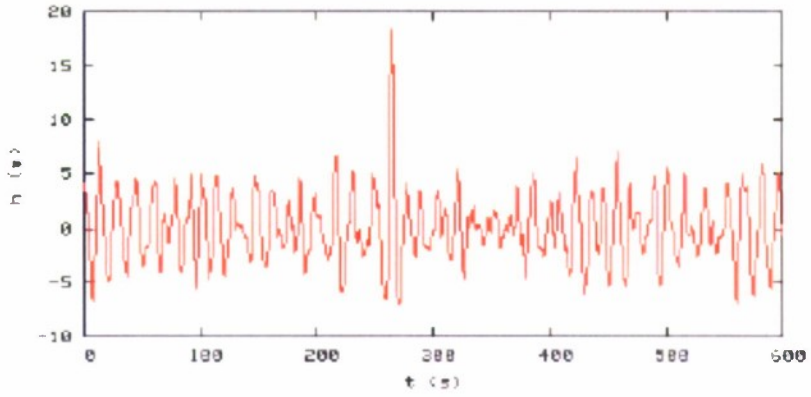

Figure 1. The Draupner Platform wave, January 1, 1995, Time-history of the wave amplitude, in meters (Rosenthal and Lehner, 2004)

During Hurricane Ivan, measurements made by Naval Research Laboratory instruments on the floor of the continental shelf in the Gulf of Mexico, recorded significant wave heights of 17.9 m (58.8 ft) and individual maximum wave heights of 27.7 m (91 ft). NRL researchers have stated that, although not recorded, additional analysis indicated significant wave heights may have exceeded 21 m (69 ft), with individual wave heights exceeding 40 m (132 ft) during the storm (Wang, et al., 2005). However, within hurricane regions, small data samples have been shown to underestimate wave heights for extreme waves (Jonathan and Ewans, 2007), resulting in the possibility that current measurements may not even provide an accurate indication of the upper limit of extreme wave heights.

Additional accounts of ships experiencing groups of exteme waves, such as the "Three Sisters," have been reported (Buckley, 2005; Smith, 2006). A wave group is defined as a series of waves, with wave heights larger than a specified threshold, and with approximately equal periods (Masson and Chandler, 1993; Ochi, 1998). A 2005 U. S. National Transportation Safety Board investigation conducted on a maritime accident in the Atlantic Ocean, off the coast of Georgia involving the *Norwegian Dawn*--indicated that the vessel had encountered three large waves in succession (NTSB, 2005). Experimental generation of groups of extreme waves, has only focused on a symmetric three wave group of heights, H_s, $2H_s$, H_s (Clauss, 2002a). While useful for determining critical motions, the symmetric wave group does not represent many of the characteristics of extreme wave groups observed in the ocean environment.

To model extreme ship motions experimentally, a large test matrix of runs must be performed. Model experiments conducted in random waves, to assess severe ship motions, dynamic stability, slamming, and ultimate strength; require long test run times to ensure that the

low probability extreme wave events, which still occur in the seaway, have been encountered.

The first approach to reduce the number of required tests for regular wave seakeeping was the transient wave technique, developed analytically by Davis and Zarnick (1964). At the David Taylor Model Basin, Davis and Zarnick, and Gersten and Johnson (1969) applied the transient wave technique to regular wave model experiments for heave and pitch, at zero and forward speed. These tests demonstrated a potential reduction by an order of magnitude of the total necessary testing time. The transient wave technique was also applied to model testing in Japan in the mid-1970s (Takezawa and Takekawa, 1976; Takezawa and Hirayama, 1976).

Clauss and Bergmann (1986), Clauss and Kuehnlein (1994, 1995), and Matos, et al. (2005) used a transient wave technique with Gaussian wave-packets to excite model ships and offshore structures in an experimental basin. Further revisions to this technique included using nonlinear transient wave trains and modified wave celerity to generate extreme waves (Clauss, 1999). Transient waves have even been proposed for use as part of a wave-maker calibration procedure (Masterton and Swan, 2008). Model tests have been performed with large transient waves, embedded in both regular and random wave trains. These waves were calculated both linearly and nonlinearly, with empirically-based terms for the particle orbital motion and shallow-water effects (Clauss and Hennig, 2002). Experimentally, single extreme waves have been shown to have larger asymmetry than full-scale storm waves, but with a profile more similar to real extreme waves than second-order numerical simulations (Antao and Guedes Soares, 2008).

To generate desired deterministic wave sequences in the experimental basin, techniques where singular extreme waves were embedded in irregular seas with a linear wave theory "first approach," and then optimized using a fully nonlinear approach have been investigated (Clauss, 2000; Clauss, 2002a; Clauss and Schmittner, 2005). Experiments using a modified "New Year Wave" have been conducted to assess both motions and structural response for floating offshore structures (Clauss, et al., 2008). Model tests, to induce extreme roll and capsize for a ship, must consider wave characteristics such as wave height and steepness, wave groupiness, and the velocity and direction of wave propagation (Clauss and Hennig, 2004).

Envelope theory (Longuet-Higgins, 1957), used to mathematically describe the ocean wave environment, assumes the wave spectra is Gaussian and narrow-banded. Kimura (1980) proposed describing a series of waves above a specified threshold, using a Markov chain to obtain the probability distribution of wave groups in a random sea. Additional revisions were proposed by Longuet-Higgins (1984) to simplify the application of Markov theory to describe the statistics of steep wave groups, and by Battjes and Van Vledder (1984) to link the wave group properties to the energy spectrum. Neither spectral method is able to fully describe the

groupiness characteristics of a given wave-field (Masson and Chandler, 1993). However, recent analysis of environmental data from the North Sea has shown the ability of a Markov chain model to better predict wave group properties than a Rayleigh distribution model, except for large wave heights (Stansell, et al., 2002). Because of the Gaussian assumption, application of both envelope and Markov theory may be limited for realistic extreme waves and extreme wave groups. Directionality has also been shown to be an important factor for accurately modeling extreme waves observed in the ocean (Johannessen and Swan, 2001; Gibson and Swan, 2007). Other analytical methods, based on the nonlinear Schroedinger equation (Osborne, 2001, 2006; Slunyaev, et al., 2005; Grue, 2002) and the Kadomtsev-Petviashvili equation (Porubov, et al., 2005), have been used both to model single large-amplitude waves in an experimental basin and to numerically recreate full-scale ocean wave measurements.

"Numerical wave tanks" have been developed for the deterministic analysis of ocean structure behavior in simulated single extreme waves (Clauss, et al., 2005; Ning, et al., 2008). One numerical tank applies potential flow codes for fast computations and RANS codes to model breaking waves and fluid-structure interaction (Clauss, et al., 2005). Some agreement exists between computations and experiments, with potential flow and RANS used either separately, or coupled. However, wave heights are shown to be generally over-predicted in a numerical wave tank. Extreme waves simulated in numerical tanks have also been applied to predict structural loading on ships (Guedes Soares, et al., 2008) and offshore structures (Clauss, 2002b). However, loads predictions have been shown to vary widely, depending on the wave kinematics model employed for the evaluation (Stansberg, et al., 2008), models such as second-order (Bitner-Gregersen and Hagen, 2004), Grue's method (Grue, et al., 2003), or the well-known Wheeler stretching method (Wheeler, 1969). Some comparisons between numerical predictions and extreme wave model experiments were performed by Hennig, et al. (2006).

Tools for ship design have been developed where waves or wave groups are used to induce a specific ship motion response. This approach was first applied by Tikka and Paulling (1990), using wave groups to induce large roll excitations caused by parametric roll. Additional studies of applications of wave groups to parametric roll response have been made by Boukhanovsky and Degtyarev (1996). Alford has used a design wave train method to produce a desired motion response (Alford, et al., 2006; Alford, 2008). The method has also shown that wave grouping and directionality are significant factors in the realization of worst-case ship motions (Alford, et al., 2007). To determine particular severe instabilities for a ship, Themelis and Spyrou (2007) applied critical wave groups deterministically by predicting the required critical wave groups to induce the instability, for a given ship. Then the probability of encountering one of these critical wave groups, for a given route and time, was computed. Using

this critical wave group method, instabilities were assessed including beam-seas resonance, parametric roll, and pure loss of stability.

All wave conditions do not have the same probability of occurrence. To predict rare response events, wave groups can present a scenario of higher probability for extreme response than a single large-amplitude wave. For both experiments and simulations, realistic groups of large-amplitude waves can be applied to overcome the "problem of rarity" (Belenky, et al., 2008) by inducing realistic severe conditions for large roll motions or stability failure, at a known time and location.

During large-scale model testing at Patuxent River Naval Air Station (NAS) in the fall of 2006 (Carrico, 2007), wave time-histories taken from buoys deployed in the Chesapeake Bay testing site showed waves with characteristic groupiness (Figures 2–5). Both singular and grouped extreme waves were present in some of the dynamic stability events observed during these tests.

The ability to reliably reproduce these grouped extreme waves in the experimental basin at NSWCCD will enable reduced test time and improved repeatability for seakeeping and dynamic stability tests. This technique can also be used to generate improved spectra for irregular wave testing. Because of the temporal and spatial limitations of the basin, it is difficult to reproduce the entire frequency range for a given spectrum. Generation of grouped extreme waves in an experimental basin will enable the realistic representation of more severe wave environmental conditions in model experiments, which is impractical with current irregular wave testing techniques.

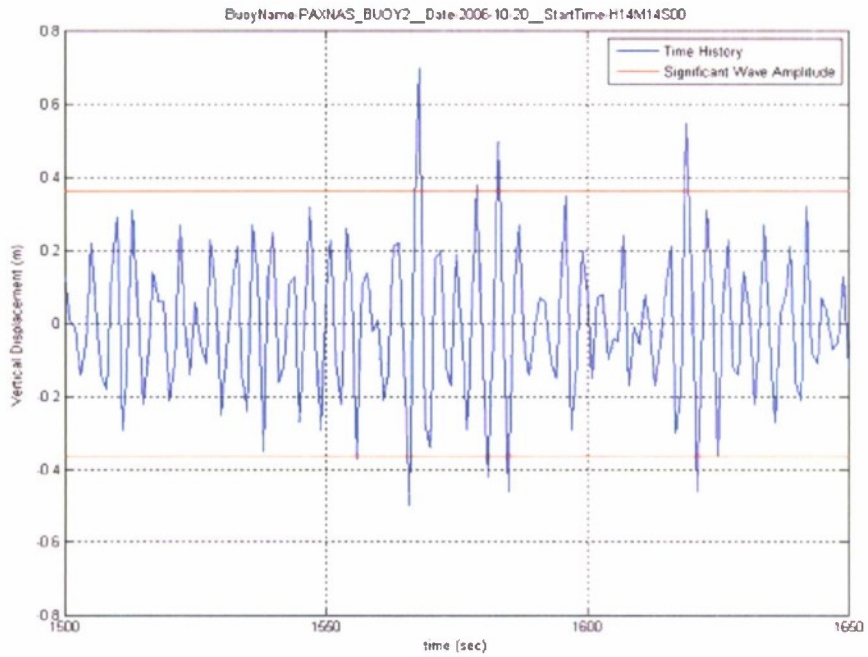

Figure 2. Wave time-history from Chesapeake Bay Buoy 2, on 10-20-2006 at 1414 hrs, significant wave height as reported for the previous 30 min. period.

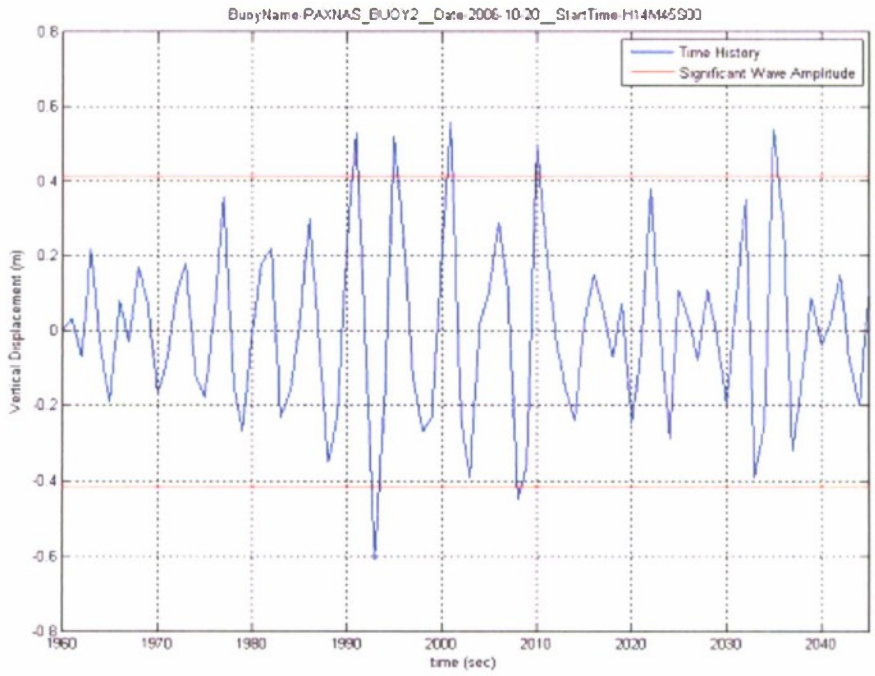

Figure 3. Wave time-history from Chesapeake Bay Buoy 2, on 10-20-2006 at 1445 hrs, significant wave height as reported for the previous 30 min. period.

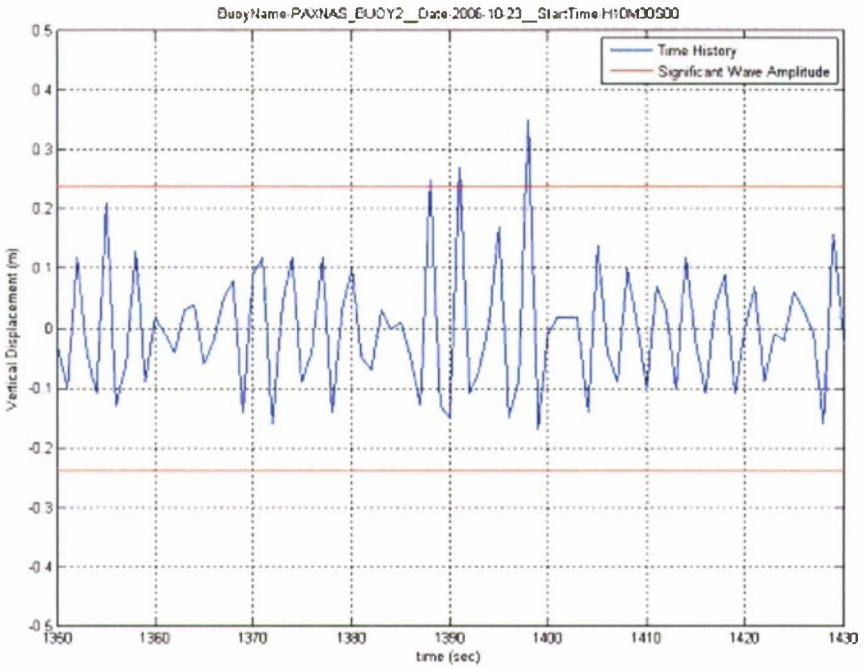

Figure 4: Wave time-history from Chesapeake Bay Buoy 2, on 10-23-2006 at 1030 hrs, significant wave height as reported for the previous 30 min. period.

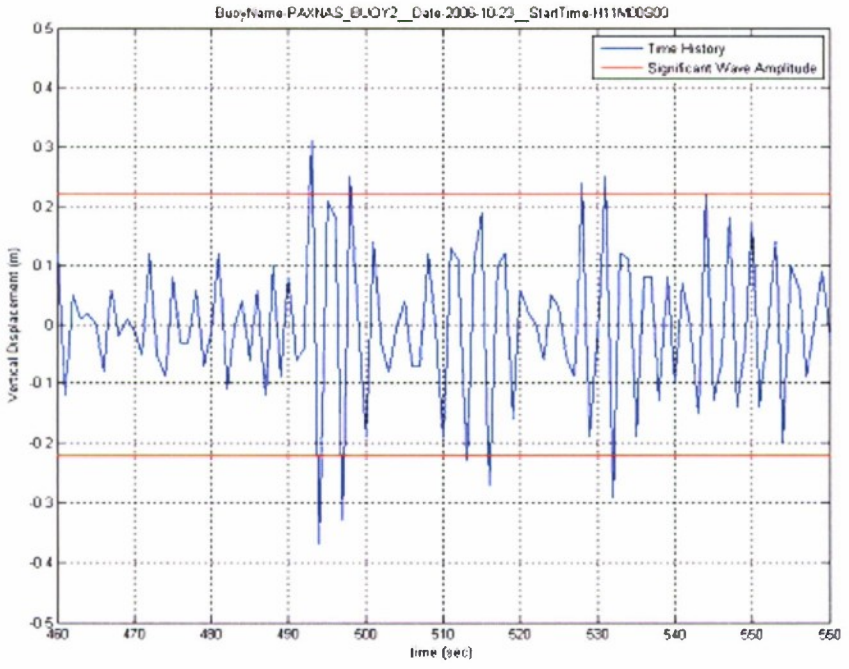

Figure 5: Wave time-history from Chesapeake Bay Buoy 2, on 10-23-2006 at 1100 hrs, significant wave height as reported for the previous 30 min. period.

Theory

Wave Groups with Regular Wave Superposition

Groups of asymmetric extreme waves have been observed in nature, but have not been produced experimentally. For this investigation, two approaches to generate extreme waves were studied: the wave-packet method and finite-wave linear superposition. The wave-packet method is well known and has previously been demonstrated as a method to produce repeatable single large-amplitude waves, at a fixed location in an experimental basin. To generate groups of extreme waves, linear superposition of a series of finite regular waves were examined. Superposition can be utilized to combine wave trains of variable periods, amplitudes, and cycles into larger or smaller amplitude waves, by either constructive or destructive interference. This technique will be referred to as the finite-wave linear superposition method.

Wave-Packet Method

The underlying principles of the wave-packet method are the deep-water dispersion relation and phase velocity, which dictate that longer waves propagate faster than shorter ones. This method, previously demonstrated both numerically and experimentally, may be utilized to generate single large amplitude waves. At the upstream position, a wave-packet consisting of a band of frequencies is generated by a wave-maker. High frequency components with small amplitudes are generated first and lower frequency components are generated subsequently. As wave components propagate downstream, lower frequency components coalesce with the higher frequency components and increasingly larger waves are formed. In general, larger waves can be produced with increased distance between the wave-maker and concentration position.

When wave components are superimposed in-phase, single large waves or symmetric groups can be produced in irregular seas. The characteristics of large waves are governed by nonlinear theory. However, linear theory was used for the first stage of development. A wave-packet can be expressed by linear superposition of the wave components,

$$a(x,t) = \mathrm{Re}\sum_{n=0}^{N/2} \hat{a}_n \exp[i\,2\pi f_n(t-t_a) - ik_n(x-x_a)] \qquad (1)$$

where x_a and t_a represent the concentration position and time, respectively. At the concentration position and time, wave components are superimposed in-phase and a large-amplitude wave may be produced. The nth frequency, f_n, is given by

$$f_n = \frac{n}{\Delta N} \tag{2}$$

where Δ represents the uniform sampling interval, in seconds, and N is the total number of discrete signals, which was assumed to be an even number for simplification. The duration of the signal, t, is given by $t = \Delta N$ and the signals are given at discrete times $t_n \equiv n\Delta$ for $n = 0, 1, ..., N-1$. The wave number, k_n, is related to the frequency, f_n, by the deep water dispersion relation,

$$k_n = \frac{\omega_n^2}{g} = \frac{(2\pi f_n)^2}{g} \tag{3}$$

For a wave-packet that propagates in the downstream (positive x) direction, negative frequencies, corresponding to $-N/2 \le n \le -1$, are not included. Equation (1) describes the wave-field of a wave-packet, at a given position and time. A Rayleigh distribution can be employed as a normalized spectrum,

$$\hat{s}_n = \frac{f_n}{\sigma^2} \exp\left[\frac{-f_n^2}{2\sigma^2}\right] \tag{4}$$

Figure 6 shows the spectrum amplitude, $\hat{s}_n$, computed from equation (4), for $\sigma = 0.2$, $N = 8192$ and $\Delta = 1/40$ seconds. Since the Nyquist critical frequency, f_c, is 20 Hz ($f_{N/2} = f_c \equiv \frac{1}{(2\Delta)}$), the frequency range is from 0 to 20 Hz.

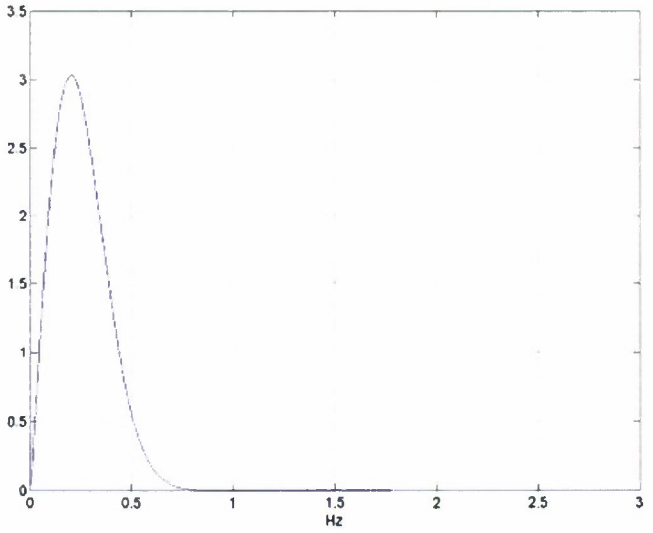

Figure 6. Spectrum, $\hat{s}_n$ when $\sigma = 0.2$

To produce large waves with the wave-packet method, the important parameters are concentration position, x_a, concentration time, t_a, and spectrum, $\hat{s}_n$. The concentration position is limited by the length of basin, the concentration time may be arbitrarily chosen for a fixed concentration position, and the shape and width of the amplitude spectrum may be selected to provide sufficient energy in the relevant frequency range. Given these three parameters, the wave-field is described by equation (1), and the amplitude, steepness, and breaking point of the large-amplitude wave can also be estimated. Different types of large-amplitude waves may be obtained with combinations of different amplitude spectra and concentration positions.

Figure 7 shows a numerical prediction of the amplitudes for a wave-packet at various stream-wise positions when the concentration position and time are $x_a = 60$ m and $t_a = 100$ sec, respectively. From the amplitude spectrum given in equation (4), the amplitudes were calculated from equation (1), at positions $x = 0$, 20, 40, 50, 60, and 70 m. High frequency components were followed by lower frequency components in the upstream locations. All wave components were superimposed in-phase and a single large-amplitude wave was formed at x = 60 m, the desired concentration position. Because long (low frequency) waves propagate faster than short (high frequency) waves, due to the phase velocity relationship (c = λ/T), the long wave components coalesce with the short waves at the concentration position. Then, for the same reason, the higher frequency components lag behind the lower ones after the concentration position. At various positions, although magnitudes of the fast Fourier transform (FFT) of the time series are the same, the phases are different.

Figure 8 presents numerical predictions of the wave-packet amplitudes at times $t = 70$, 80, 90, 100, 110, and 120 seconds so the examine wave steepness could be examined. At the concentration time the steepness of the wave is large. Once an amplitude scaling factor is chosen to scale the normalized amplitude to a desired dimensional value, the wave-breaking point may be estimated by examining the steepness of the waves.

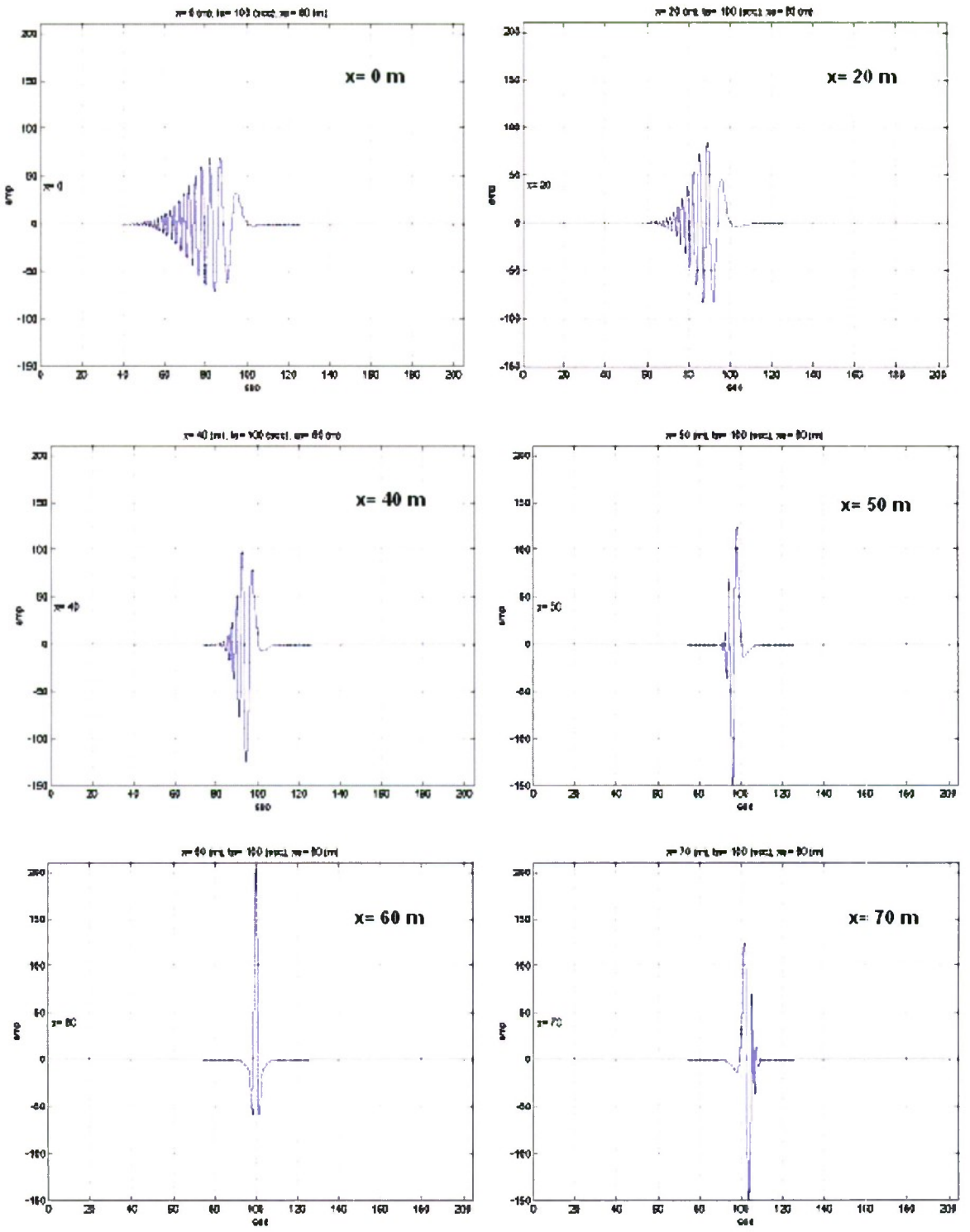

Figure 7. Time-history of packet amplitude for a notional numerical example, at $x = 0$, 20, 40, 50, 60, and 70 m when $x_a = 60$ m and $t_a = 100$ sec

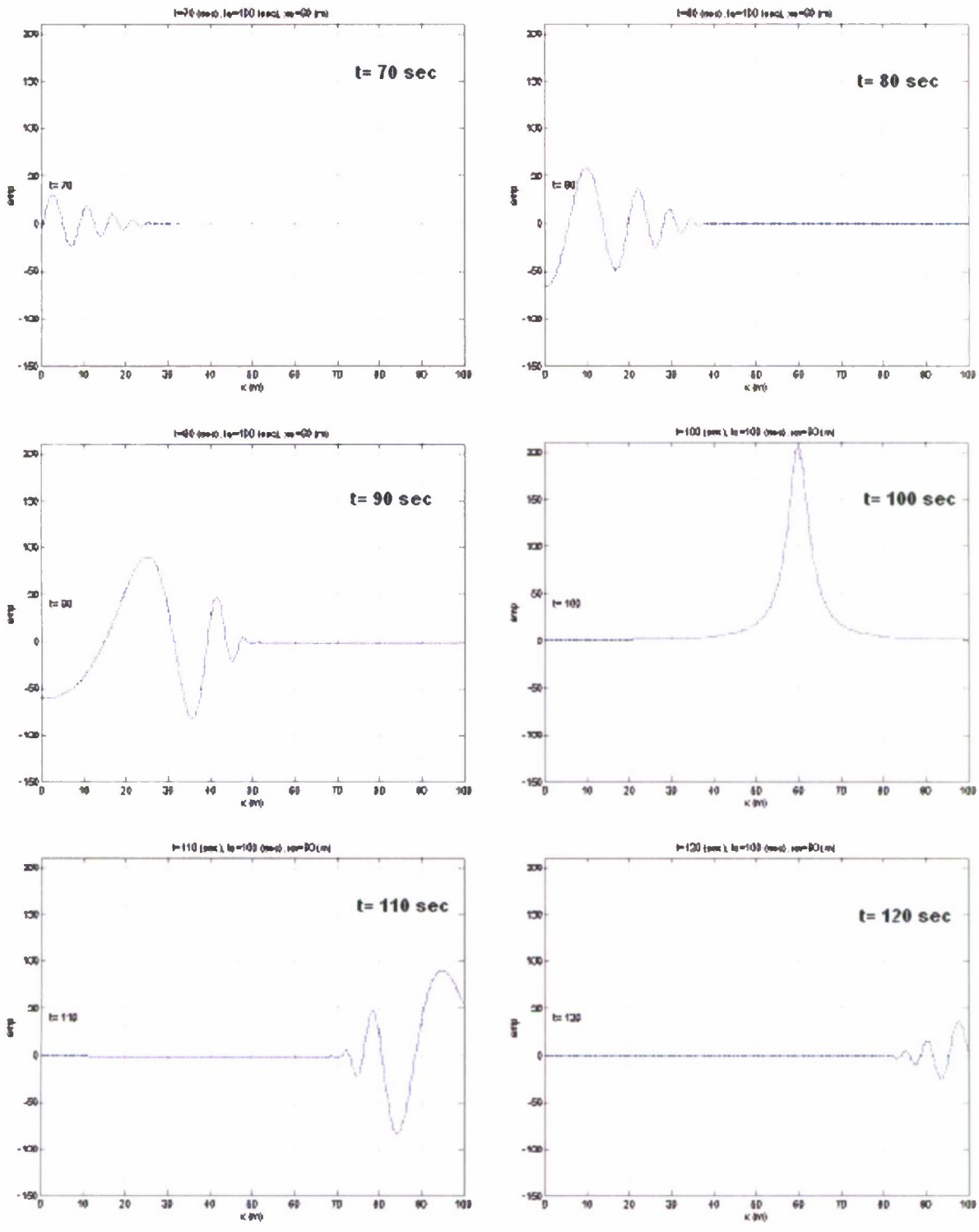

Figure 8. Time-history of wave height for a notional numerical example, at $t = 70, 80, 90, 100, 110,$ and 120 sec when $x_a = 60$ m and $t_a = 100$ sec

Finite-Wave Linear Superposition Method

The finite-wave linear superposition method employs the interaction between sequential finite length regular waves, of varied amplitude and frequency, to superimposed at a desired location in the basin, resulting in a group of asymmetric large-amplitude waves. For a given finite wave-train, consideration of the wave amplitude, period, and number of cycles enabled the different finite regular waves to superpose as a group of extreme waves at a desired, repeatable location in the basin.

This theory was examined numerically by superposition of four sine waves of varying amplitudes and frequencies: $x_1 = 1.1\sin(t_1)$, $x_2 = \sin(0.9t_1)$, $x_3 = 1.2\sin(1.1t_1)$, $x_4 = \sin(0.8t_1)$. The four sine waves were combined to form periodic asymmetric groups of three large waves (Figure 9).

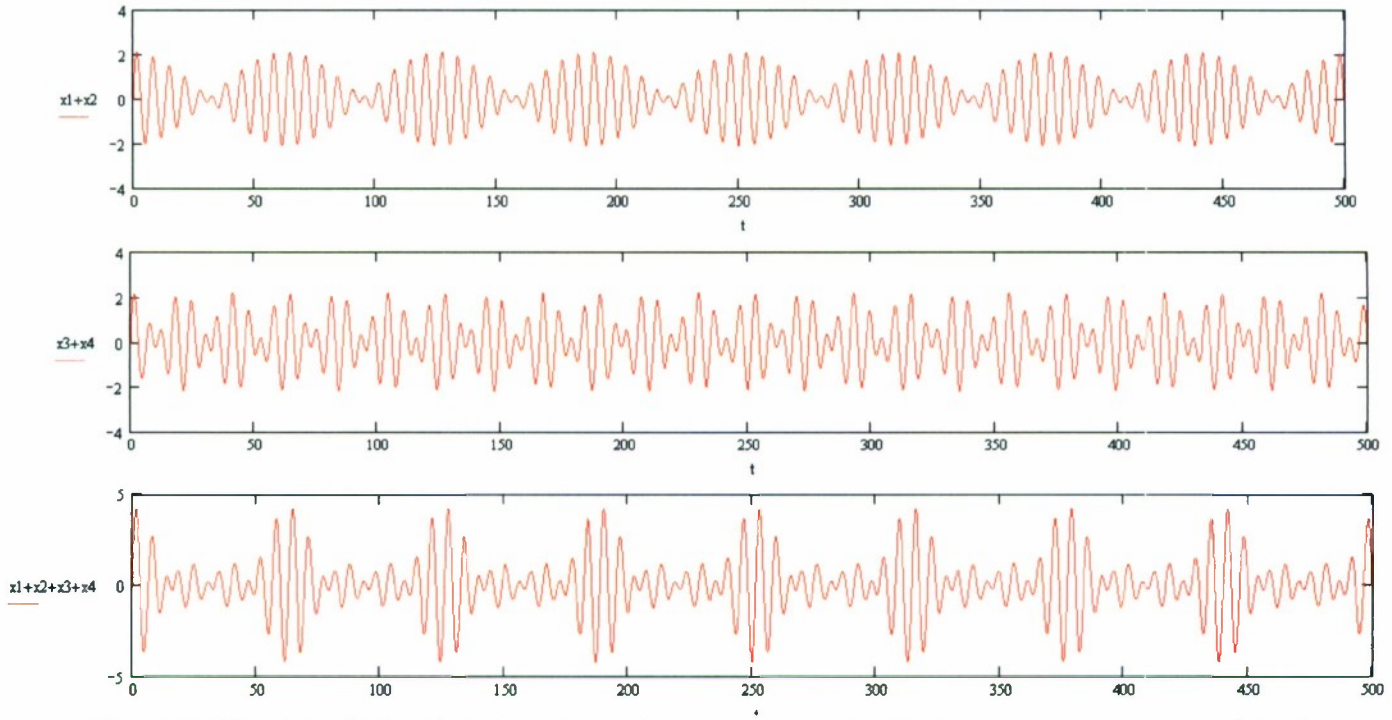

Figure 9. Combined signal output from sine wave superposition, two sine waves combined: $x_1 + x_2$ (top) and $x_3 + x_4$ (middle), all four waves ($x_1 + x_2 + x_3 + x_4$) combined to form groups of three large waves (bottom)

In this example, four sine waves of infinite length were superposed, and the three-wave group was shown to occur periodically. However, four finite-wave sequences would result in a three-wave group occurring at only one location, which could be varied based on the individual finite-wave amplitudes and periods.

Linear wave theory was applied to calculate the group velocity and regular wave groups were calculated to coalesce at a determined concentration position. The sequence files for wave generation were determined using equations (5–10).

Start time for nth regular wave train: $t_n = t_0 + \frac{T_n}{4} - T_n\left(Cyc_n - 1\right)$ (5)

Voltage for nth wave train at time t: $V(t) = H_n \cos\left[\frac{2\pi\left(t - t_n - T_n/4\right)}{T_n}\right]$ (6)

Time for the nth regular wave to reach test point: $t_P = \frac{x_a}{c_{Gn}} + \frac{T_n}{4}$ (7)

Deep-water group velocity of nth regular wave: $c_{Gn} = \frac{d\omega}{dk} = \frac{gT_n}{4\pi}$ (8)

Wavelength, $\lambda = \frac{g}{2\pi} T_n^{\,2}$ (9)

Wave steepness, $s = \frac{H}{\lambda}$ (10)

where T_n is the period of the nth regular wave in seconds, H_n is the voltage of the nth regular wave (amplitude of flap motion), Cyc_n is the number of cycles of the nth regular wave, x_a is the distance to the concentration location (in meters), and t_0 is the zero time before waves start in seconds. Local g is $9.80100\,\mathrm{m/s^2} \pm 0.0004$.

Wave Groups in an Irregular Seaway

Because the emphasis of this study was the generation of asymmetric groups of extreme waves, the wave-packet method was not considered for this part of the study. Previous work has shown the wave-packet technique to be successful for generating single large-amplitude waves, or symmetric wave groups, and embedding single extreme waves into irregular seas. Much of the previous work has focused on single large-amplitude waves and the ability to generate steep asymmetric wave groups was not investigated. For this investigation, the finite-wave linear superposition method was developed and employed to generate asymmetric groups of extreme waves and embed them into two scaled irregular sea spectra, a Bretschneider sea state 8 and Hurricane Camille.

Experimental Methods and Test Procedures

Experiments were conducted in August and November 2007 in the Maneuvering and Seakeeping (MASK) basin at NSWCCD to investigate the feasibility of producing grouped extreme waves in an experimental basin. The first experiment (Phase I) consisted of producing several combinations of finite regular waves with varying parameters, including amplitude, frequency, and signal duration. A second experiment (Phase II) was conducted and consisted of two parts. The first part applied the wave-packet method to produce single large-amplitude waves, based on the technique developed by Clauss and Bergmann (1986) and Clauss and Kuehnlein (1994, 1995). The second part employed the achievements from Phase I to embed grouped extreme waves, obtained through finite regular wave superposition in two scaled irregular seaways: a Bretschneider sea state 8 spectrum and a Hurricane Camille spectrum. Wave-maker settings used in Phase I and Phase II testing are detailed in Appendix A. Descriptions of the MASK basin, wake-maker operations for regular and irregular waves, and two wave height measurement systems, the Senix wave gage and Global Laser Rangefinder Profilometry (GLRP) is provided in the following sections.

MASK Description

The wave generation experiments were conducted in the Maneuvering and Seakeeping (MASK) basin at NSWCCD (Figure 10). Eight pneumatic wave-maker units are located along the 73 m (240 ft) side of the basin and thirteen units along the 110 m (360 ft) side of the basin. The basin is 6 m (20 ft) deep. A 115 m (376 ft) bridge traverses the basin and can be moved to a 45 degree offset from the longitudinal center of the basin. The two perpendicular banks of wave-makers can be operated individually to produce long-crested waves, or simultaneously to generate a bi-directional wave-field. Sloping, perforated, concrete beaches are located on each of the sides of the basin opposite the wave-makers to minimize wave reflections.

Two methods are used to control the flow of energy into the wave-field: varying blower motor speeds supplying air to the pneumatic domes and motion amplitude variation of the flapper valve that controls air being pumped in and out of the domes. Hydraulic cylinders with a $\pm$ 10V control signal are employed to actuate the flapper valves. The wave-maker also has a series of lips on each of the pneumatic domes, which can be set in a position of either up or down. The lips can be used to modify high frequency disturbances in the generated wave-field.

For these experiments, the MASK bridge was located in the middle of the basin, parallel to the long bank. Wave data collected from sonic probes on the bridge were recorded at 20 Hz, after being filtered with fixed 10 Hz low-pass filters. Zeroes were taken at the beginning of each testing session to obtain more accurate test data and to account for small changes in the water level of the basin.

Wave-maker Operation

To generate long crested waves, individual wave-maker units in each bank are operated in-phase and produce wave segments of the same nominal amplitude. Wave periods can be either regular or random. For this test, waves were generated from the short bank wave-makers on the left side and travel from West to East across the basin, as shown in Figure 10.

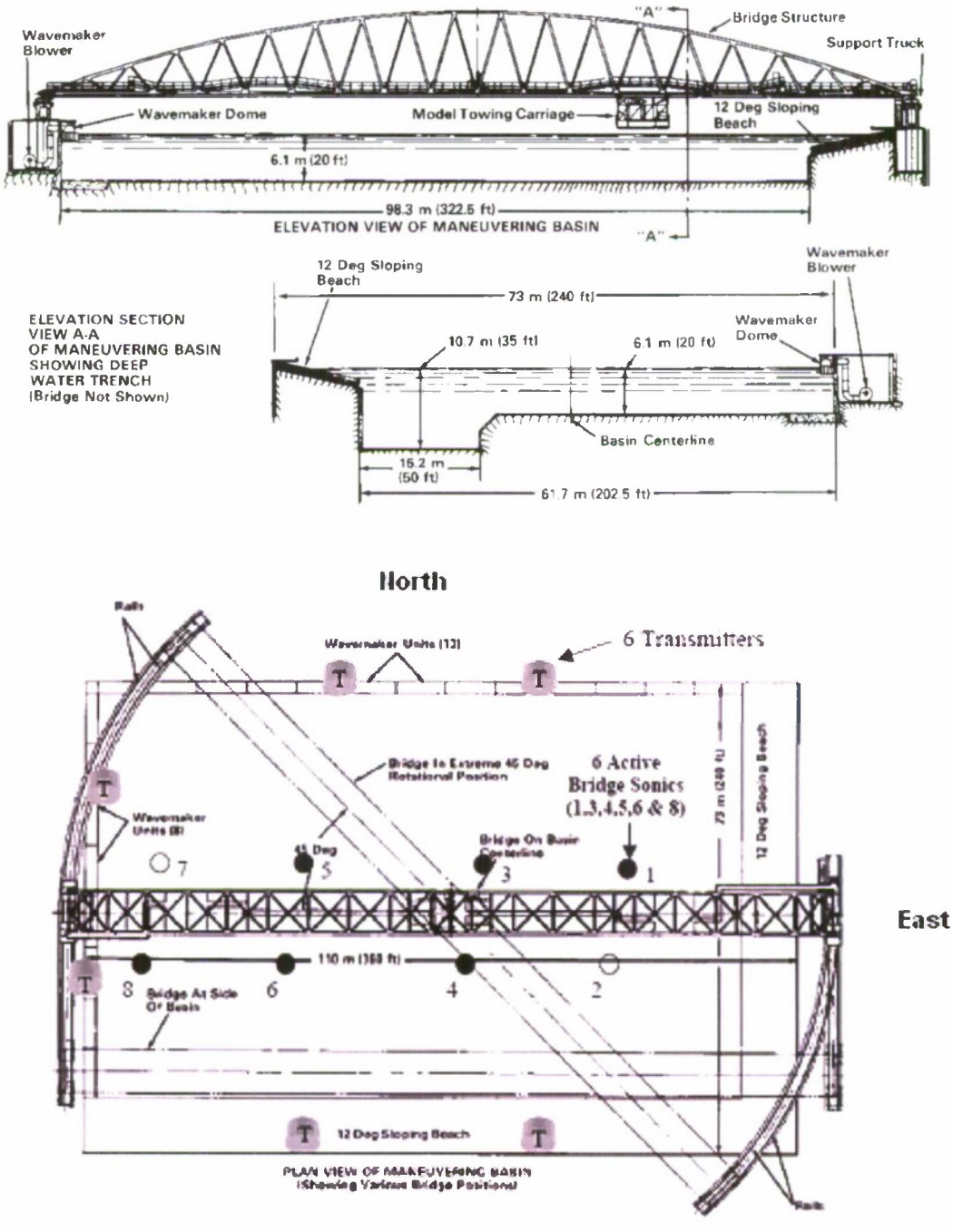

Figure 10. Maneuvering and Seakeeping (MASK) Basin

Regular Waves

To generate regular waves the wave-maker control program employs a sequence file of voltages programmed at 40 cycles per second. The computer generated digital control voltage sequences are created with a digital-to-analog (D/A) converter. The digitized voltage signal is filtered with a low-pass smoothing filter and a high-pass cutoff frequency prior to being input into the wave-maker.

In this study, a sequence file is a summation of four finitc regular waves converted to a voltage signal for the hydraulic wave-maker piston. Each of the four regular waves was controlled by blower rpm, maximum voltage (the amplitude of flapper motion), frequency, and the number of wave cycles. Other variables for the calculation of a wavc sequence were the zero time at start, which indicates a series of zero volts before initializing the wave, and the concentration point, which is the point at which the waves will coalescc to form a desired group of three large-amplitude waves.

Wave sequences, varying four separate regular wave cycles for particular pneumatic wave-maker blower rpm, signal amplitudes, and frequencies (Table 1) were applied to generate wave trains designed for the desired groupiness, with repeatable wave properties, at a fixed location within the MASK. The finalized sequence file was a summation of the voltages for the four wave trains. In some sequences, a flat spot existed, due to the signal frequency interaction, and was removed manually to smooth the motion of the hydraulic pistons.

Table 1. Experimental Parameters

Parameter	Value
Blower (rpm)	1100, 1300, 1500
Amplitude (V)	± 1.0, 2.0, 6.0, 8.0, 9.0, 9.5
Frequency (Hz)	0.4–3.3
Number of cycles	1–5

Irregular Waves

A computer program was used to generate irregular waves. The program produced digital control signal sequences and supplied them to the wave-maker controller through a digital-to-analog (D/A) converter. The digital control sequence software uses a filtered white noise technique. To produce a desired wave spectrum, a computer generated white noise signal is used to actuate the flapper valves, resulting in wave-maker dome pressure fluctuations. The wave energy distribution, as a function of the frequency, is adjusted with the driving frequencies for the valves controls. The blower speed is adjusted to control the wave amplitude. To represent nominal conditions for extreme waves, two long-crested irregular wave spectra were considered for this study, a Bretschneider wave spectrum for sea state 8 and a Hurricane Camille wave spectrum. Both spectra were modeled using two different scale ratios. Plots of the theoretical Bretschneider spectral energy distribution for sea state 8 and the Hurricane Camille spectral energy distribution, which was actually measured during the hurricane, are shown in Appendix C.

Senix Wave Gages

To measure the generated waves, the MASK basin contains an array of non-contact ultrasonic sensors, suspended from the MASK Bridge (Table 2). Locations (xy) of the sensors are referenced from the south-east corner of the MASK basin (Figure 10). The Senix Corporation model ULTRA-SR-BP sonic sensor transmits an ultrasonic wave and measures the time of reflection from the target to calculate the distance. Wave height measurements are collected from an array of six bridge-mounted wave probes (Figure 10). The probes are connected to a computer on the bridge that transmits the wave data to a shore computer, where the data are collected and stored.

Each probe (Figure 11) emits a conical sonic beam with a nominal 12-degree total angle. Measurements for steep waves may have drop-outs because the water surface tends to scatter the sonic beam away from the sensor. When attempting to measure large, steep waves, the probes can have signal drop-outs or inaccurate measurements due to scattering, which may result in measurement error. Calibration results and uncertainty estimates for the tests are described in the next section of the report.

Table 2. Wave Height Sonics Located on MASK Bridge

Gage Name	Units	Cal Factor (units /V)	Offset Units @ 0 V	Type Instrument	Mfg	Model No.	Serial No.	Barcode No.	Location x (m)	Location y (m)
Bridge Wave Ht #1	mm	-76.60	+386	Ultrasonic Distance Transducer	Senix Corp	Ultra-SR-BP	00105878	039325	5.88	29.57
Bridge Wave Ht #3	mm	-76.42	+394	Ultrasonic Distance Transducer	Senix Corp	Ultra-SR-BP	00105301	039326	32.55	29.75
Bridge Wave Ht #4	mm	-76.50	+362	Ultrasonic Distance Transducer	Senix Corp	Ultra-SR-BP	00105878	039327	36.36	39.65
Bridge Wave Ht #5	mm	-81.64	+387	Ultrasonic Distance Transducer	Senix Corp	Ultra-SR-BP	00105875	039328	56.66	29.57
Bridge Wave Ht #6	mm	-76.78	+345	Ultrasonic Distance Transducer	Senix Corp	Ultra-SR-BP	00105740	039329	60.69	39.59
Bridge Wave Ht #8	mm	-76.46	+395	Ultrasonic Distance Transducer	Senix Corp	Ultra-SR-BP	00105300	039330	78.73	39.59

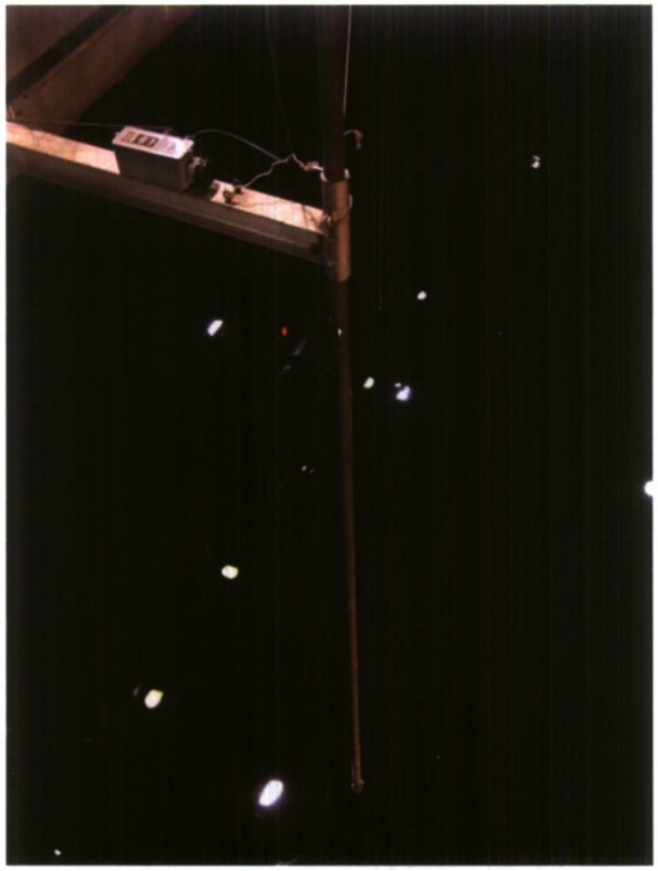

Figure 11. Senix ULTRA-SR-BP wave gage and attachment on the MASK bridge

GLRP

Global Laser Rangefinder Profilometry (GLRP) was developed at NSWCCD to provide a capability for a time-resolved field measurement of wave elevations. GLRP provides high-rate, three-dimensional mapping of surface waves over a large physical area. It is suitable for the study of large-amplitude transient wave dynamics in experimental facilities. The GLRP concept and original prototypes were demonstrated and documented previously, and a fully-functional GLRP system was constructed in the Maneuvering and Seakeeping (MASK) basin at NSWCCD (Atsavapranee, et al., 2005; Carneal, et al., 2005a).

The MASK GLRP system was designed to provide accurate model-scale whole-field measurements of wave surface profiles during free-running and captive model tests. The GLRP system illuminates the water surface with distinct points using laser diodes and measures vertical fluctuations (Figure 12). The apparent position of each diode was calibrated and recorded on a charge-coupled device (CCD) detector. The capability of the system to measure waves created in the MASK facility, as well as the wave-field generated by a scaled ship model, was demonstrated in previous testing (Carneal, et al. 2005b; Carneal and Atsavapranee, 2006). The absolute uncertainty of the system was estimated at 3 mm, which represents a relative

uncertainty on the order of 0.5% of the full measurement range (Carneal, et al., 2005b; Carneal and Atsavapranee, 2006). Calibration results and uncertainty estimates for the tests are described in the next section of the report.

The GLRP system implemented in the MASK facility is shown in Figure 13. The system used for this experiment consisted of two panels, with 200 diodes in each panel, spanning an area of 1.5 m by 3 m (4.92 ft by 9.84 ft), at a spatial resolution of 7.62 cm (19.35 in.) in each direction. Two CCD cameras, with a frequency of 30 Hz and a resolution of 1392 X 1040 pixels, are also mounted on each panel. Each panel is mounted to the GLRP platform with an ACME screw and two linear bearings to allow traversal of the entire panel. The platform has a seeding system consisting of two seeding rakes, with three nozzles each, to disperse fluorescent dye across the measurement area. The platform contains all the necessary hardware for seeding and data acquisition (Figure 14). A more complete description of the system, calibration procedures, and data processing methods used in the MASK GLRP system is contained in Carneal, et al. (2005) and Carneal and Atsavapranee (2006).

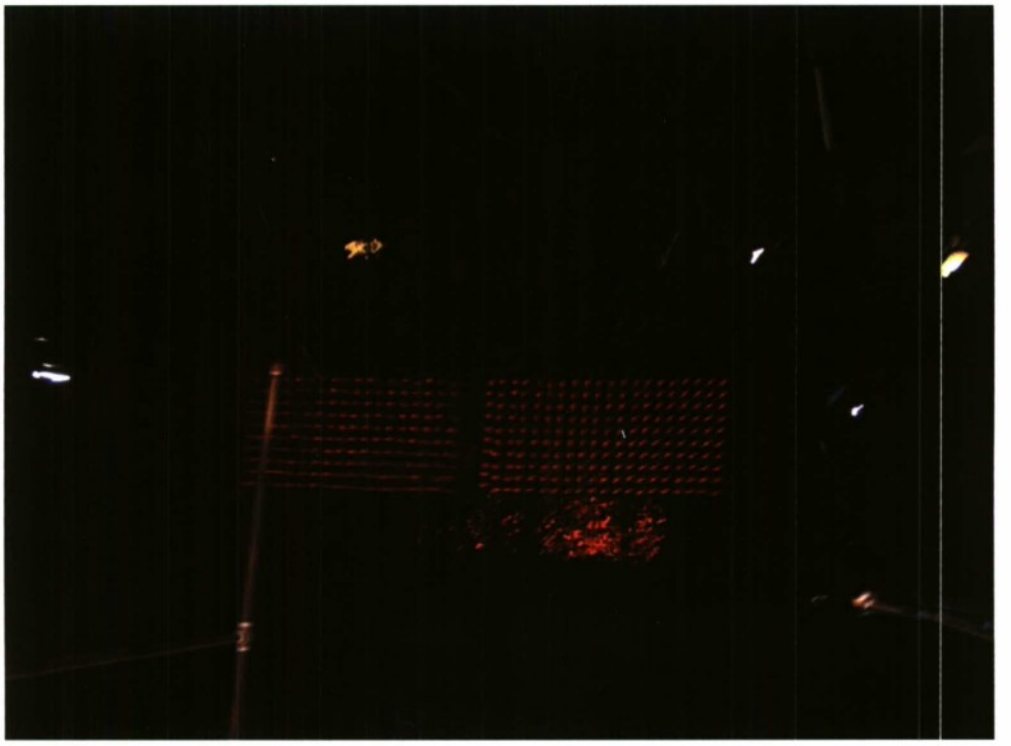

Figure 12. GLRP array illuminating water surface in MASK, as viewed from the MASK Bridge

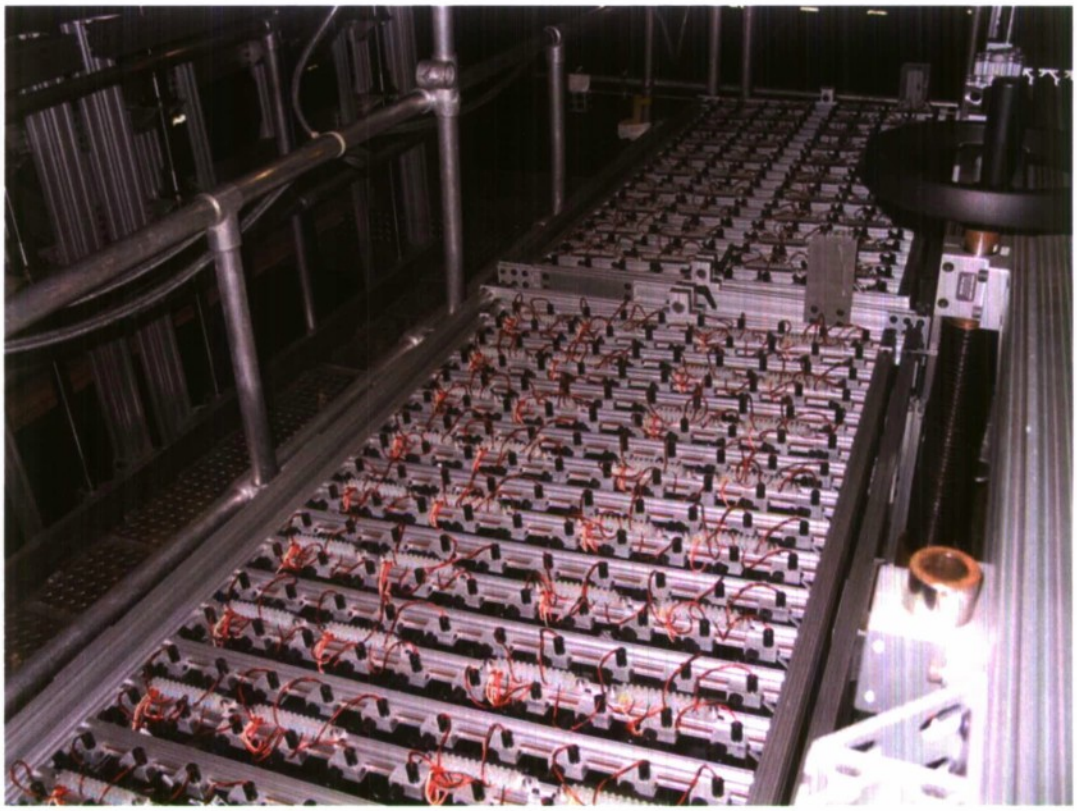

Figure 13. GLRP array panel in MASK

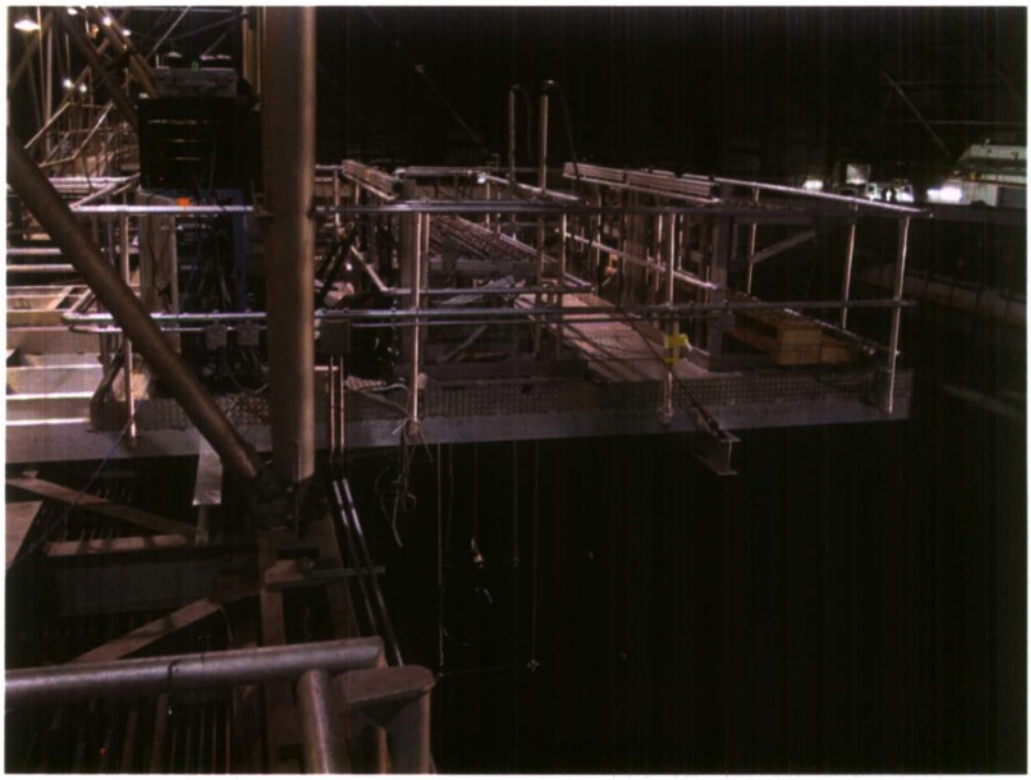

Figure 14. GLRP platform and seeder configuration

Instrumentation Calibration and Uncertainty

The following section describes the calibration of the Senix Ultra-SR-BP wave gages and Global Laser Rangefinder Profilometry (GLRP) and the uncertainty estimates of the calibrations.

Senix Ultrasonic Wave Gages

The Senix wave gages were calibrated in-situ, by varying the distance above a measured calm water level in the MASK. The transducers were located via precision machined pin locations with an estimated uncertainty of ±0.127 mm (±0.005 inch). The calibration range was ±381 mm (±15 inches), in 127-mm (5-inch) increments. The calibration locations were –381, -254, -127, 0, +127, +254, +381 mm (-15, -10, -5, 0, +5, +10, +15 inches).

The analog output for the Senix is 0 to 10 Vdc. Data from the Senix were collected and processed on a PC. The data were digitized with a National Instruments 16-bit data acquisition card, NI 6036, at a sample rate of 24 Hz. The anti-aliasing filters are Frequency Devices D78L8L, set at a cutoff frequency of 8 Hz. Typical data collection time was at least 60 s.

Normal Calibration

The normal nominal gain setting for the Senix is 76.2 mm/V (3 inches/V). The noise level of the Senix for measurements over calm water is typically between 1 and 10 mV. The maximum Type A expanded uncertainty from the ISO GUM (1995) is ±0.048 mm (±0.0019 inch) for 1,000 samples, or 41.7 s averaging time. The Type A standard uncertainty is defined as

$$u_A = \frac{s_h}{\sqrt{n}} \tag{11}$$

where s_h is the standard deviation of the height and n is the number of samples. The expanded uncertainty is defined as

$$U = k_f u \tag{12}$$

where k_f is the coverage factor. Normally at the 95% confidence level, $k_f = 1.959 \approx 2$. The maximum combined and expanded uncertainty from these two elements is 0.135 mm (0.0053 inch). The contribution of the Senix noise is negligible, compared to the machining accuracy of ±0.127 mm (±0.005 inch) for the positioning device.

An example calibration plot is presented in Figure 15, as a residual plot, for Senix wave gage #1. A residual plot is the difference between the data and a linear regression fit. The dashed line in Figure 15 is the prediction limit at the 95% confidence level, from the calibration theory of Scheffe (1973) and Carroll, et al. (1988). The uncertainty in the measurement from the

instrument noise and position is smaller than the symbols in the figure. The red symbol in the figure is an outlier and was excluded from the linear regression analysis.

The outlier is caused by the over-ranging of the Senix, in this case at 10 V. Due to the location of the Senix sensor relative to the water at 0 (zero) mm, the transducer may over-range at either 0 or 10 V, but not both. In a few cases, the sensor was located relative to the water so that over-ranging did not occur.

Most of the calibration uncertainty is due to the data scatter in the calibration. The contributions from instrument noise and position are quite small by comparison. The relative uncertainty in the calibration is presented in Figure 16. As Figure 16 indicates, the maximum relative uncertainty is about ±2%. The relative uncertainty is computed from the full-range (fr) value, which is nominally 381 mm (15 inches).

Table 3 is a summary of the calibration data acquired before the test. In this case, the calibration data were reported for the position of the probe above the water. In the experiment, the gage remained fixed, and the water moved relative to the gage. In the data processing routine, the signs of the gain and slope were opposite those in the table. The slope is negative and the intercept positive for the wave measurements.

In Table 3, the column *SEE* is the standard error estimate from the linear regression analysis, while the *r* in the next column is the correlation coefficient. The *SEE* is essentially the standard deviation of the curve fit and is a measure of the randomness of the data. The precise definition may be found in most texts on statistical analysis, such as Ross (2004). For a highly linear curve fit, *r* is near one as indicated in the table, and *SEE* will be near zero.

The column *t-test*, is the result of a hypothesis test for a comparison of the measured slope to the nominal slope of 76.2 mm/V (3 inches/V) from Ross (2004). The column t_{95} is the value of the inverse Student-*t* from the hypothesis test. Any value from the *t-test* that is less than t_{95} is statistically the same as the nominal slope. From the table, the only wave gage that is different from the nominal slope is #6.

The last two columns are the expanded uncertainty of the gages at the 95% confidence level, at 10 Vdc. The last column is percent full-range (% fr) from the measured slope, where the nominal full-scale value is 381 mm (15 inches). As the table indicates, the largest uncertainty was about ±8 mm (±0.31 inches), or ±2% fr, at the 95% confidence level.

Higher Range Calibration

To measure larger waves, the gain for the Senix wave gages was changed to a nominal value of 101.6 mm/V (4 inches/V). However, the gages were not calibrated until after the Phase II test. The results described here are from the post-test calibration. The calibration was limited by the calibration fixture, over a total range of 762 mm (30 inches). The required range for 0 to 10 Vdc was ±508 mm (±20 inches). From the limitations of the fixture, the 7 calibration locations were then –508, -381, –254, -127, 0, +127, and +254 (-20, -15, -10, -5, 0, +5, and +10 inches).

The calibration results for Senix wave gage #1 are presented in Figure 17. The measured uncertainty for each point is again smaller than the symbols. The noise level for the Senix was 0.8 to 6.2 mV, which was similar to the noise level from the normal range calibration. The Type A uncertainty had a maximum expanded uncertainty of ±0.040 mm (±0.0016 inch). The resulting combined uncertainty was then ±0.13 mm (±0.0052 inch). The uncertainty from the instrument noise was small in comparison to uncertainty of the probe location, and most of the uncertainty was in the curve fit.

As Figure 17 indicates, the maximum uncertainty was about ±17 mm. The uncertainty at +508 mm (+20 inches) was significantly higher than at –508 mm (-20 inches). The larger value is from the extrapolation of the calibration data from +254 mm (+10 inches) to +508 inches (+20 inches). The relative uncertainty is shown in Figure 18. The maximum relative uncertainty for this gage was ±3.4% fr.

The calibration results are summarized in Table 4. The data trends are similar to the normal calibration (Table 3). All of the probes, with the exception of #6, have a slope that is statistically the same as the nominal gain setting of 101.6 mm/V (4 inches/V). With the exception of gage #1, the relative uncertainty of the gages was less than or equal to ±2% fr, similar to previous results. The cause of the larger uncertainty in probe #1 is unknown. Calibration over the full range, ±508 mm (±20 inches), of the Senix wave gages may reduce the uncertainty.

Because both the normal and higher range calibrations are performed on a flat-plane surface, the accuracy associated with signal drop-outs when attempting to measure steep waves should be considered. However, the influence of wave steepness on signal drop-outs for the Senix probes is not currently known.

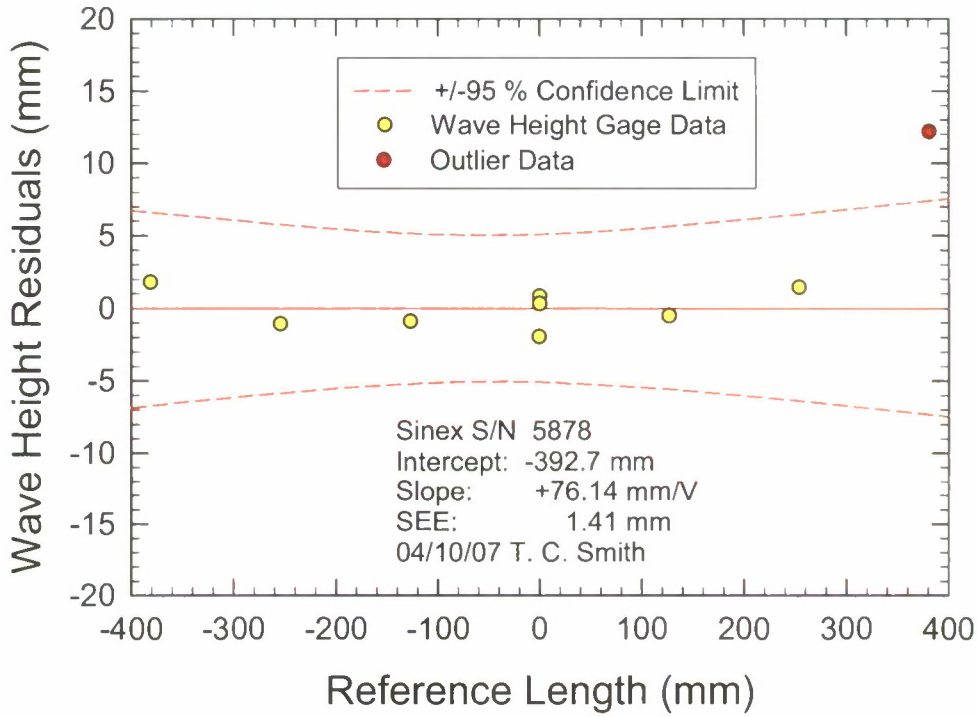

Figure 15. Calibration of Senix Wave Gage #1 for Normal Range

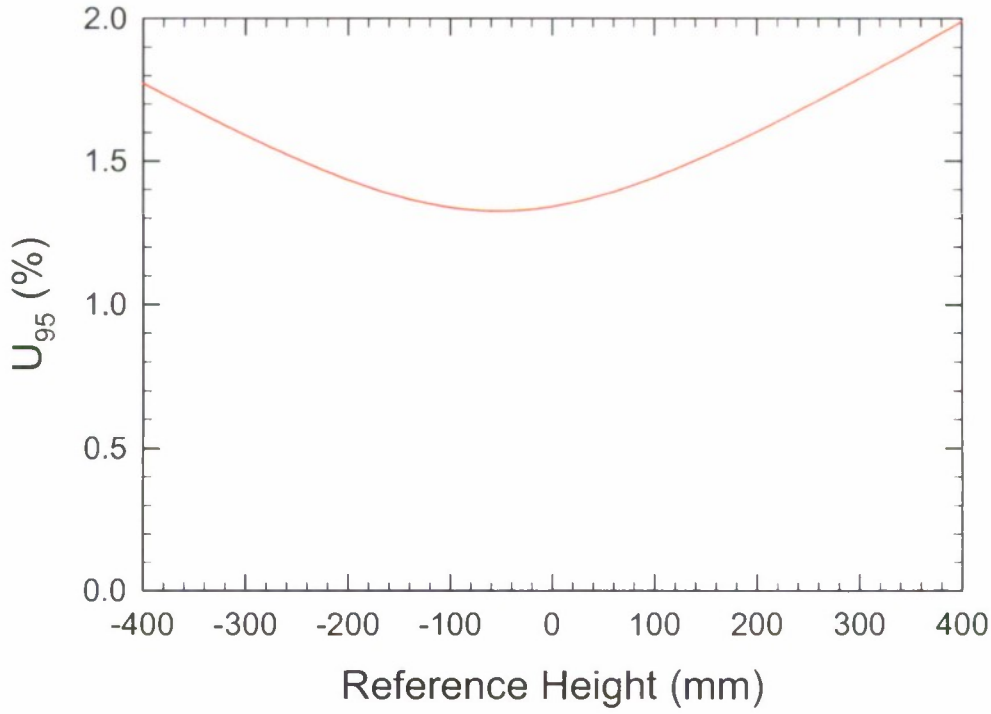

Figure 16. Relative Calibration Uncertainty of Senix Wave Gage #1 for Normal Range

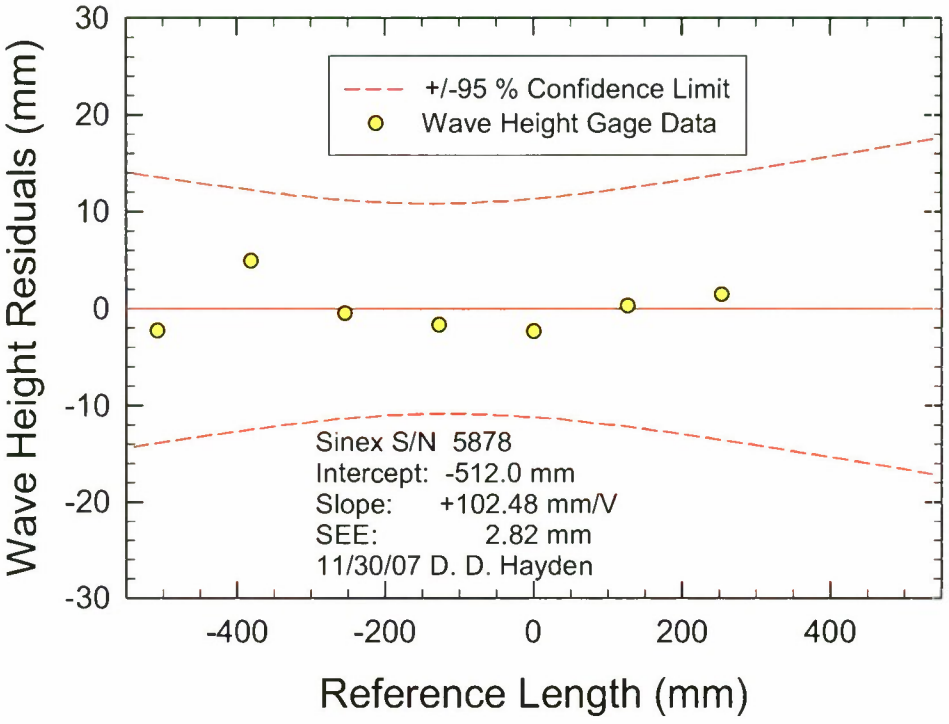

Figure 17. Calibration of Senix Wave Gage #1 for High Range

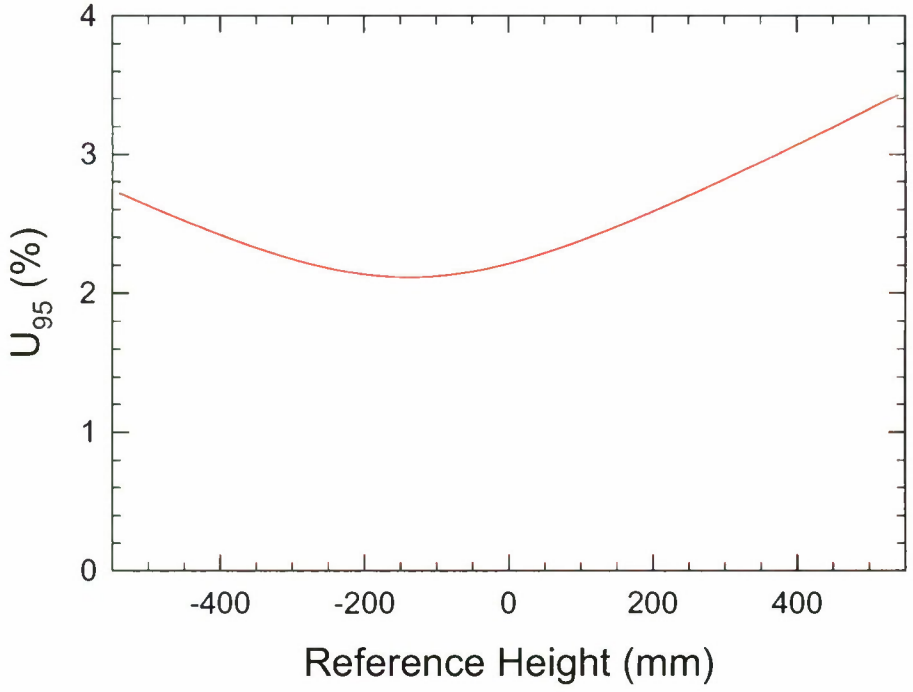

Figure 18. Relative Calibration Uncertainty of Senix Wave Gage #1 for High Range

Table 3. Summary of Senix Wave Gage Calibrations for Normal Range

Probe #	Slope (mm/V)	Intercept (mm)	SEE (mm)	r	t-test	t_{95}	U_{95} (mm)	U_{95} (% fr)
1	76.138	-392.67	1.410	0.999979	0.308	2.45	7.33	1.93
3	76.325	-380.34	1.808	0.999975	0.611	2.36	7.99	2.09
4	76.269	-390.20	0.945	0.999991	0.515	2.45	4.92	1.29
5	76.314	-381.16	1.844	0.999977	0.545	2.45	8.50	2.23
6	76.538	-392.73	0.679	0.999995	3.51	2.45	3.53	0.92
8	76.313	-395.16	0.358	0.999999	2.24	2.45	1.85	0.49

Table 4. Summary of Senix Wave Gage Calibrations for High Range

Probe #	Slope (mm/V)	Intercept (mm)	SEE (mm)	r	t-test	t_{95}	U_{95} (mm)	U_{95} (% fr)
1	102.477	-512.02	2.821	0.999956	2.06	2.57	17.29	3.38
3	101.458	-491.95	1.054	0.999992	0.704	2.78	7.53	1.48
4	101.442	-512.87	1.221	0.999992	0.857	2.57	7.33	1.44
5	101.883	-502.24	1.469	0.999985	1.002	2.78	10.47	2.06
6	102.260	-511.20	0.621	0.999997	5.56	2.78	4.38	0.86
8	101.635	-515.52	0.622	0.999997	0.290	2.78	4.35	0.86

GLRP

Calibration of the GLRP measurement was performed by raising and lowering the GLRP panels to several standoff heights. Images of the laser diode's intersection with the water surface were reeorded at eaeh height to simulate vertieal motion of the water surface. This process is termed surfaee height ealibration, and a superimposed ealibration image for a single eamera is shown in Figure 19. In this experiment, ealibration heights ranged from -304.8 mm to +304.8 mm (-1 ft. to +12 ft.) in increments of 25.4 mm (1 in.). The ealibration data provided the positions of the images of the laser diodes on the CCD eamera in pixels versus the height or z-coordinate. A typieal result is shown in Figure 20. Results are presented for two resolutions of the measurements. Calibration data for this report were based upon 7 points (Figure 20a), at an inerement of 101.6 mm (4 in.). The full data set is shown in Figure 20b, at a resolution of 25.4 mm (1 in.).

The calibration for this report was obtained from a seeond-order polynomial fit. Figure 20a indieates that a seeond-order fit may not be justified. A measure of the uneertainty is the Standard Error of Estimate (*SEE*). As the figure indieates, the *SEE* is signifieantly redueed with an inereased number of data points. For 7 points, the *SEE* was nearly 19 mm, eompared to 12.1 mm for 23 points, where one point was exeluded as an outlier from the 24 point data set.

The data were then evaluated for an optimal curve fit with a reasonably lower value of *SEE*. The results are summarized in Table 5 for diode #80, which had one of the lower values of *SEE* in the data set of 80 diodes. As the table indicates, a third-order polynomial fit has a significantly lower value of *SEE,* 4.6 mm, compared to an *SEE* of 10 mm for the second-order fit, with 7 points for the data in this report.

Table 5. Comparison of Polynomial Fits of Different Orders and Number of Points for GLRP Diode #80 Calibration for Wave Height

No. Points	Order	SEE (mm)	r
7	1	18.6	0.9970
7	2	10.4	0.9993
23	1	12.1	0.9981
23	2	7.8	0.9992
23	3	4.6	0.9997

The calibration result for diode #80, as a third-order polynomial, is presented in Figure 21 as a residual plot. As the figure indicates, on the basis of the prediction limit at the 95% confidence level, the uncertainty was 10 mm, which is similar to the high range calibration of Senix gage #5 in Table 4. Senix gage #5 was the closest to the GLRP. However, the uncertainty varies with diode number, or location, as indicated by the *SEE* in Figure 22. The SEE decreased systematically from a value of 14.6 mm at diode # 1 to 4.6 mm at diode #80. The value from the prediction is about 2.2 **SEE*. Thus, the uncertainty in the wave height calibration varied between 10 mm and 32 mm. The variation of the 3rd-order polynomial coefficients with diode number is shown in Figure 23. These coefficients also vary systematically with diode number, with trends similar to *SEE*.

In addition to calibration of the system in the z-coordinate, an xy-mapping calibration was also performed. Because the camera was at an angle to the water surface, the xy-positions of the diodes must be determined as a function of water height. This was accomplished by recording images of a precision machined calibration target at several heights, at a known position in the MASK facility. A sample image is shown in Figure 24. These images were then de-warped using standard image processing techniques. The calibration positions of each diode image were calculated from a corresponding x- and y-position in the MASK facility, for each diode at each height. A second-order polynomial fit for x and y, as a function of distance from neutral position, was computed for each measurement point. The second-order polynomial fits were obtained for x, y, z physical coordinates in the MASK facility, as a function of diode position on the CCD detector.

Data proeessing was aeeomplished by blob analysis of the raw data images and loeating the diode image in eaeh frame. Information from the ealibration proeess was used to assign the deteeted blobs to the appropriate calibration curves. The centroid of the detected blob was determined and the ealibration eurves were applied to determine the loeation (x, y, z) of each blob in each frame, and the data were stored. Beeause the eurrent MASK system generates a large amount of raw data, approximately 170MB/s in a four eamera, two panel eonfiguration, the data proeessing must be performed offline. A more eomplete deseription of the system, ealibration proeedures, and data processing methods in the MASK GLRP system is doeumented in Atsavapranee, et al. (2005), Carneal, et al. (2005), and Carneal and Atsavapranee (2006).

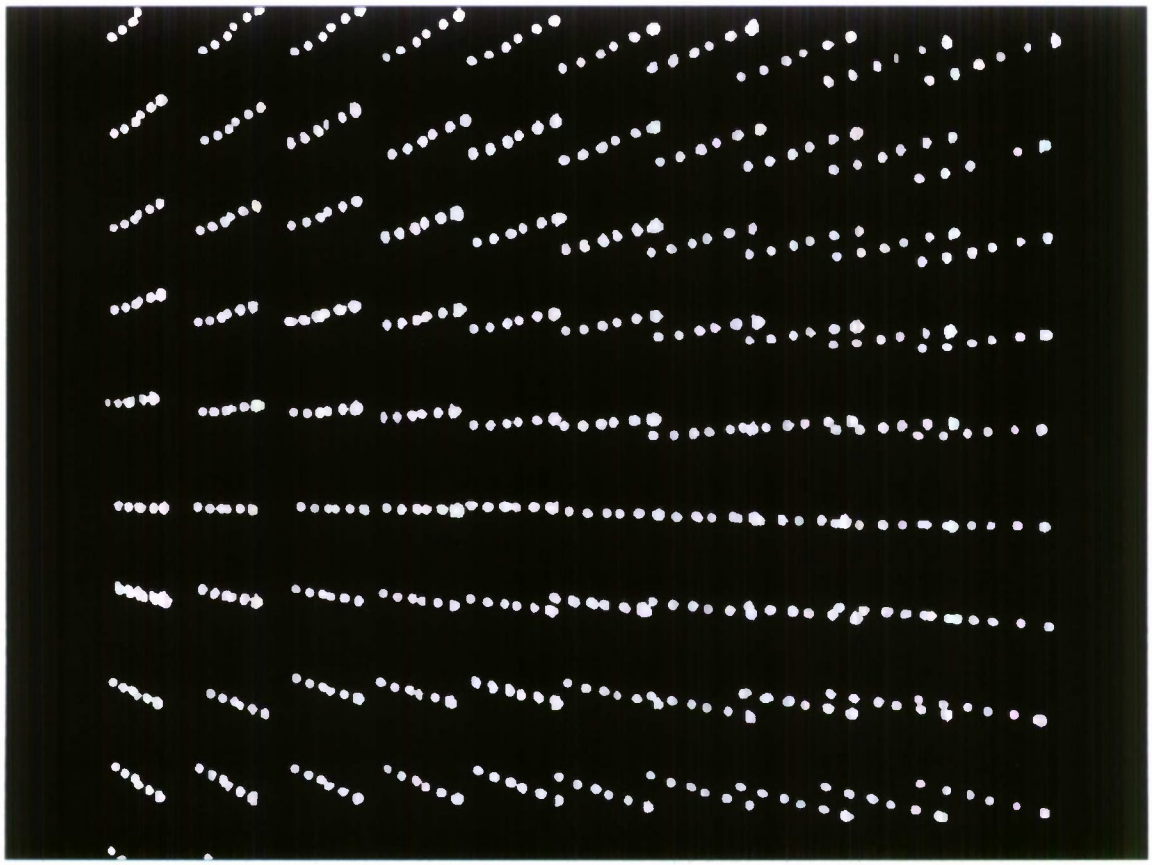

Figure 19. Superimposed surface height calibration image

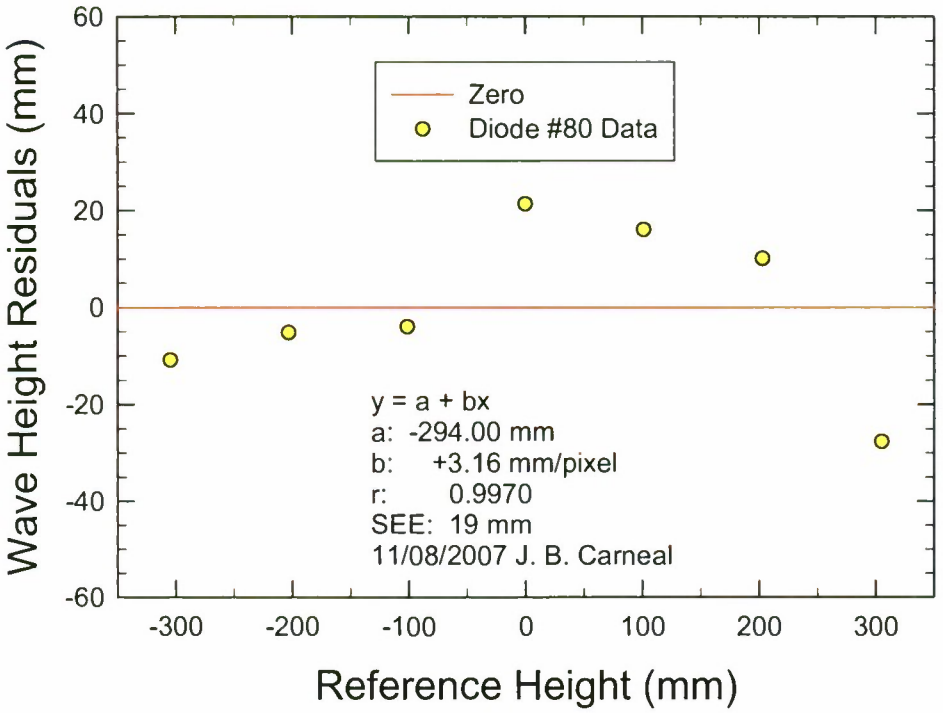

a. Calibration with 7 points

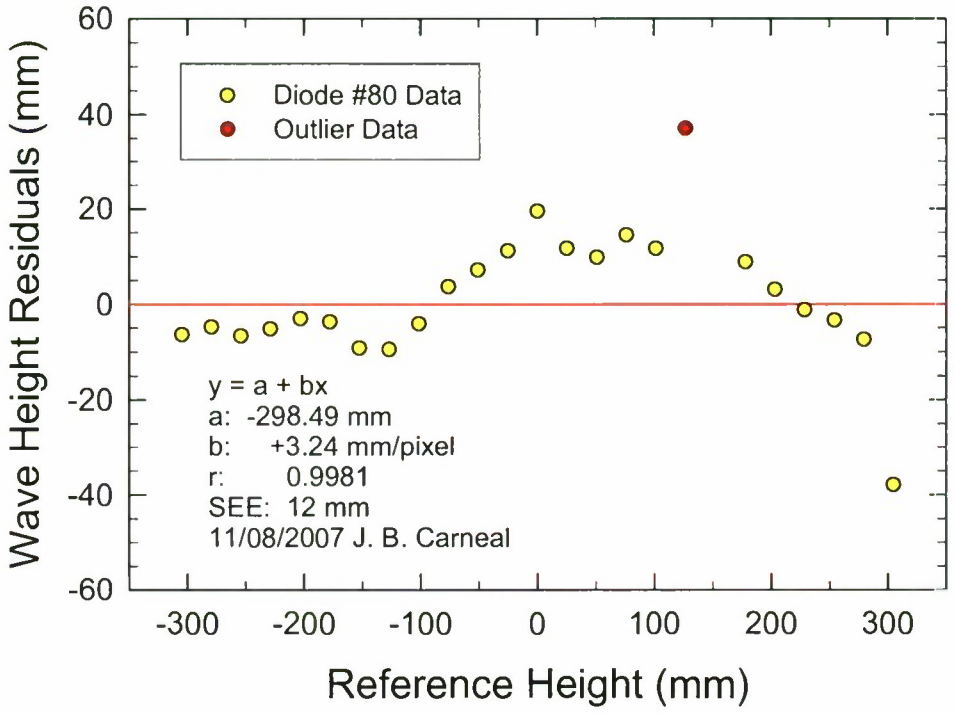

b. Calibration with 24 points

Figure 20. GLRP Linear Wave Height Calibration for Diode #80

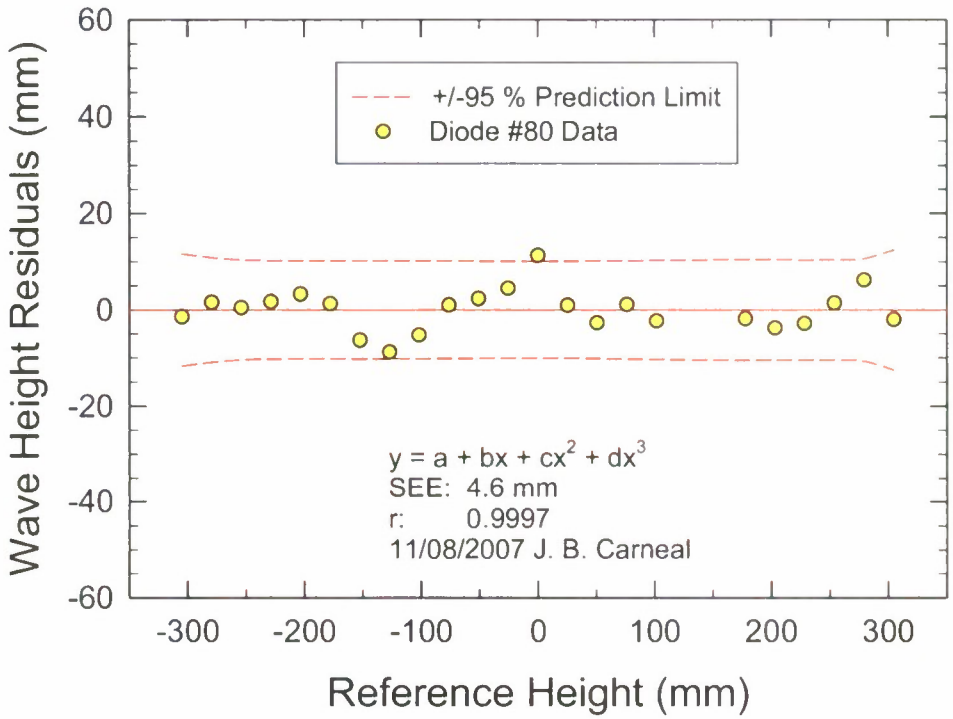

Figure 21. GLRP Calibration of Diode #80 with 3rd-Order Polynomial

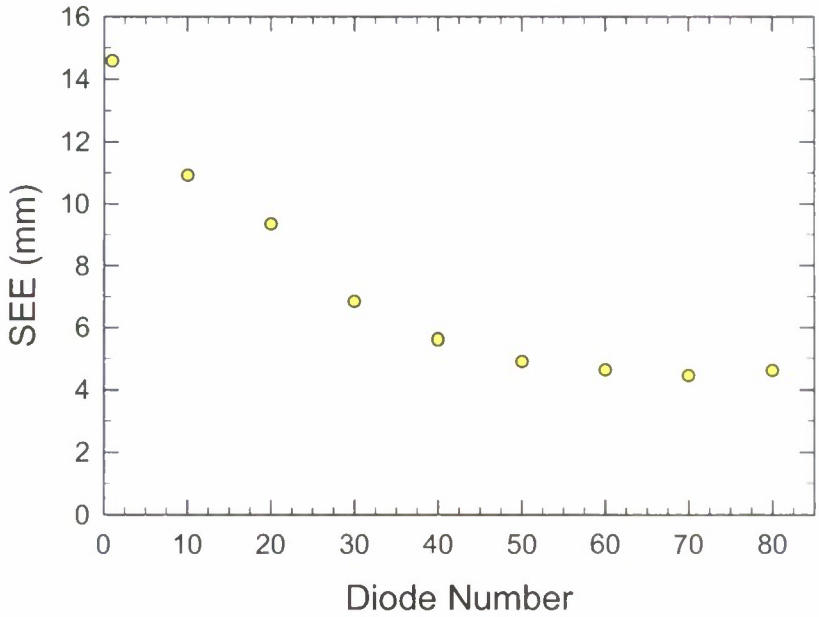

Figure 22. Standard Error of Estimate for GLRP

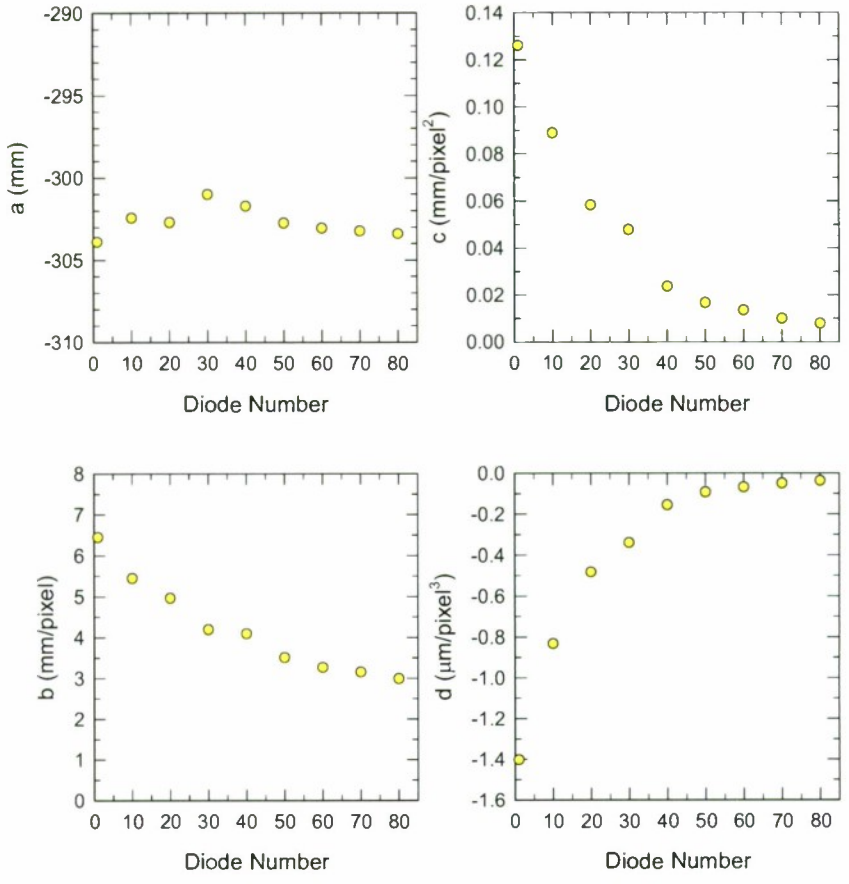

Figure 23. Coefficients of 3rd-Order Polynomial Calibration of GLRP for Wave Height

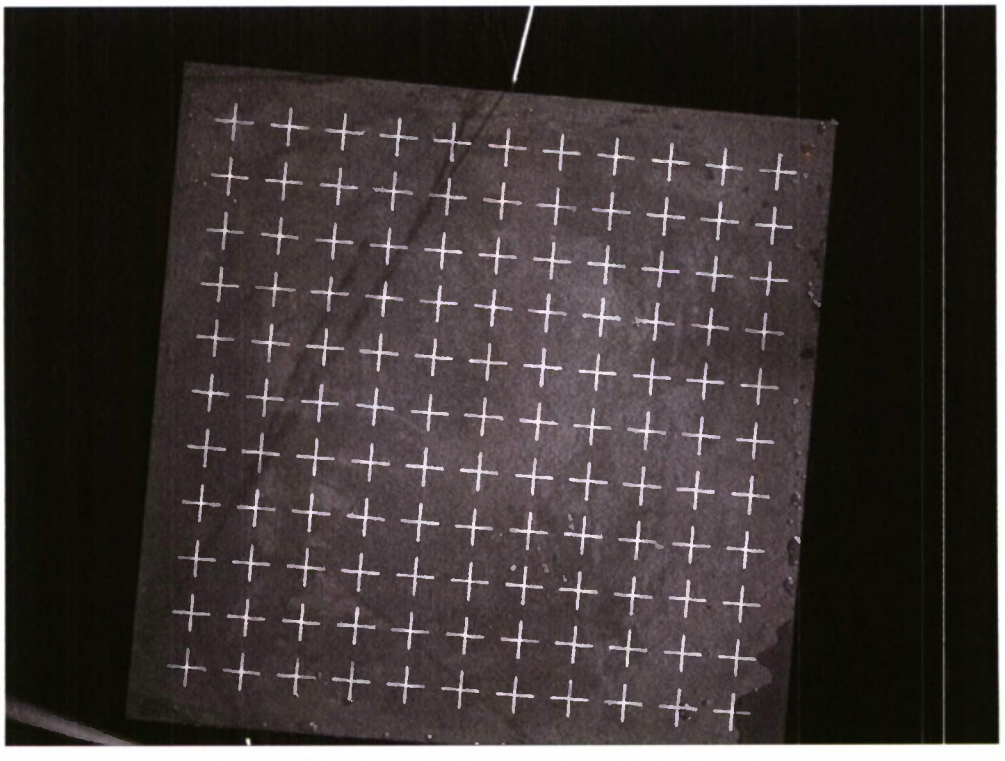

Figure 24. Sample image for XY calibration

Experimental Results

Wave Groups with Regular Wave Superposition

The wave-paeket method and finite-wave linear superposition method were used to generate extreme waves. The wave-paeket method is well known and has been demonstrated as a method to produee repeatable single large-amplitude waves, at a fixed loeation in an experimental basin. Earlier researeh did not investigate or indieate the eapability of this method to generate realistic groups of asymmetrie extreme waves. To develop this later eapability, the finite-wave linear superposition method was used. Through linear superposition of these finite regular waves, unidireetional asymmetrie groups of extreme waves were produeed at repeatable, fixed loeations in the basin. Regular wave results from the wave-paeket method and the finite-wave linear superposition method are shown in Appendix B. Results from embedded wave groups in irregular waves are shown in Appendix C. GLRP results and eomparisons to Senix Probe measurements are shown in Appendix D.

Wave-Packet Method

The wave-paeket method applies wave eomponents, which are superimposed in-phase, to produee single large waves in irregular seas. This method was applied to generate a single large-amplitude wave at a fixed loeation in the MASK basin. Linear superposition of eomponents using Rayleigh distributions as a speetrum, eoupled with varied scale parameters and amplitudes, were used to generate large-amplitude waves for this part of the study. For comparison, additional measurements were taken of pure sine waves generated with varied frequencies and amplitudes. The test results with a single frequeney sinusoidal input signal and with a wave-paeket input signal are diseussed. Results are shown in Appendix B.

As a baseline test, a sine wave with the frequeney of 0.3 Hz was given as an input for the wave-maker. Figure 25 shows the time series data from the six wave gages installed along the bridge in the basin. The positions of the wave gages are shown in Figure 10. In general, the measured frequencies of the Senix signals were in good agreement with the input frequeney. However, the amplitude of the sine wave measured at probe 8, located at the most upstream position, was much smaller than the other downstream probe signals. The wave amplitude at probe 4 was a little larger than at probe 3. The generated wave-field in the model basin is not completely uniform (O'Dea and Newman, 2007; Smith, et al., 2007).

Linear theory indieates that if an upstream wave-paeket, for example at $x = 0$, can be generated, then a large wave at a desired eoneentration position, at $x = 60$ m, ean be expeeted (Figure 7). The input signal for the wave-maker ean be determined if the transfer function of the wave maker is known. However, the transfer function of the MASK wave-maker is not clearly known, particularly the phase. Additionally, in many cases, the transfer functions are not linear.

Because the wave-maker transfer function of the MASK is not well known, the signal at x = 0 (Figure 7) was utilized as an input to the wave-maker. The probe data are plotted in Figures 25 and 26. The probe signals indicate that the concentration position was located between probes 3 and 1. The maximum wave height measured at probe 3 is about 18 cm and at the upstream probe 8 is 7.65 cm. Additional measurements between probes 3 and 1 are necessary to determine the exact location of the concentration position and the maximum wave height.

To evaluate the effect of the amplitude on the wave-maker signal, three input signals with different amplitudes were supplied to the wave-maker. The maximum values of the wave-maker flapper control signals were 3, 6, and 9 V, shown in Figure 27 by the blue, green, and red lines, respectively. The measured probe data are plotted in Figure 28. In these figures, the probe data were multiplied by scale factors of the input signals, 3 for blue, 1.5 for green, and 1 for red. The probe data from three different input amplitudes agree quite well.

The results (Figure 28) demonstrate that linear theory can identify an optimum input signal. Various input signals, with different amplitude spectra, can produce a desired large wave signal, at a given position. Once an input signal is selected, the signal can be amplified to produce a larger wave, as long as a breaking wave does not occur in the wave-packet during the process. Linear theory also shows that a wave-field at any position and time can be determined by a few parameters: concentration position, x_a, concentration time, t_a, and amplitude spectrum, $\hat{a}_n$. Because concentration position is limited by the length of the model basin and concentration time may be chosen arbitrarily, the amplitude spectrum is the only free parameter. Comparisons of the amplitudes for different voltages and the resulting waves are shown in Figures 29 and 30.

Results of this study indicate that a database with different wave-maker input signals is an essential first step in producing single large-amplitude waves deterministically. This database will identify an input signal that will produce a desired wave-packet, at a specified position. The shape of the wave-packet should be the primary focus. The test results show that a larger wave can be produced by multiplying an input signal by a desired scale factor. Because the generated wave-field in the MASK was shown to be repeatable, large waves may be produced with the identified input signals. The results of this study confirm that a wave-field may be modeled well with linear theory.

Finite-Wave Linear Superposition Method

Based on the principle of superposition, regular waves of finite length and varying amplitude were considered as a method to produce groups of asymmetric large-amplitude waves. For this part of the study, fifty-six runs were completed in the MASK. The influence of the different parameters were examined by thirty-six different wave sequence files and a repeatable group of large-amplitude waves were obtained at a fixed location in the basin. Time-histories of the waves, recorded by the Senix probes, are shown in Appendix C.

A number of runs containing large wave groups were observed. Some sample runs: 15, 35, 43, 51, and 61 are presented where the wave sequences produced coalesced to form a group of three waves of successively increasing amplitudes that occur at probes 3 and 4 (Figure 31). In some cases, the third wave in the group reached a wave height of nearly 0.76 m (30 inches) (Figure 32). The wave characteristics of these groups, obtained from the wave-time histories recorded by the sonic probes, are shown (Figures 41–55). Some of the observed trends are discussed below.

The wave time-histories show a wave-packet generated by the wave-maker, as defined in Table 11, arriving at probe 8. The varying speeds of the waves within the packet caused the waves to form the desired three-wave group formation within the region measured by probes 4 and 3, before dissipating toward the end of the basin, as shown in the measurements from probe 1 (Figures 41–55).

From the conditions tested, an increase in the blower rpm led to an overall increase in the generated wave amplitudes. Setting the lips on the wave-maker to the down position resulted in a slight improvement in the overall shape of the waves, because the lips filter out high frequency disturbances. For the range of parameters tested, a generalized limit for the wave-maker blower rpm was established. For wave cycles with large amplitudes, indicated by large voltage signals, a blower setting of 1300 rpm could not be exceeded without breaking waves occurring. For some cases (ex. Run 61), reduced signal voltages for the 1st and 4th cycles enabled a blower setting of 1500 rpm to be applied without breaking waves resulting.

As observed in runs 15 and 43, a high voltage signal was applied for the first of the wave cycles. This was combined with small amplitude signals and a low number of cycles for the second and third waves. For the fourth wave cycle signal, there was a decrease in the amplitude and increase in the frequency. The combination of these four waves resulted in the occurrence of a larger and steeper third wave in the group, at probe 4 in the basin.

As observed in runs 15 and 35, a small increase in the third and fourth wave cycle frequencies, with other parameters constant, resulted in a larger amplitude, but slightly less steep second wave, at probe 4. As observed in runs 35 and 43, a small increase in frequency and decrease in amplitude of the third wave cycle, and a small decrease in the frequency and increase in amplitude of the fourth wave cycle, resulted in larger amplitude and steeper second waves at probe 4. However, neglecting changes to the third and fourth wave cycles most likely results in a larger and steeper third wave. Because the wave characteristics exceeded the calibration limits of the Senix probes and the steepness of the largest wave, this was unconfirmed during this set of experiments due to saturation and drop-outs in the sonic probe measurements.

As observed in runs 51 and 61, a decrease in the first and fourth cycle amplitudes, with one additional cycle added to the second wave signal, resulted in a greater wave height for the third wave in the group, still with 1/10 wave steepness. This decrease also resulted in larger and

steeper first and second waves in the wave group.

At probe 3, many of the runs showed a decrease in the first and second wave heights of the three-wave group compared to the wave heights of the group measured at probe 4. For the third wave in the group, the largest wave amplitude was typically observed at probe 4. However, the greatest steepness of the third wave in the group was typically measured at probe 3. At probe 3, the second wave in the group was slightly less steep, but the third wave was slightly steeper than the same group at probe 4. This difference in the wave group characteristics is important because it provides variations in wave heights and steepness at two locations close together in the basin, to enable a model test to accurately simulate a range of conditions.

As part of Phase II testing, runs 5–8 and 42, were performed to repeat the optimal wave groups obtained through the finite-wave linear superposition method in Phase I. The wave time-histories of the wave groups were in good agreement between the August and November 2007 tests (Tables 6 and 7). Recalibration and gain change of the Senix probes enabled measurements of larger wave amplitudes without saturation, although some runs still had wave amplitudes larger than $\pm$ 50 cm, which remained beyond the recalibrated range of the Senix probes.

Table 6. Summary of Maximum Wave Height Results for Finite-Wave Linear Superposition Method- Probe #3

Run #	h (m)	h/λ	h/L	h_{fs} (m)**
15	0.615	0.125	0.157	28.7
7*	0.738	0.143	0.189	34.4
35	0.595	0.111	0.152	27.7
42*	0.678	0.111	0.173	31.6
43	0.606	0.125	0.155	28.2
8*	0.744	0.143	0.190	34.7
51	0.633	0.111	0.162	29.5
5*	0.633	0.111	0.162	29.5
61	0.595	0.125	0.152	27.7
6*	0.705	0.143	0.180	32.9

*Run numbers from Phase II repeat runs

** For a scale ratio of 46.6

Table 7. Summary of Maximum Wave Height Results for Finite-Wave Linear Superposition Method- Probe #4

Run #	h (m)	h/λ	h/L	h_{fs} (m)**
15	0.743	0.100	0.190	34.6
7*	0.739	0.091	0.189	34.4
35	0.722	0.100	0.185	33.6
42*	0.669	0.077	0.0.171	31.2
43	0.706	0.091	0.180	32.9
8*	0.732	0.091	0.187	34.1
51	0.666	0.100	0.170	31.0
5*	0.507	0.100	0.130	23.6
61	0.727	0.111	0.185	33.9
6*	0.672	0.100	0.172	31.3

*Run numbers from Phase II repeat runs

** For a scale ratio of 46.6

Wave Groups in an Irregular Seaway

These experiments were performed as part of Phase II, and consisted of extending the methodology for generating large-amplitude wave groups using the finite-wave linear superposition method, developed in Phase I. In the Phase II experiments, the large-amplitude wave groups were embedded in two different irregular seaways. A list of the conditions tested is shown in Table 12. Throughout this phase, additional measurements of the wave-field were acquired with the Global Laser Rangefinder Profilometery (GLRP) system. Results are shown in Appendix C.

Senix Results

Two wave spectra were examined to determine the feasibility of the embedding method, a 30th scale Bretschneider Sea State 8, with H_s= 38.1 cm (15.0 in.) and T_m= 3.0 s, and two Hurricane Camille spectra, a 30th scale, with H_s= 40.64 cm (16.0 in.) and T_m= 2.45 s, and a 46th scale, with H_s= 26.16 cm (10.30 in.) and T_m= 1.96 s. The two scales considered in this study represent typical scale ratios for ship model testing at NSWCCD, used to assess seakeeping and dynamic stability performance.

As a first comparison, run 15 from the Phase I testing was embedded at both the end and in the middle of the 30th scale Bretschneider Sea State 8 spectra. In both cases the wave group retained the general characteristics after being embedded. Because of the desired application to

dynamic stability model testing, the process was continued with the wave group embedded in the middle of the irregular seaway time series (Figures 61–71). Results from Senix probe measurements at probes 3 and 4 for the embedded large-amplitude wave group are shown in Tables 8 and 9.

To assess the impact of the embedded wave group on the spectral shape, spectral analysis was performed of runs with both the Bretschneider and Hurricane Camille spectra (Figures 94–96). Examination of the spectra shows a good agreement between the idealized and generated spectra with the embedded wave group for the 30th scale Bretschneider Sea State 8. With the embedded wave group, the peak of the spectra was significantly higher, but the overall spectral shape was still close to the idealized value. However, the idealized and generated spectra for the two scaled Hurricane Camille seaways did not agree as well. The 30th scale spectrum with the embedded wave groups had higher spectral values at the lower frequencies and a lower peak value compared to the idealized spectrum. The 46th scale Hurricane Camille spectrum with the embedded wave group had a higher peak than the idealized spectrum, but also a secondary peak, near a frequency of 3.8 rad/s. Because a deterministic time series was used for the Hurricane Camille sequence, it is possible that not enough of the spectral components were included to define a realistic spectral shape, skewing the peak of the spectral shape. With the extreme wave group embedded in the time series, a secondary, larger peak may have occurred, more closely approximating the peak of the idealized Camille spectrum. Additional testing will have to be performed to confirm this conjecture.

Variation of the embedded wave groups in irregular seaways produced runs where three-wave groups occurred in the seaway with two outcomes. In the first, successively larger waves led to a steep wave, which could be classified as an extreme wave ($H > 2.0\ H_s$). In the second, a wave of larger amplitude than the previous two in the group, and at least two waves still exceeding the criteria for an extreme wave, were observed. Both of these outcomes were reproducible and repeatable (Figures 61–71). Processing of the characteristics of the wave groups, as each of the three waves occurred in the irregular seaway, was completed (Figures 72–93).

Table 8. Summary of Maximum Wave Height Results for Finite-Wave Linear Superposition Method Embedded Into Irregular Waves- Probe #3

Run #	Spectrum*	h (m)	h/λ	h/L	h_{fs} (m)**
11	BS SS8	0.804	0.143	0.205	37.5
14	BS SS8	0.799	0.143	0.204	37.2
21	BS SS8	0.602	0.111	0.153	28.1
22	BS SS8	0.644	0.111	0.164	30.0
24	BS SS8	0.718	0.125	0.184	33.4
26	HC	0.647	0.018	0.165	30.2
27	HC	0.530	0.071	0.136	24.7
30	HC	0.542	0.015	0.139	25.3
41	HC	0.480	0.063	0.123	22.4
43	HC	0.649	0.091	0.165	30.2

Table 9. Summary of Maximum Wave Height Results for Finite-Wave Linear Superposition Method Embedded Into Irregular Waves- Probe #4

Run #	Spectrum*	h (m)	h/λ	h/L	h_{fs} (m)**
11	BS SS8	0.714	0.091	0.183	33.3
14	BS SS8	0.710	0.100	0.182	33.1
21	BS SS8	0.525	0.063	0.134	24.5
22	BS SS8	0.530	0.050	0.136	24.7
24	BS SS8	0.540	0.526	0.138	25.2
26	HC	0.761	0.040	0.195	35.5
27	HC	0.582	0.067	0.149	27.1
30	HC	0.786	0.100	0.201	36.6
41	HC	0.478	0.040	0.122	22.3
43	HC	0.494	0.048	0.126	23.0

*Embedded into Bretschneider sea state 8 (BS SS8) and Hurricane Camille (HC) spectra

** For a scale ratio of 46.6

GLRP Results

Results from GLRP measurements and comparisons to Senix probe data are shown in Appendix D. Three-dimensional representations of GLRP data are presented every third figure, in Figures 97–121. These representations show several snapshots of the wave group evolution in the measurement region. The first frame shows the water surface before the wave group enters the measurement region. The second frame shows the beginning of the wave group. In the third and fourth frames, the maximum and minimum wave heights encountered in the measurement are shown. The final frame shows the calm water surface at the end of the run.

A single point time-history for a selected GLRP diode is shown every third figure, in Figures 98–122. The time-history clearly shows the evolution of the wave group, from the occurrence of the smaller waves at the beginning to the larger waves in the middle of the wave group. At the end of the measurement, the water surface returns to a relatively calm state after the wave group has traversed the measurement area. In addition, sonic measurements were taken simultaneously with GLRP measurements. The sonic probe in closest proximity to the GLRP platform was probe 5. A comparison between the time histories of a single GLRP point and sonic probe 5 is shown every third figure, in Figures 99–123. Qualitatively the measurements agree very well. Because the systems were not spatially co-located in the basin, a truly quantitative comparison cannot be made. However, the amplitudes appear to be within the uncertainty in the measurements, and most of the difference may be the phase shift due to location. These details have not been evaluated for this data. in future tests, a sonic probe should be placed within the measurement region of the GLRP platform to provide a direct comparison between the two measurement techniques.

During Run 7 (Figures 97–99), the GLRP system began collecting data after the smallest waves in the wave group had already reached the measurement area. The evolution of the wave group is apparent, as the interaction between waves produced minimum and maximum wave heights occurring at approximately 17 and 18 seconds, respectively. After the maximum wave arrived, the wave height fluctuations decayed quickly, and the basin began to settle. The GLRP measurement showed a similar peak, with a slightly lower minimum than the sonic measurements, as well as a faster decrease in wave activity after the maximum wave encounter occurred.

In Run 9 (Figures 103–105), a selected portion of the time series is shown to emphasize the evolution of the beginning of the wave group. For this case, a set of grouped extreme waves were added to the wave-field after the development of Bretschneider sea state 8. A comparison between the time histories of a single GLRP point and sonic probe 5 is shown (Figure 105) and the GLRP and sonic measurements show a strong qualitative agreement.

For Run 11, and all successive runs, data are shown for Cameras 1 and 2 only. The data from Camera 3 exhibited a high noise level. Data could be extracted from Camera 3 with further

software modification, but it was decided to replace the camera for future tests instead of exhausting resources to develop unneeessary high noise level data processing applications.

A single point time-history for a seleeted GLRP diode and Senix probe 5 is shown (Figure 108). For this case, waves were generated to simulate a Bretschneider sea state 8 with a large-amplitude wave group embedded in the wave-field. The minimum and maximum wave heights occurred at approximately 52 and 54 seconds. The GLRP and sonic measurements show a strong qualitative agreement. The GLRP system measured a lower trough and peak than the sonic probe, but these differences could stem from the differenee in measurement locations and capabilities of the two systems.

A single point time-history for a selected GLRP diode is shown in Figure 116, which shows a seetion of the time-history in the middle of the wave generation sequence. For this case, waves were generated to simulate conditions during Hurrieane Camille with a wave group embedded into the wave-field. The maximum and minimum wave heights oeeurred at approximately 61 and 62 seconds after the GLRP system data collection began. The large-amplitude wave group is elearly evident in the middle of the GLRP time series, surrounded by waves occurring in the simulated hurricane conditions. A comparison between the time-histories of a single GLRP point and sonie probe 5 is shown in Figure 117. In this ease, the maximum wave height eneounters measured by the GLRP and sonie systems were very similar, while the GLRP system eontinued to deteet a deeper trough for the largest wave than the sonic probe.

A single point time-history for a seleeted GLRP diode is shown in Figure 122. For this case, waves were generated to simulate the conditions during Hurricane Camille with a wave group embedded in the wave-field. The maximum wave encounter occurred at approximately 57 seconds after GLRP system data collection began. A eomparison between the time histories of a single GLRP point and sonic probe 5 is shown in Figure 123. The GLRP and sonic measurements show a strong qualitative agreement. As in previous measurements, the GLRP system measured a lower trough and peak than the sonie probe. Only a few peaks and troughs exhibited major differences in this run.

The GLRP measurements performed in this work were very successful in obtaining 3-D spatially dense measurements of the wave-fields. Comparisons to Senix probes show very strong qualitative agreement between the measurement techniques. The observed differences between the measurement techniques can be attributed to several factors. The most important faetor is that the measurements were taken in different locations in the basin, since the sonie probe is approximately 4.57 m (15 ft) closer to the short bank wave-maker than the closest GLRP point. Given that the wave-fields generated in this experiment ranged from sinusoidal to highly random, the qualitative agreement between the GLRP and sonie measurements was expected to decrease with additional random wave interaction. The data collected in this experiment supported this expectation, and for the isolated large-amplitude wave groups (runs 7 and 8), the

qualitative agreement between the measurements was very favorable. For the Bretschneider sea state 8 and Hurricane Camille test runs, the qualitative agreement between the measurement systems was less favorable, especially in regions of random wave interaction away from the wave groups. However, the measurements display a level of qualitative agreement that was very close, even in the random seaway cases, despite the different location from probe 5.

In future tests, a sonic probe will be placed in the same location as the GLRP system to provide a quantitative comparison between the measurement systems. In addition, directional wave probes will be deployed to determine the ability of GLRP measurements to provide directional wave spectra. In order to exactly locate the sonic probes, laser measurement and alignment systems will be used to precisely determine the sonic locations in the basin, as well as the exact position of the GLRP platform and measurement areas as a function of grid angle. Future work may also include reprocessing of the data contained in this report to extract directional wave information from the collected data to determine the capability of the current GLRP system in the measurement of directional wave spectra. Additionally, the differences in amplitudes of the waves from both systems should be compared quantitatively to the estimated uncertainties. The phase shift in the measurements should be checked for consistency in the relative location of the two types of sensors.

Comparison of Senix and GLRP Results

Results including the measured maximum wave heights from the Senix Probe #5 and GLRP point measurements for probes within at x=3.4-3.5 m, y=1.3-1.4 m, at one of the middle points on the first panel. The percent difference for each run are shown in Table 10. The percent difference was calculated using the following standard formula:

$$\%\,Diff = \frac{\left|h_{Senix} - h_{GLRP}\right|}{\left(\frac{h_{Senix} + h_{GLRP}}{2}\right)} \cdot 100 \tag{13}$$

Table 10. Summary of Comparison of Maximum Wave Height Results GLRP and Senix Probe #5 Measurements

Run #	Senix h (m)	GLRP h (m)	Difference (%)
7	0.629	0.651	3.44
8	0.613	0.634	3.37
11	0.653	0.635	2.80
21	0.561	0.573	2.12
22	0.626	0.629	0.478
24	0.661	0.616	7.05
26	0.635	0.618	2.71
27	0.435	0.482	10.25
30	0.552	0.494	11.09

All of the data in Table 10 are within the limits of the Senix ealibration (h= 1.016 m), but some exeeed the ealibration range of the GLRP system (H= 0.610 m). Additional work is neeessary to determine the ealibration limit of GLRP. Runs 7, 9, 11, 21, 22, and 26 in Table 10 are within the measurement uneertainty of Senix probe #5 and probably have a signifieant overlap of uneertainty estimates between the two systems.

Summary of Results

The maximum ealibrated attained wave height, as normalized with a nominal representative ship model length (h/L), was 0.205 eompared to 0.1 for the typieal largest regular wave height to ship model length ratio used for testing. This is double the maximum wave height normally achieved in the MASK. The maximum wave steepness (h/λ) observed was approximately 1/7, approaching the theoretical limit for a non-breaking wave, eompared to a 1/10 wave steepness whieh is typieally the maximum for regular wave testing. The largest estimated full-seale wave height observed was 37.5 m (123 ft.) at a 46.6 seale ratio.

Conclusions and Recommendations

The purpose of this investigation was to demonstrate the feasibility of producing extreme waves, both singularly and in groups, in an experimental basin for applications to surface-ship model experiments. Physical model experiments provide a valuable evaluation tool to assess surface ship performance in extreme conditions. Currently, the best representation of a seaway in the model basin is through the modeling of spectral shapes by generating random waves. Model experiments conducted in random waves to assess dynamic stability, slamming, and ultimate strength require very long run times to ensure that the extreme wave events, which are probable for the seaway, have been encountered. Employing a deterministic model testing technique will reduce testing time in the model basin, enhance the realistic representation of the seaway, and increase confidence in the assessment of dynamic stability and secondary structural loads performance in extreme conditions.

Grouped extreme waves of varied, yet repeatable, amplitudes and locations were produced during the course of this investigation. The NSWCCD MASK basin pneumatic wave-maker generated extreme wave groups in the basin. Superposition of regular waves created wave groups and embedded them in an irregular seaway. The wave-packet method generated single large-amplitude waves. The generation of large-amplitude wave groups was demonstrated in the basin, with the goal of eventually producing simulated extreme wave groups in irregular waves, similar to those observed in nature. GRLP measurements were shown to provide a similar level of accuracy as measurements using the Senix wave probes, but also enabled 3D wave-field measurements, in addition to point measurements, of very large, steep waves. This study demonstrated the initial steps for the development of a sophisticated and efficient experimental technique for dynamic stability model testing which will enable the realization of wave groups within a given seaway that will induce severe motions.

Future Work

The work outlined in this report details progress made in FY07 and the first half of FY08. Expanding on the initial success of this work, the eventual objective of improved dynamic stability and structural testing of a free-running ship model with wave groups in the MASK may be achieved. Plans for future work are presented below.

One of the first tasks will be additional investigation of the Chesapeake Bay wave buoy data. The wave buoy data can be evaluated to develop assessment methods to determine the frequency of occurrence of groups of extreme waves, better characterize these wave groups, and possibly correlate the groups to dynamic stability events. A criterion to identify extreme wave groups could be applied to buoy and satellite imagery data from ocean measurements, for several geographic regions and time-periods. This would aid with initial development to determine the

probability of oeeurrenee for groups of extreme waves, which eould be expanded to assess the global oeean wave environment.

A signifieant emphasis of additional work will inelude the generation of bidireetional waves from the short bank and long bank in the MASK. A primary goal of this work is to re-ereate wave time histories seen in nature, such as those measured from the Chesapeake Bay wave buoys or other oeean measurements, to provide realistie extreme wave groups for applieation in experimental testing. Investigation of teehniques for embedding additional multiple large-amplitude waves groups, sueh as a five wave group, in an irregular wave speetrum, in both sea states 7 and 8, ean be investigated. Further adjustment of wave eyele parameters, to aehieve a range of grouped wave amplitudes and loeations, may be investigated. Although the finite-wave linear superposition method enabled repeatable, predietable generation of three wave groups, further applieation of the wave-paeket approaeh should also be examined to attempt to produee wave groups with large-amplitude, asymmetrie, steep waves and embed them in an irregular seaway.

The applieation of the methodology for dynamie stability testing may be demonstrated by testing of seale models with the wave groups, initially for dead-ship eonditions, but also with forward speed, to assess dynamie stability performanee. In addition to dynamie stability performanee evaluation, the large-amplitude wave group teehnique can be utilized to evaluate seeondary loads on ships and offshore struetures. A theory will need to be developed for understanding how to perform statistieal extrapolation of ship motion response from extreme wave groups to determine lifetime risks for ship stability failures, perhaps building on some of the reeent work of Alford (Alford, et al., 2006; Alford, 2008).

Continuing throughout this future work, additional measurements of wave-fields will be taken with the Global Laser Rangefinder Profilometery (GLRP) system. Development of a Infrared Global Laser Rangefinder Profilometery (IRGLRP) system whieh does not require dye seeding of the water surfaee is eurrently underway. Applications of this system to large-amplitude wave group testing will also be explored.

The ealibration range of the measurement systems should be extended to match the maximum wave heights of the eurrent research. Some of the wave heights in the experiments eontinued to exeeed the reealibrated range of the Senix probes, ± 0.508 m. The ealibration limit of the GLRP system has not yet been investigated. Calibration fixtures for both systems should be modified for a wave height measurement range larger than ± 0.6m

This page intentionally left blank

References

Alford, L. K., A. W. Troesch, and L. S. McCue (2006), "Design Wave Elevations Leading to Extreme Roll Motion," *Marine Systems and Ocean Technology*, 1(4), June.

Alford, L. K., M. S. Khalid, D. Kim, K. Maki, and A. W. Troesch (2007), "A Methodology for Creating Design Ship Responses," *10th International Symposium on Practical Design of Ships and Other Floating Structures*, Houston, TX, 1-5 October.

Alford, L. K. (2008), Estimating Extreme Responses Using A Non-Uniform Phase Distribution, *Ph.D. Dissertation*, The University of Michigan.

Anato, E. M. and C. Guedes Soares (2008), "On the Occurrence of Abnormal Waves in an Offshore Tank," *Journal of Offshore Mechanics and Artic Engineering*, 130, May.

Atsavapranee, P., J. B. Carneal, C. W. Baumann, J. H. Hamilton, and J. W. Shan (2005), "Global Laser Rangefinder Profilometry (GLRP): A Novel Optieal Surfaee-Wave Measurement System," NSWCCD-50-TR-2005/022, April.

Battjes, J. A. and G. Ph. Van Vledder (1984), "Verification of Kimura's Theory for Wave Group Statisties" *Proceedings of the 19th International Coastal Engineering Conference*, Houston, TX, 3-7 Scptember.

Belenky, V., J. O. de Kat, and N. Umeda (2008), "Toward Performance-Based Criteria for Intact Stability," *Marine Technology* 45(2), April.

Bitner-Gregersen, E. M. and O. Hagen (2004), "Freak Wave Events Within the Second Order Wave Model," *23rd International Conference on Offshore Mechanics and Artic Engineering*, Vancouver, Canada, June.

Boukhanovsky, A. V. and A. B. Degtyarev (1996), "Nonlinear Stochastic Ship Motion Stability in Different Wave Regime," *Proceedings of 3rd International Conference in Commemoration of the 300th Anniversary of Creating Russian Fleet by Peter the Great (CRF'96)*, St. Petersburg, Russia,.

Buckley, W. H. (2005), "Extreme Waves for Ship and Offshore Platform Design," *SNAME Technical and Research Report No. 57*,

Carneal, J. B., P. Atsavapranee, C. W. Baumann, J. H. Hamilton, and J. Shan (2005a), "A Global Laser Rangefinder Profilometry System for the Measurement of Three Dimensional Wave Surfaces," *ASME Fluids Engineering Division Summer Meeting and Exhibition (FEDSM05)*, Houston, TX, 19-23 June.

Carncal, J. B., P. Atsavapranee, and J. T. Curight (2005b), "Global Laser Rangefinder Profilometry: Initial Test and Uncertainity Analysis," NSWCCD-50-TR-2005/069, August.

Carneal, J. B. and P. Atsavapranee (2006), "Global Laser Rangefinder Profilometry: Initial Test and Uneertainty Analysis," *2006 ASME Joint European Fluids Summer Meeting*, Miami, FL, 17-23 July.

Carrico, T. (2007), "DDG 1000 Large Seale Experimentation," *28th American Towing Tank Conference (ATTC)*, Ann Arbor, MI, 9-10 August.

Carroll, R. J., C. H. Spiegelman,, and J. Sacks (1988), "A Quiek and Easy Multiple-Use Calibration-Curve Procedure," *Technometrics*, 30(2), pp. 137-141.

Clauss, G. F. and J. Bergmann (1986), "Gaussian Wave Packets- A New Approach to Seakeeping Tests of Ocean Structures," *Applied Ocean Research*, 8(4).

Clauss, G. F. and W. L. Kuehnlein (1994), "Seakeeping Tests of Marine Structures with Deterministic Wave Groups and Tank Side Wall Wave Absorbers," *7th International Conference on the Behavior of Offshore Strucutures*, Boston, MA, 12-15 July.

Clauss, G. F. and W. L. Kuehnlein (1995), "A New Approach to Seakeeping Tests of Self-Propelled Models in Oblique Waves with Transient Wave Packets," *14th International Conference on Offshore Mechanics and Artic Engineering*, Copenhagen, Denmark, June.

Clauss, G. F. (1999), "Task-Related Wave Groups for Seakeeping Tests or Simulation of Design Storm Waves," *Applied Ocean Research*, 21(5), October.

Clauss, G. F. (2000) "Tailor-Made Transient Wave Groups for Capsizing Tests," *7th International Conference on Stability and Seakeeping of Ships and Ocean Vehicles (STAB 2000)*, Launceston, Australia, 7-12 February.

Clauss, G. F. and J. Hennig (2002), "Computer Controlled Capsizing Tests Using Tailored Wave Sequences," *21st International Conference on Offshore Mechanics and Artic Engineering*, Oslo, Norway, 23-28 June.

Clauss, G. F. (2002a), "Task-Related Rogue Waves Embedded in Extreme Seas," *21st International Conference on Offshore Mechanics and Artic Engineering*, Oslo, Norway, 23-28 June.

Clauss, G. F. (2002b), "Dramas of the Sea: Episodic Waves and Their Impact on Offshore Structures," *Applied Ocean Research*, 24(3), June.

Clauss, G. F. and J. Hennig (2004), "Deterministic Analysis of Extreme Roll Motions and Subsequent Evaluation of Capsizing Risk," *International Shipbuilding Progress*, 51(2/3),.

Clauss, G. F. and C.E. Schmittner (2005), "Experimental Optimization of Extreme Wave Sequences for the Deterministic Analysis of Wave/Structure Interaction," *24th International Conference on Offshore Mechanics and Artic Engineering*, Halkidiki, Greece, 12-17 June.

Clauss, G. F., C.E. Schmittner, and R. Stuck (2005), "Numerical Wave Tank-Simulation of Extreme Waves for the Investigation of Structural Response," *24th International Conference on Offshore Mechanics and Artic Engineering*, Halkidiki, Greece, 12-17 June.

Clauss, G. F., C.E. Schmittner, and J. Hennig (2008), "Systematically Varied Rogue Wave Sequences for the Experimental Investigation of Extreme Structure Behavior, " *Journal of Offshore Mechanics and Artic Engineering*, 130, May.

Davis, M. C. and E. E. Zarnick (1964), "Testing Ship Models in Transient Waves," *5th Symposium on Naval Hydrodynamics*.

Draper, L. (1971), "Severe Wave Conditions at Sea," *Journal of the Institute of Navigation*, 24(3), July.

Fedele, F. (2006a), "Extreme Events in Nonlinear Random Seas," *Journal of Offshore Mechanics and Artic Engineering*, 128, February.

Fedele, F. (2006b), "On Wave Groups in a Gaussian Sea," *Ocean Engineering*, 33(17-18).

Gersten, A. and R. J. Johnson (1969), "Notes on Ship Model Testing in Transient Waves," NSRDC Report 2960, April.

Gibson, R. S. and C. Swan (2007), "The Evolution of Large Ocean Waves: The Role of Local and Rapid Spectral Changes," *Proceedings of the Royal Society of London,Series A*, 463.

Gruc, J. (2002), "On Four Highly Nonlinear Phenomena in Wave Theory and Marine Hydrodynamics," *Applied Ocean Research*, 24(5), October.

Gruc, J., D. Clamond, M. Huseby, and A. Jensen (2003), "Kinematics of Extreme Waves in Deep Water," *Applied Ocean Research*, 25.

Guedes Soares, C., and R. Pascoal (2005), "On the Profile of Large Ocean Waves," *Journal of Offshore Mechanics and Artic Engineering*, 127, November.

Guedes Soares, C., N. Fonseca, and R. Pascoal (2008), "Abnormal Wave-Indueed Load Effects in Ship Structures," *Journal of Ship Research*, 52(1), March.

Hayden, D. D., R.C. Bishop, J. T. Park, and S. M. Laverty (2006), "Model 5514 Capsize Experiments Representing the Pre-Contraet DDG51 Hull Form at End of Service Life Conditions," NSWCCD-50-TR-2006/020, April.

Hennig, J., H. Billerbeck, G. F. Clauss, D. Testa, K. E. Brink, and W. L. Kuhnlein (2006), "Quantitative and Qualitative Validation of a Numerieal Code for the Realistic Simulation of Various Ship Motion Scenarios," *25th International Conference on Offshore Mechanics and Artic Engineering*, Hamburg, Germany, 4-9 June.

Holliday, N. P., M. J. Yelland, R. W. Paseal, V. R. Swail, P. K. Taylor, C. R. Griffiths, and E. C. Kent (2006), "Were extreme waves in the Roekall Trough the largest ever reeorded?," *Geophysical Research Letters*, Vol. 33.

Smith, T.C., L. K. Hanyok, and M.J. Hughes (2007), "MASK Waves Benehmark," NSWCCD-50-TR-2007/052, October.

ISO (1995), "Guide to the Expression of Uncertainty in Measurement," International Organization for Standardization (ISO), Gencva, Switzerland.

Johannessen, T. B. and C. Swan (2001), "A Laboratory Study of the Foeusing of Transient and Directionally Spread Surface Water Waves," *Proceedings of the Royal Society of London, Series A*, 457.

Johannessen, T. B. and C. Swan (2003), "On the Nonlinear Dynamics of Wave Groups Produced by the Foeusing of Surfaee-Water Waves," *Proceedings of the Royal Society of London,Series A*, 459.

Jonathan, P. and K. Ewans (2007), "Uncertainties in Extreme Wave Height Estimates for Hurricane Dominated Regions," *Journal of Offshore Mechanics and Artic Engineering*, 129, November.

Kimura, A. (1980), "Statistical Properties of Random Wave Groups," *Proceedings of the 17th Coastal Engineering Conference*, Sydney, Australia, 23-28 Mareh.

Liu, P. C. and K. R. MacHutchon (2008), "Are There Different Kinds of Rogue Waves?," *Journal of Offshore Mechanics and Artic Engineering*, 130, May.

Longuet-Higgins, M. S. (1957), "The Statistieal Analysis of a Random, Moving Surface," *Philosophical Transactions A*, 249.

Longuet-Higgins, M. S. (1984), "Statistical Properties of Wave Groups in a Random Sea State," *Philosophical Transactions A*, 312.

Lopatoukhin, L. J. and A.V. Boukhanovsky (2004), "Freak Wave Generation and Their Probability," *International Shipbuilding Progress*, 51(2/3).

Masson, D. and P. Chandler (1993), "Wave Groups: A Closer Look at Spectral Methods," *Coastal Engineering*, 20.

Masterton, S. R. and C. Swan (2008), "On the Accurate and Efficient Calibration of a 3D Wave Basin," *Ocean Engineering*, 35(8-9), June.

Matos, V., J. S. Sales Jr., and S. H. Sphaier (2005), "Seakeeping Tests with Gaussian Wave Packets," *24th International Conference on Offshore Mechanics and Artic Engineering*, Halkidiki, Greece, 12-17 June.

National Transportation Safety Board (2005), NTSB Marine Accident Brief: Heavy-Weather Damage to Bahamas-Flag Passenger Vessel Norwegian Dawn, NTSB/MAB-05/03, 16 April.

Ning, D. Z., B. Teng, R. E. Eatock Taylor, and J. Zang (2008), "Numerical Simulation of Non-Linear Regular and Focused Waves in an Infinite Water-Depth," *Ocean Engineering*, 35(8-9), June.

Ochi, M. K. (1998), *Ocean Waves: The Stochastic Approach*, Cambridge, U.K.: The Cambridge University Press.

O'Dea, J.F. and J. N. Newman (2007), "Numerical Studies of Directional Wavemaker Performance," *28th American Towing Tank Conference*, Ann Arbor, MI, 9-10 August.

Osborne, A. R. (2001), "The Random and Deterministic Dynamics of 'Rouge Waves' in Unidirectional, Deep-Water Wave Trains," *Marine Structures*, 14 (3), May-June.

Osbourne, A. R. (2006), "Computation and Modeling of Oceanic Freak Waves," Proceedings of the 26th Symposium on Naval Hydrodynamics, Rome, Italy, 17-22 September.

Petrova, P., Z. Cherneva, and C. Guedes Soares (2007), "On the Adequacy of Second-Order Models to Predict Abnormal Waves," *Ocean Engineering*, 34(7).

Porubov, A. V., H. Tsuji, I. V. Lavrenov, and M. Oikawa (2005), "Formation of the Rogue Wave Due to Non-Linear Two-Dimensional Waves Interaction," *Wave Motion*, 42(3), September.

Rosenthal, W. and S Lehner (2004), "Results of the MAXWAVE Project," *23rd International Conference on Offshore Mechanics and Artic Engineering*, Vancouver, Canada, June.

Rosenthal, W. and S Lehner (2008), "Rogue Waves: Results of the MaxWave Project," *Journal of Offshore Mechanics and Artic Engineering*, 130, May.

Ross, S. M. (2004), *Introduction to Probability and Statistics for Engineers and Scientists*, Third Edition, Amsterdam: Elsevier, Academic Press.

Scheffe, H., 1973, "A Statistical Theory of Calibration," *The Annals of Statistics*, 1(1), pp. 1-37.

Slunyaev, A., E. Pelinovsky, and C. Gudes Soares (2005), "Modeling Freak Waves from the North Sea," *Applied Ocean Research*, 27(1), April.

Smith, C. B. (2006), *Extreme Waves*, Washington, D. C.: Joseph Henry Press.

Stansberg, C. T., O. T. Gudmestad, and S. K. Haver (2008), "Kinematics Under Extreme Waves," *Journal of Offshore Mechanics and Artic Engineering*, 130, May.

Stansell, P., J. Wolfram, and B. Linfoot (2002), "Statisties of Wave Groups Measured in the Northern North Sea: Comparisons Between Time Series and Speetral Predietions," *Applied Ocean Research*, 24(2), April.

Sverdrup, K. A., A. C. Duxbury, and A. B. Duxbury (2003), *An Introduction to the World's Oceans,* Seventh Edition, New York: MeGraw Hill.

Takezawa, S. and M. Takekawa (1976), "Advaneed Experiment Technique for Testing Ship Models in Transient Water Waves, Part l: The Transient Test Teehnique on Ship Motions in Waves," *11th Symposium on Naval Hydrodynamics*, University College, London.

Takezawa, S. and T. Hirayama (1976), "Advaneed Experiment Teehnique for Testing Ship Models in Transient Water Waves, Part ll: The Controlled Transient Water Waves for Using in Ship Motion Tests," *11th Symposium on Naval Hydrodynamics*, University College, London.

Themelis, N. and K. J. Spyrou (2007), "Probabilistie Assessment of Ship Stability," *SNAME Maritime Technology Conference & Expo and Ship Production Symposium*, Fort Lauderdale, FL, November 14-16.

Tikka, K. K. and J. R. Paulling (1990), "Predietions of Critieal Wave Conditions for Extreme Vessel Response in Random Seas," *4th International Conference on the Stability of Ships and Ocean Vehicles (STAB '90)*, Naples, Italy,.

Wang, D. W., D. A. Mitehell, W. J. Teague, E. Jarosz, and M. S. Hulbert (2005), "Extreme Waves Under Hurriean lvan," *Science*, 309(5736), 5 August.

Wheeler, J.D. (1969), "Method of Caleulating Forees Indueed by Irregular Waves," *Proceedings of the First Offshore Technology Conference (OTC)*, Houston, TX, 1:71-82.

This page intentionally left blank

Appendix A: Wave-maker Settings

Table 11. Phase I Wave Run Matrix

Run Number*	Cycle 1	Cycle 2	Cycle 3	Cycle 4	Blower RPM	Lips	Wave sequence file
02	0.5 Hz 5 V 10 cycles	0.4 Hz 5 V 10 cycles			1300	Down	groups01.txt
03	2 Hz 9.5 V 5 cycles	2.25 Hz 9.5 V 1 cycle	2.5 Hz 9.5 V 1 cycles	2.98 Hz 9.5 V 1 cycle	1300	Down	test9.dat
04	2 Hz 9.5 V 5 cycles	2.25 Hz 9.5 V 1 cycle	2.5 Hz 9.5 V 1 cycles	2.98 Hz 9.5 V 1 cycle	1300	Down	groups02.txt
05	2 Hz 9.5 V 5 cycles	2.25 Hz 9.5 V 1 cycles	2.5 Hz 9.5 V 1 cycles	2.98 Hz 9.5 V 1 cycles	1300	Down	groups03.txt
06	2 Hz 9.5 V 5 cycles	2.25 Hz 7 V 1 cycles	2.5 Hz 7 V 1 cycles	2.98 Hz 9.5 V 1 cycles	1300	Down	groups04.txt
07	2 Hz 9.5 V 5 cycles	2.25 Hz 3 V 1 cycles	2.5 Hz 3 V 1 cycles	2.98 Hz 9.5 V 1 cycles	1300	Down	groups05.txt
09	2 Hz 9.5 V 5 cycles	2.25 Hz 1 V 1 cycles	2.5 Hz 1 V 1 cycles	2.98 Hz 9.5 V 1 cycles	1300	Down	groups06.txt
10	2 Hz 9.5 V 5 cycles	2.25 Hz 0.1 V 1 cycles	2.5 Hz 0.1 V 1 cycles	2.98 Hz 9.5 V 1 cycles	1300	Down	groups07.txt
11	2 Hz 9.5 V 5 cycles	2.25 Hz 0.1 V 1 cycles	2.5 Hz 0.1 V 1 cycles	2.98 Hz 9.5 V 2 cycles	1300	Down	groups08.txt
13	2 Hz 9.5 V 5 cycles	2.25 Hz 1 V 1 cycles	2.5 Hz 1 V 1 cycles	2.98 Hz 9.5 V 2 cycles	1300	Down	groups09.txt

14	2 Hz 6 V 4 cycles	2.25 Hz 1 V 1 cycles	2.5 Hz 1 V 1 cycles	2.98 Hz 4 V 3 cycles	1300	Down	groups10.txt
15	2 Hz 9.5 V 5 cycles	2.25 Hz 1 V 1 cycles	2.5 Hz 1 V 1 cycles	2.98 Hz 9.5 V 2 cycles	1300	Down	groups09.txt
16	2 Hz 9.5 V 5 cycles	2.25 Hz 1 V 1 cycles	2.5 Hz 1 V 1 cycles	2.98 Hz 9.5 V 2 cycles	1300	Up	groups09.txt
17	2 Hz 9.5 V 5 cycles	2.25 Hz 1 V 1 cycles	2.5 Hz 1 V 1 cycles	2.98 Hz 9.5 V 2 cycles	1300	Up	groups09.txt
18	2 Hz 9.5 V 5 cycles	2.25 Hz 1 V 1 cycles	2.5 Hz 1 V 1 cycles	2.98 Hz 9.5 V 2 cycles	1000	Up	groups09.txt
19	2 Hz 9.5 V 5 cycles	2.25 Hz 1 V 1 cycles	2.5 Hz 1 V 1 cycles	2.98 Hz 9.5 V 2 cycles	1150	Up	groups09.txt
20	2 Hz 9.5 V 5 cycles	2.25 Hz 1 V 1 cycles	2.5 Hz 1 V 1 cycles	2.98 Hz 9.5 V 2 cycles	1500	Up	groups09.txt
21	2.1 Hz 9.5 V 5 cycles	2.25 Hz 1 V 1 cycles	2.5 Hz 1 V 1 cycles	3.3 Hz 9.0 V 2 cycles	1300	Up	groups11.txt
22	2.1 Hz 9.5 V 5 cycles	2.25 Hz 1 V 1 cycles	2.5 Hz 1 V 1 cycles	3.3 Hz 9.0 V 2 cycles	1100	Up	groups11.txt
23	2.1 Hz 9.5 V 5 cycles	2.25 Hz 1 V 1 cycles	2.5 Hz 1 V 1 cycles	3.3 Hz 9.0 V 2 cycles	1100	Up	groups11.txt
24	2.1 Hz 9.5 V 5 cycles	2.25 Hz 1 V 1 cycles	2.5 Hz 1 V 1 cycles	3.4 Hz 9.0 V 2 cycles	1300	Up	groups12.txt
25	2.1 Hz 9.5 V 5 cycles	2.25 Hz 1 V 1 cycles	2.5 Hz 1 V 1 cycles	3.2 Hz 9.0 V 2 cycles	1300	Up	groups13.txt

26	2.1 Hz 9.5 V 5 cycles	2.25 Hz 1 V 1 cycles	2.6 Hz 2 V 1 cycles	3.2 Hz 9.0 V 2 cycles	1300	Up	groups14.txt
27	2.1 Hz 9.5 V 5 cycles	2.25 Hz 1 V 1 cycles	2.3 Hz 2 V 1 cycles	3.2 Hz 9.0 V 2 cycles	1300	Up	groups15.txt
29	2.1 Hz 9.5 V 5 cycles	2.25 Hz 1 V 1 cycles	2.3 Hz 2 V 1 cycles	3.2 Hz 9.0 V 2 cycles	1300	Up	groups15.txt
30	2.1 Hz 9.5 V 5 cycles	2.25 Hz 1 V 1 cycles	2.3 Hz 2 V 1 cycles	3.2 Hz 9.0 V 2 cycles	1100	Up	groups15.txt
31	2.1 Hz 9.5 V 5 cycles	2.4 Hz 1 V 1 cycles	2.3 Hz 2 V 1 cycles	3.2 Hz 9.0 V 2 cycles	1300	Up	groups16.txt
32	2.1 Hz 9.5 V 5 cycles	2.25 Hz 2 V 1 cycles	2.3 Hz 2 V 1 cycles	3.2 Hz 9.0 V 2 cycles	1300	Up	groups17.txt
33	2.1 Hz 9.5 V 5 cycles	2.25 Hz 2 V 1 cycles	2.17 Hz 2 V 1 cycles	3.2 Hz 9.0 V 2 cycles	1300	Up	groups18.txt
34	2.1 Hz 9.5 V 5 cycles	2.25 Hz 2 V 1 cycles	2.3 Hz 2 V 2 cycles	3.2 Hz 9.0 V 2 cycles	1300	Up	groups19.txt
35	2 Hz 9.5 V 5 cycles	2.25 Hz 1 V 1 cycles	2.7 Hz 1 V 1 cycles	3 Hz 9.5 V 2 cycles	1300	Up	groups20.txt
36	2 Hz 9.5 V 5 cycles	2.25 Hz 1 V 1 cycles	2.7 Hz 1 V 1 cycles	3 Hz 9.5 V 2 cycles	1500	Up	groups20.txt
37	2 Hz 9.5 V 5 cycles	2.25 Hz 1 V 1 cycles	2.7 Hz 1 V 1 cycles	3 Hz 9.5 V 2 cycles	1400	Up	groups20.txt

38	2 Hz 9.5 V 5 cycles	2.25 Hz 1 V 1 cycles	2.7 Hz 1 V 1 cycles	3.1 Hz 9.5 V 2 cycles	1300	Up	groups21.txt
39	2 Hz 9.5 V 5 cycles	2.25 Hz 1 V 1 cycles	2.5 Hz 1 V 1 cycles	3.1 Hz 9.0 V 2 cycles	1300	Up	groups22.txt
40	2 Hz 9.5 V 5 cycles	2.25 Hz 1 V 1 cycles	2.5 Hz 2 V 1 cycles	3.1 Hz 8.0 V 2 cycles	1300	Up	groups23.txt
41	2 Hz 9.5 V 5 cycles	2.25 Hz 1 V 1 cycles	2.5 Hz 2 V 1 cycles	3.1 Hz 8.0 V 2 cycles	1300	Down	groups23.txt
42	2 Hz 9.5 V 5 cycles	2.25 Hz 1 V 1 cycles	2.5 Hz 2 V 1 cycles	3.1 Hz 8.0 V 2 cycles	1300	Down	groups24.txt
43	2 Hz 9.5 V 5 cycles	2.25 Hz 1 V 1 cycles	2.5 Hz 2 V 1 cycles	3.1 Hz 8.0 V 2 cycles	1300	Down	groups25.txt
44	2 Hz 9.5 V 5 cycles	2.25 Hz 1 V 1 cycles	2.5 Hz 2 V 1 cycles	3.1 Hz 8.0 V 2 cycles	1100	Down	groups25.txt
45	2 Hz 9.5 V 5 cycles	2.25 Hz 1 V 1 cycles	2.5 Hz 2.2 V 1 cycles	3.1 Hz 8.0 V 2 cycles	1300	Down	groups26.txt
47	2 Hz 9.5 V 5 cycles	2.25 Hz 1 V 1 cycles	2.5 Hz 2.2 V 1 cycles	3.1 Hz 8.0 V 2 cycles	1300	Down	groups27.txt
48	2 Hz 9.5 V 5 cycles	2.25 Hz 1 V 1 cycles	2.5 Hz 2.2 V 1 cycles	3.1 Hz 8.0 V 2 cycles	1300	Down	groups28.txt
49	2 Hz 9.5 V 5 cycles	2.25 Hz 1 V 1 cycles	2.5 Hz 2.2 V 1 cycles	3.1 Hz 8.0 V 2 cycles	1500	Down	groups26.txt
50	2 Hz 9.5 V 5 cycles	2.25 Hz 1 V 1 cycles	2.5 Hz 2.2 V 1 cycles	3.1 Hz 8.0 V 2 cycles	1400	Down	groups26.txt

51	2 Hz 8.0 V 5 cycles	2.25 Hz 1 V 1 cycles	2.5 Hz 2.2 V 1 cycles	3.1 Hz 8.0 V 2 cycles	1300	Down	groups29.txt
52	2 Hz 8.0 V 4 cycles	2.25 Hz 1 V 1 cycles	2.5 Hz 2.2 V 1 cycles	3.1 Hz 8.0 V 2 cycles	1300	Down	groups30.txt
53	2 Hz 8.0 V 3 cycles	2.25 Hz 1 V 1 cycles	2.5 Hz 2.2 V 1 cycles	3.1 Hz 8.0 V 2 cycles	1300	Down	groups31.txt
54	1.6 Hz 8.0 V 5 cycles	2.25 Hz 1 V 1 cycles	2.5 Hz 2.2 V 1 cycles	3.1 Hz 8.0 V 2 cycles	1300	Down	groups32.txt
55	1.6 Hz 8.0 V 5 cycles	2.25 Hz 1 V 1 cycles	2.5 Hz 2.2 V 1 cycles	3.1 Hz 8.0 V 2 cycles	1300	Down	groups33.txt
56	2 Hz 9.5 V 5 cycles	2.25 Hz 1 V 1 cycles	2.5 Hz 2.2 V 1 cycles	3.1 Hz 8.0 V 2 cycles	1300	Down	groups26.txt
57	2 Hz 9.5 V 5 cycles	2.25 Hz 1 V 1 cycles	2.5 Hz 2.2 V 1 cycles	3.1 Hz 8.0 V 2 cycles	1100	Down	groups26.txt
58	2 Hz 8 V 5 cycles	2.25 Hz 1 V 1 cycles	2.5 Hz 2.2 V 1 cycles	3.1 Hz 6.5 V 2 cycles	1300	Down	groups34.txt
59	2 Hz 8 V 5 cycles	2.25 Hz 0.5 V 1 cycles	2.5 Hz 1.1 V 1 cycles	3.1 Hz 6.5 V 2 cycles	1300	Down	groups35.txt
60	2 Hz 8 V 5 cycles	2.25 Hz 1 V 2 cycles	2.5 Hz 1.1 V 1 cycles	3.1 Hz 6.5 V 2 cycles	1300	Down	groups36.txt
61	2 Hz 8 V 5 cycles	2.25 Hz 1 V 2 cycles	2.5 Hz 1.1 V 1 cycles	3.1 Hz 6.5 V 2 cycles	1500	Down	groups36.txt

* Run numbers omitted were either runs where zeros were taken or bad runs.

Table 12. Phase II Wave Run Matrix

Run Number**	Wave sequence file	Blower RPM	Lips	Spectra Embedded Into	GLRP Measurement
05	groups29.txt	1300	Down	N/A, repeat of run 51 from Aug 07	No
06	groups36.txt	1500	Down	N/A, repeat of run 61 from Aug 07	No
07	groups09.txt	1300	Down	N/A, repeat of run 15 from Aug 07	Yes
08	groups25.txt	1300	Down	N/A, repeat of run 43 from Aug 07	Yes
09	BR15130S.gen	1440	Down	Bretsehneider SS8, λ=30, Hs= 15.0 in., Tm= 3.0s	Yes
10	groups37.txt	1300	Down	groups09.txt at end of Bretsehneider SS8, λ=30	Yes
11	groups38.txt	1300	Down	groups09.txt in middle of Bretsehneider SS8, λ=30	Yes
14	groups39.txt	1300	Down	groups25.txt in middle of Bretsehneider SS8, λ=30	Yes
15	ray01.txt	1300	Down	N/A, Rayleigh distribution superposition, σ= 0.2, 3 V max	Yes
16	ray02.txt	1300	Down	N/A, Rayleigh distribution superposition, σ= 0.2, 6 V max	Yes
17	ray03.txt	1300	Down	N/A, Rayleigh distribution superposition, σ= 0.2, 9 V max	Yes
18	ray04.txt	1300	Down	N/A, Rayleigh distribution superposition, σ= 0.25, 3 V max	Yes
19	ray05.txt	1300	Down	N/A, Rayleigh distribution superposition, σ= 0.25, 6 V max	Yes
20	ray06.txt	1300	Down	N/A, Rayleigh distribution superposition, σ= 0.25, 9 V max	Yes
21	groups40.txt	1300	Down	groups36.txt in middle of Bretsehneider SS8, λ=30	Yes
22	groups41.txt	1300	Down	groups29.txt in middle of Bretsehneider SS8, λ=30	Yes
25***	Camlsr30.gen	1600	Down	Hurricane Camille spectra, λ=30, Hs= 16.0 in., Tm= 2.45s	Yes
26	Groups42.txt	1600	Down	groups36.txt in middle of Hurricane Camille spectra, λ=30	Yes

27	groups42.txt	1300	Down	groups36.txt in middle of Hurricane Camille spectra, λ=30	Yes
28	groups43.txt	1300	Down	groups09.txt in middle of Hurricane Camille spectra, λ=30	Yes
31***	ray15.txt	1300	Down	N/A, Rayleigh distribution superposition, σ= 0.5, 9 V max	Yes
32	ray13.txt	1300	Down	N/A, Rayleigh distribution superposition, σ= 0.5, 3 V max	Yes
33	ray10.txt	1300	Down	N/A, Rayleigh distribution superposition, σ= 0.4, 3 V max	Yes
34	ray07.txt	1300	Down	N/A, Rayleigh distribution superposition, σ= 0.3, 3 V max	Yes
35	ray11.txt	1300	Down	N/A, Rayleigh distribution superposition, σ= 0.4, 6 V max	Yes
36	sine01.txt	1300	Down	N/A, Sine wave, freq=0.3 Hz, 3 V max	Yes
37	sine04.txt	1300	Down	N/A, Sine wave, freq=0.5 Hz, 3 V max	Yes
38	sine07.txt	1300	Down	N/A, Sine wave, freq=0.7 Hz, 3 V max	Yes
39	sine03.txt	1300	Down	N/A, Sine wave, freq=0.3 Hz, 9 V max	Yes
40	cpszcaml.gen	1600	Down	Hurricane Camille spectra, λ=46.6, Hs= 10.30 in., Tm= 1.96s	Yes
41	groups44.txt	1300	Down	groups36.txt in middle of Hurricane Camille spectra, λ=46.6	Yes
42	groups20.txt	1300	Up	N/A, repeat of run 35 from Aug 07	Yes
43	groups45.txt	1300	Up	groups20.txt in middle of Hurricane Camille spectra, λ=46.6	Yes

**Run numbers omitted were either runs where zeros were taken, where additional repeat runs were performed, or were bad runs.

***Runs 24 and 30 were repeat runs of 14 and 28, where additional GLRP measurements were taken.

This page intentionally left blank

Appendix B: Senix Results— Regular Waves

Senix probe results from the wave-packet method and the finite-wave linear superposition method are shown in this Appendix. Wave group characteristics are also shown.

Wave-Packet Method

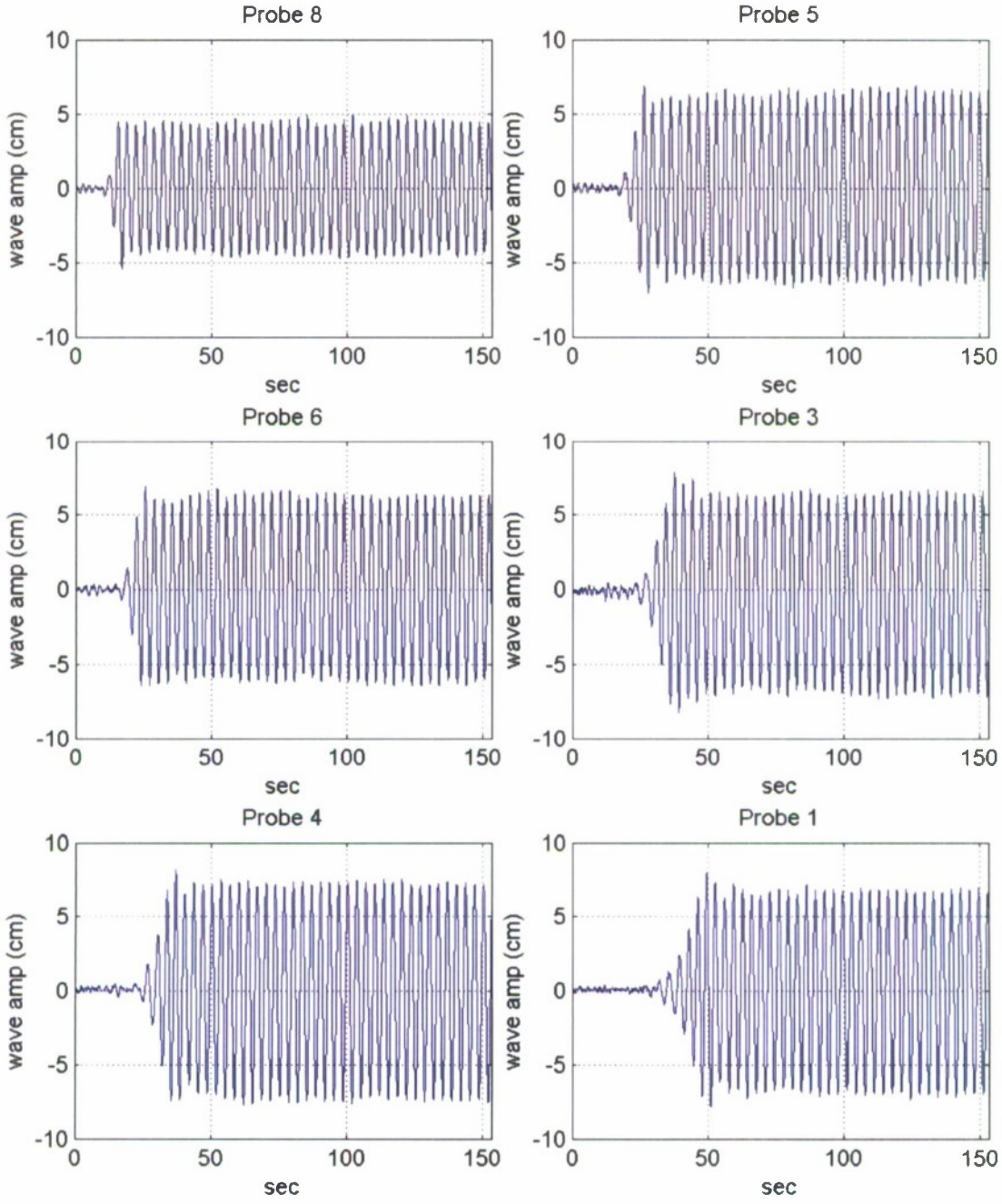

Figure 25. Phase II, Run 36 Time series data from sonic probes 8, 6, 5, 4, 3, and 1 with the sinusoidal wave-maker signal at 0.3 Hz

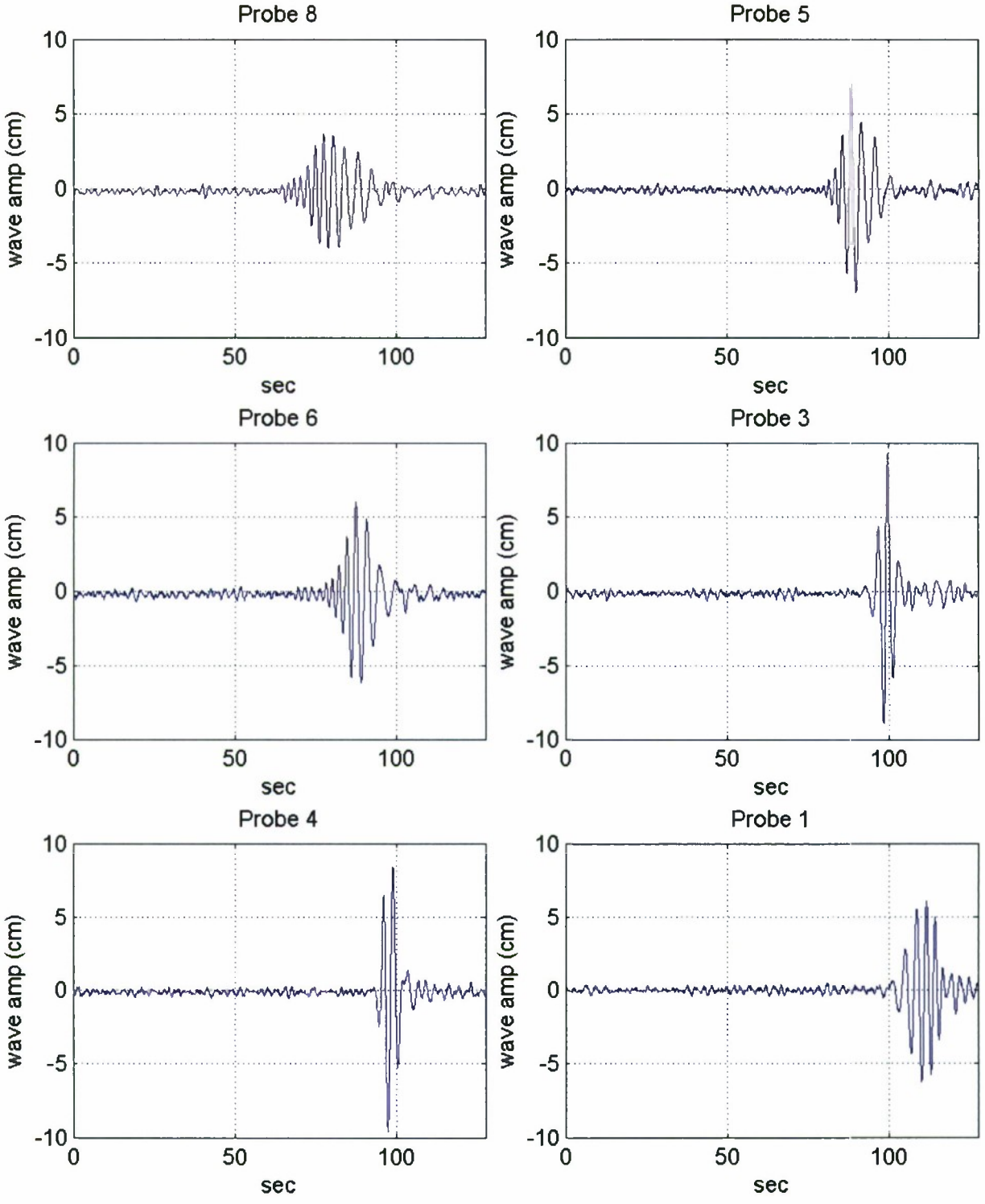

Figure 26. Phase II Run 15 Time series data from sonic probes 8, 6, 5, 4, 3, and 1 for wave-packet generation

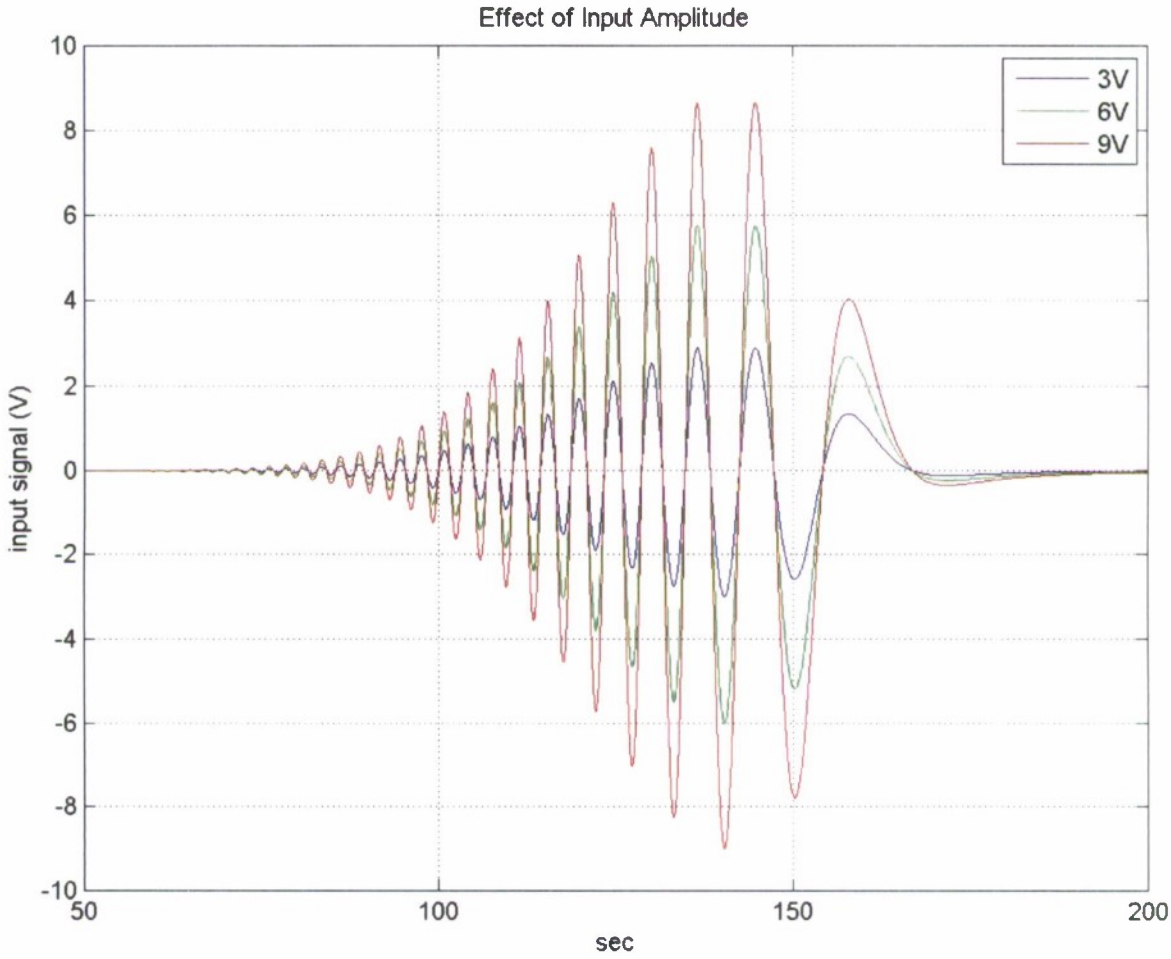

Figure 27. Input signals for the wave-maker. Maximum amplitudes are 3, 6 and 9 Volts for the blue, green and red lines, respectively.

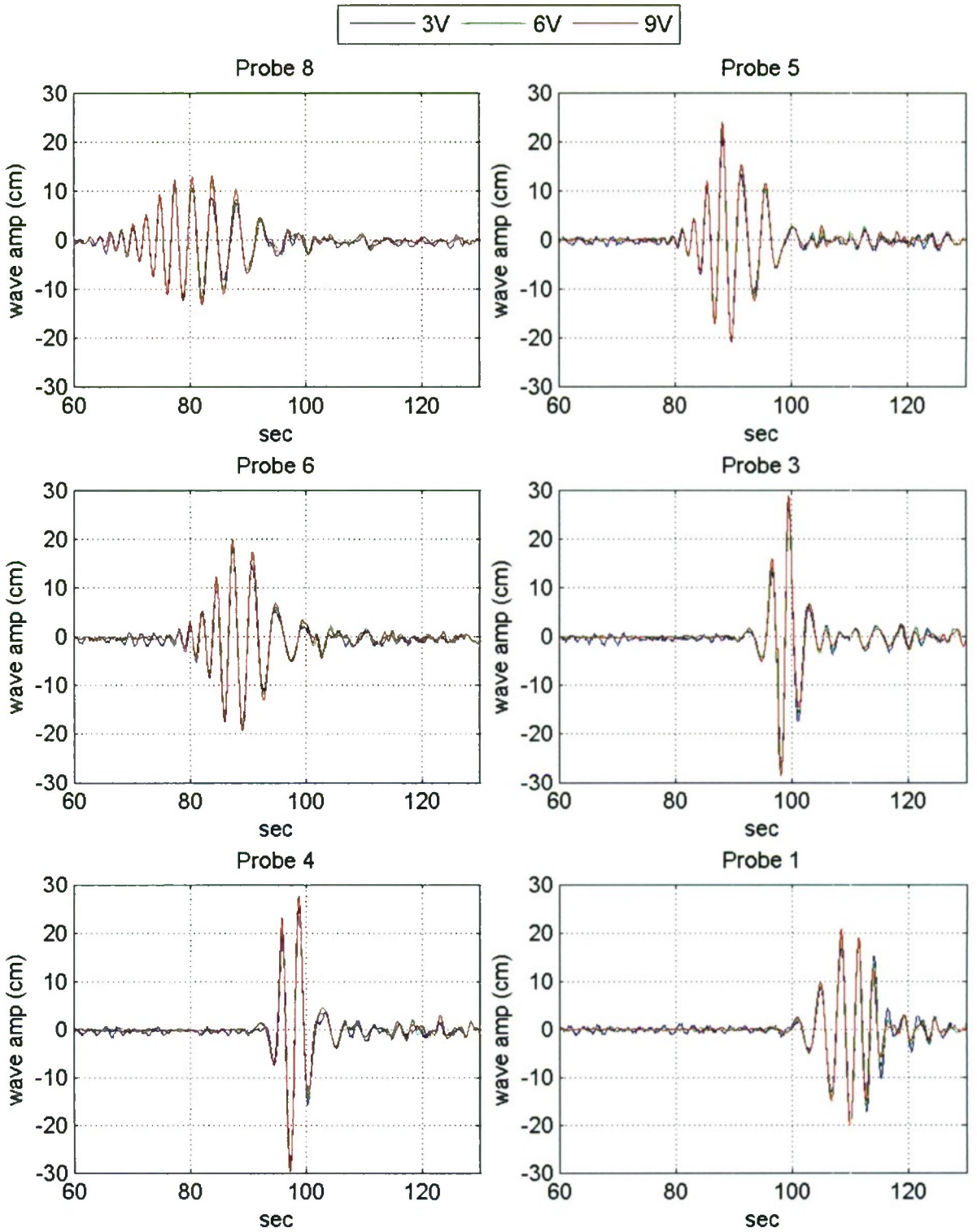

Figure 28. Phase II, Run 15 Time series data from sonic probes 8, 6, 5, 4, 3, and 1. The probe signals were multiplied by 3, 1.5 and 1 for the blue, green and red lines, respectively. Maximum amplitudes of wave-maker input signals are 3, 6 and 9 Volts for the blue, green and red lines, respectively

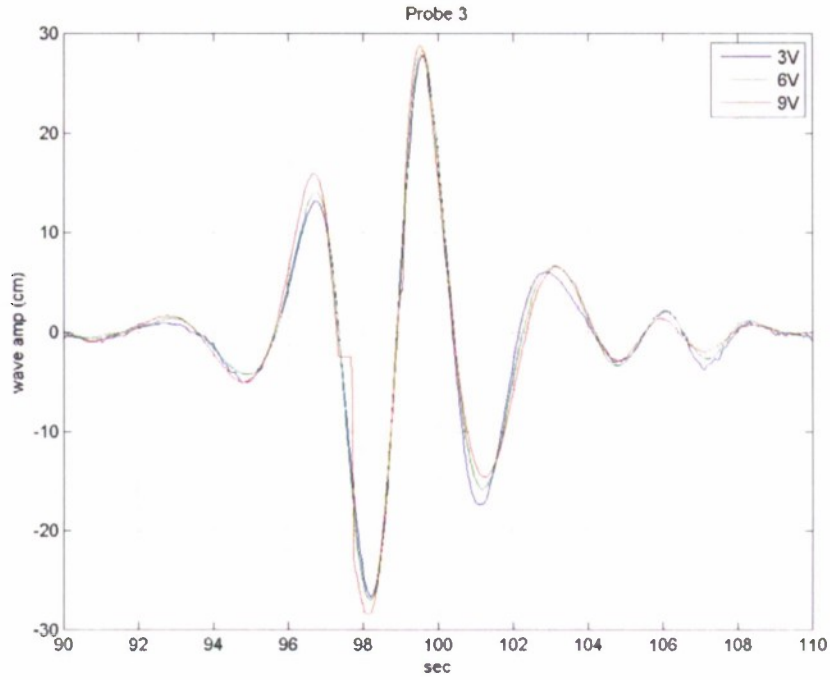

Figure 29. Phase II, Run 15 wave amplitude time series for probe 3

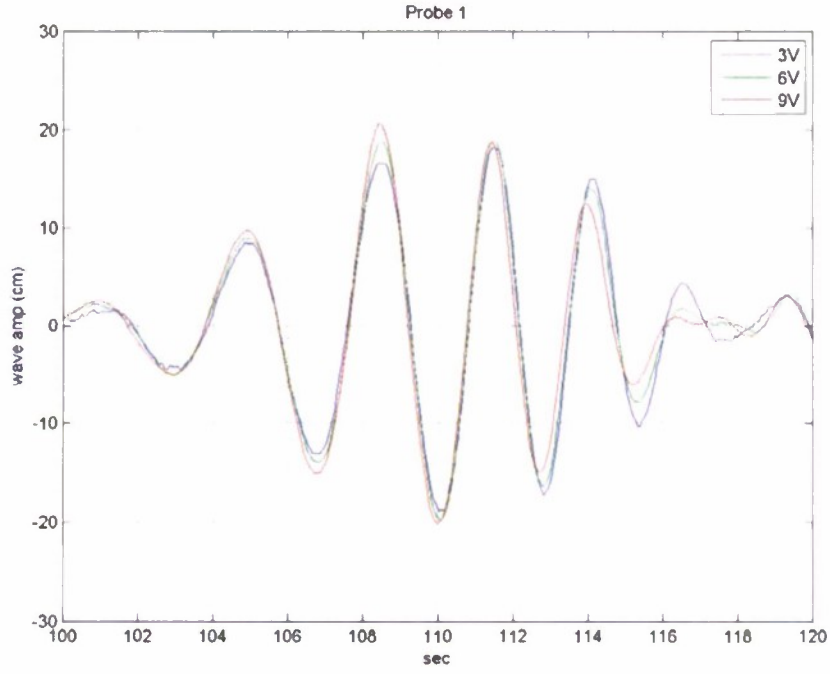

Figure 30. Phase II, Run 15 wave amplitude time series for probe 1

Finite-Wave Linear Superposition Method

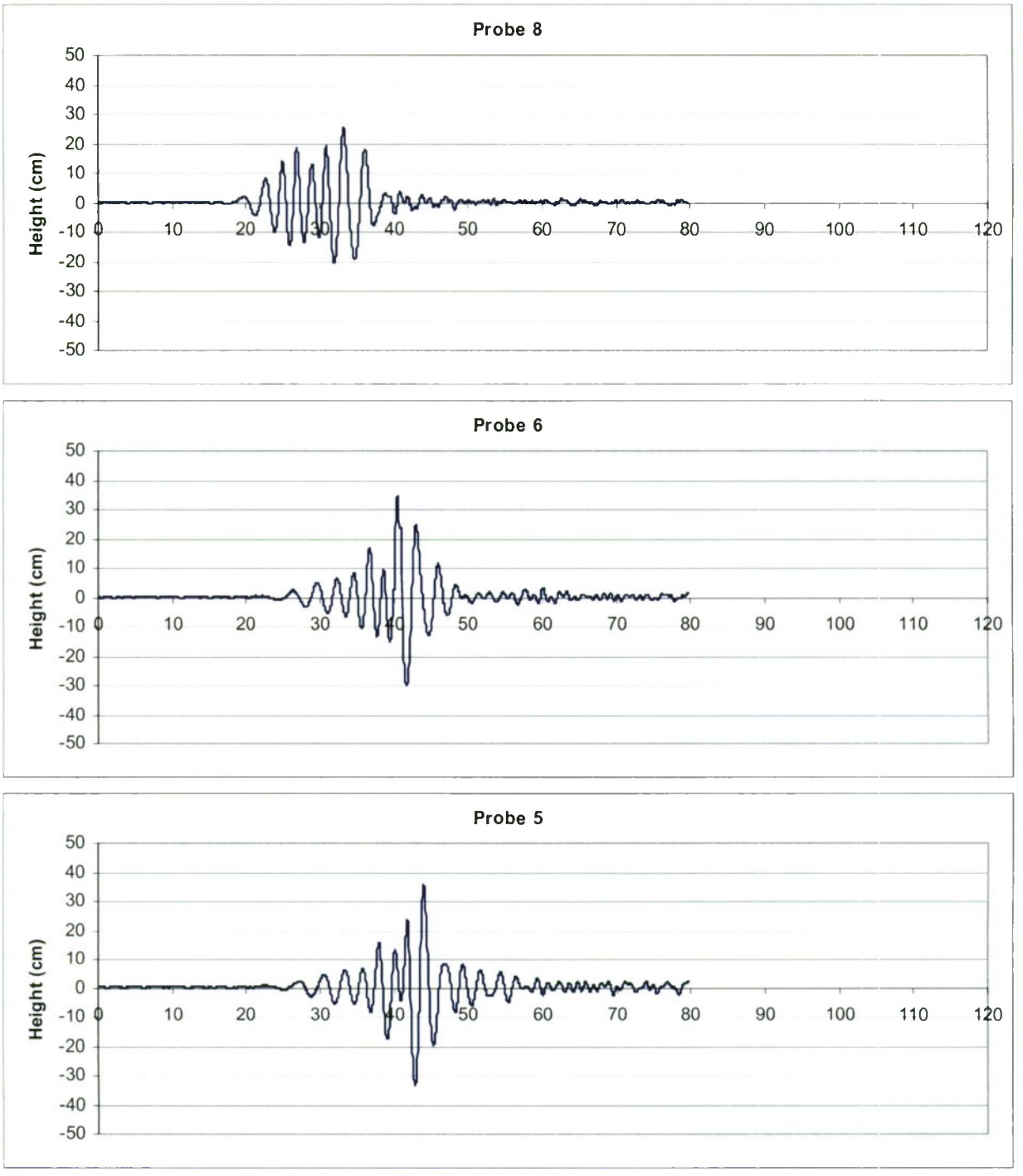

Figure 31. Measured wave time-history of sonic probes 8 (closest to wave-maker) to 1 (closest to the beach), Phase I, Run 15

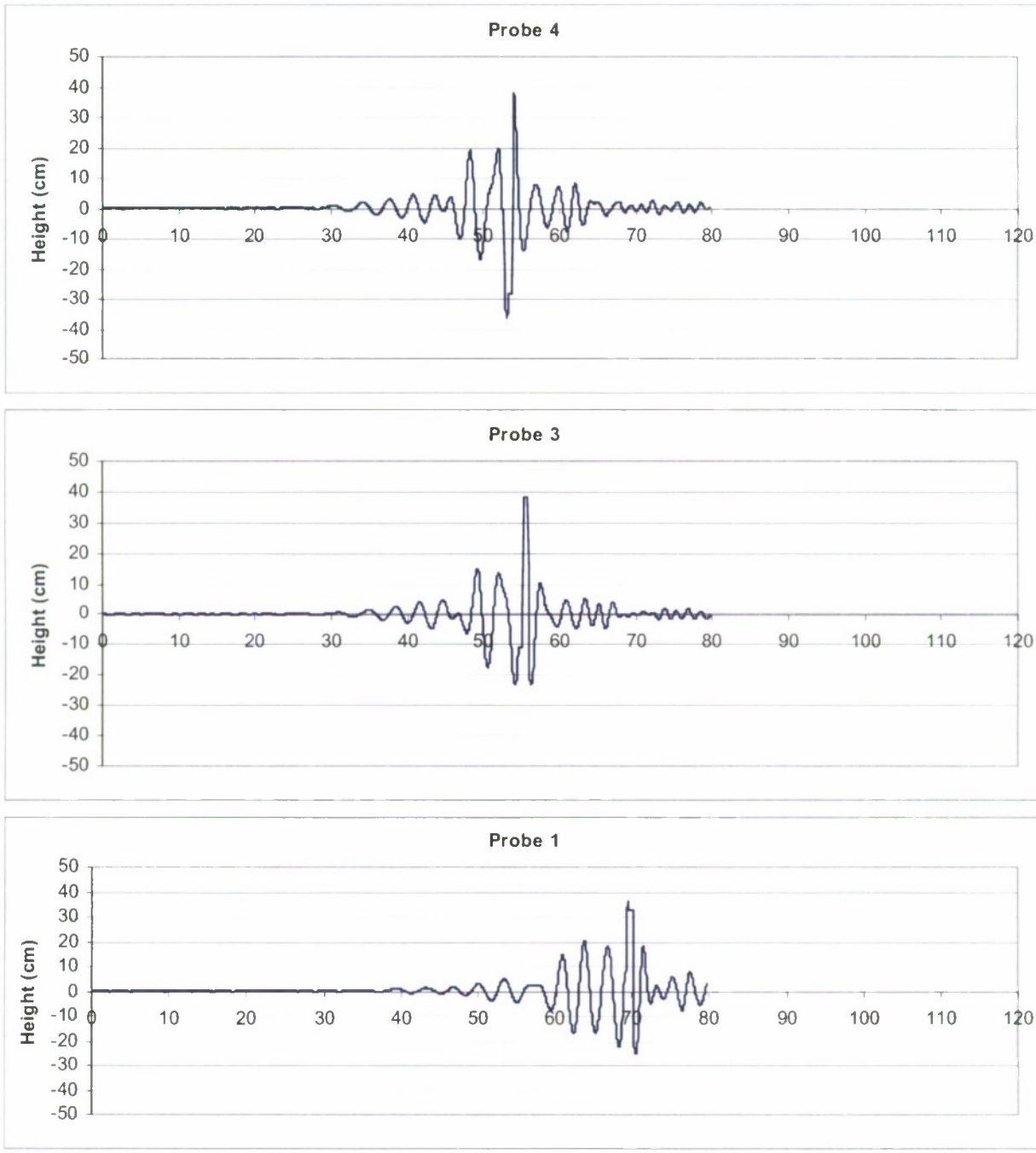

Figure 31 (continued)

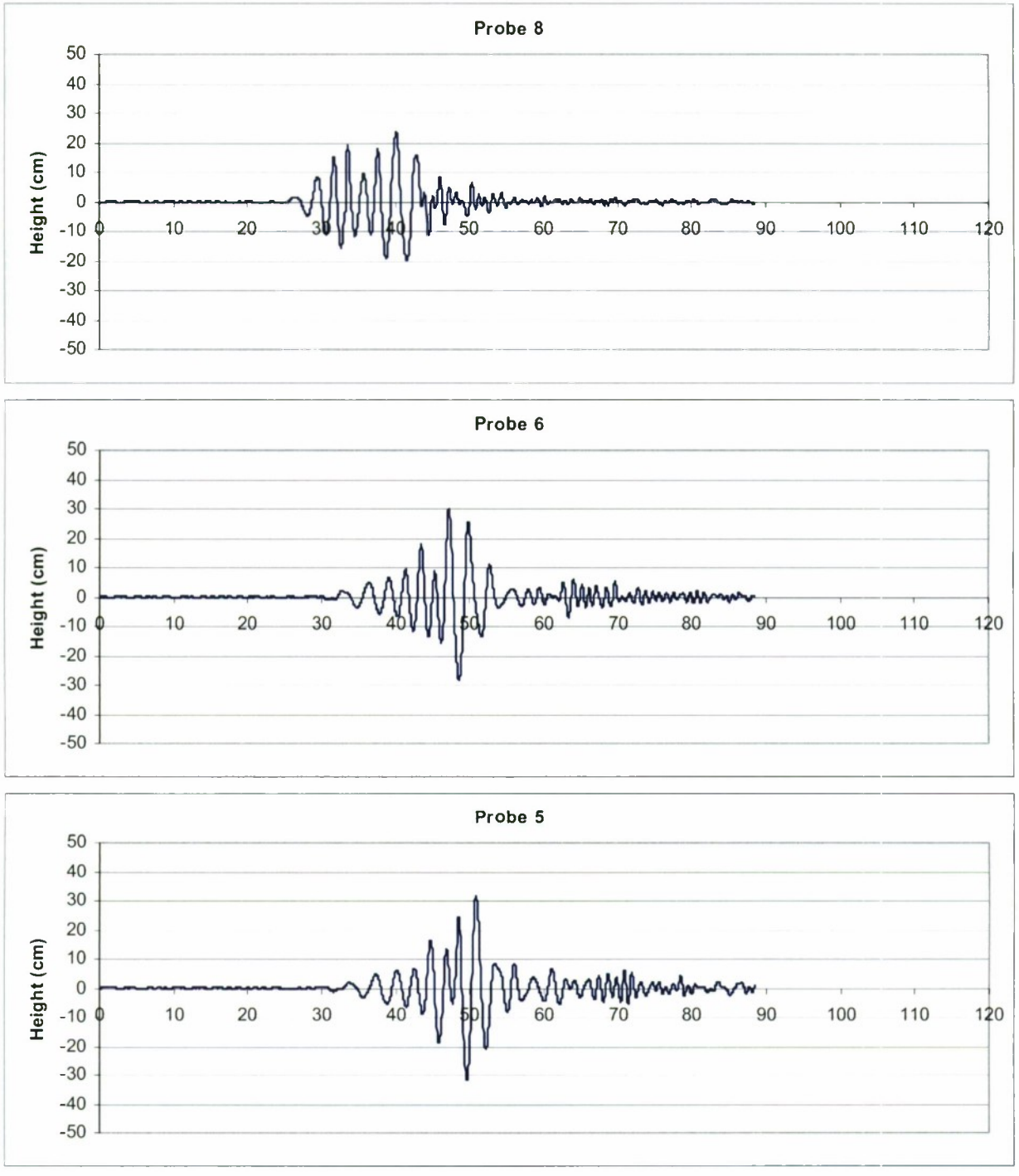

Figure 32. Measured wave time-history of sonic probes 8 (closest to wave-maker) to 1 (closest to the beach), Phase I, Run 35

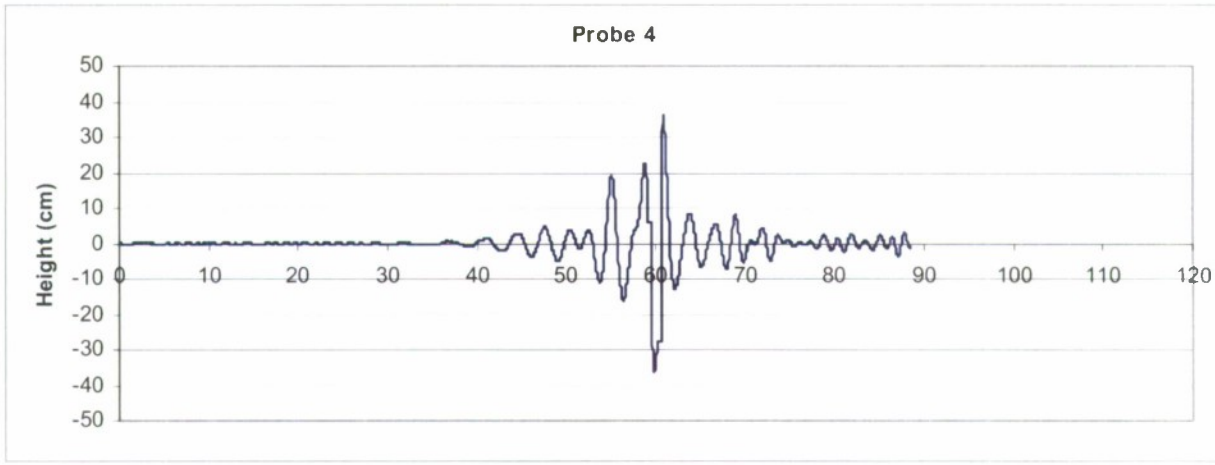

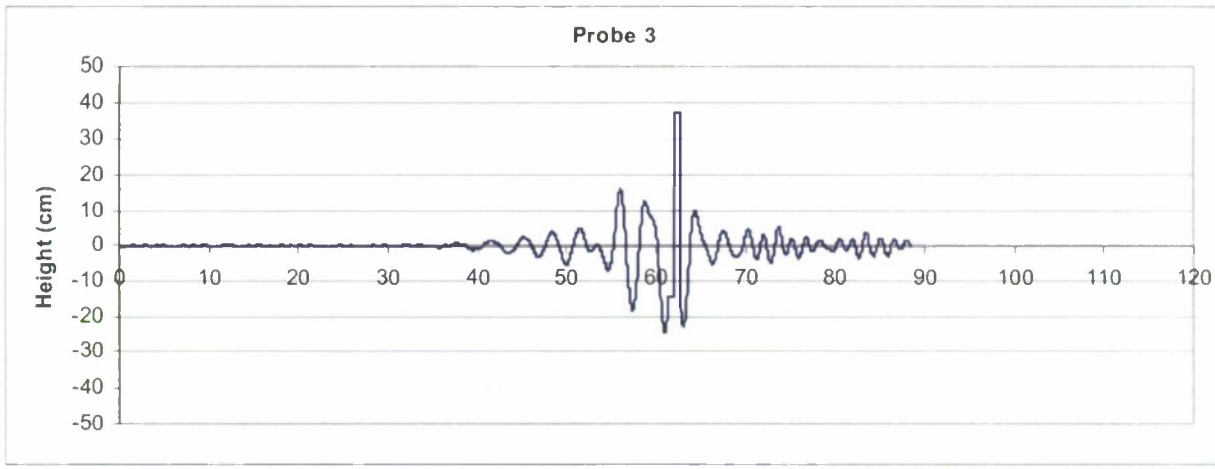

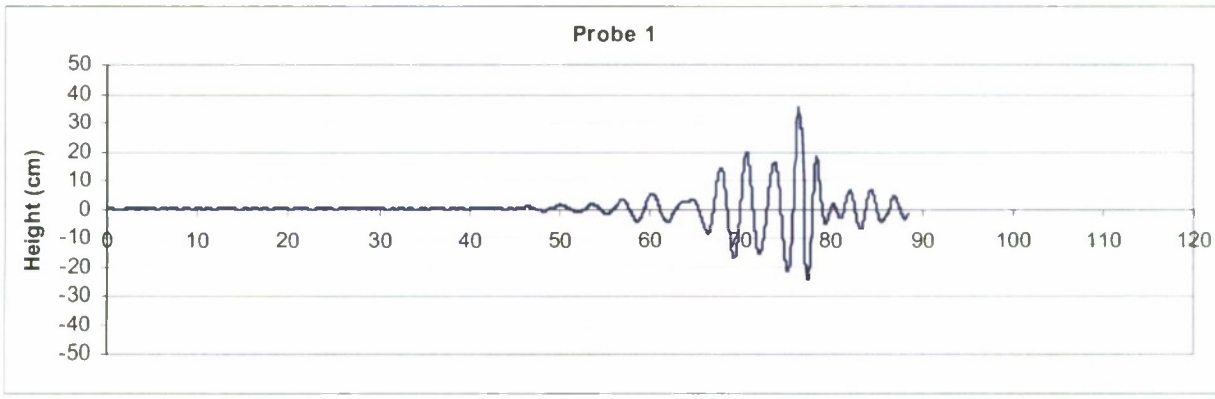

Figure 32 (continued)

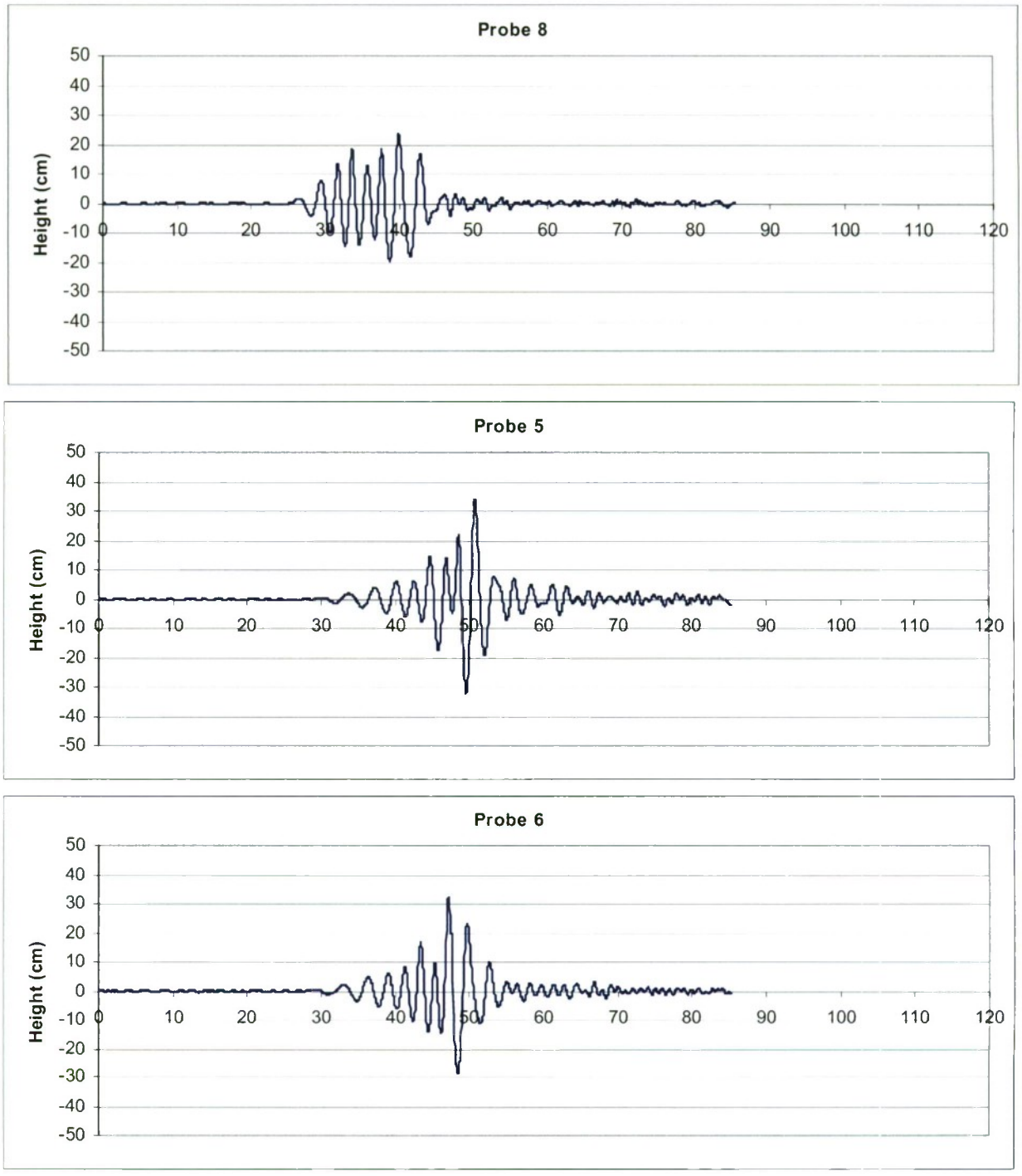

Figure 33. Measured wave time-history of sonic probes 8 (closest to wave-maker) to 1 (closest to the beach), Phase I, Run 43

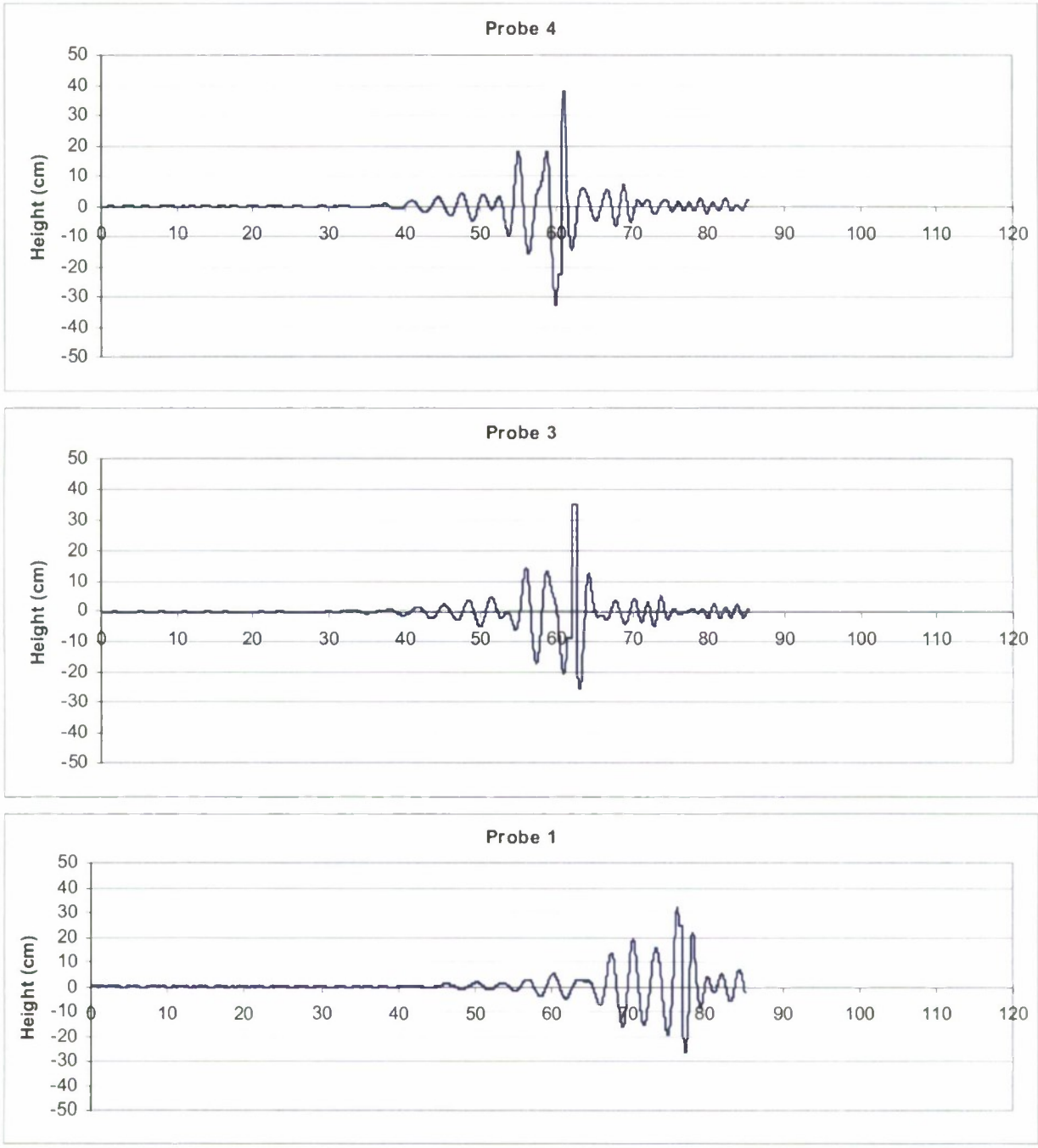

Figure 33 (continued)

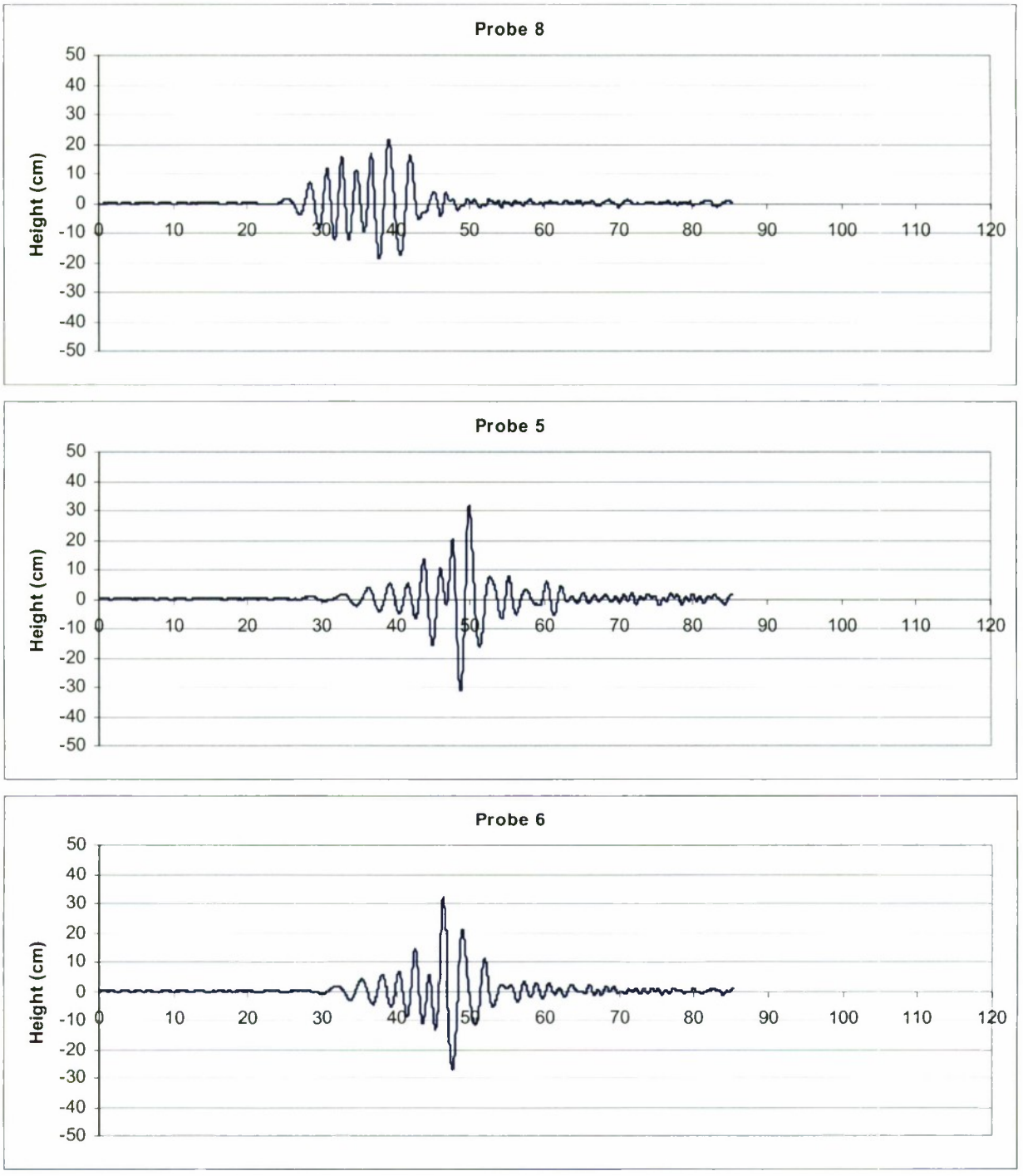

Figure 34. Measured wave time-history of sonic probes 8 (closest to wave-maker) to 1 (closest to the beach), Phase I, Run 51

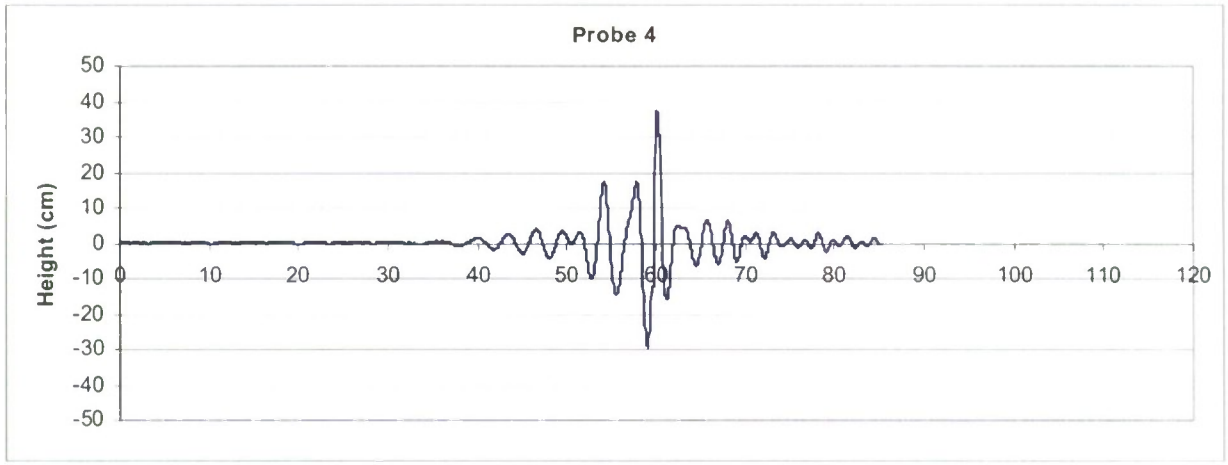

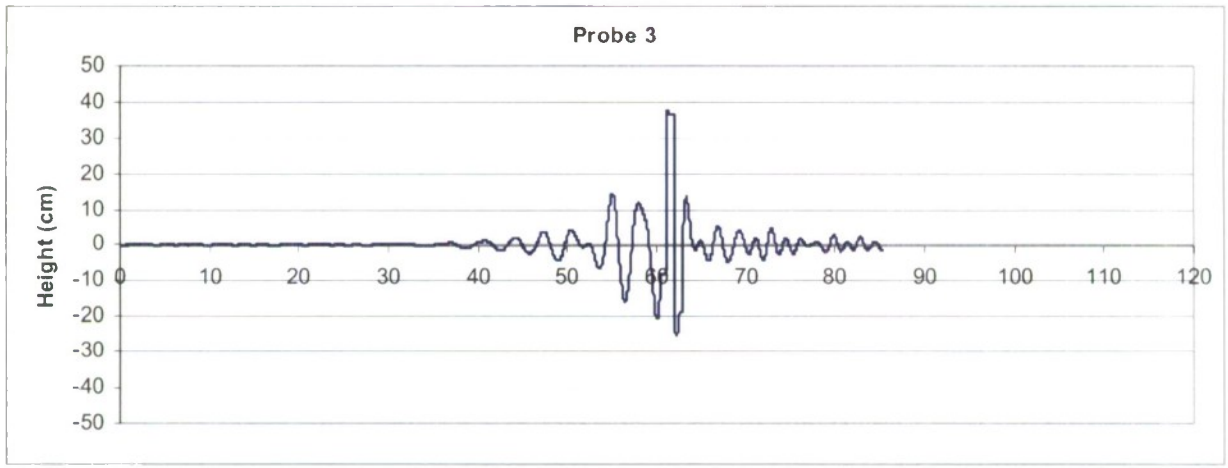

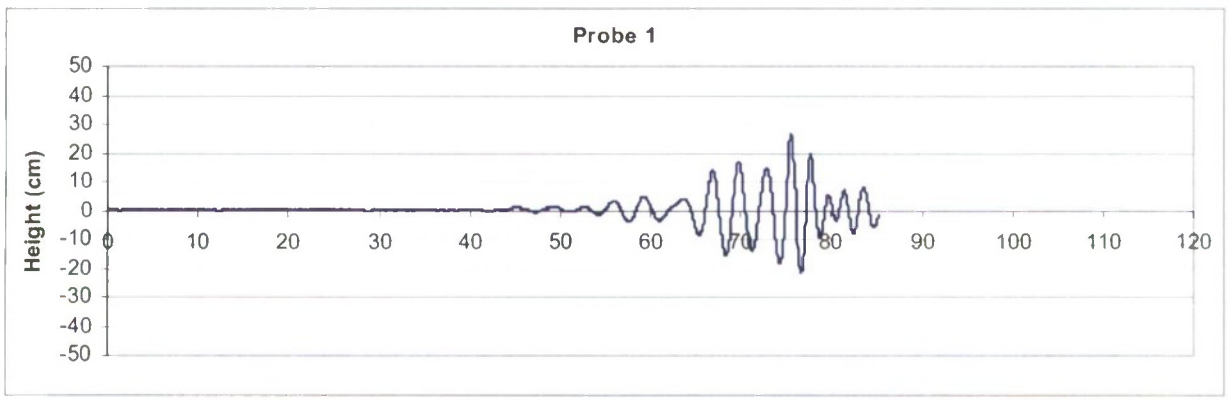

Figure 34 (continued)

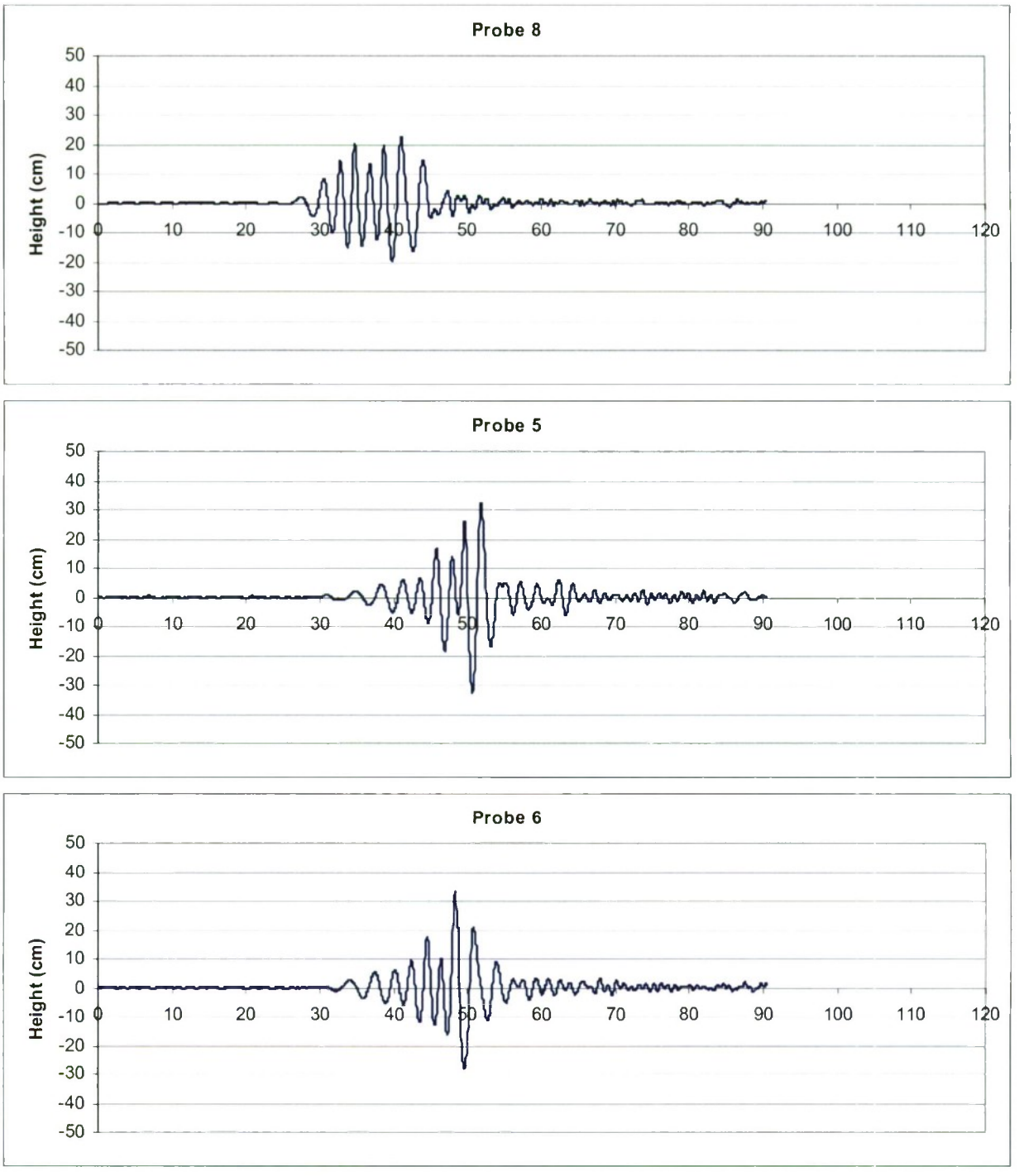

Figure 35. Measured wave time-history of sonic probes 8 (closest to wave-maker) to 1 (closest to the beach), Phase I, Run 61

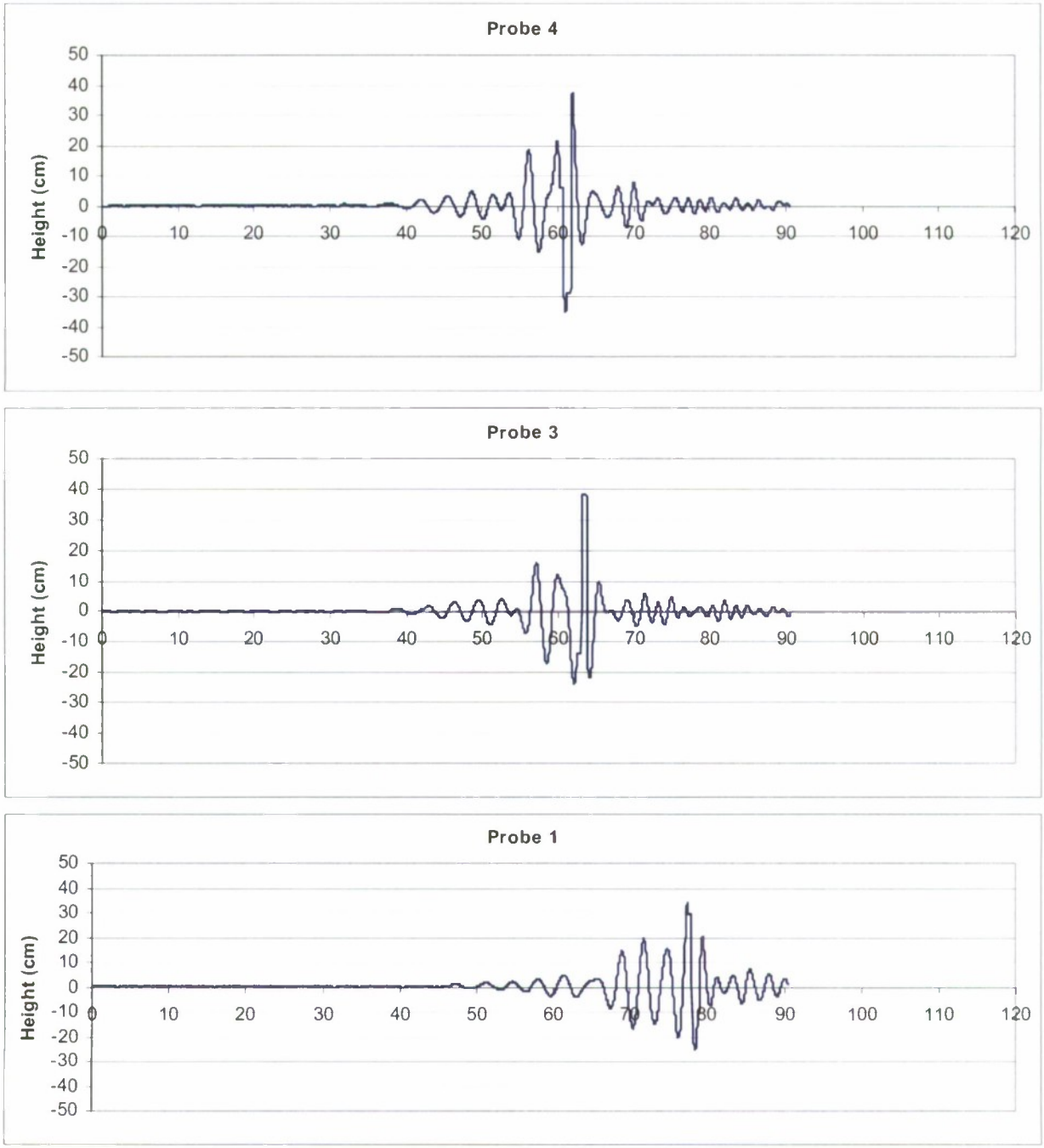

Figure 35 (continued)

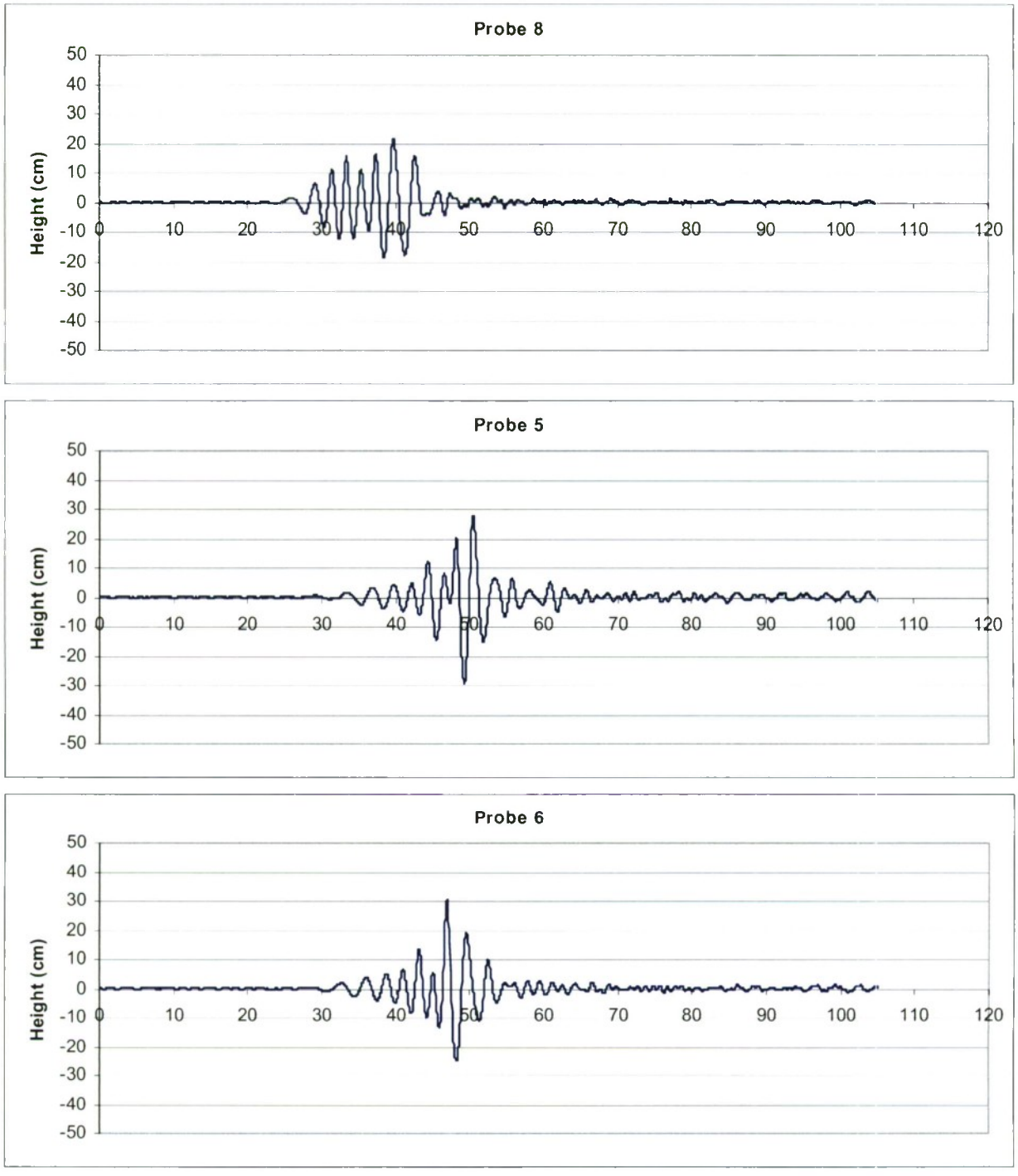

Figure 36. Measured wave time-history of sonic probes 8 (closest to wave-maker) to 1 (closest to the beach), Phase II, Run 5

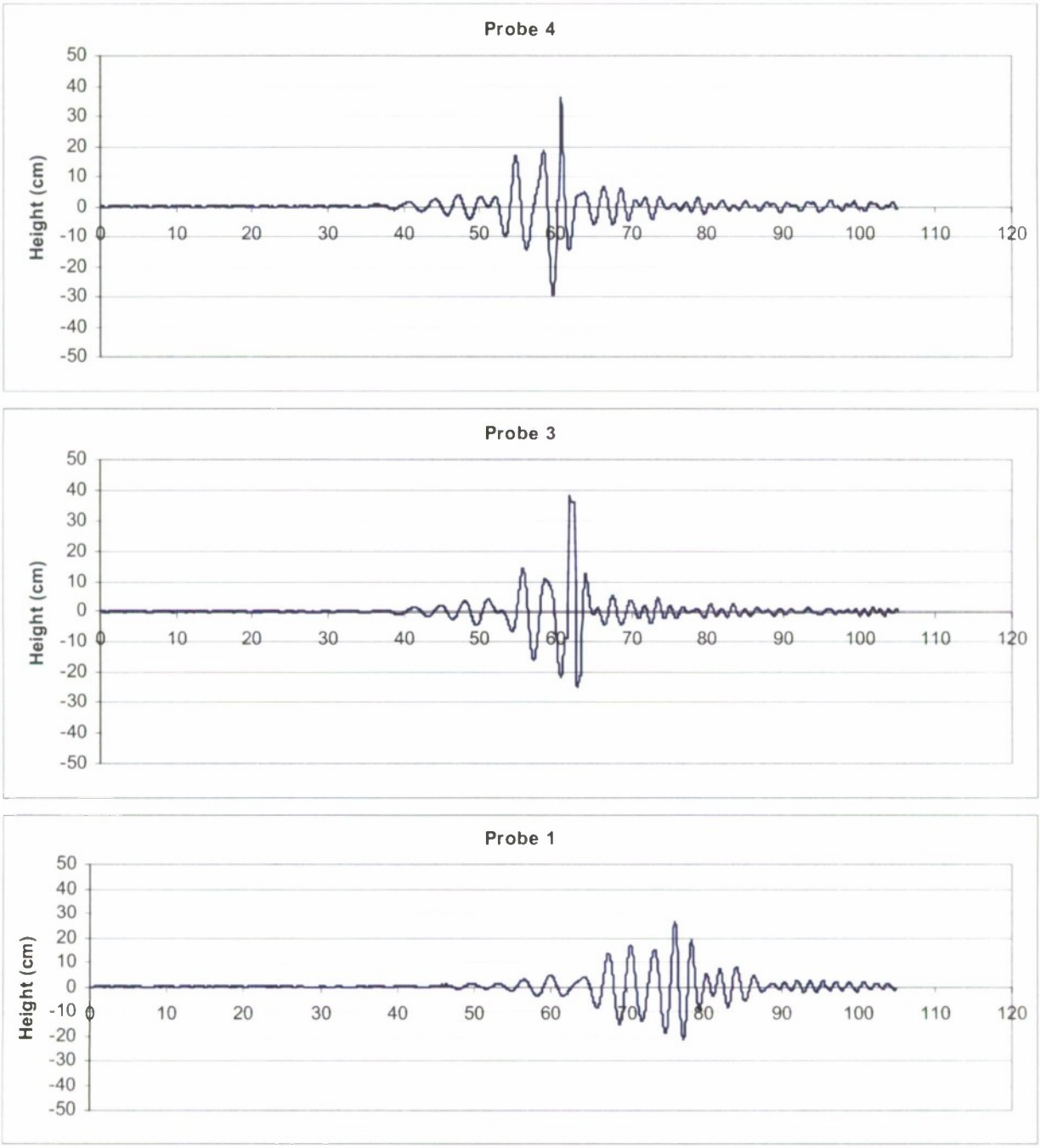

Figure 36 (continued)

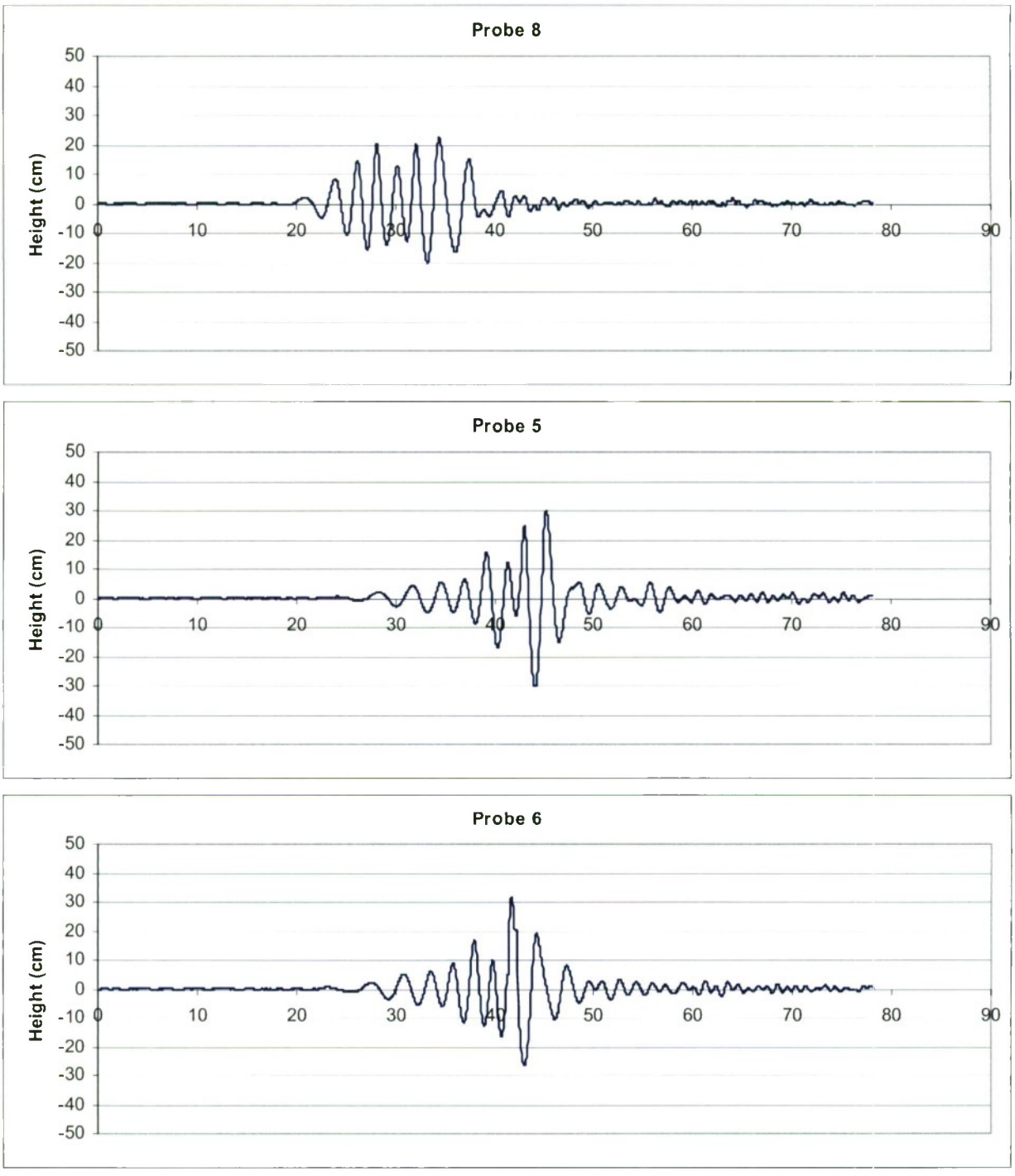

Figure 37. Measured wave time-history of sonic probes 8 (closest to wave-maker) to 1 (closest to the beach), Phase II, Run 6

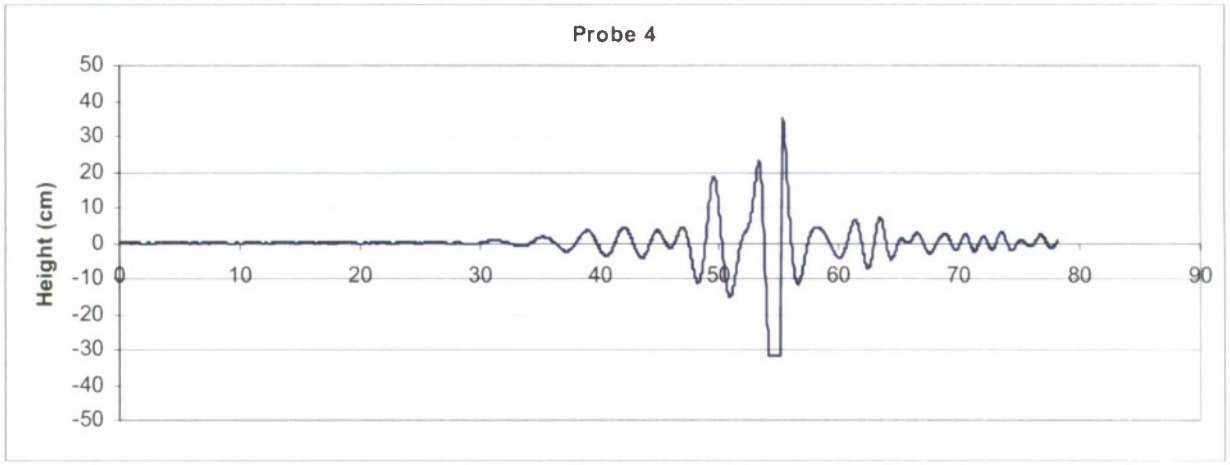

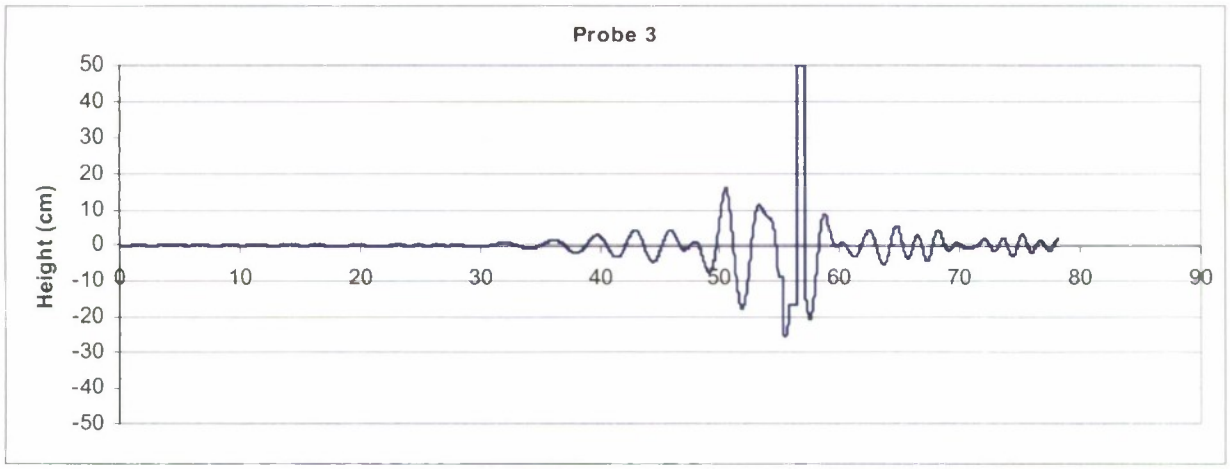

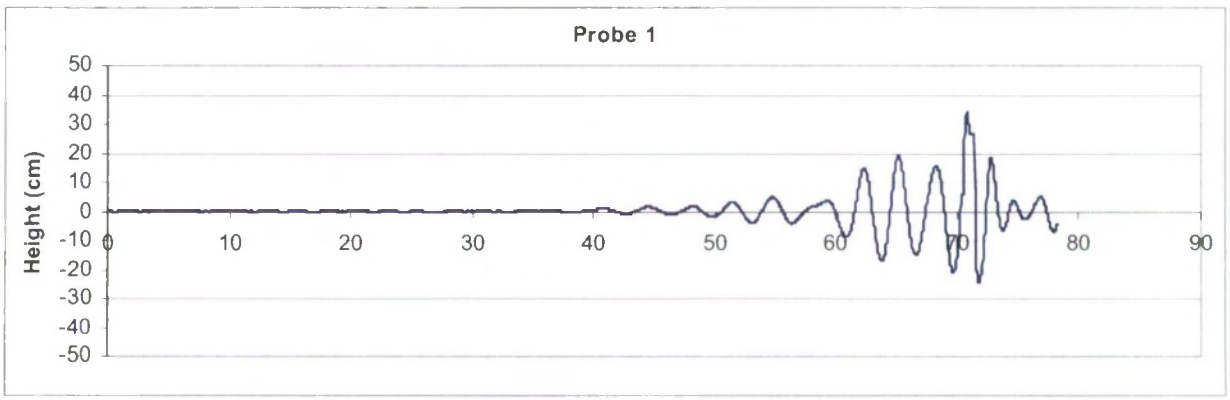

Figure 37 (continued)

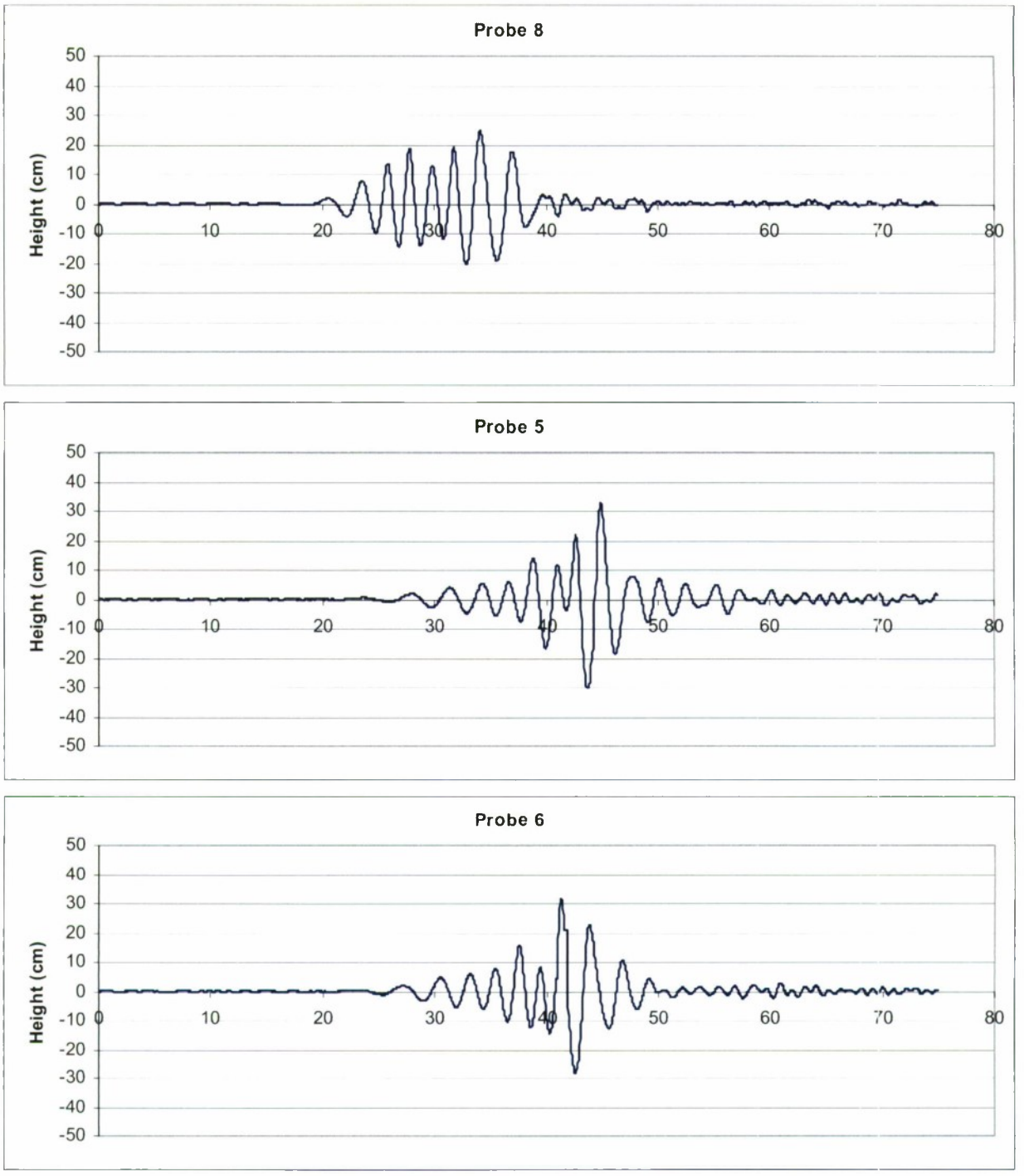

Figure 38. Measured wave time-history of sonic probes 8 (closest to wave-maker) to 1 (closest to the beach), Phase II, Run 7

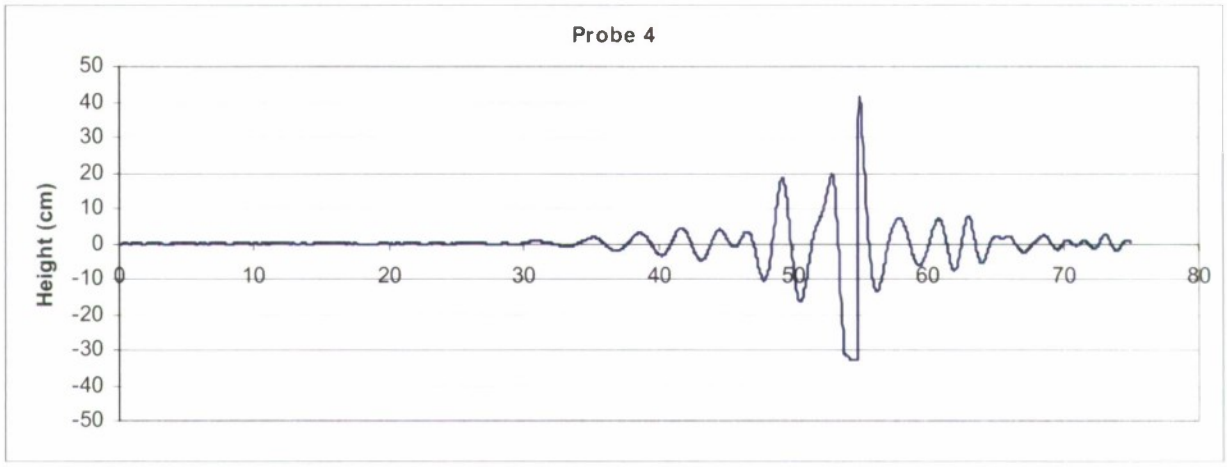

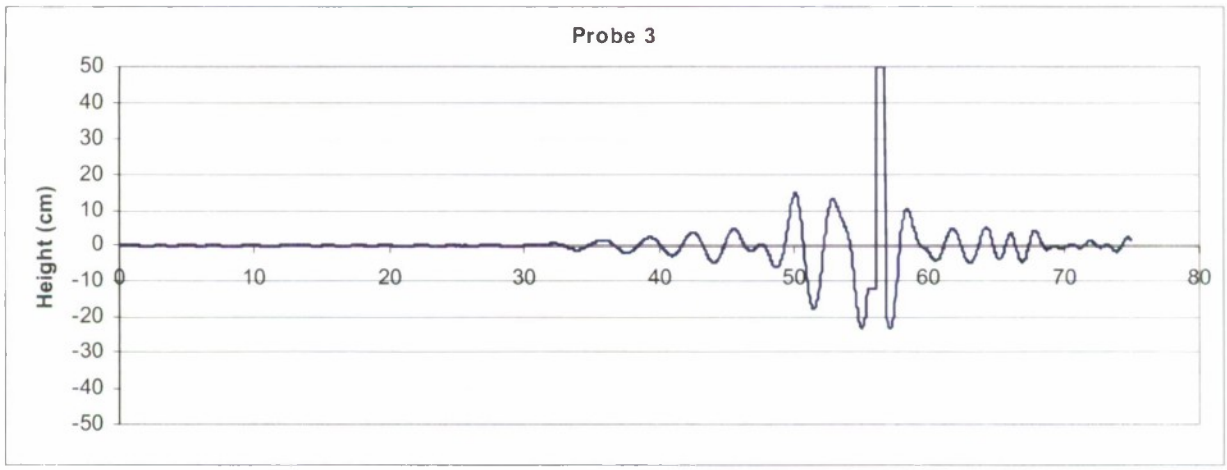

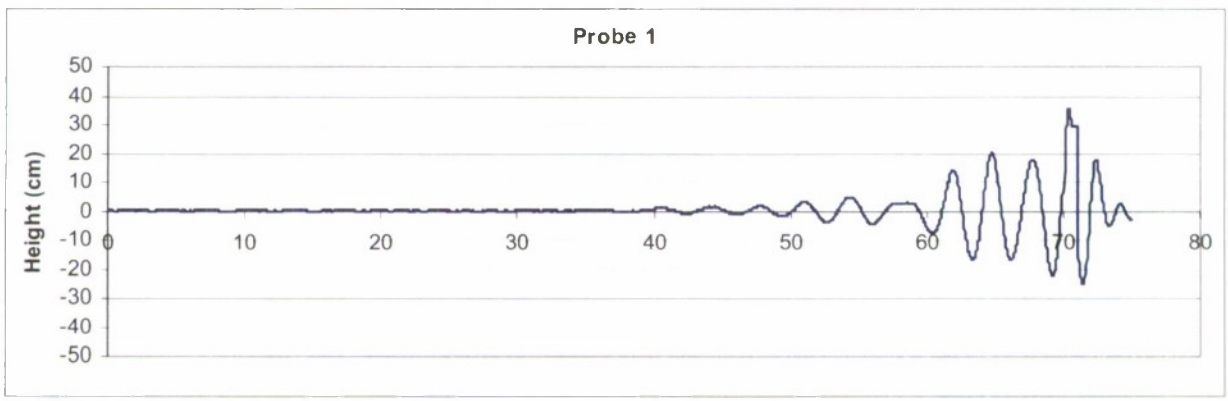

Figure 38 (continued)

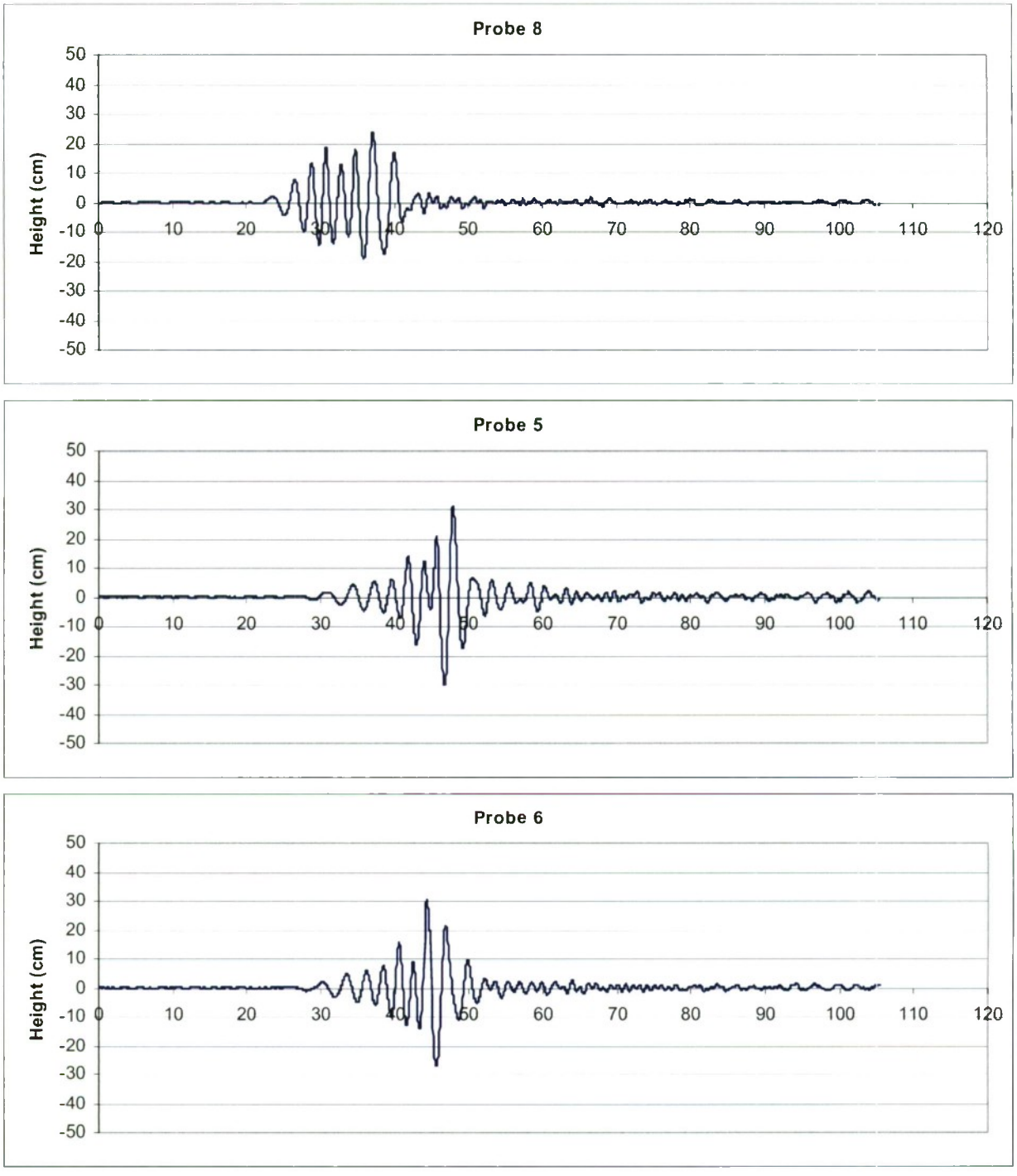

Figure 39. Measured wave time-history of sonic probes 8 (closest to wave-maker) to 1 (closest to the beach), Phase II, Run 8

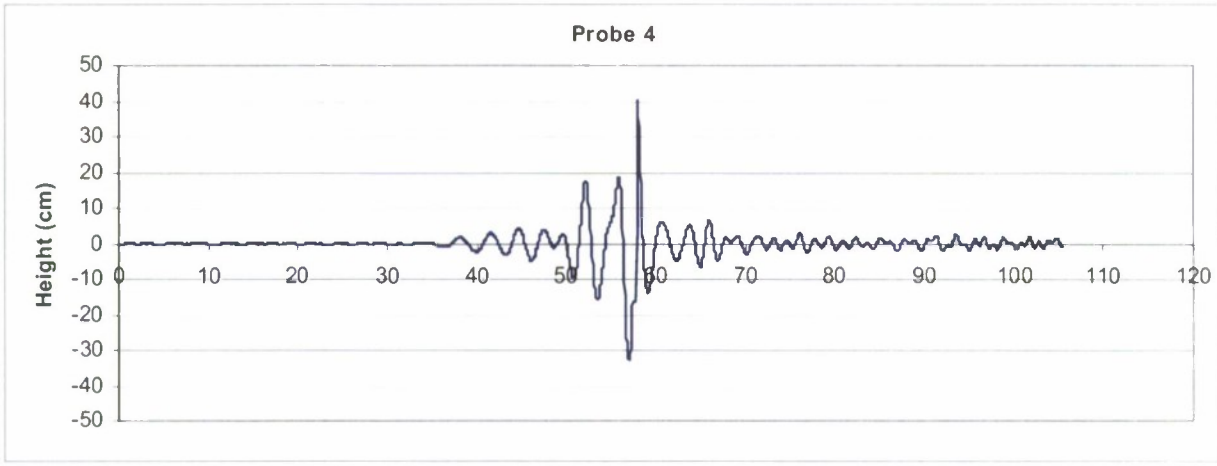

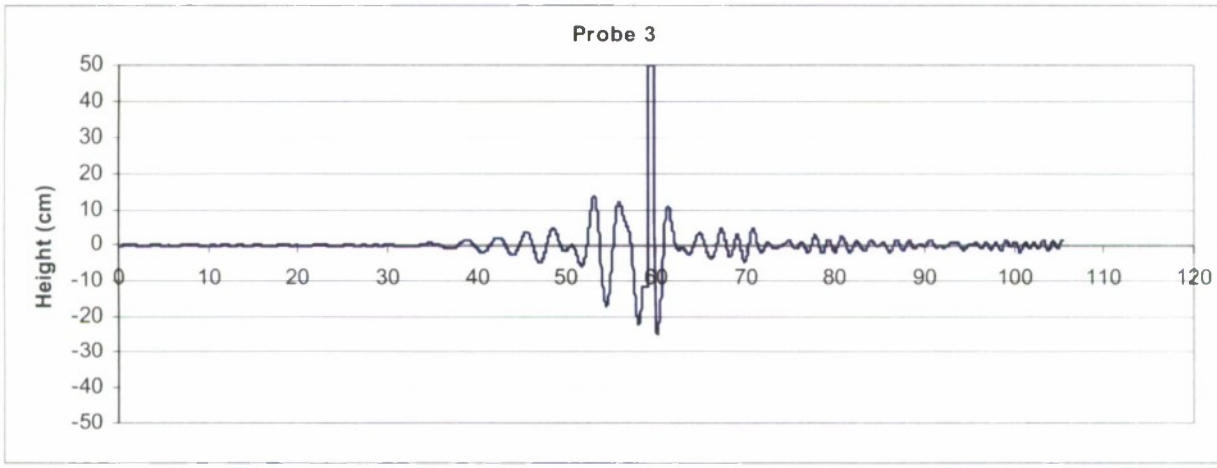

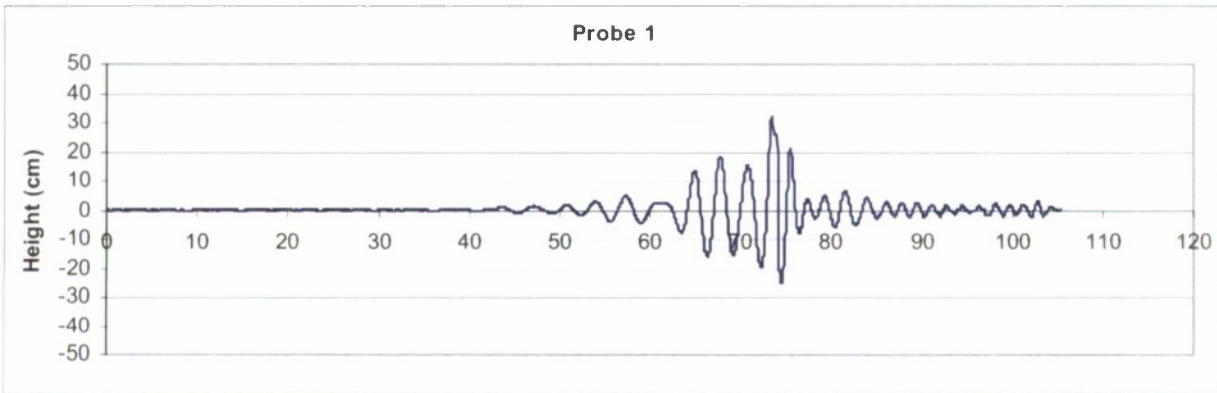

Figure 39 (continued)

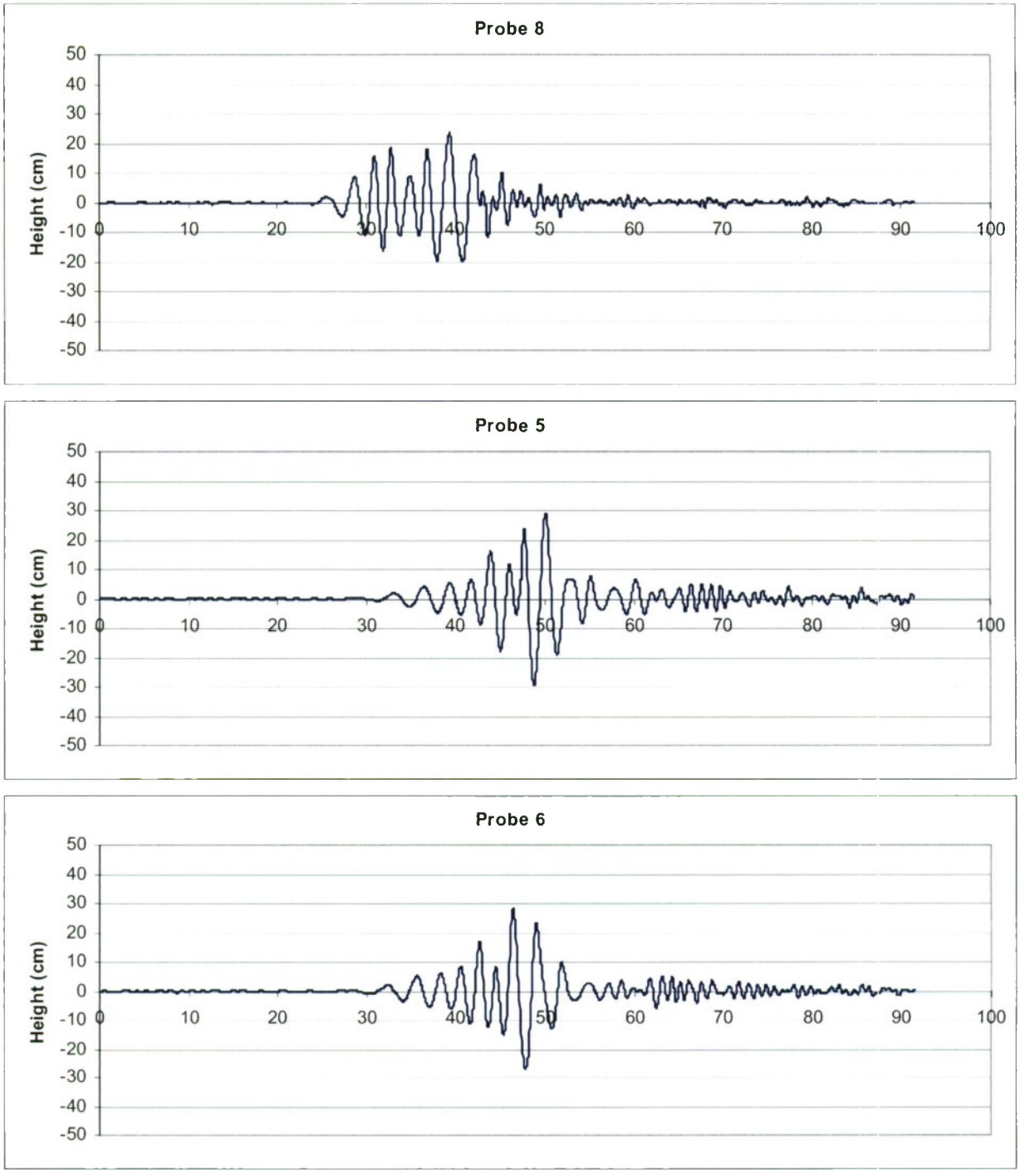

Figure 40. Measured wave time-history of sonic probes 8 (closest to wave-maker) to 1 (closest to the beach), Phase II, Run 42

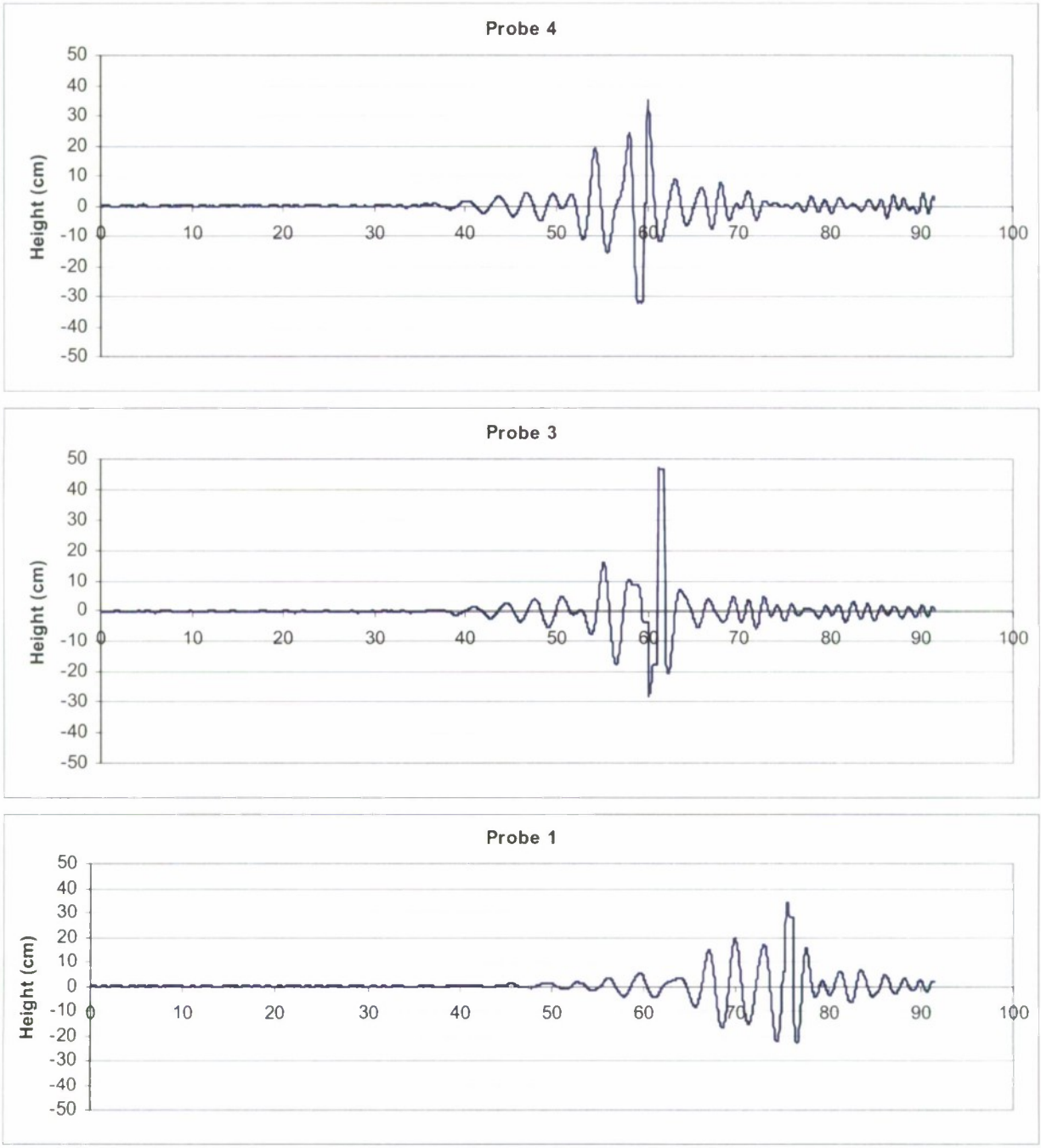

Figure 40 (continued)

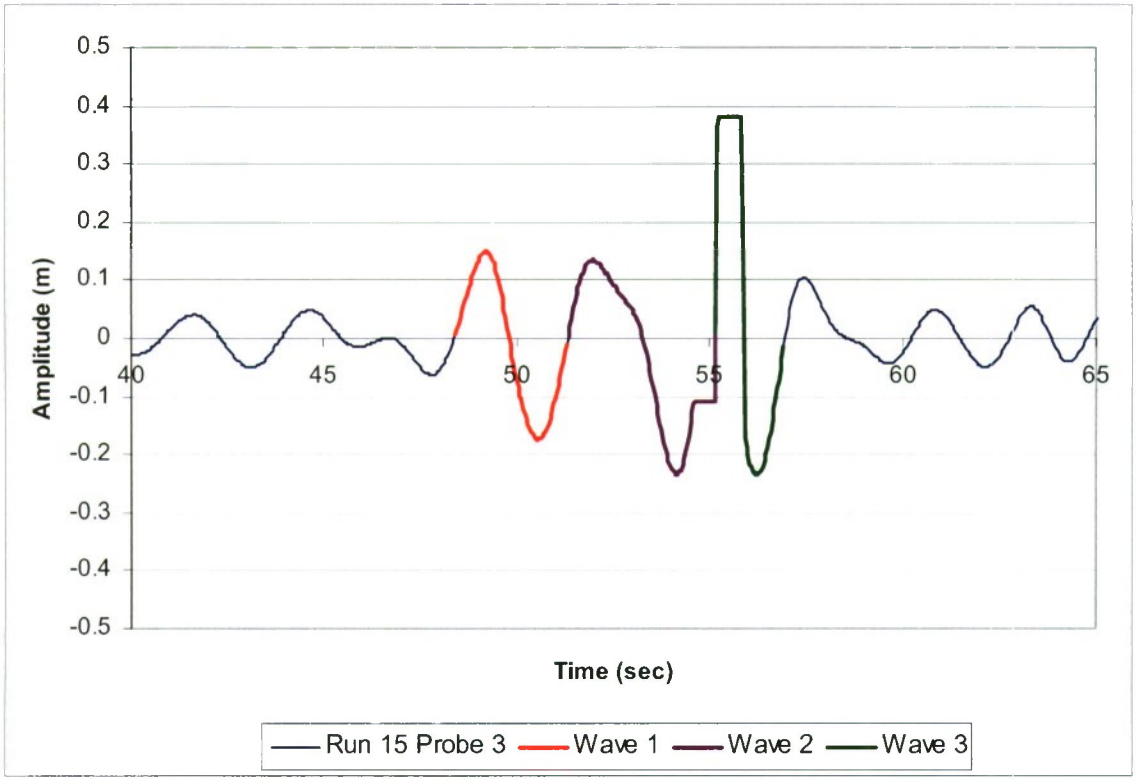

	Wave 1	Wave 2	Wave 3
Max Amplitude (m)	0.150	0.135	0.380
Min Amplitude (m)	-0.174	-0.233	-0.235
Wave Height (m)	0.323	0.368	0.615
Wave Period (sec)	2.9	3.8	1.7
Wave Length (m)	12.9	22.9	4.8
Steepness	1/40	1/62	1/8

Scale ratio:	Scaled wave heights (m):		
10	3.2	3.7	6.1
20.8	6.7	7.7	12.8
30	9.7	11.0	18.4
40	12.9	14.7	24.6
46.6	15.1	17.1	28.7

Figure 41. Wave characteristics at sonic probe 3, Phase I, Run 15

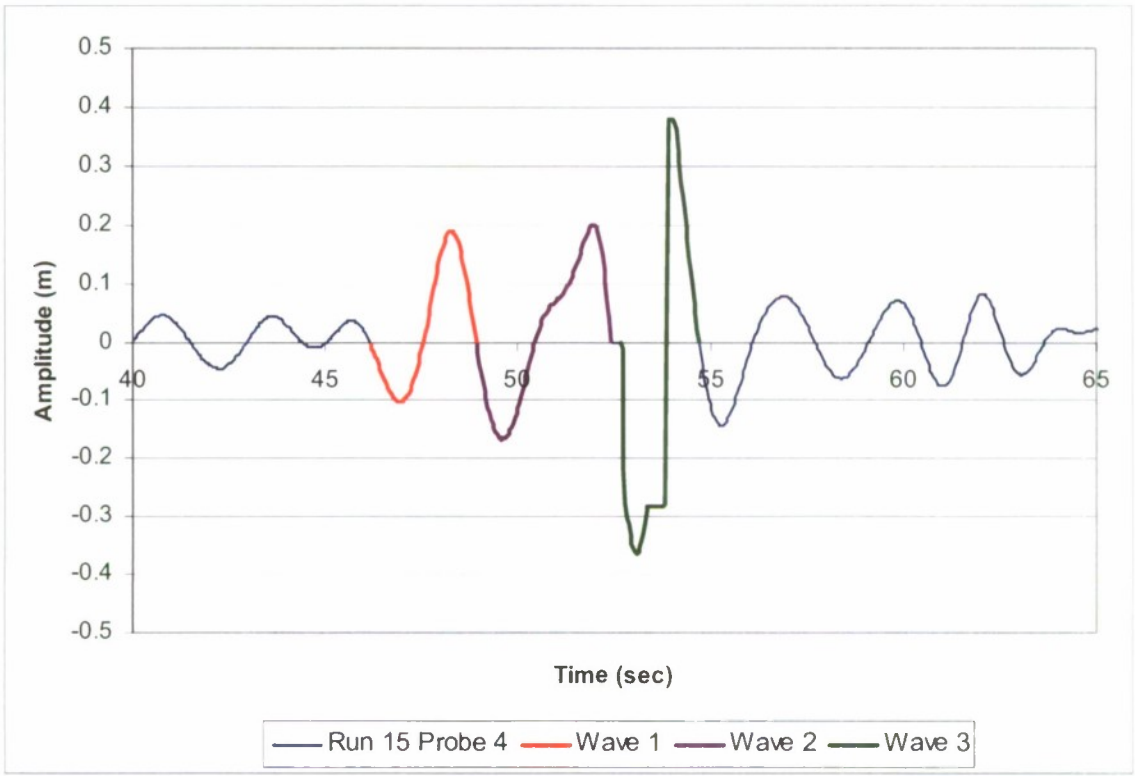

	Wave 1	Wave 2	Wave 3
Max Amplitude (m)	0.189	0.199	0.380
Min Amplitude (m)	-0.103	-0.167	-0.364
Wave Height (m)	0.292	0.367	0.743
Wave Period (sec)	2.7	3.5	2.0
Wave Length (m)	11.8	19.1	6.5
Steepness	1/41	1/48	1/10

Scale ratio:	Scaled wave heights (m):		
10	2.9	3.7	7.4
20.8	6.1	7.6	15.5
30	8.8	11.0	22.3
40	11.7	14.7	29.7
46.6	13.6	17.1	34.6

Figure 42. Wave characteristics at sonic probe 4, Phase I, Run 15

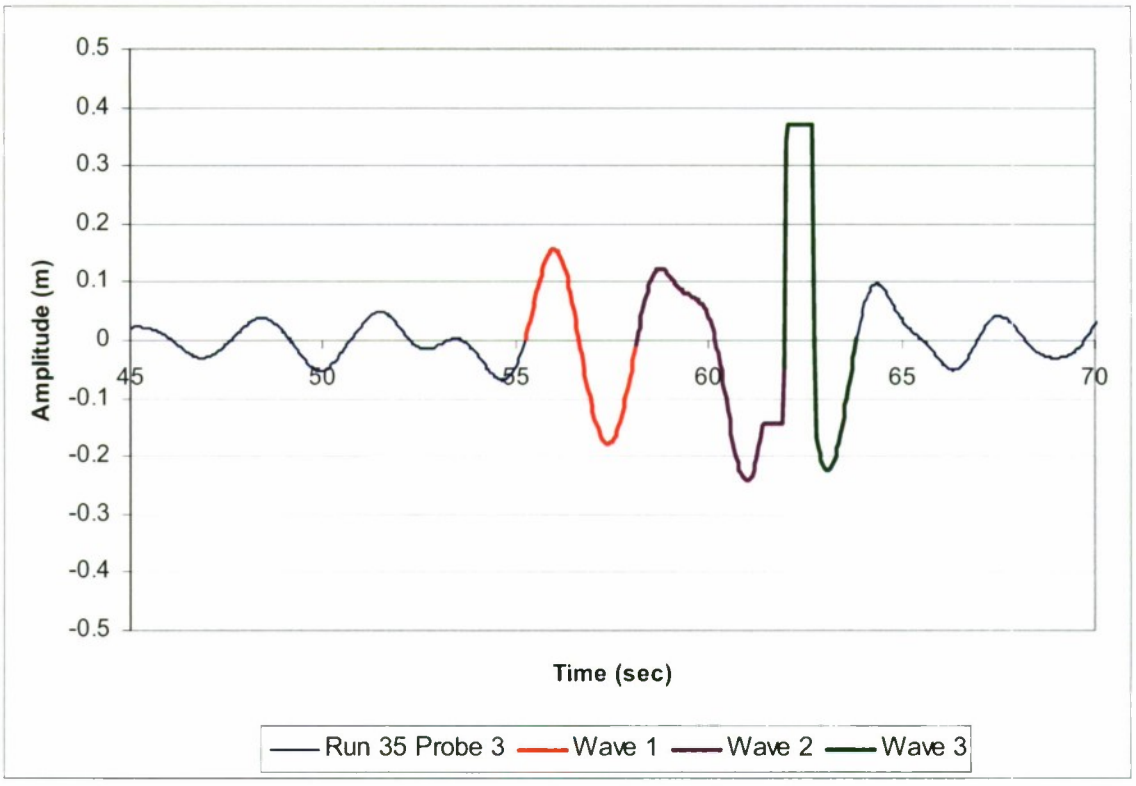

	Wave 1	Wave 2	Wave 3
Max Amplitude (m)	0.157	0.123	0.371
Min Amplitude (m)	-0.179	-0.241	-0.224
Wave Height (m)	0.336	0.365	0.595
Wave Period (sec)	2.9	3.8	1.9
Wave Length (m)	12.9	22.4	5.5
Steepness	1/43	1/62	1/9

Scale ratio:	Scaled wave heights (m):		
10	3.4	3.6	5.9
20.8	7.0	7.6	12.4
30	10.1	10.9	17.8
40	13.4	14.6	23.8
46.6	15.6	17.0	27.7

Figure 43. Wave characteristics at sonic probe 3, Phase I, Run 35

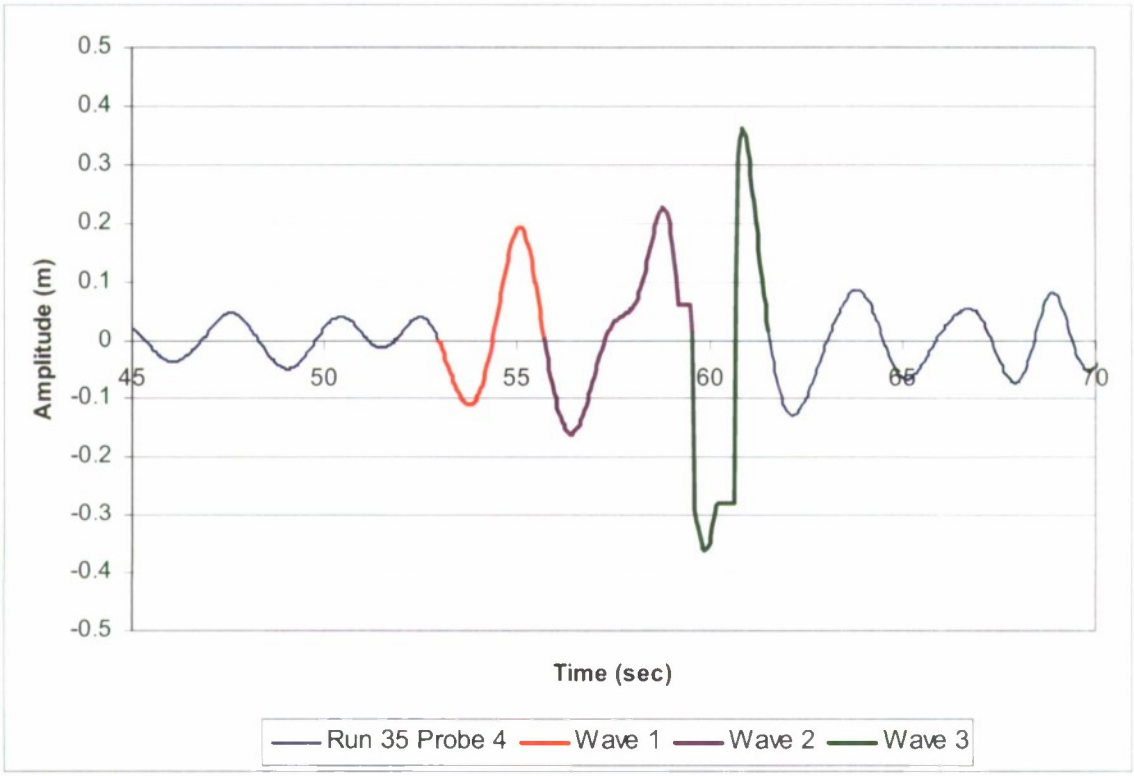

	Wave 1	Wave 2	Wave 3
Max Amplitude (m)	0.193	0.225	0.361
Min Amplitude (m)	-0.111	-0.160	-0.361
Wave Height (m)	0.303	0.386	0.722
Wave Period (sec)	2.7	3.8	2.0
Wave Length (m)	11.8	22.9	6.2
Steepness	1/39	1/57	1/10

Scale ratio:	Scaled wave heights (m):		
10	3.0	3.9	7.2
20.8	6.3	8.0	15.0
30	9.1	11.6	21.7
40	12.1	15.4	28.9
46.6	14.1	18.0	33.6

Figure 44. Wave characteristics at sonic probe 4, Phase I, Run 35

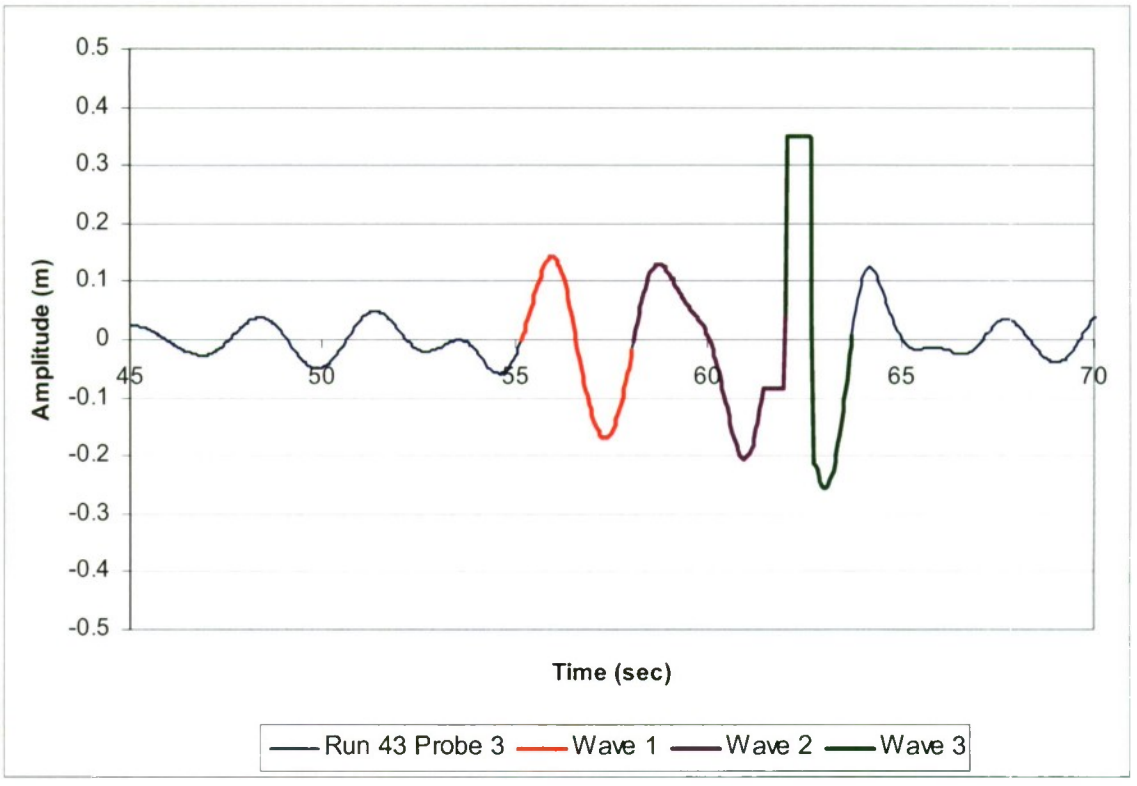

	Wave 1	Wave 2	Wave 3
Max Amplitude (m)	0.142	0.130	0.350
Min Amplitude (m)	-0.169	-0.205	-0.256
Wave Height (m)	0.311	0.335	0.606
Wave Period (sec)	2.9	3.9	1.7
Wave Length (m)	12.9	23.9	4.8
Steepness	1/43	1/80	1/8

Scale ratio:	Scaled wave heights (m):		
10	3.1	3.4	6.1
20.8	6.5	7.0	12.6
30	9.3	10.1	18.2
40	12.5	13.4	24.2
46.6	14.5	15.6	28.2

Figure 45. Wave characteristics at sonic probe 3, Phase I, Run 43

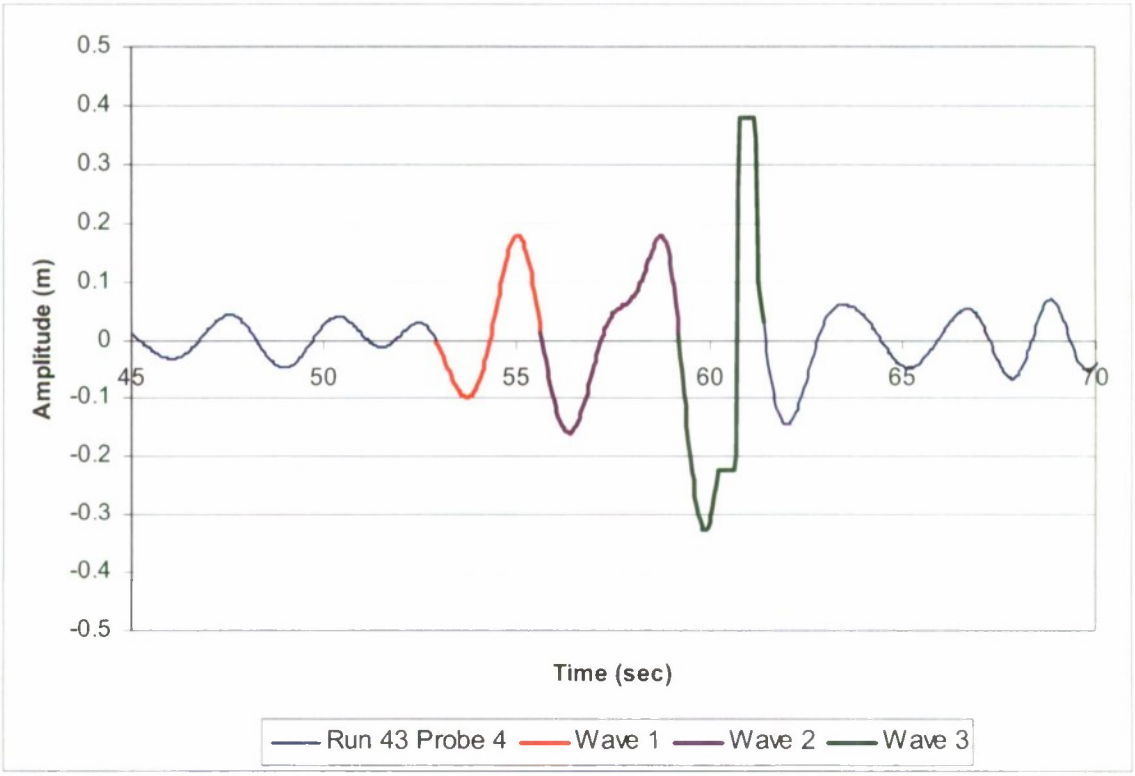

	Wave 1	Wave 2	Wave 3
Max Amplitude (m)	0.179	0.178	0.379
Min Amplitude (m)	-0.098	-0.160	-0.328
Wave Height (m)	0.277	0.338	0.706
Wave Period (sec)	2.7	3.6	2.2
Wave Length (m)	11.4	20.0	7.6
Steepness	1/38	1/67	1/11

Scale ratio:	Scaled wave heights (m):		
10	2.8	3.4	7.1
20.8	5.8	7.0	14.7
30	8.3	10.1	21.2
40	11.1	13.5	28.3
46.6	12.9	15.7	32.9

Figure 46. Wave characteristics at sonic probe 4, Phase I, Run 43

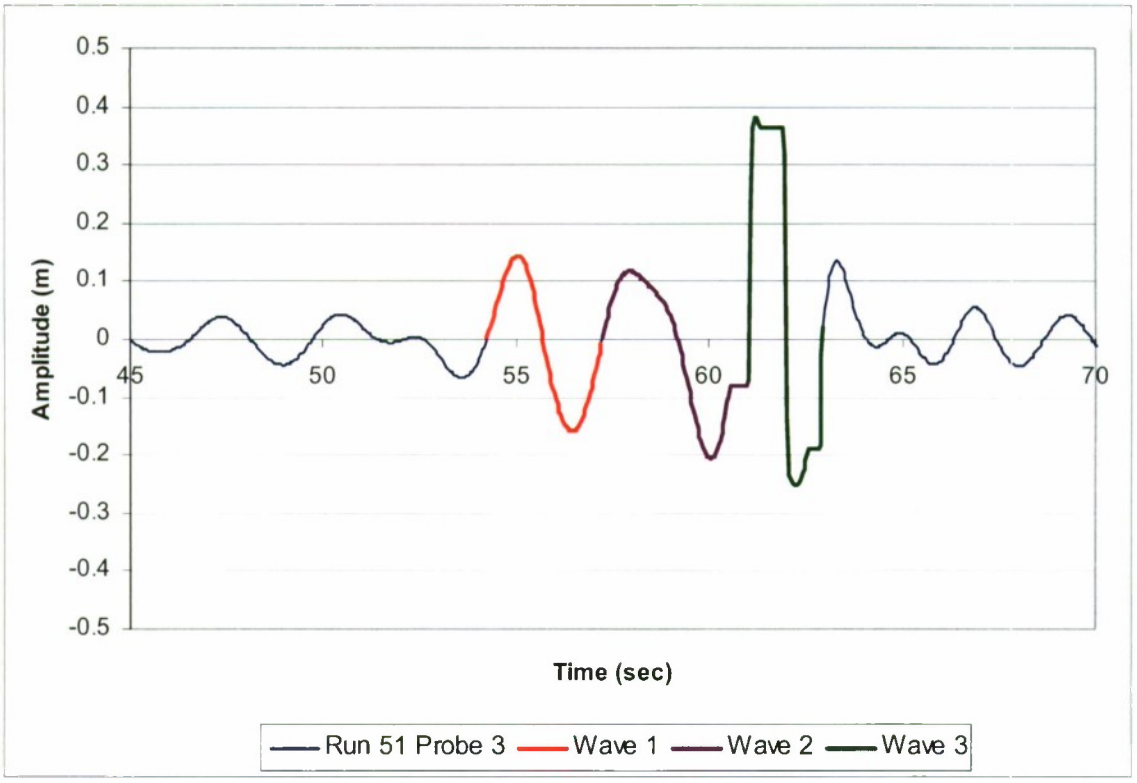

	Wave 1	Wave 2	Wave 3
Max Amplitude (m)	0.144	0.118	0.380
Min Amplitude (m)	-0.159	-0.205	-0.253
Wave Height (m)	0.303	0.323	0.633
Wave Period (sec)	3.0	3.8	1.9
Wave Length (m)	13.7	22.4	5.7
Steepness	2/91	1/70	1/9

Scale ratio:	Scaled wave heights (m):		
10	3.0	3.2	6.3
20.8	6.3	6.7	13.2
30	9.1	9.7	19.0
40	12.1	12.9	25.3
46.6	14.1	15.1	29.5

Figure 47. Wave characteristics at sonic probe 3, Phase I, Run 51

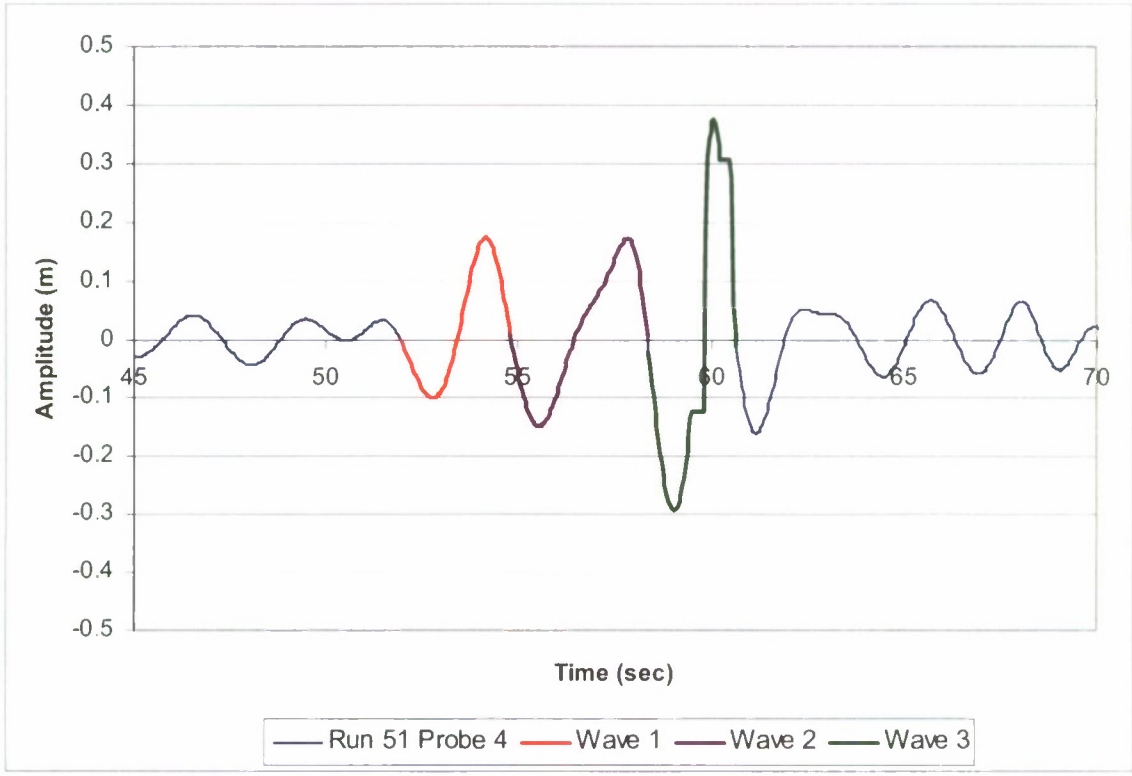

	Wave 1	Wave 2	Wave 3
Max Amplitude (m)	0.174	0.172	0.374
Min Amplitude (m)	-0.099	-0.148	-0.292
Wave Height (m)	0.273	0.320	0.666
Wave Period (sec)	2.8	3.5	2.3
Wave Length (m)	12.5	19.6	8.2
Steepness	1/46	1/65	1/10

Scale ratio:	Scaled wave heights (m):		
10	2.7	3.2	6.7
20.8	5.7	6.7	13.8
30	8.2	9.6	20.0
40	10.9	12.8	26.6
46.6	12.7	14.9	31.0

Figure 48. Wave characteristics at sonic probe 4, Phase I, Run 51

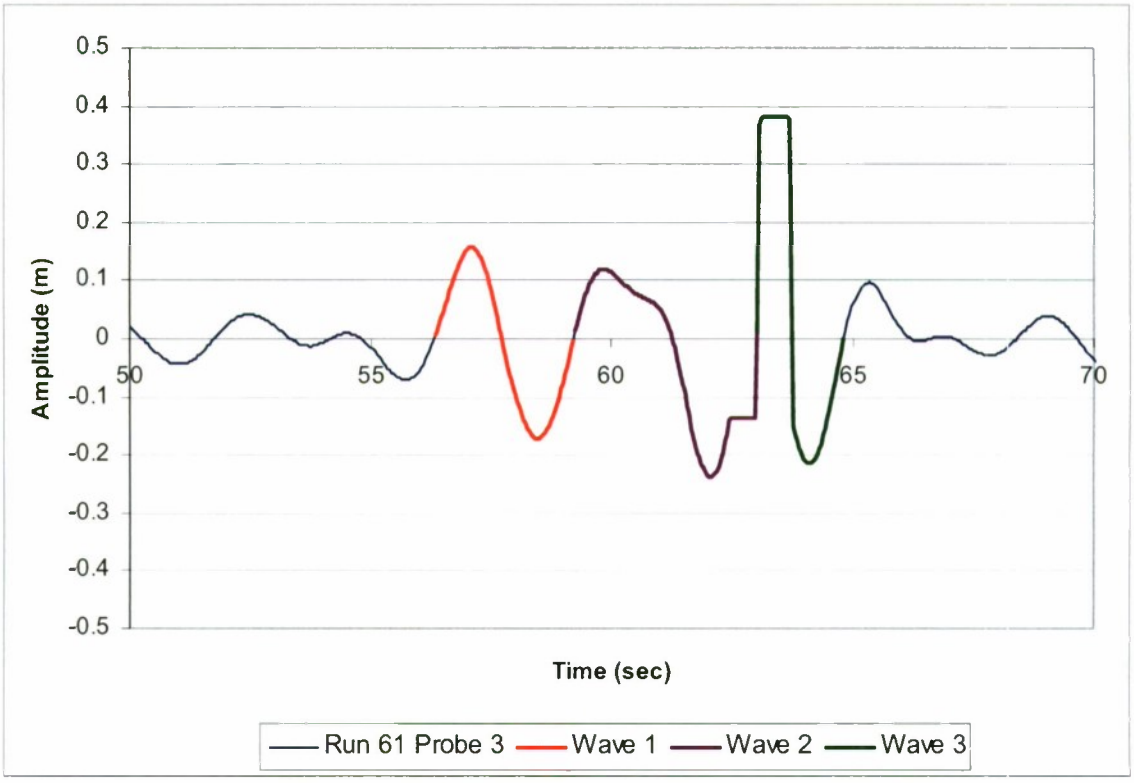

	Wave 1	Wave 2	Wave 3
Max Amplitude (m)	0.157	0.120	0.380
Min Amplitude (m)	-0.171	-0.237	-0.215
Wave Height (m)	0.328	0.357	0.595
Wave Period (sec)	2.9	3.8	1.8
Wave Length (m)	12.9	22.4	5.0
Steepness	1/39	1/56	1/8

Scale ratio:	Scaled wave heights (m):		
10	3.3	3.6	6.0
20.8	6.8	7.4	12.4
30	9.8	10.7	17.9
40	13.1	14.3	23.8
46.6	15.3	16.6	27.7

Figure 49. Wave characteristics at sonic probe 3, Phase I, Run 61

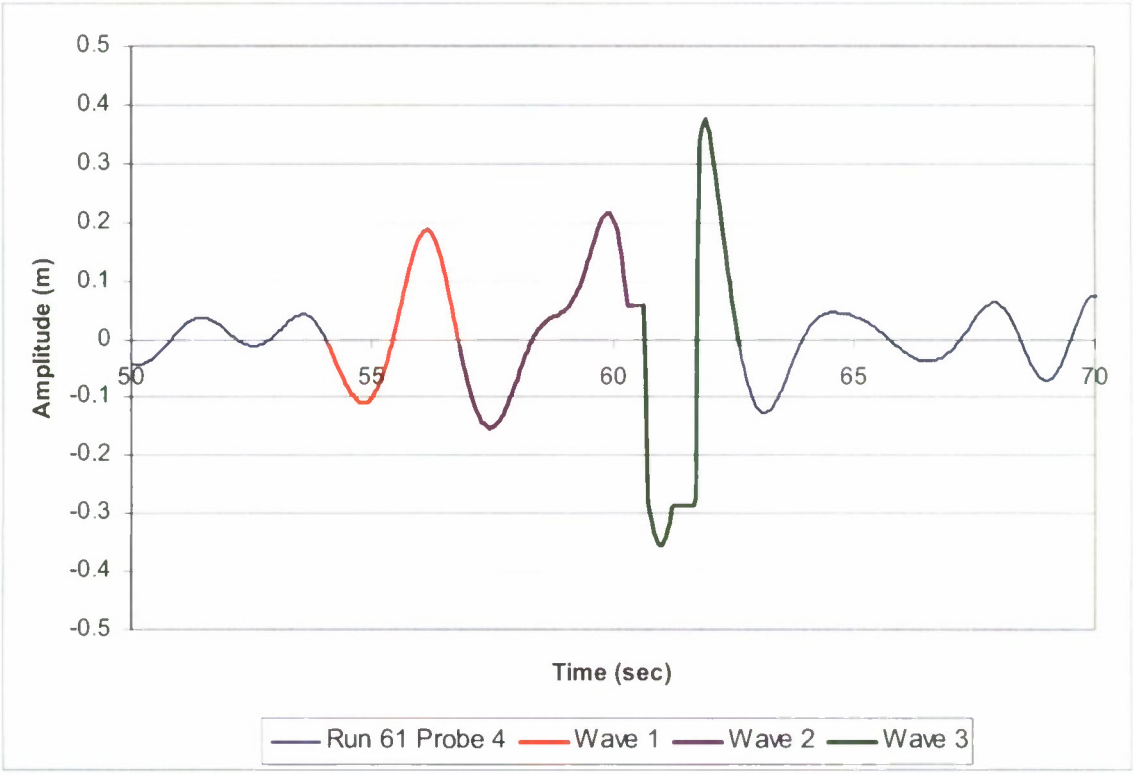

	Wave 1	Wave 2	Wave 3
Max Amplitude (m)	0.187	0.216	0.374
Min Amplitude (m)	-0.110	-0.153	-0.353
Wave Height (m)	0.297	0.369	0.727
Wave Period (sec)	2.7	3.6	2.0
Wave Length (m)	11.4	20.0	6.2
Steepness	1/38	1/50	1/9

Scale ratio:	Scaled wave heights (m):		
10	3.0	3.7	7.3
20.8	6.2	7.7	15.1
30	8.9	11.1	21.8
40	11.9	14.8	29.1
46.6	13.8	17.2	33.9

Figure 50. Wave characteristics at sonic probe 4, Phase I, Run 61

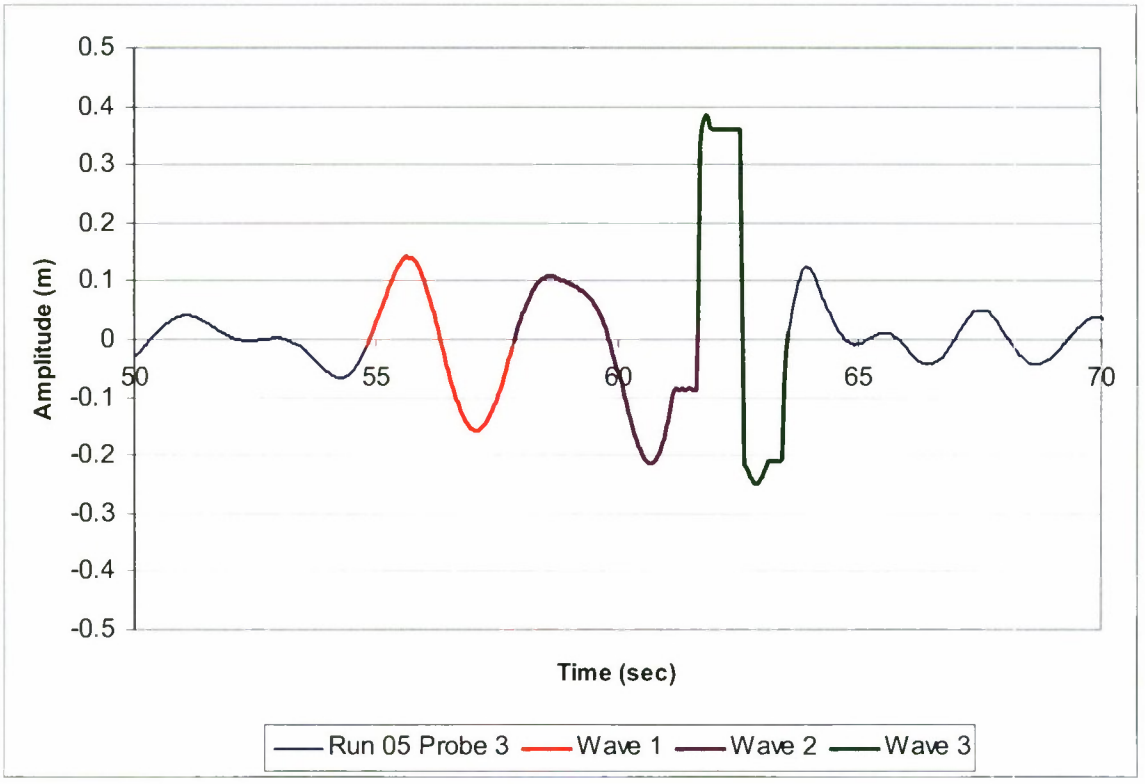

	Wave 1	Wave 2	Wave 3
Max Amplitude (m)	0.142	0.108	0.385
Min Amplitude (m)	-0.157	-0.213	-0.248
Wave Height (m)	0.299	0.321	0.633
Wave Period (sec)	3.0	3.8	1.9
Wave Length (m)	14.0	22.4	5.5
Steepness	1/47	1/75	1/9

Scale ratio:	Scaled wave heights (m):		
10	3.0	3.2	6.3
20.8	6.2	6.7	13.2
30	9.0	9.6	19.0
40	12.0	12.8	25.3
46.6	13.9	15.0	29.5

Figure 51. Wave characteristics at sonic probe 3, Phase II, Run 5

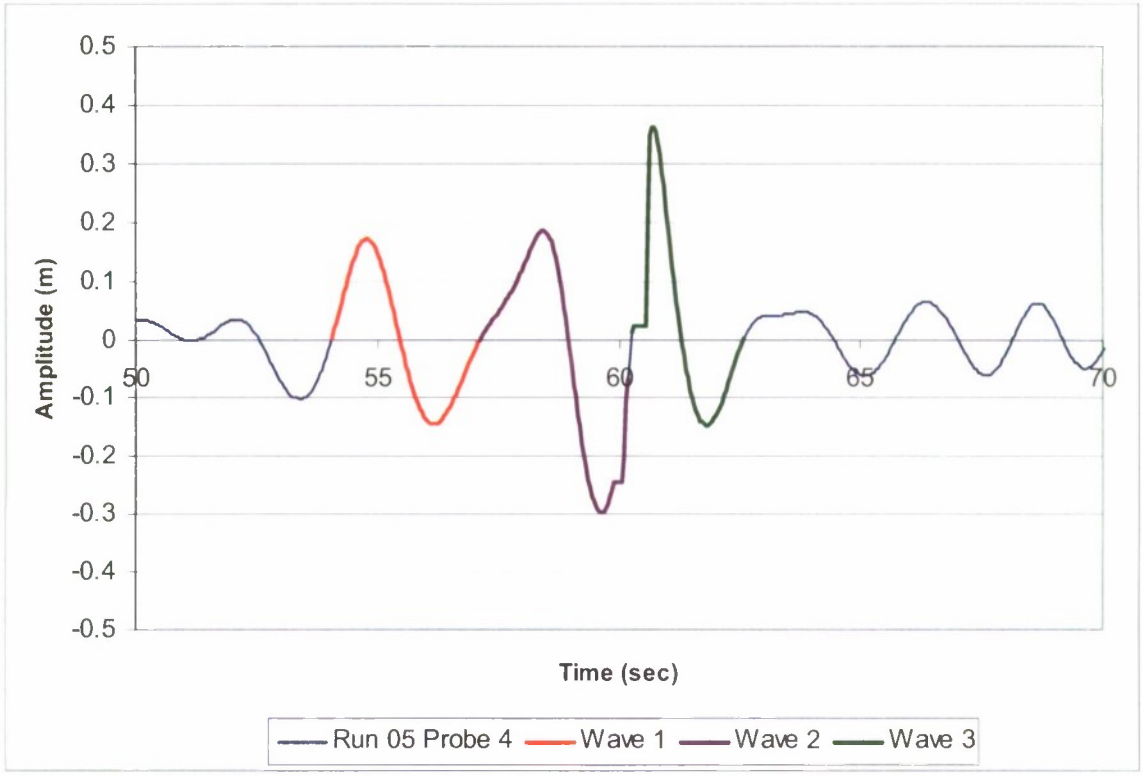

	Wave 1	Wave 2	Wave 3
Max Amplitude (m)	0.171	0.185	0.361
Min Amplitude (m)	-0.145	-0.297	-0.146
Wave Height (m)	0.316	0.482	0.507
Wave Period (sec)	3.1	3.1	2.3
Wave Length (m)	14.8	14.8	8.5
Steepness	1/46	1/31	1/10

Scale ratio:	Scaled wave heights (m):		
10	3.2	4.8	5.1
20.8	6.6	10.0	10.6
30	9.5	14.5	15.2
40	12.6	19.3	20.3
46.6	14.7	22.5	23.6

Figure 52. Wave characteristics at sonic probe 4, Phase II, Run 5

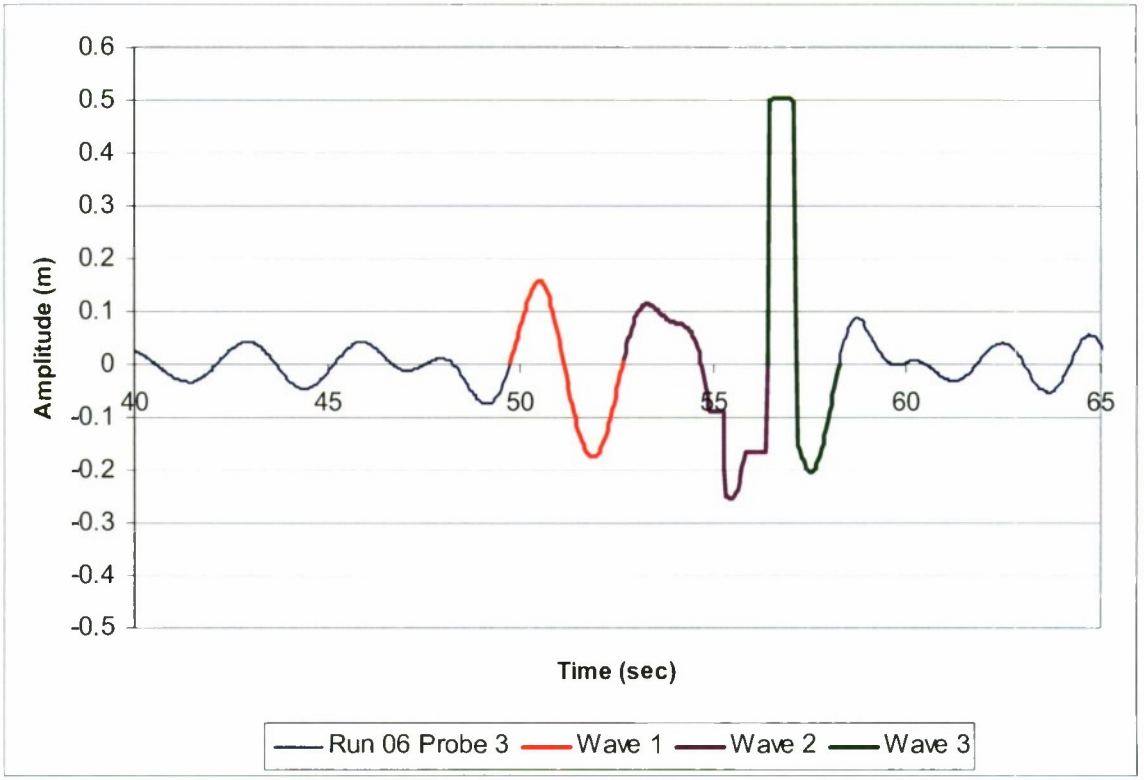

	Wave 1	Wave 2	Wave 3
Max Amplitude (m)	0.157	0.114	0.502
Min Amplitude (m)	-0.174	-0.254	-0.203
Wave Height (m)	0.332	0.368	0.705
Wave Period (sec)	2.9	3.7	1.8
Wave Length (m)	13.3	21.9	5.2
Steepness	1/40	1/60	1/7

Scale ratio:	Scaled wave heights (m):		
10	3.3	3.7	7.1
20.8	6.9	7.6	14.7
30	9.9	11.0	21.2
40	13.3	14.7	28.2
46.6	15.5	17.1	32.9

Figure 53. Wave characteristics at sonic probe 3, Phase II, Run 6

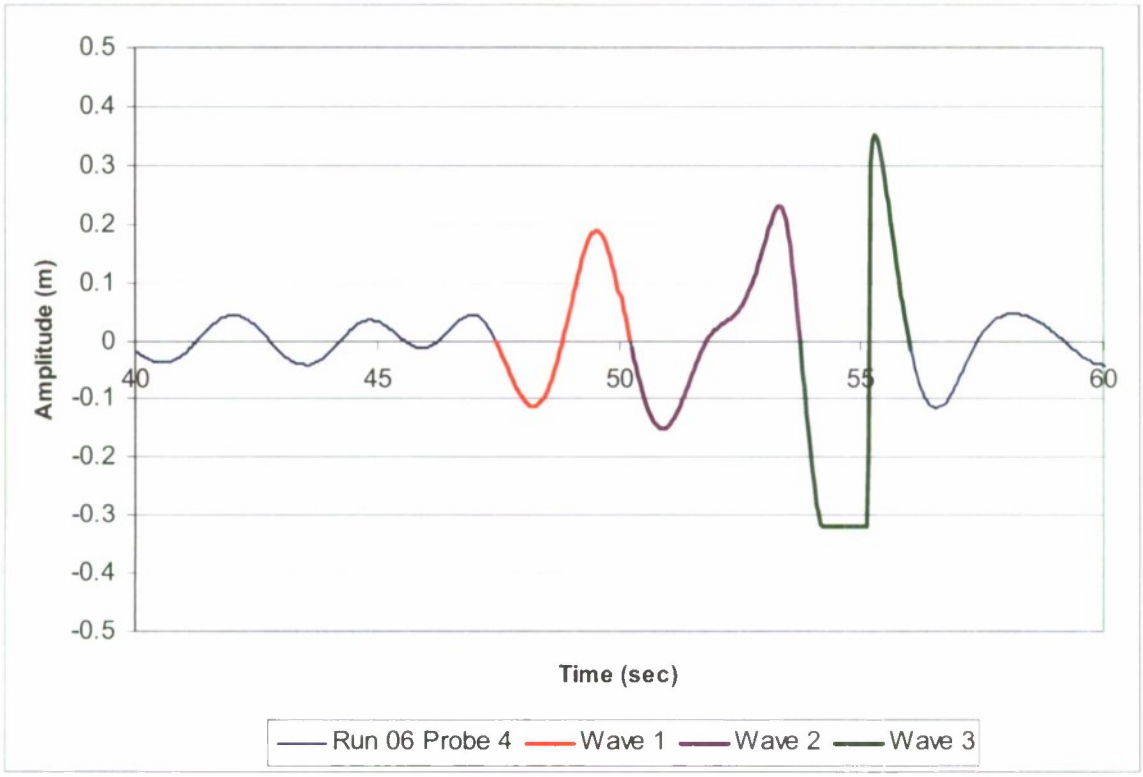

	Wave 1	Wave 2	Wave 3
Max Amplitude (m)	0.188	0.231	0.352
Min Amplitude (m)	-0.113	-0.150	-0.319
Wave Height (m)	0.301	0.381	0.672
Wave Period (sec)	2.7	3.5	2.3
Wave Length (m)	11.8	19.1	8.2
Steepness	1/40	1/50	1/10

Scale ratio:	Scaled wave heights (m):		
10	3.0	3.8	6.7
20.8	6.3	7.9	14.0
30	9.0	11.4	20.1
40	12.1	15.2	26.9
46.6	14.0	17.8	31.3

Figure 54. Wave characteristics at sonic probe 4, Phase II, Run 6

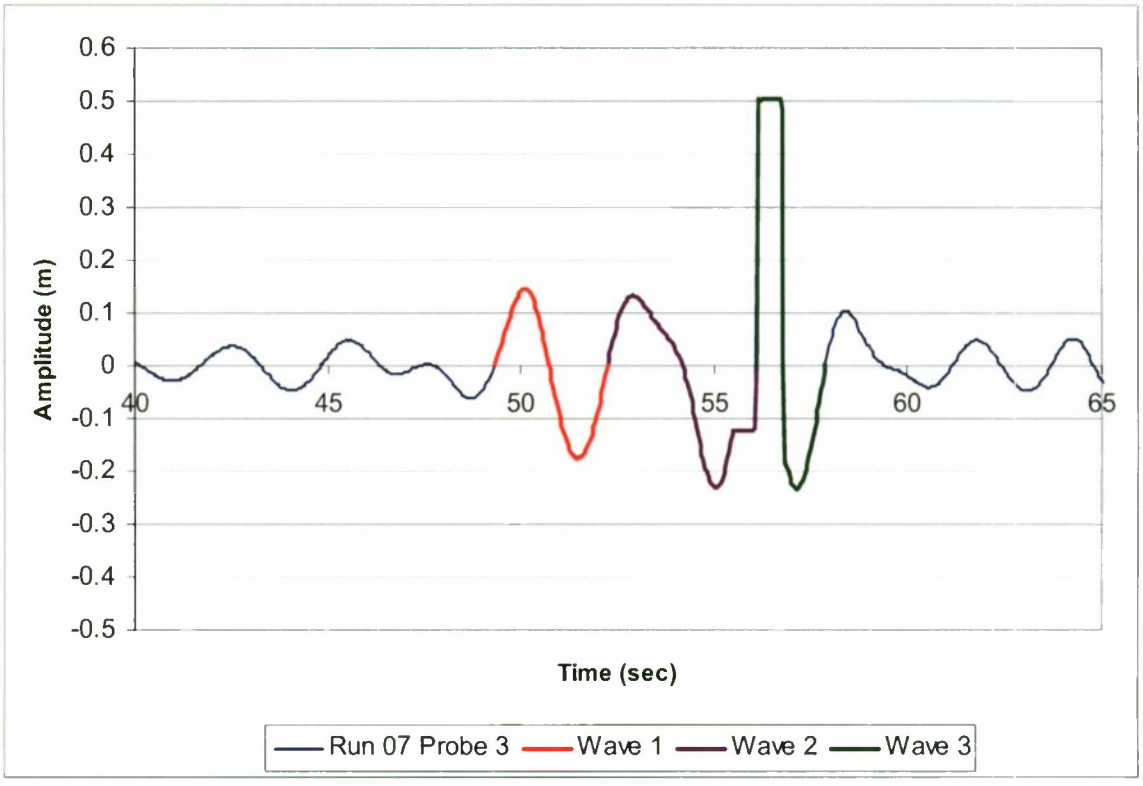

	Wave 1	Wave 2	Wave 3
Max Amplitude (m)	0.148	0.133	0.504
Min Amplitude (m)	-0.176	-0.230	-0.234
Wave Height (m)	0.324	0.363	0.738
Wave Period (sec)	2.9	3.8	1.8
Wave Length (m)	13.3	22.9	5.0
Steepness	1/41	1/63	1/7

Scale ratio:	Scaled wave heights (m):		
10	3.2	3.6	7.4
20.8	6.7	7.6	15.3
30	9.7	10.9	22.1
40	13.0	14.5	29.5
46.6	15.1	16.9	34.4

Figure 55. Wave characteristics at sonic probe 3, Phase II, Run 7

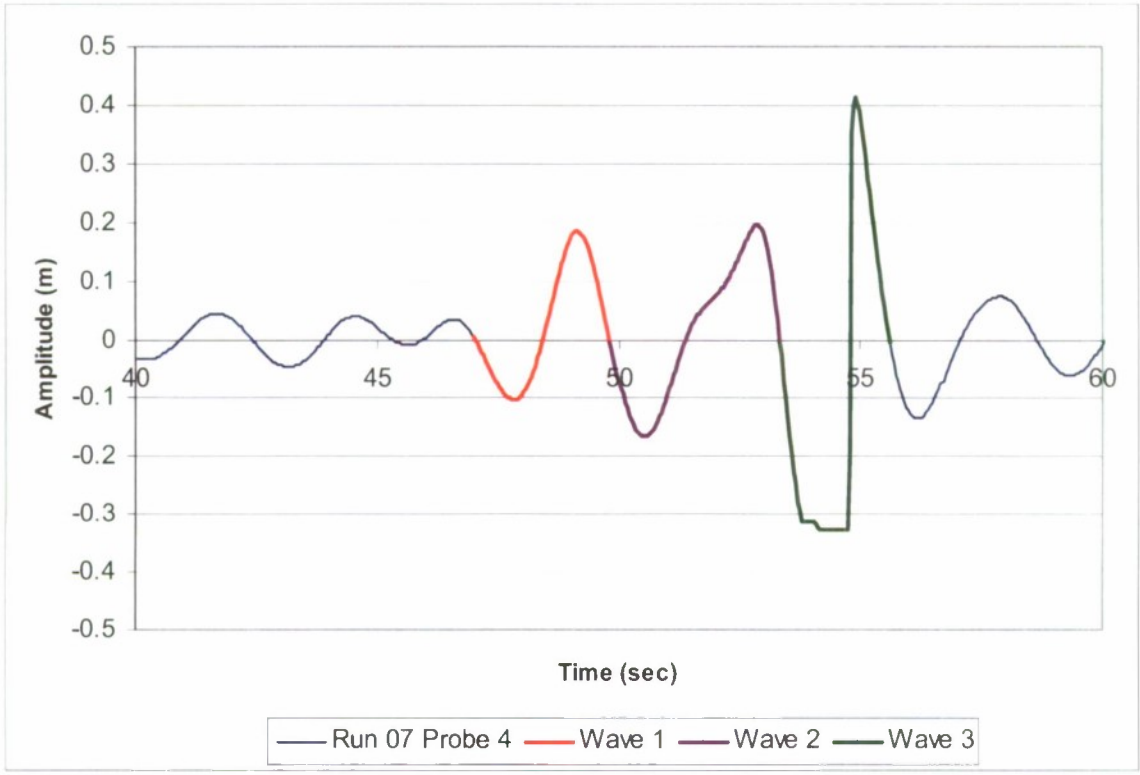

	Wave 1	Wave 2	Wave 3
Max Amplitude (m)	0.184	0.195	0.412
Min Amplitude (m)	-0.103	-0.166	-0.327
Wave Height (m)	0.287	0.361	0.739
Wave Period (sec)	2.8	3.5	2.3
Wave Length (m)	12.5	19.1	8.2
Steepness	1/43	1/53	1/11

Scale ratio:	Scaled wave heights (m):		
10	2.9	3.6	7.4
20.8	6.0	7.5	15.4
30	8.6	10.8	22.2
40	11.5	14.4	29.6
46.6	13.4	16.8	34.4

Figure 56. Wave characteristics at sonic probe 4, Phase II, Run 7

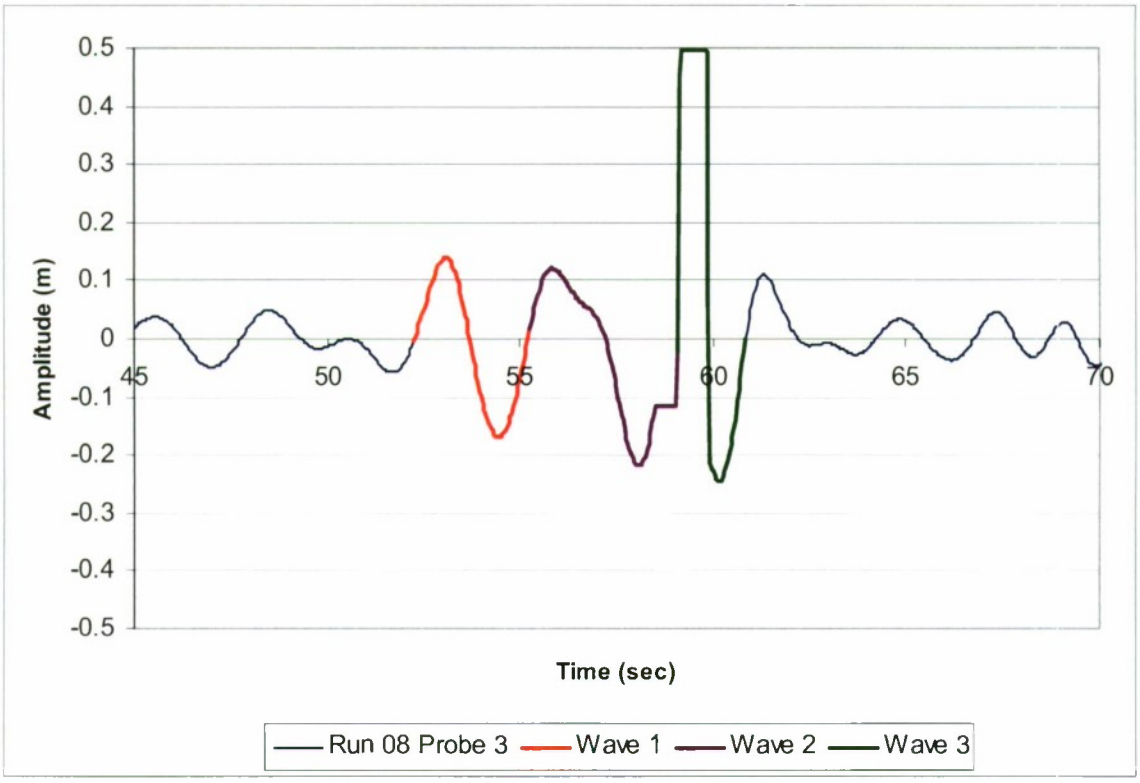

	Wave 1	Wave 2	Wave 3
Max Amplitude (m)	0.139	0.121	0.498
Min Amplitude (m)	-0.168	-0.218	-0.246
Wave Height (m)	0.307	0.339	0.744
Wave Period (sec)	3.0	3.8	1.7
Wave Length (m)	14.0	22.9	4.8
Steepness	1/46	1/68	1/7

Scale ratio:	Scaled wave heights (m):		
10	3.1	3.4	7.4
20.8	6.4	7.1	15.5
30	9.2	10.2	22.3
40	12.3	13.6	29.8
46.6	14.3	15.8	34.7

Figure 57. Wave characteristics at sonic probe 3, Phase II, Run 8

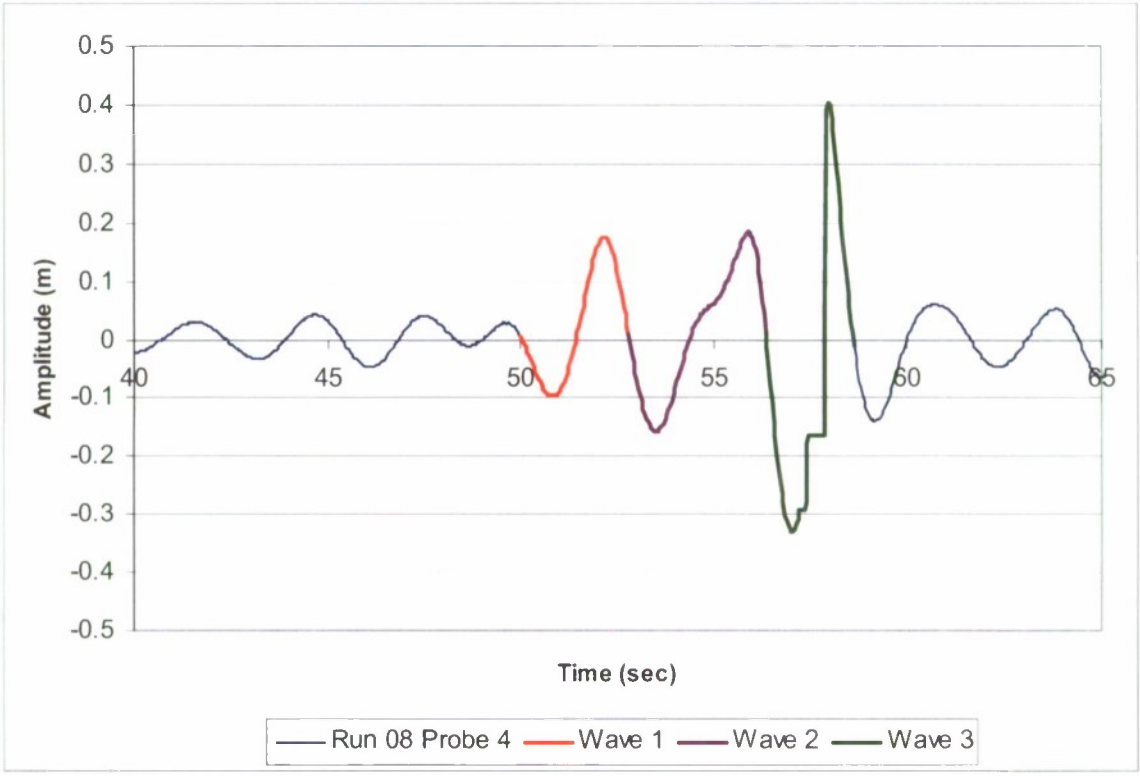

	Wave 1	Wave 2	Wave 3
Max Amplitude (m)	0.176	0.184	0.402
Min Amplitude (m)	-0.097	-0.157	-0.331
Wave Height (m)	0.273	0.341	0.732
Wave Period (sec)	2.8	3.5	2.3
Wave Length (m)	12.2	19.6	8.2
Steepness	1/45	1/57	1/11

Scale ratio:	Scaled wave heights (m):		
10	2.7	3.4	7.3
20.8	5.7	7.1	15.2
30	8.2	10.2	22.0
40	10.9	13.6	29.3
46.6	12.7	15.9	34.1

Figure 58. Wave characteristics at sonic probe 4, Phase II, Run 8

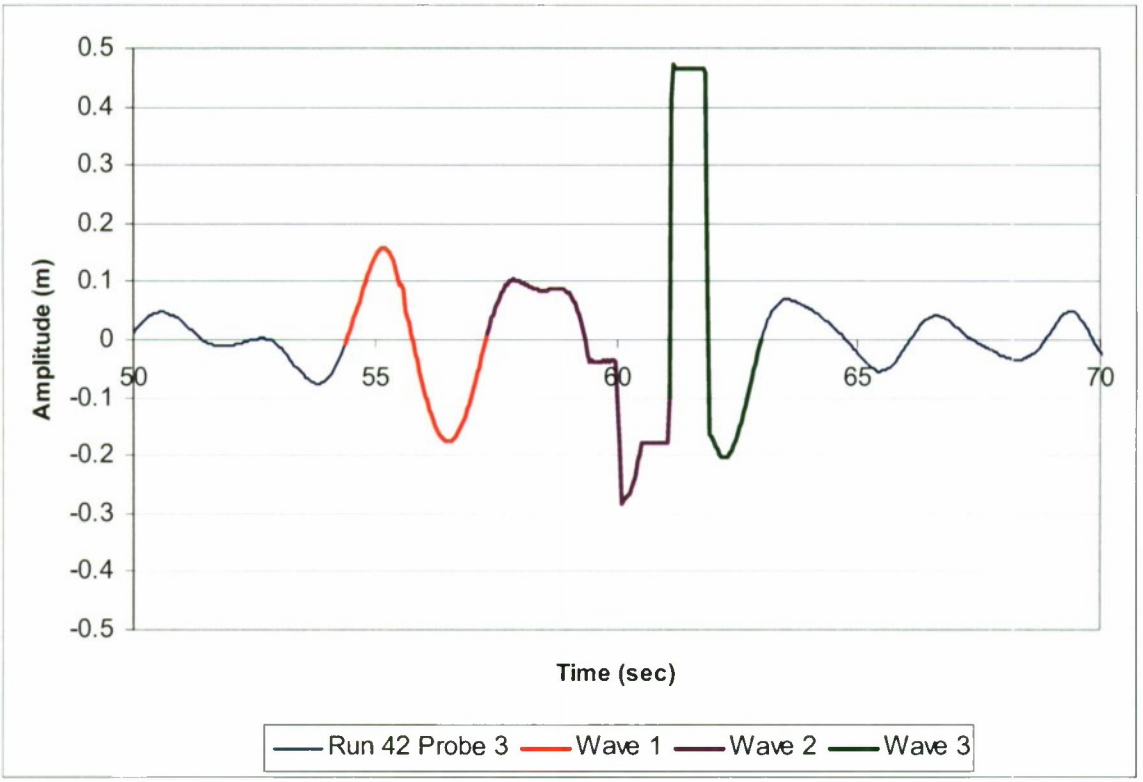

	Wave 1	Wave 2	Wave 3
Max Amplitude (m)	0.158	0.104	0.474
Min Amplitude (m)	-0.176	-0.282	-0.204
Wave Height (m)	0.334	0.386	0.678
Wave Period (sec)	3.0	3.7	1.8
Wave Length (m)	13.7	21.9	5.2
Steepness	1/50	1/57	1/9

Scale ratio:	Scaled wave heights (m):		
10	3.3	3.9	6.8
20.8	6.9	8.0	14.1
30	10.0	11.6	20.3
40	13.3	15.4	27.1
46.6	15.5	18.0	31.6

Figure 59. Wave characteristics at sonic probe 3, Phase II, Run 42

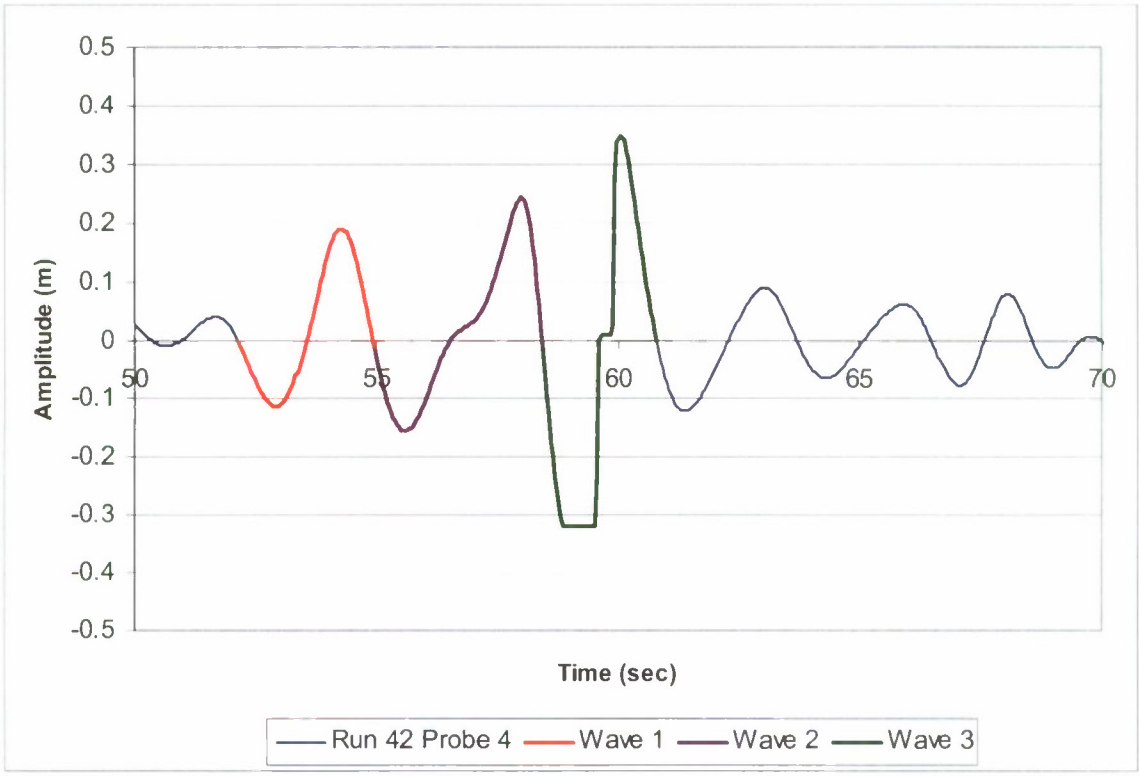

	Wave 1	Wave 2	Wave 3
Max Amplitude (m)	0.190	0.243	0.349
Min Amplitude (m)	-0.113	-0.154	-0.320
Wave Height (m)	0.304	0.398	0.669
Wave Period (sec)	2.8	3.5	2.3
Wave Length (m)	12.2	19.1	8.5
Steepness	1/40	1/48	1/13

Scale ratio:	Scaled wave heights (m):		
10	3.0	4.0	6.7
20.8	6.3	8.3	13.9
30	9.1	11.9	20.1
40	12.1	15.9	26.8
46.6	14.1	18.5	31.2

Figure 60. Wave characteristics at sonic probe 4, Phase II, Run 42

This page intentionally left blank

Appendix C: Senix Results— Irregular Waves

Results from the Phase II testing, with embedded wave groups in irregular waves, are shown in this Appendix. The results include Senix probe time-histories and analysis of the wave group characteristics.

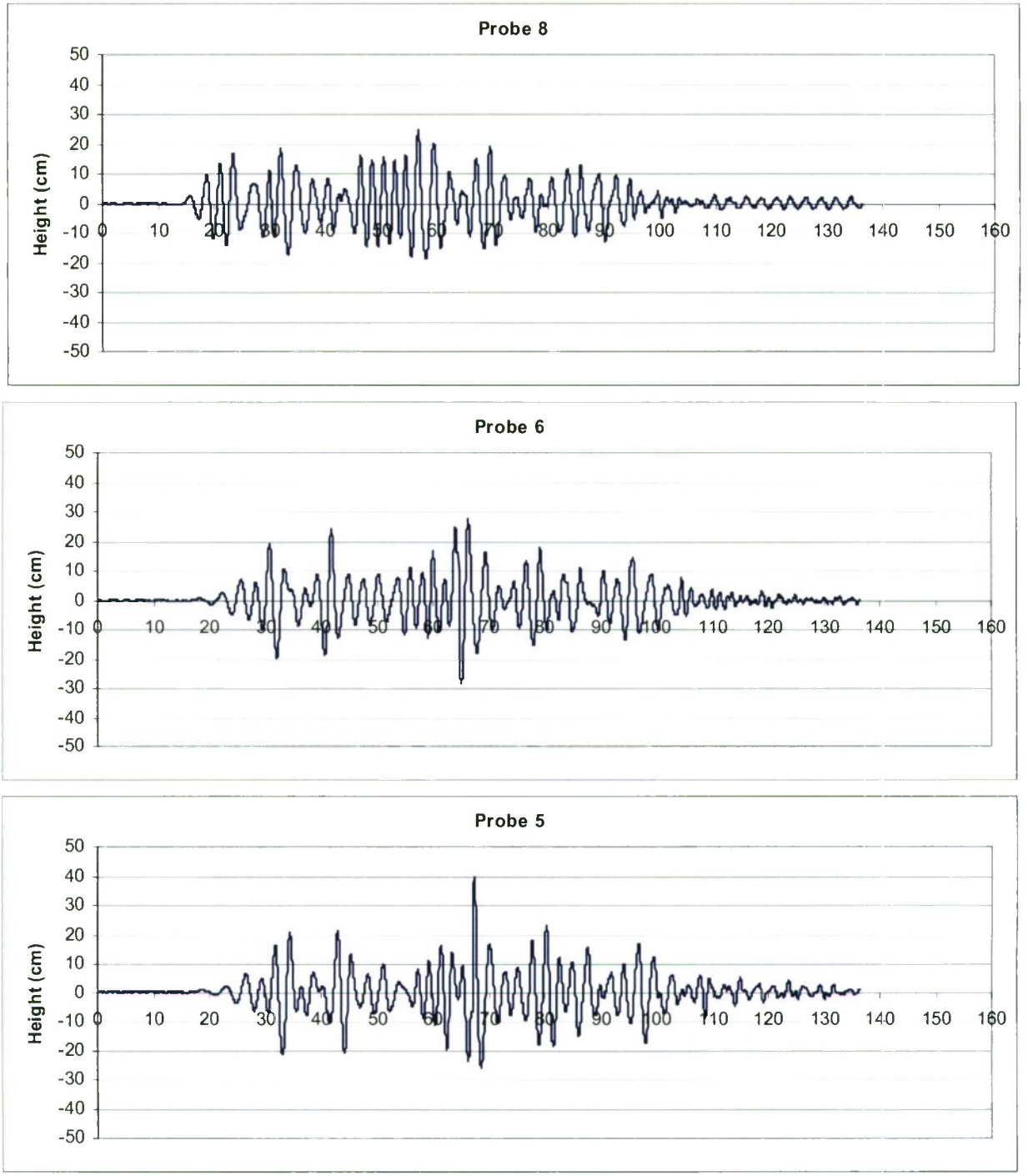

Figure 61. Measured wave time-history of sonic probes 8 (closest to wave-maker) to 1 (closest to the beach), Phase II, Run 11

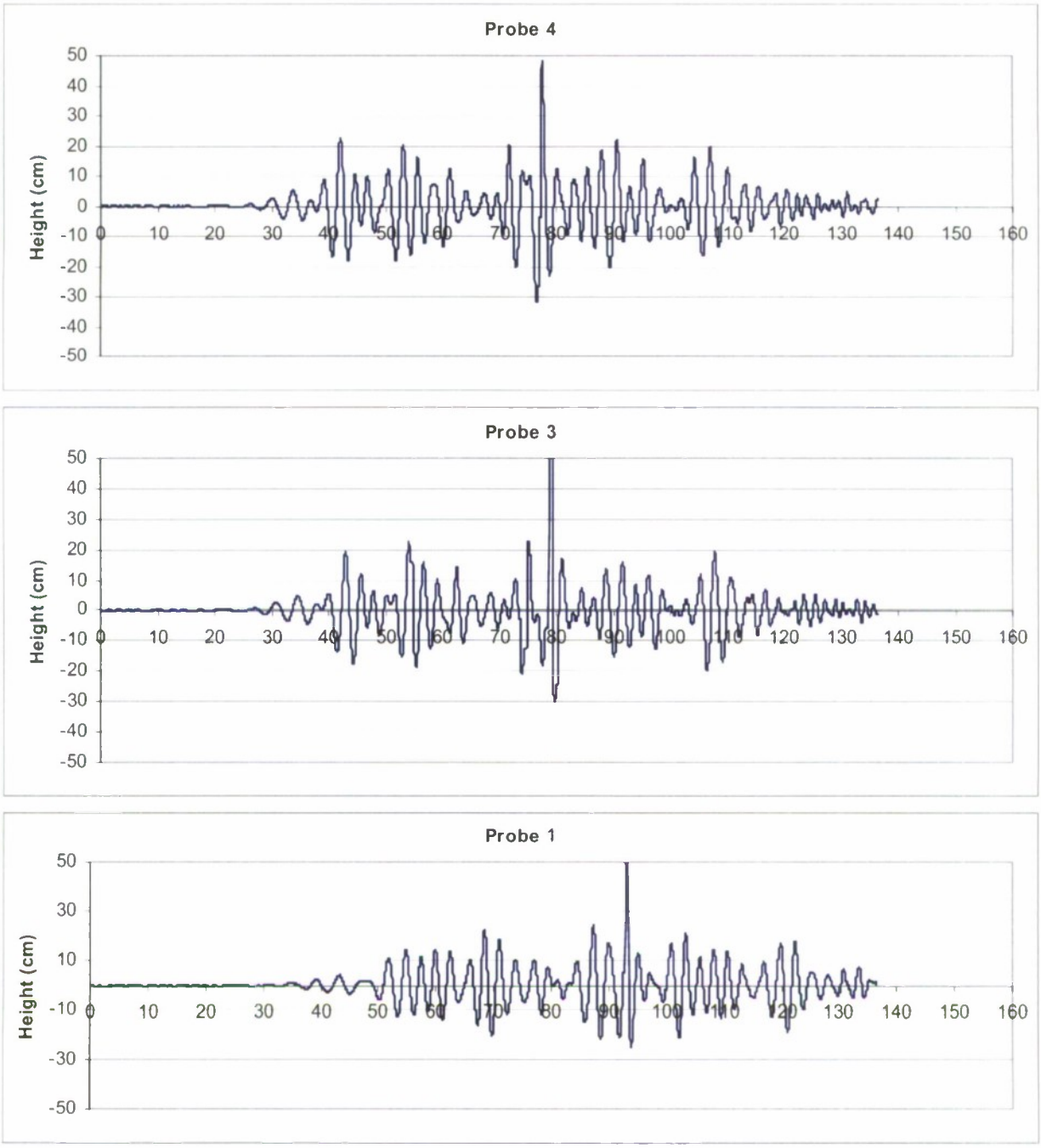

Figure 61 (continued)

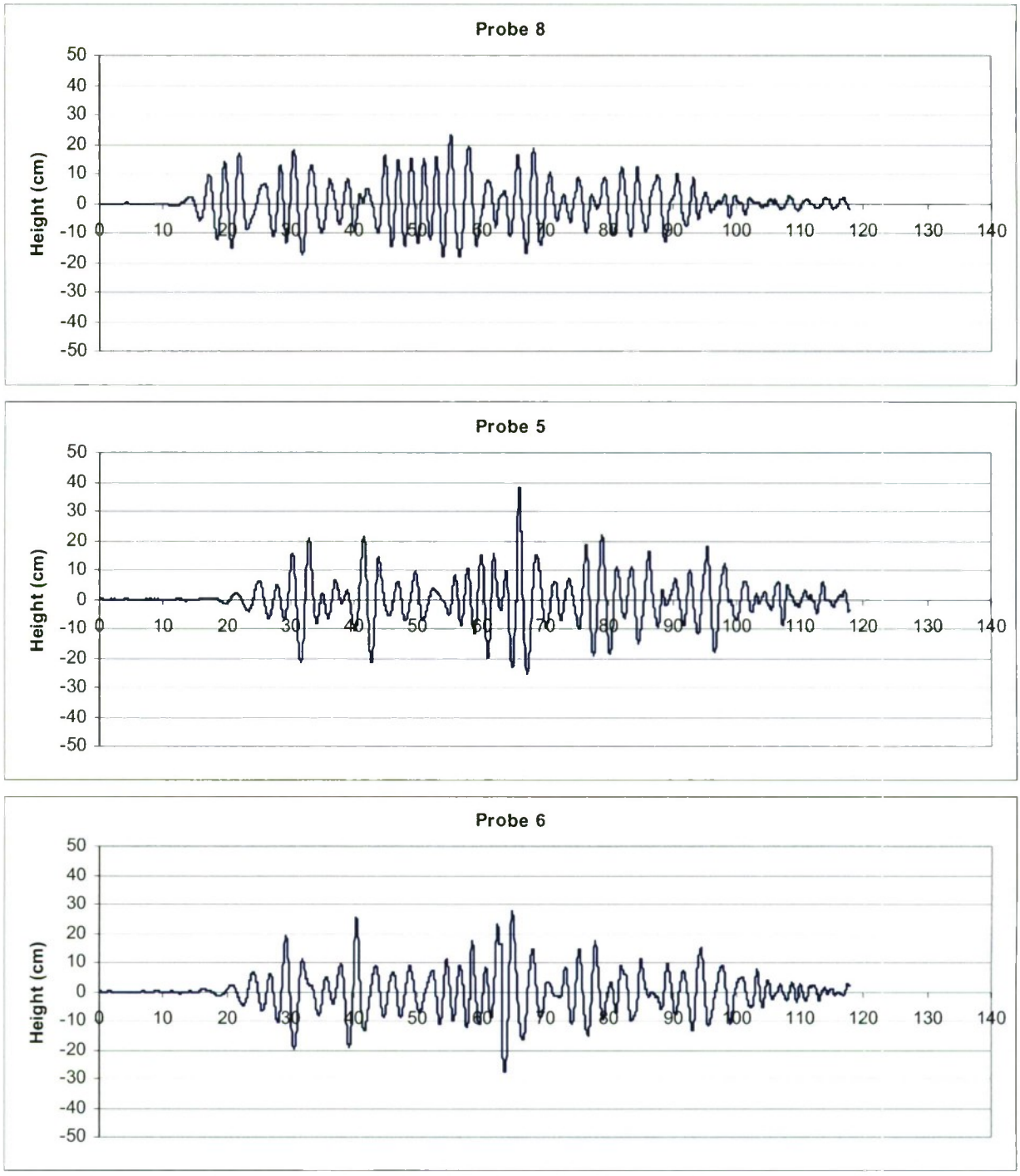

Figure 62. Measured wave time-history of sonic probes 8 (closest to wave-maker) to 1 (closest to the beach), Phase II, Run 14

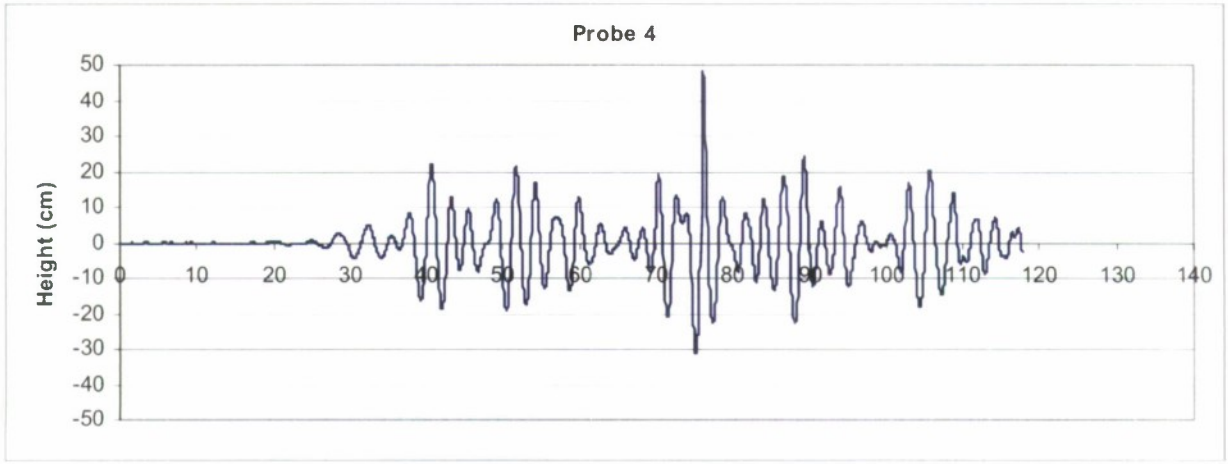

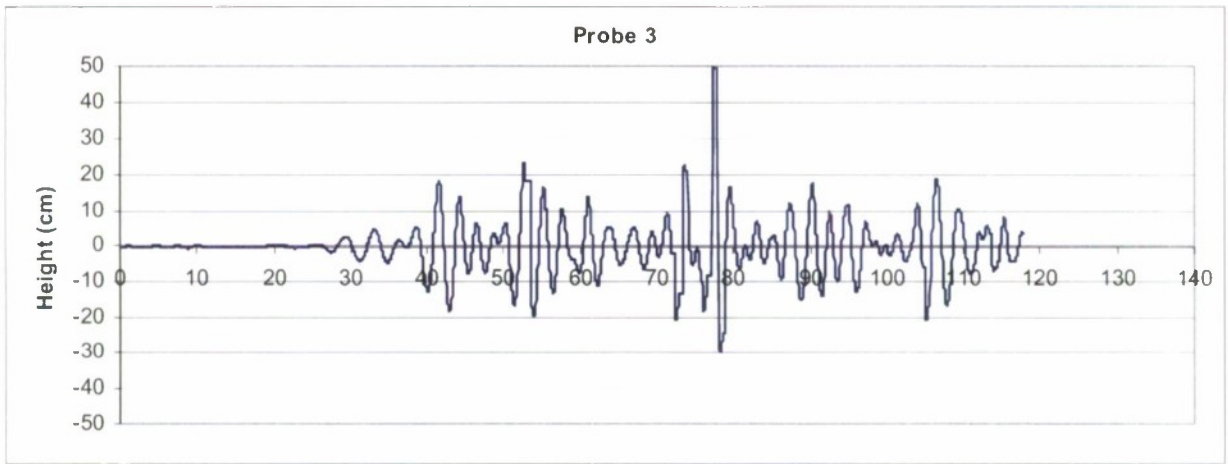

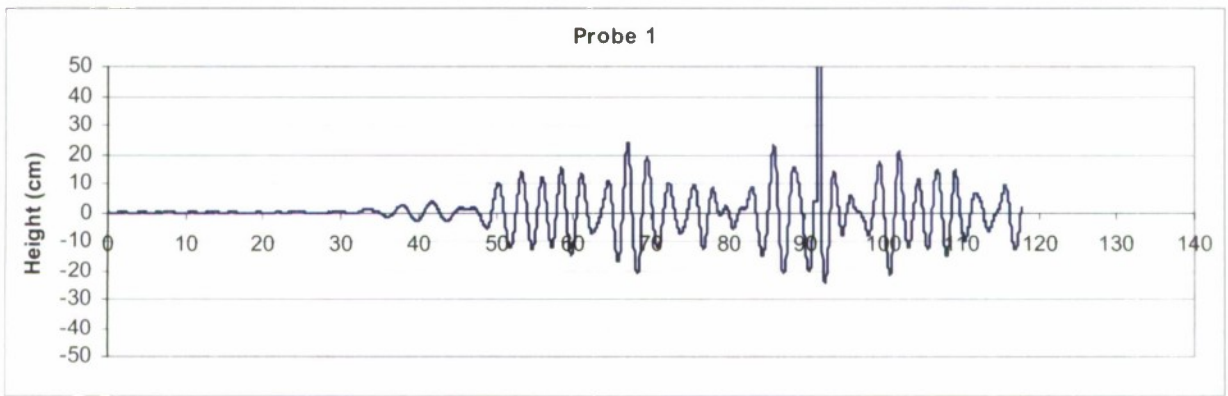

Figure 62 (continued)

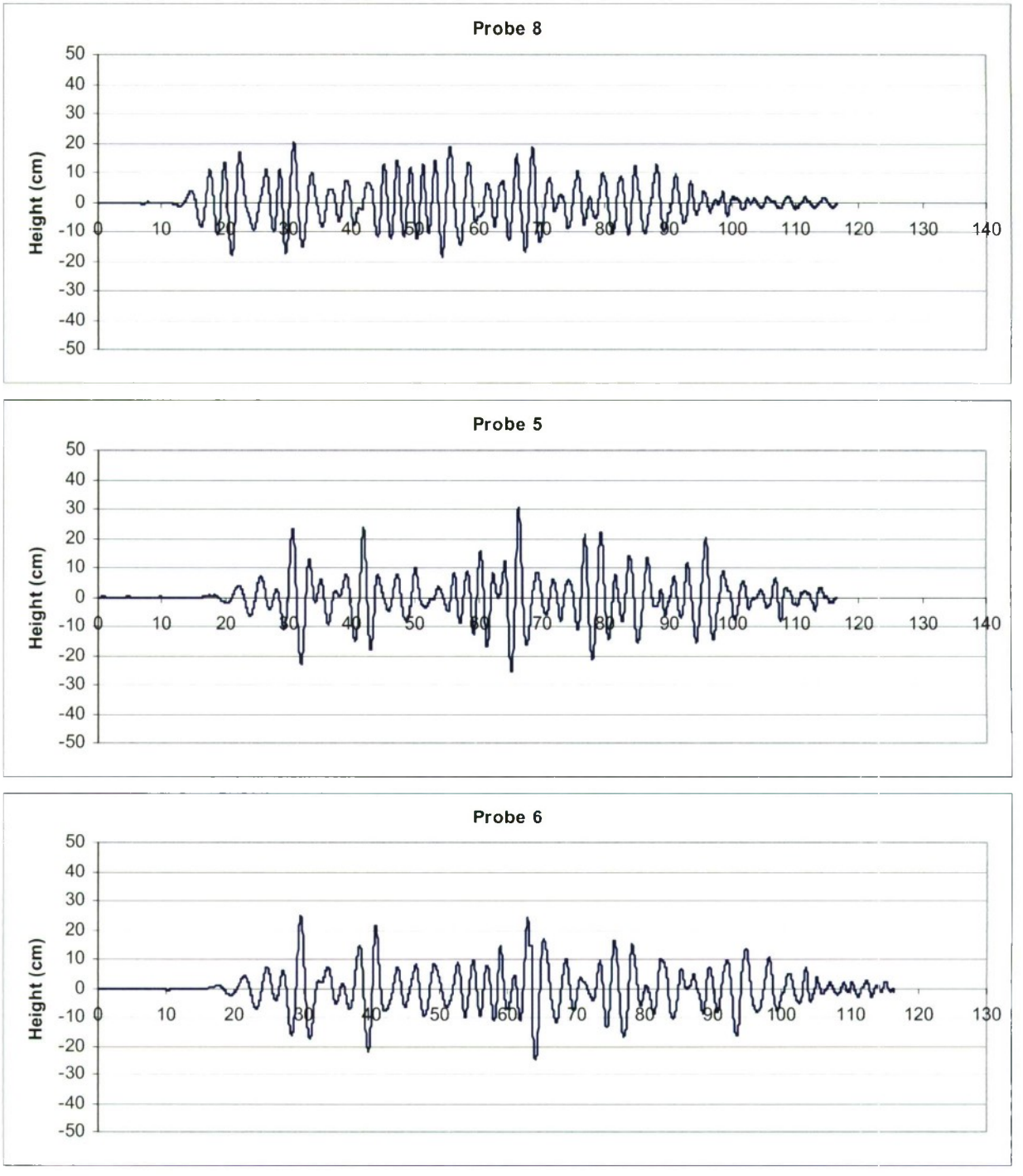

Figure 63. Measured wave time-history of sonic probes 8 (closest to wave-maker) to 1 (closest to the beach), Phase II, Run 21

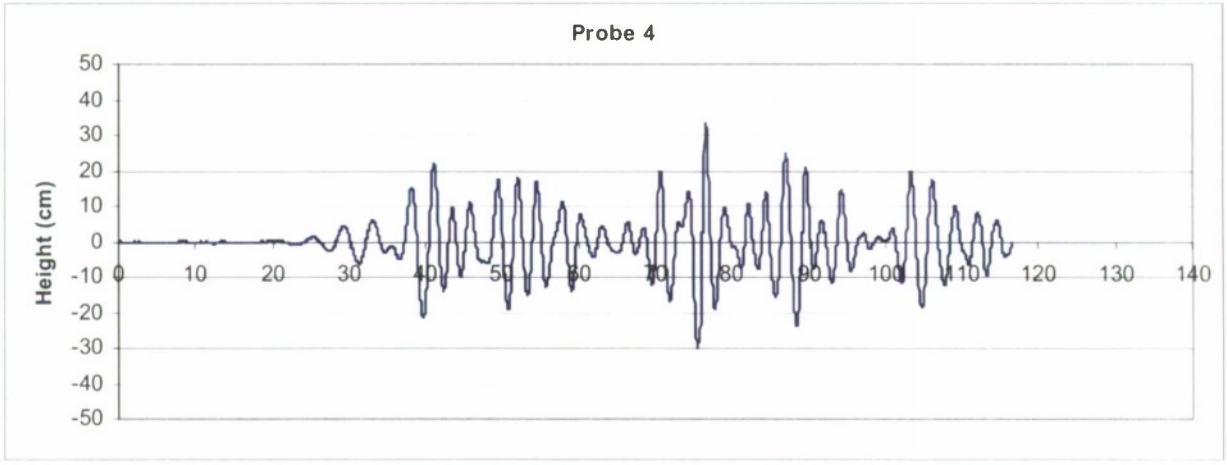

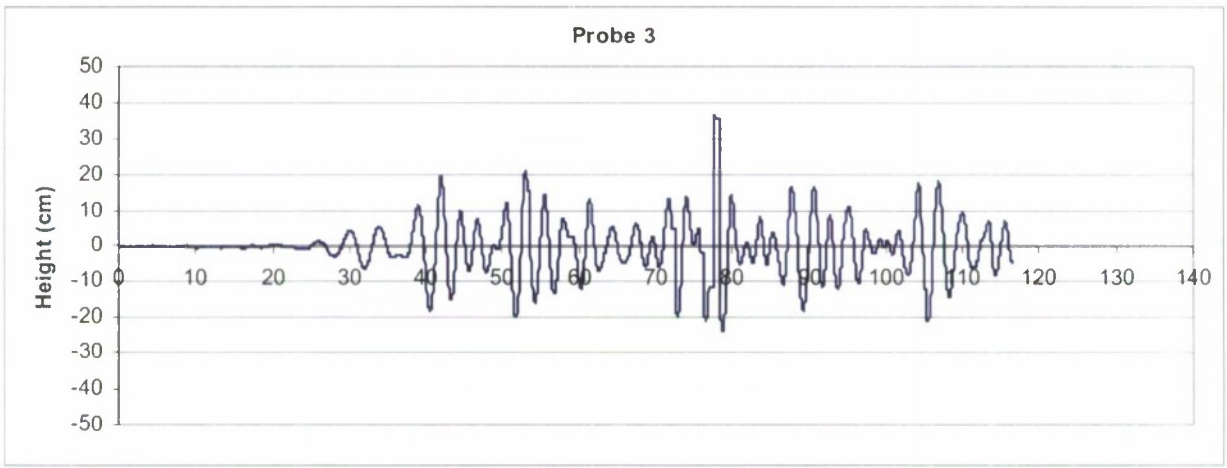

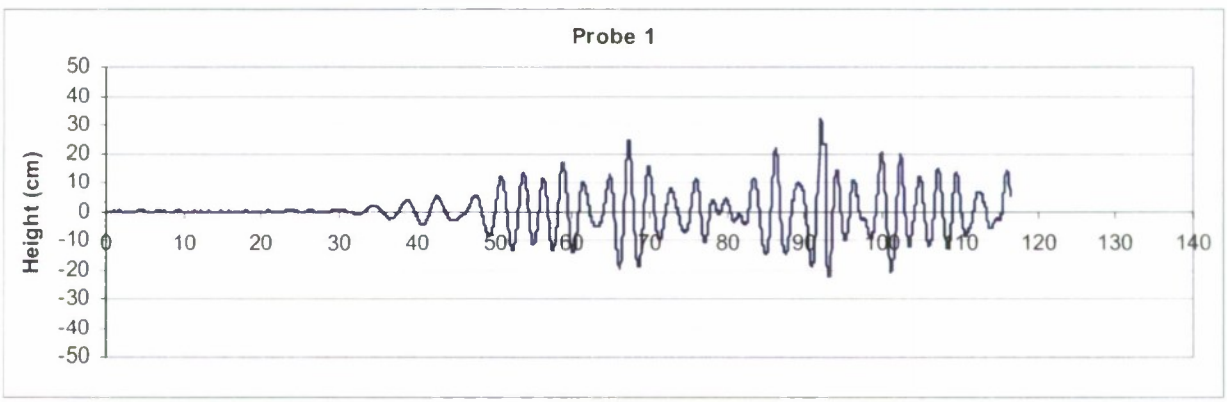

Figure 63 (continued)

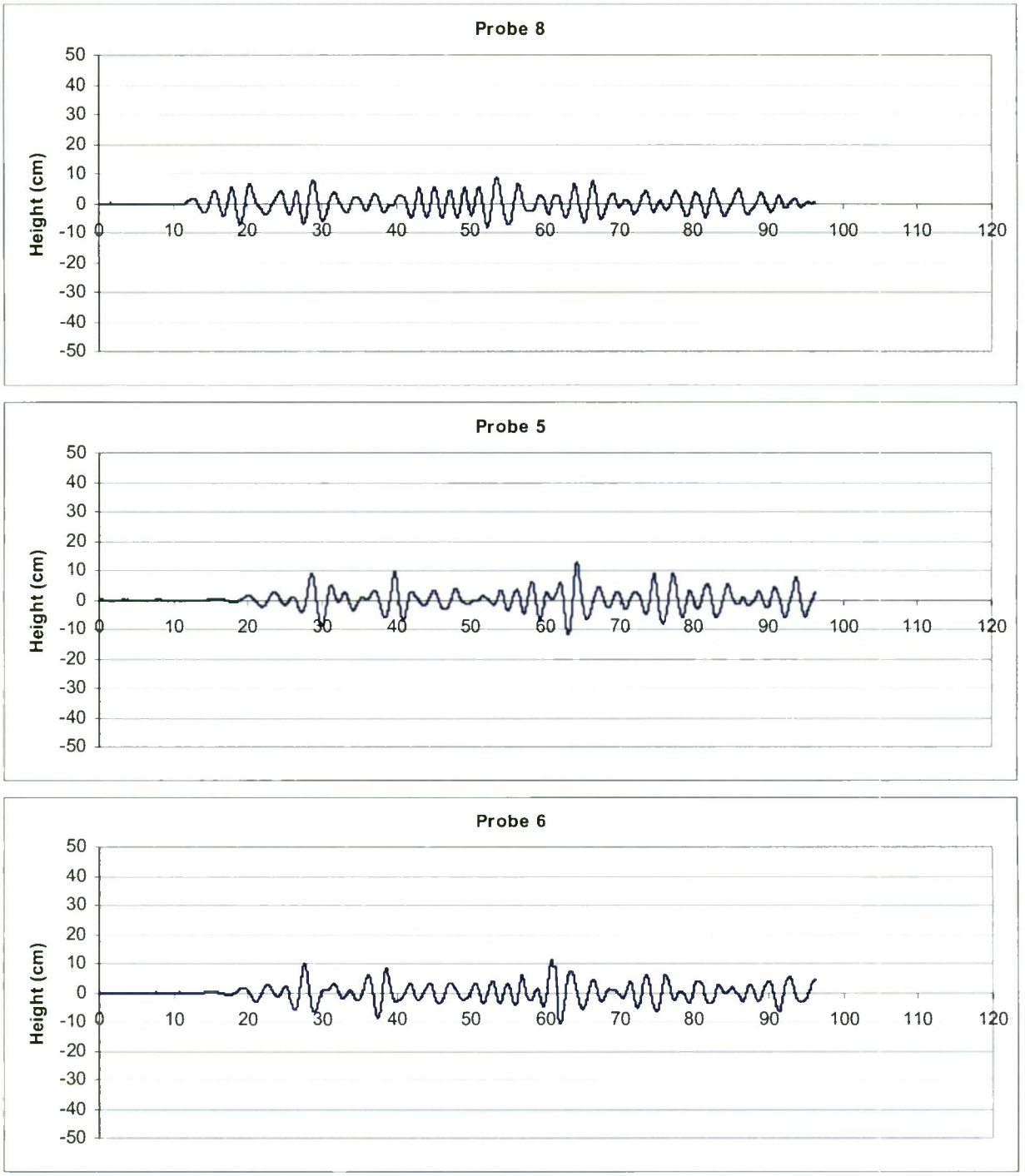

Figure 64. Measured wave time-history of sonic probes 8 (closest to wave-maker) to 1 (closest to the beach), Phase II, Run 22

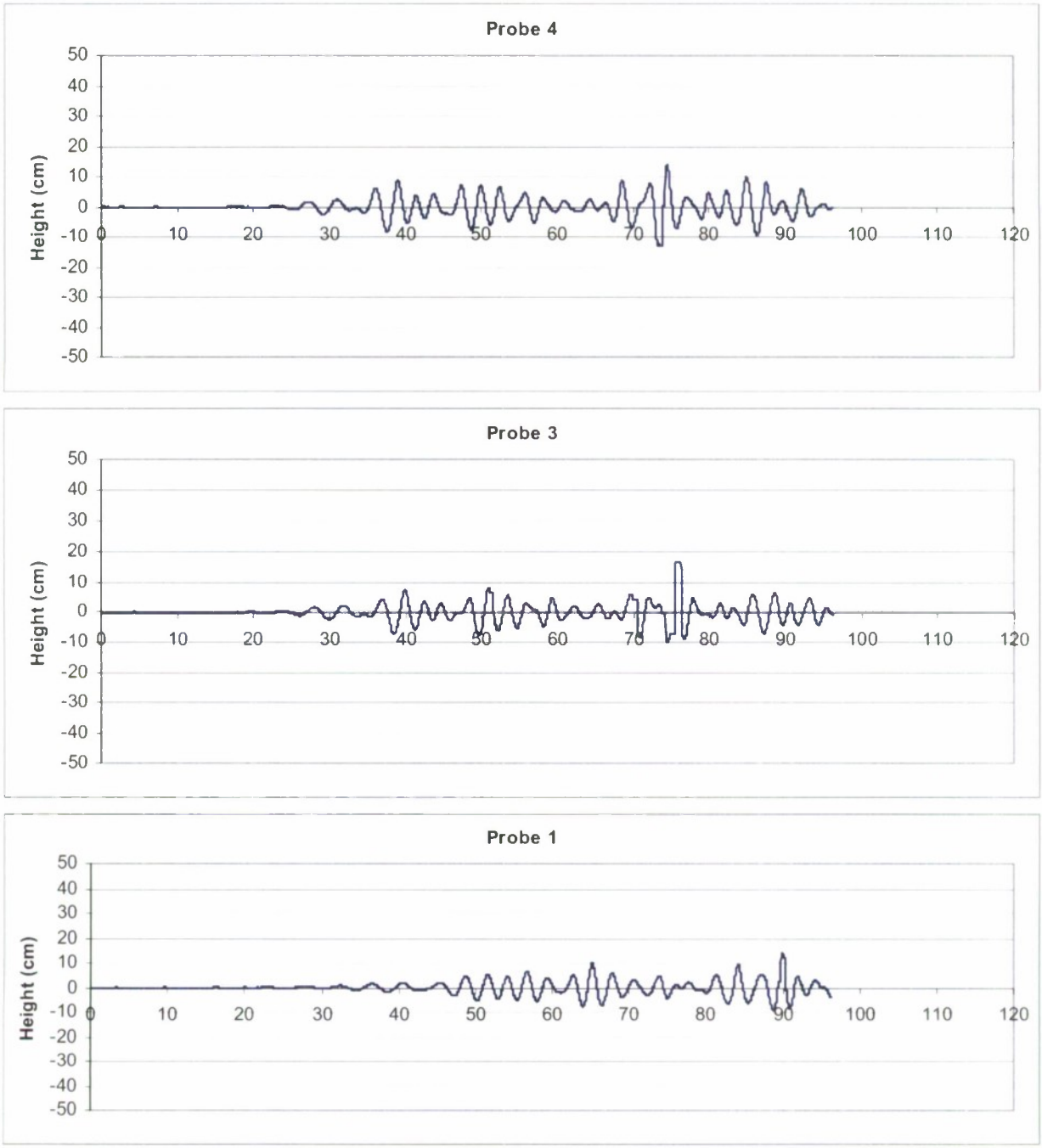

Figure 64 (continued)

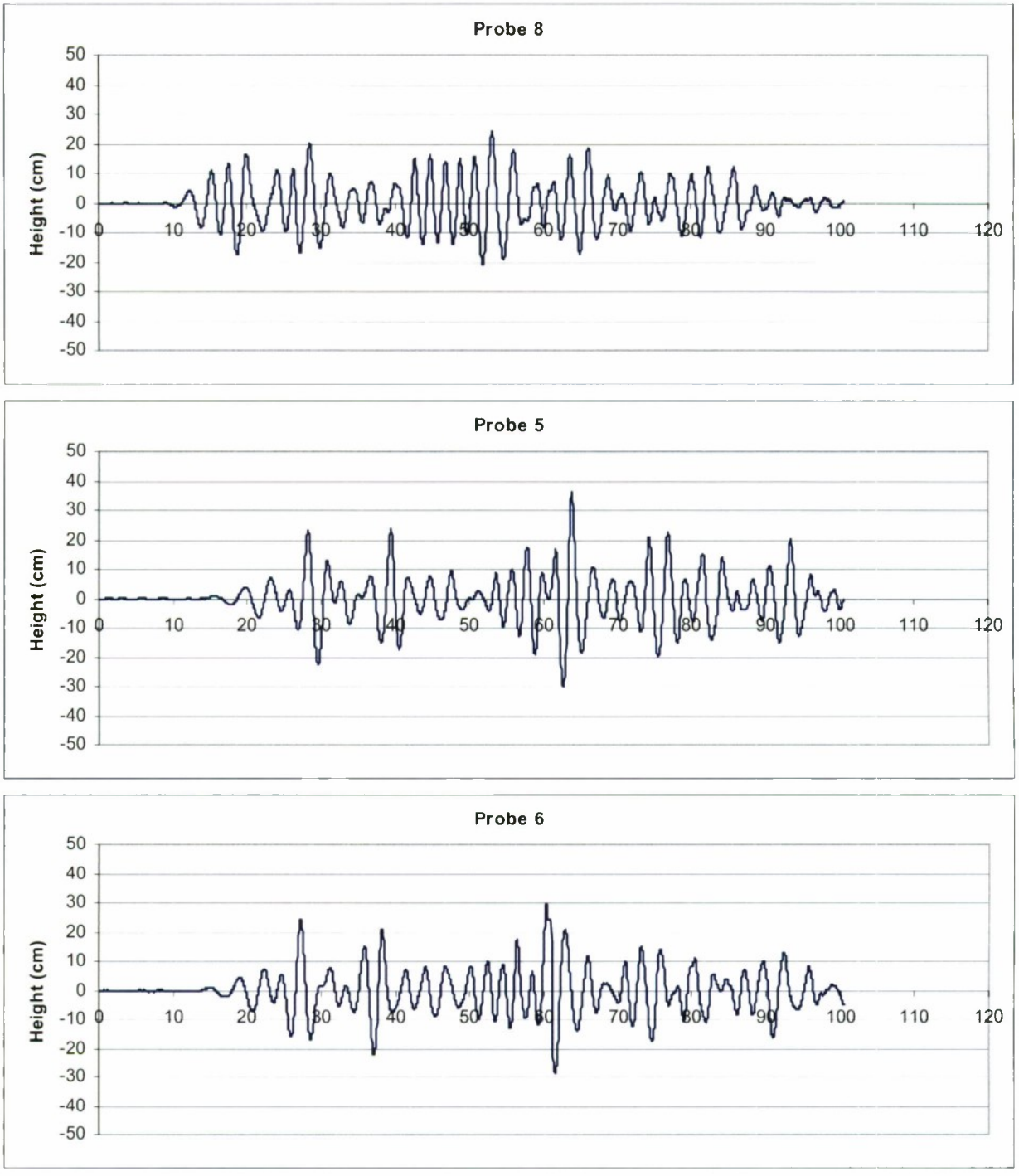

Figure 65. Measured wave time-history of sonic probes 8 (closest to wave-maker) to 1 (closest to the beach), Phase II, Run 24

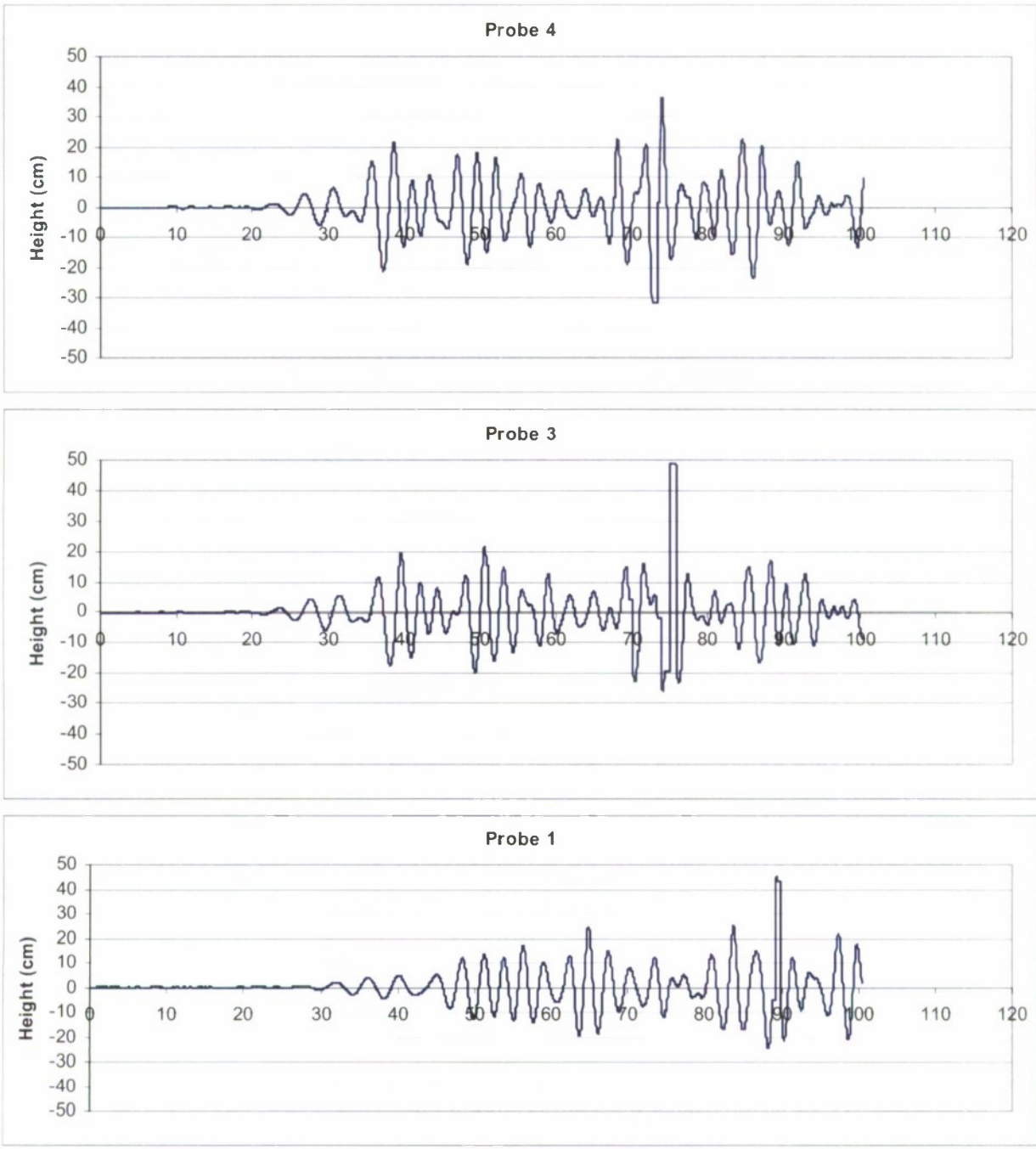

Figure 65 (continued)

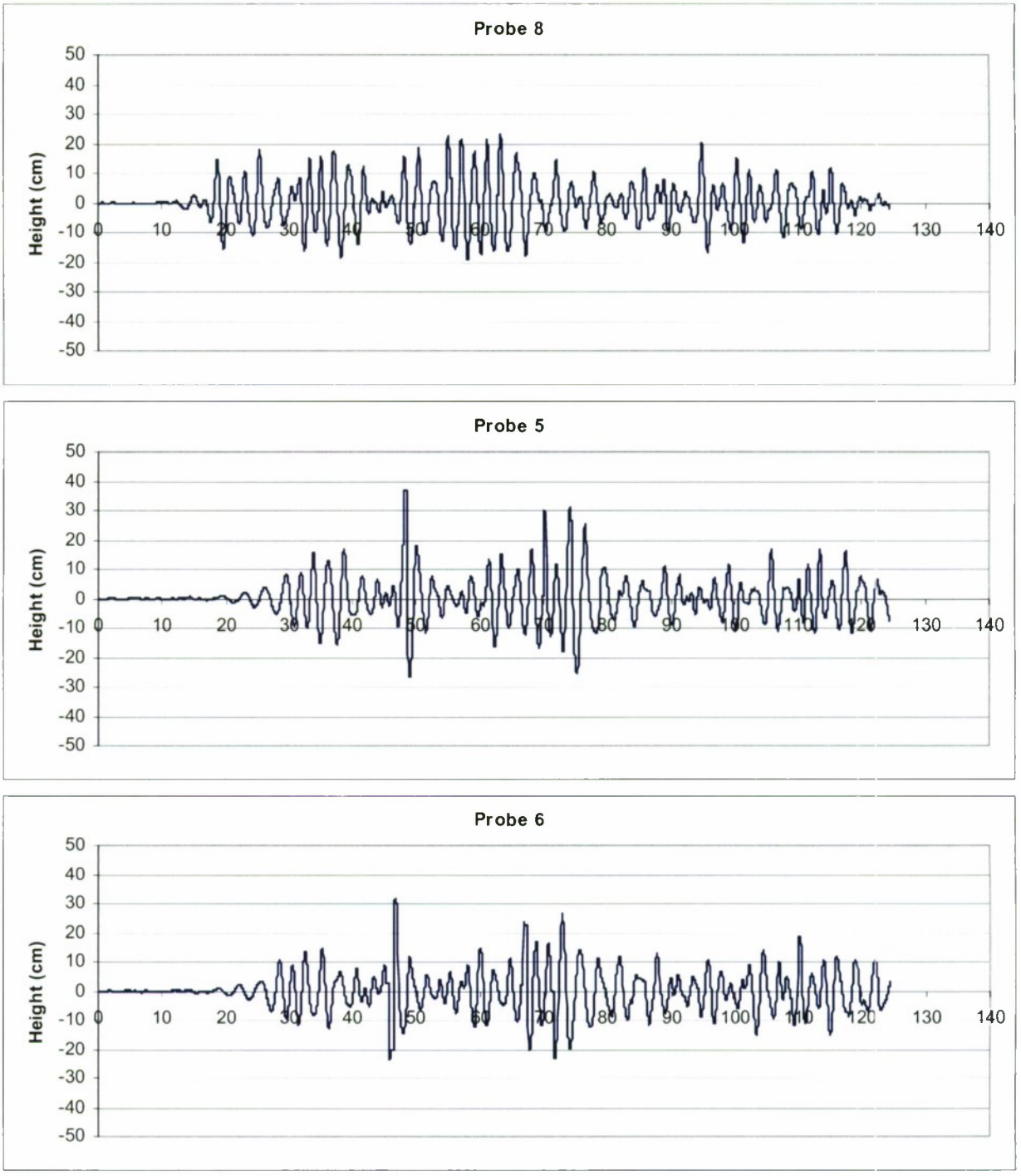

Figure 66. Measured wave time-history of sonic probes 8 (closest to wave-maker) to 1 (closest to the beach), Phase II, Run 26

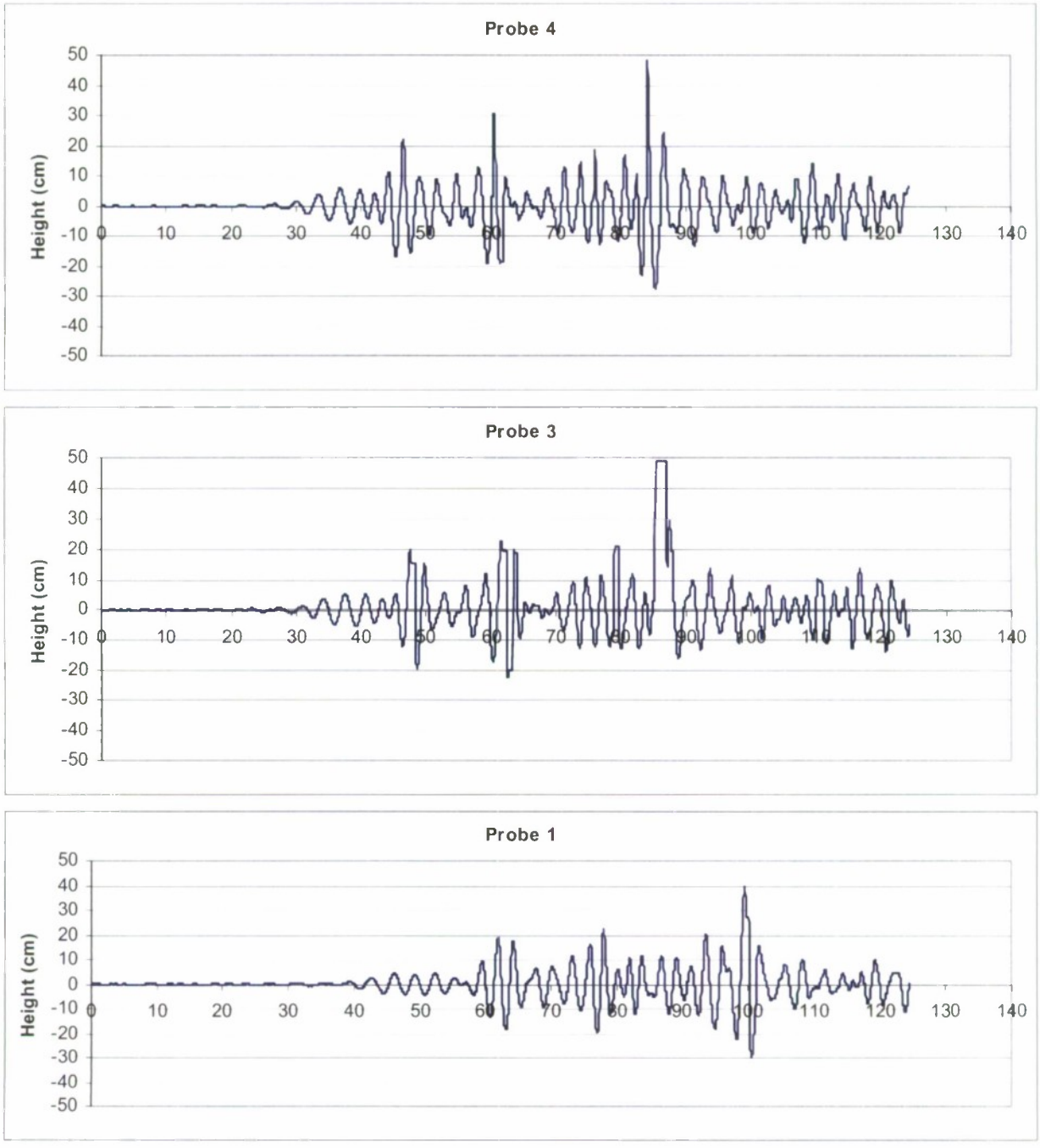

Figure 66 (continued)

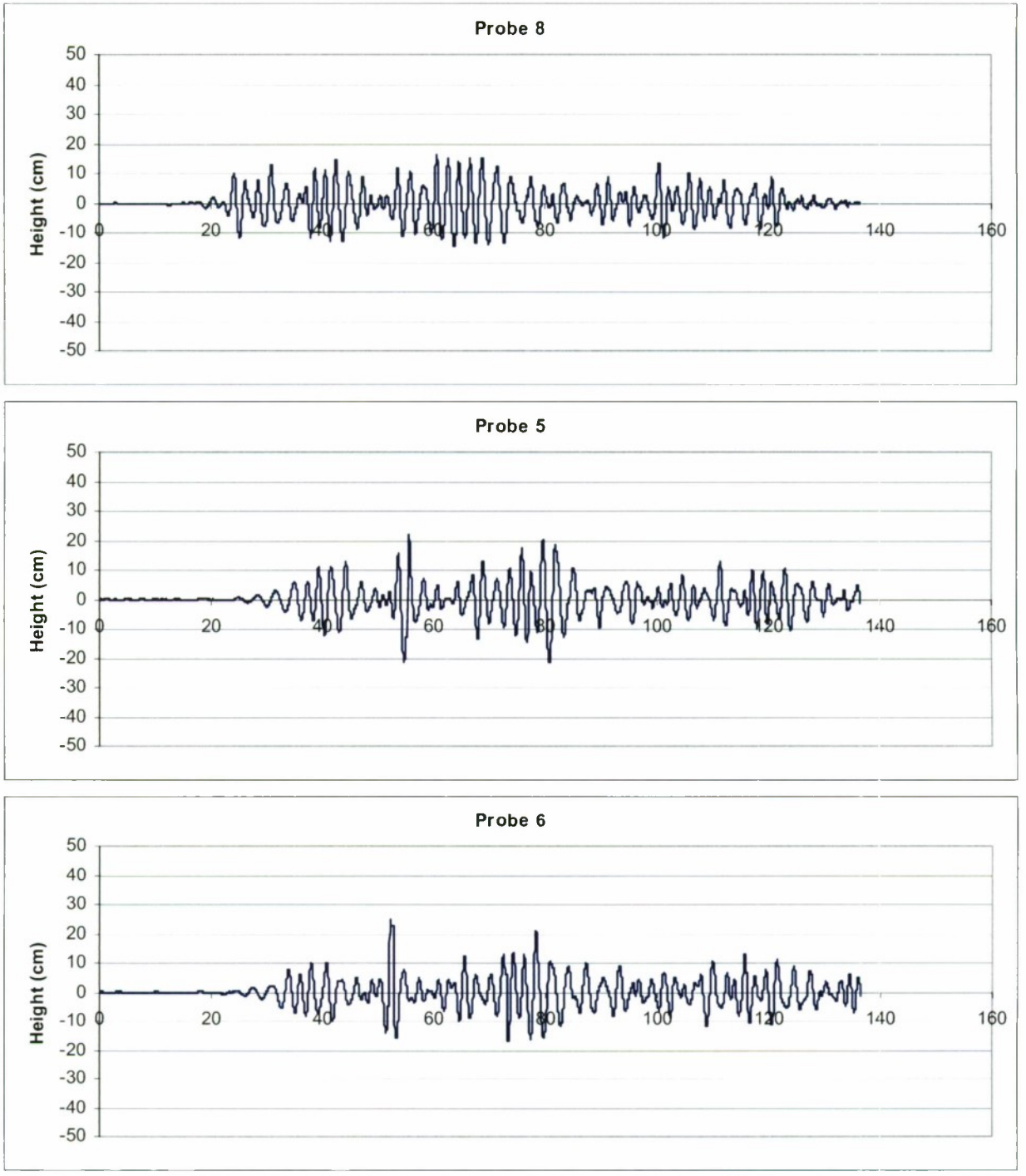

Figure 67. Measured wave time-history of sonic probes 8 (closest to wave-maker) to 1 (closest to the beach), Phase II, Run 27

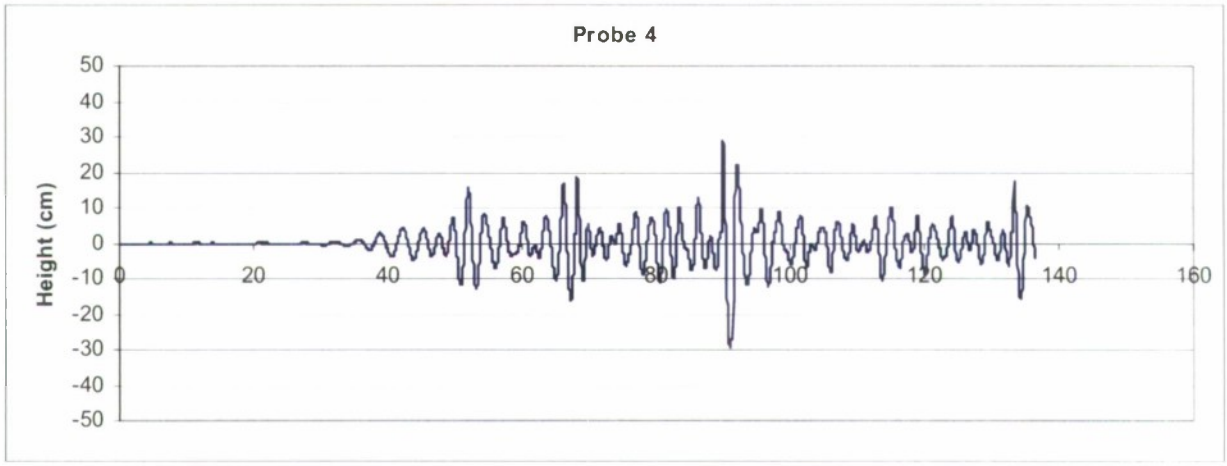

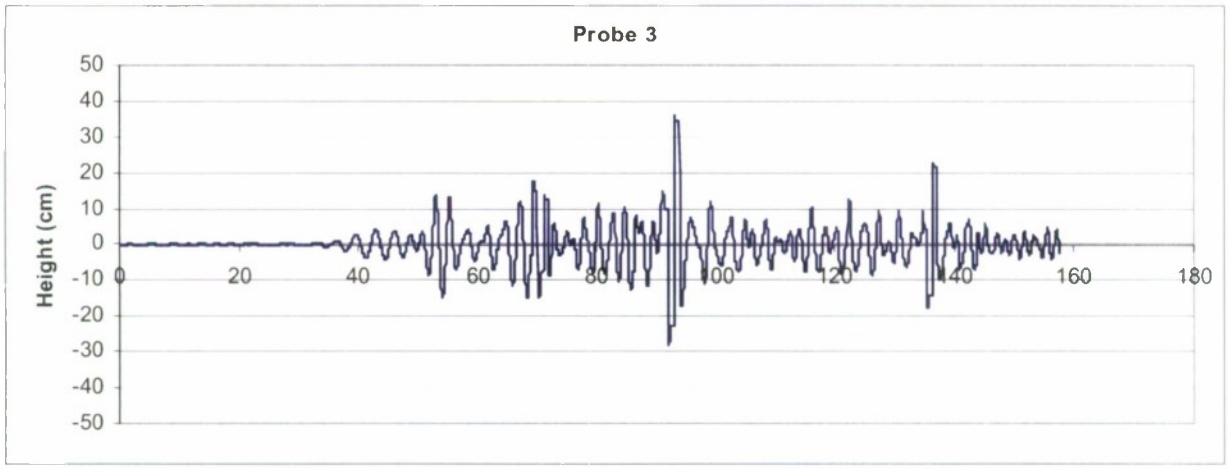

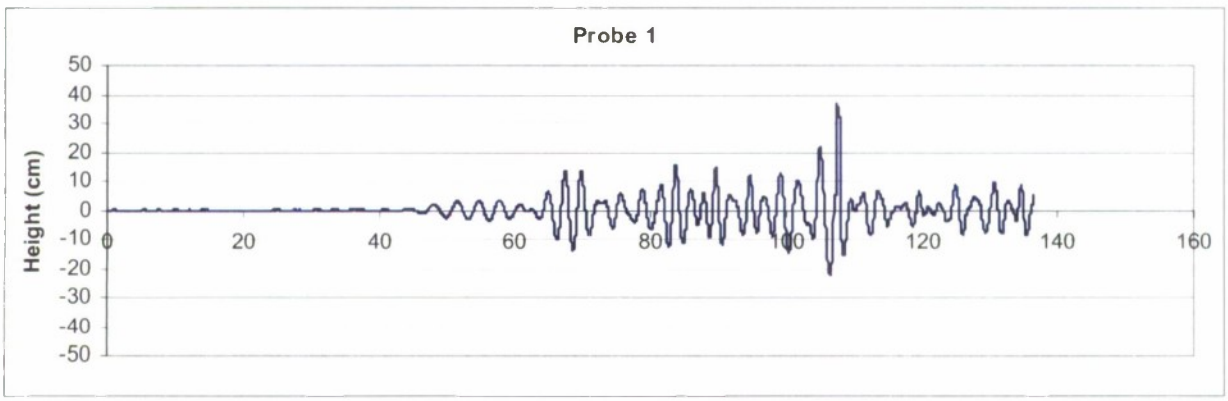

Figure 67 (continued)

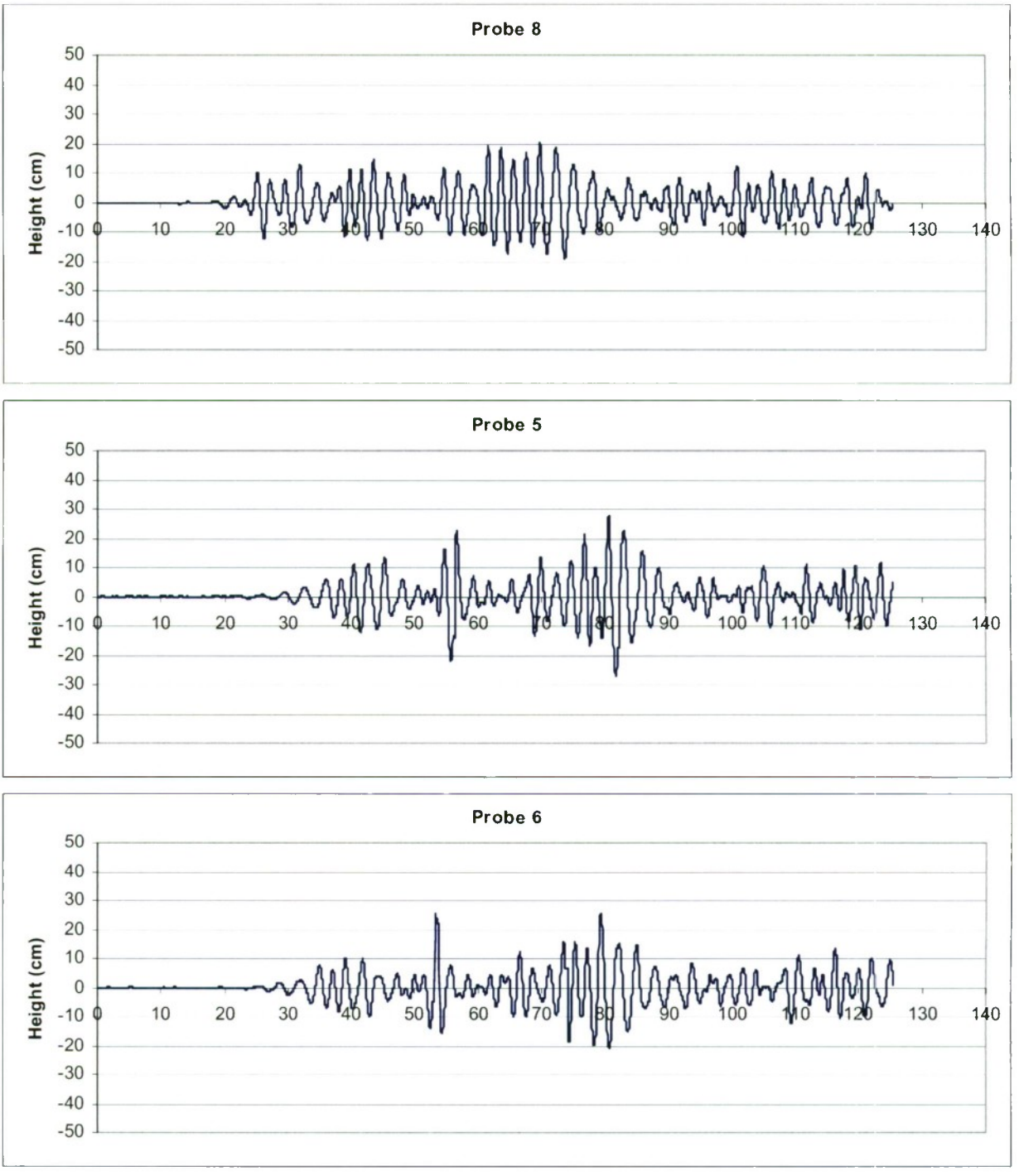

Figure 68. Measured wave time-history of sonic probes 8 (closest to wave-maker) to 1 (closest to the beach), Phase II, Run 28

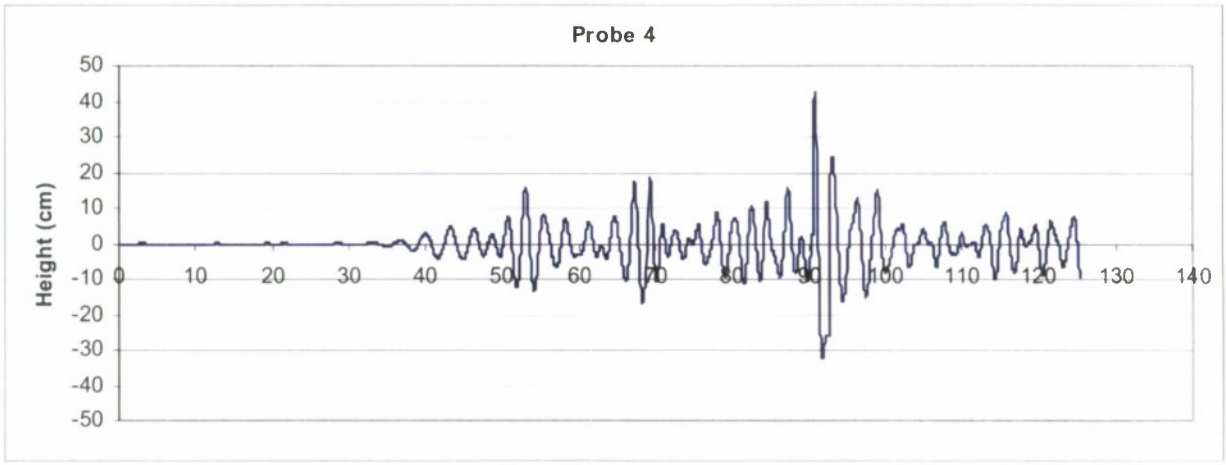

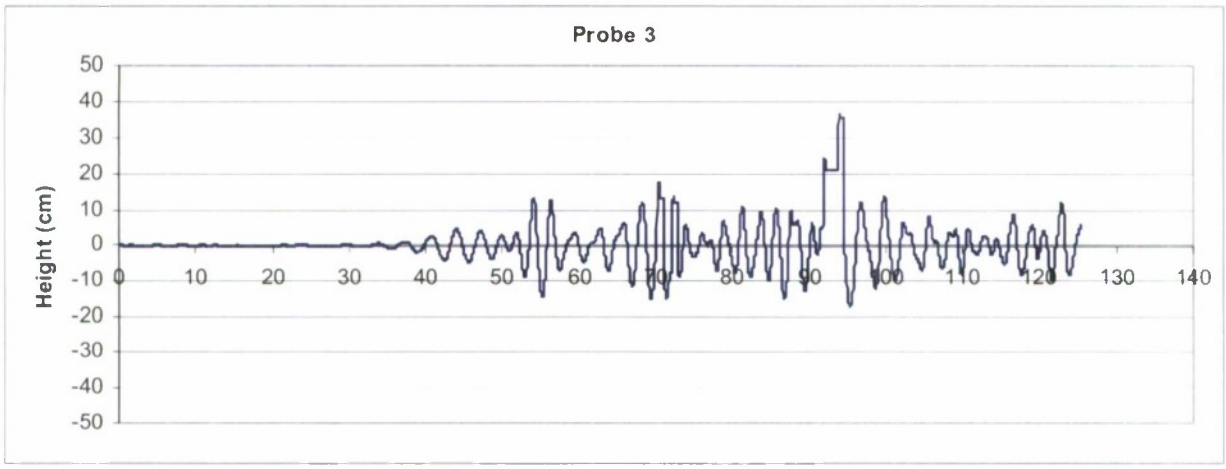

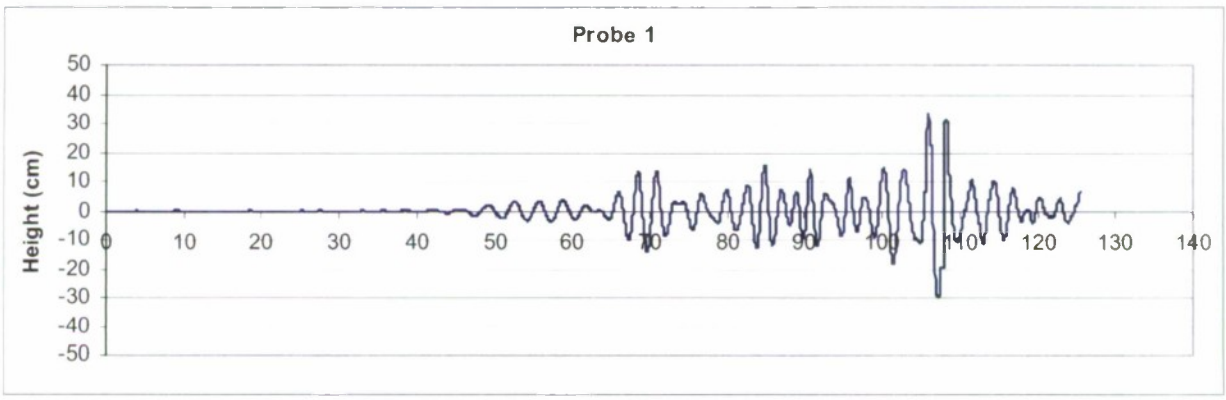

Figure 68 (continued)

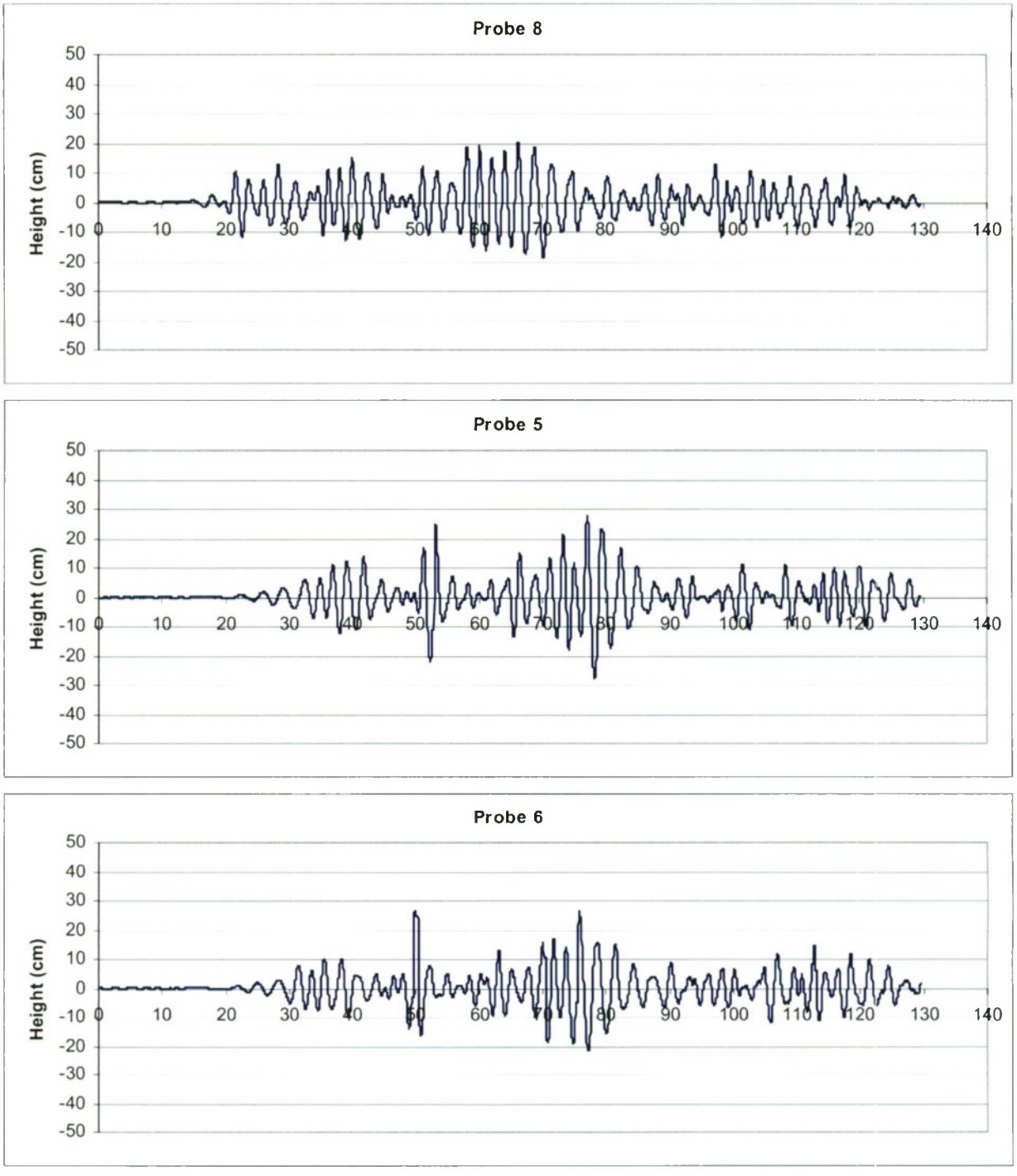

Figure 69. Measured wave time-history of sonic probes 8 (closest to wave-maker) to 1 (closest to the beach), Phase II, Run 30

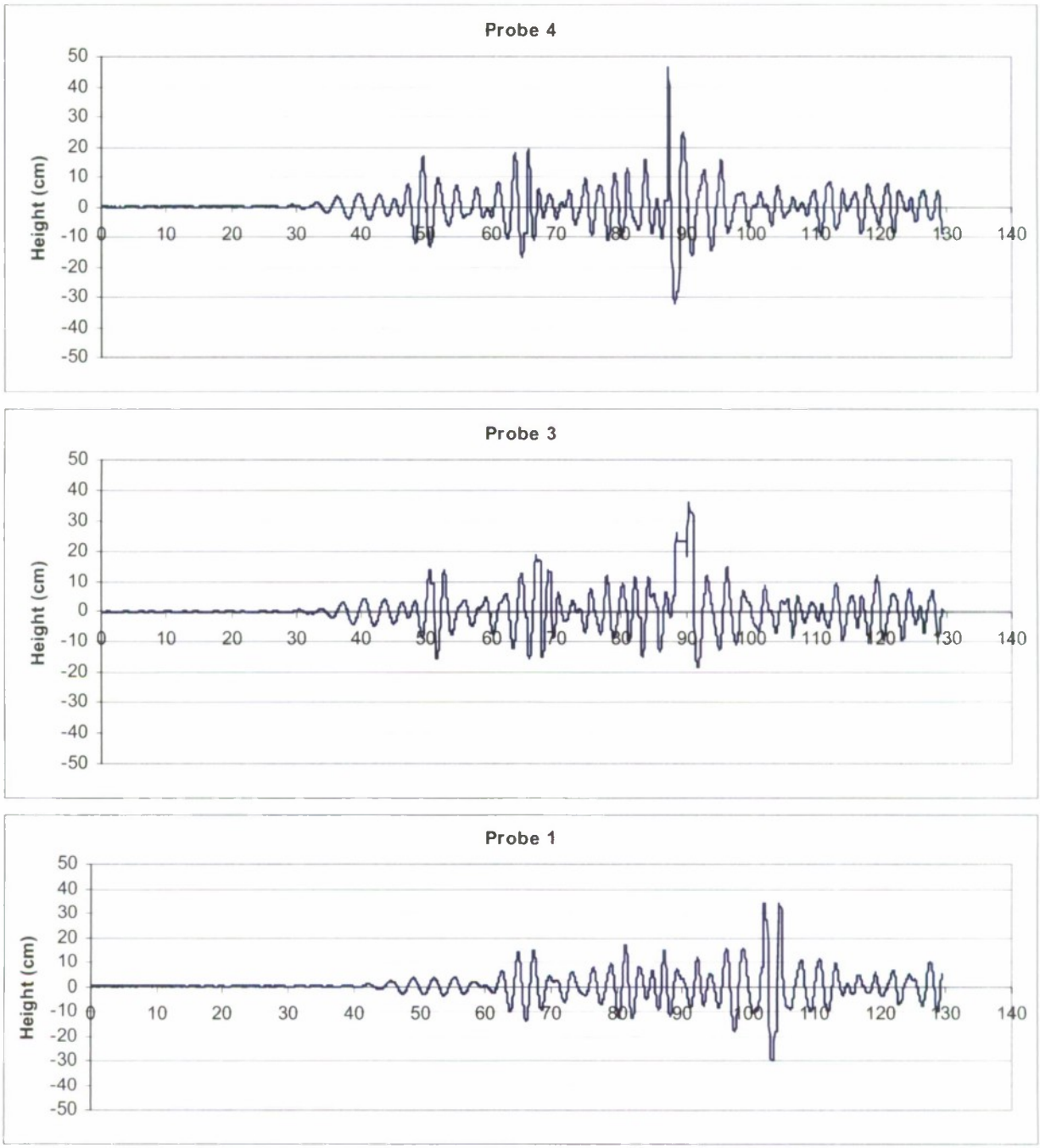

Figure 69 (continued)

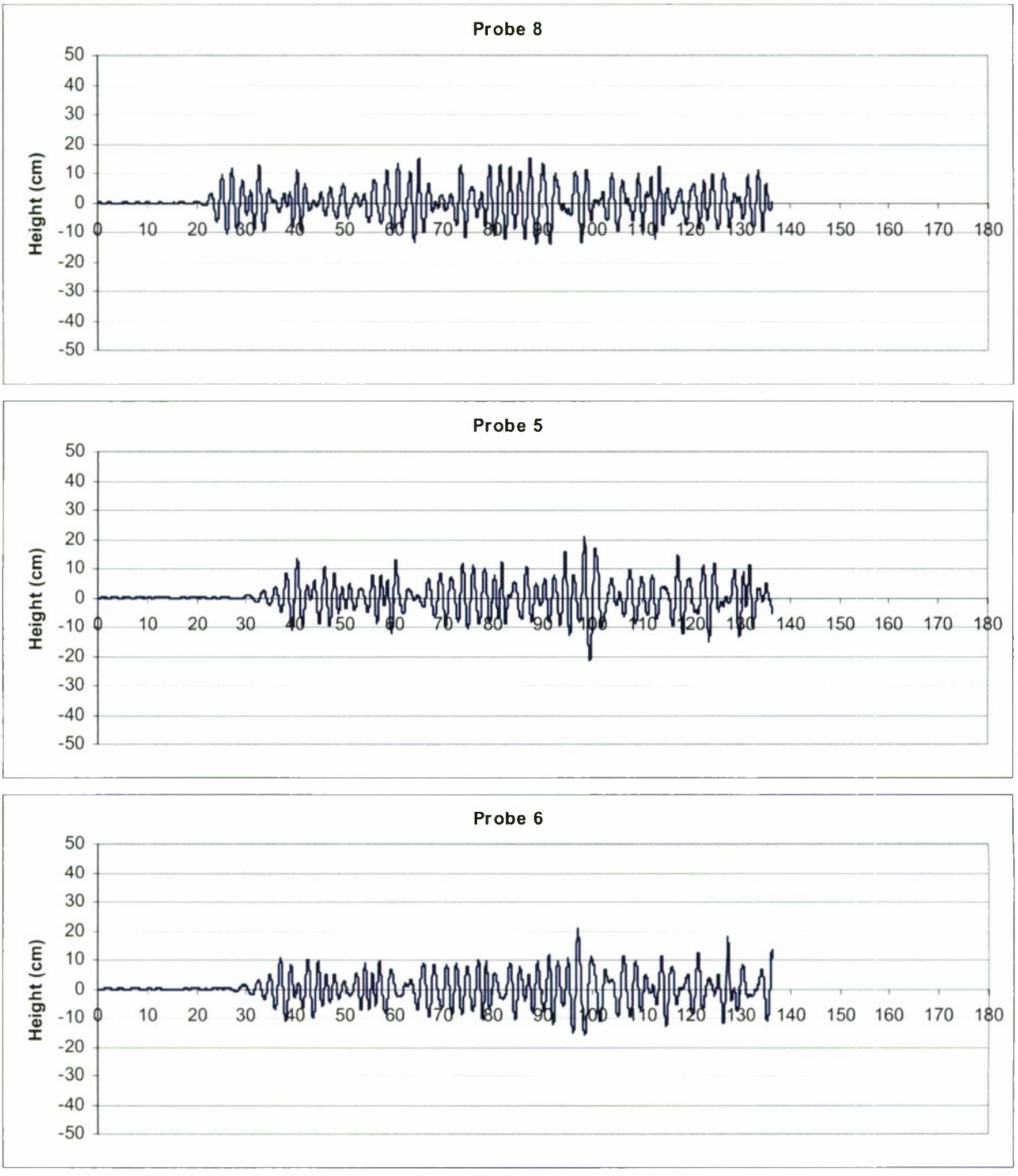

Figure 70. Measured wave time-history of sonic probes 8 (closest to wave-maker) to 1 (closest to the beach), Phase II, Run 41

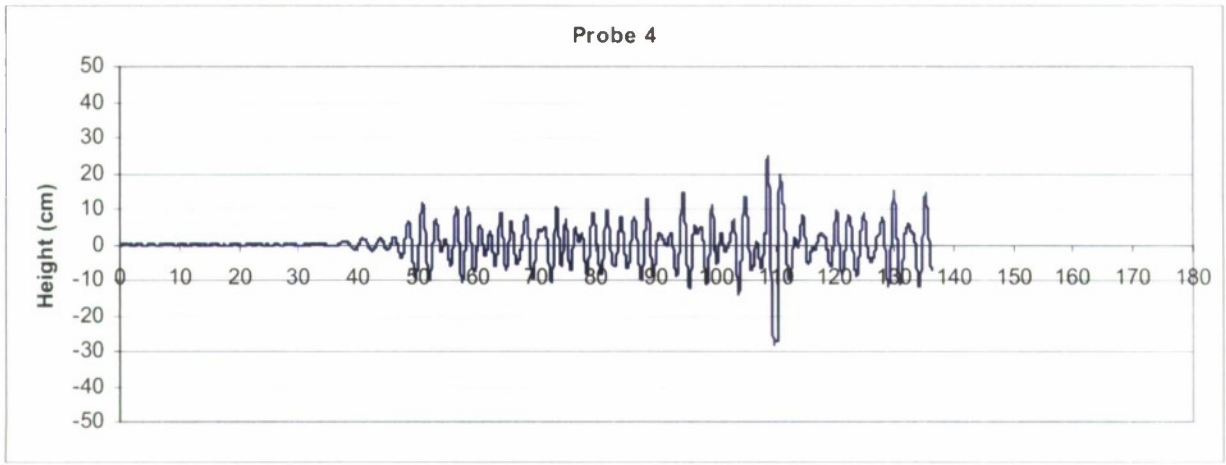

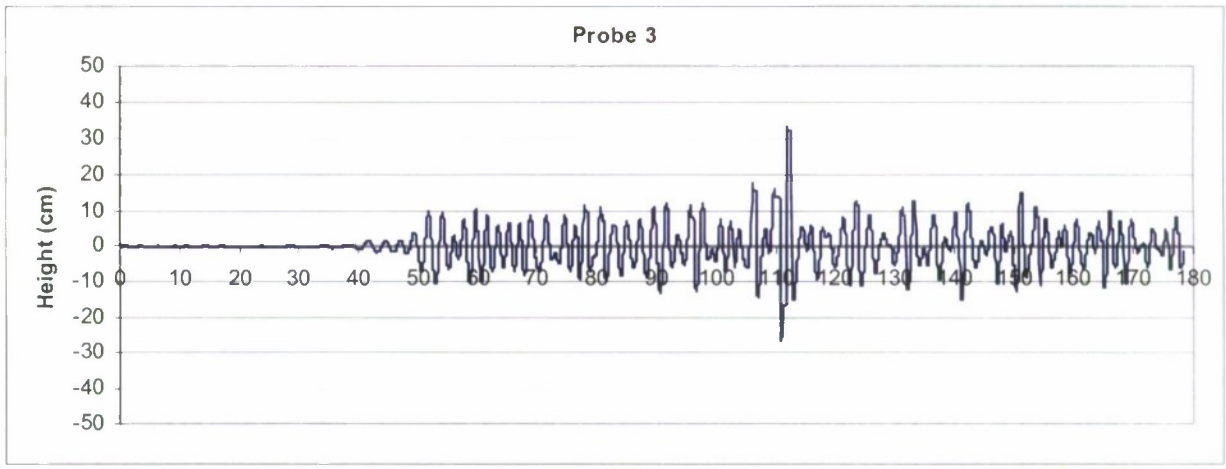

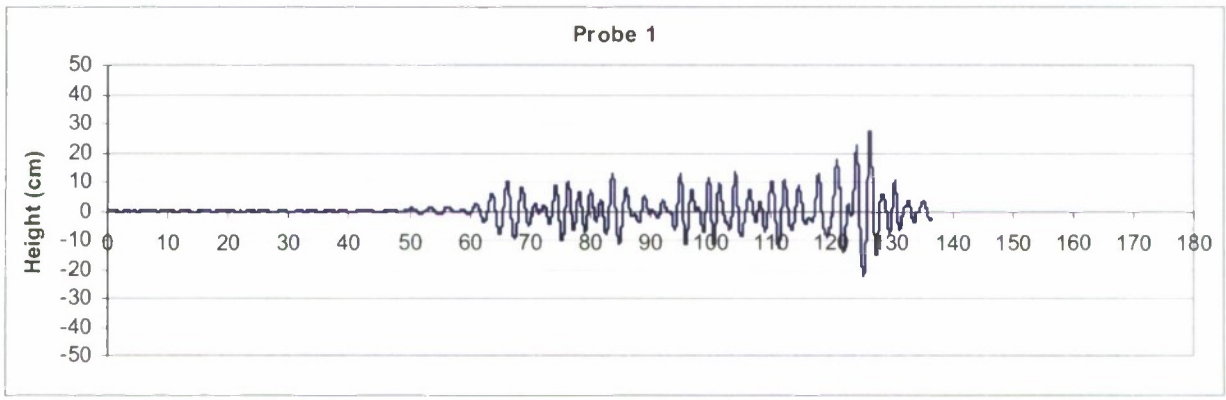

Figure 70 (continued)

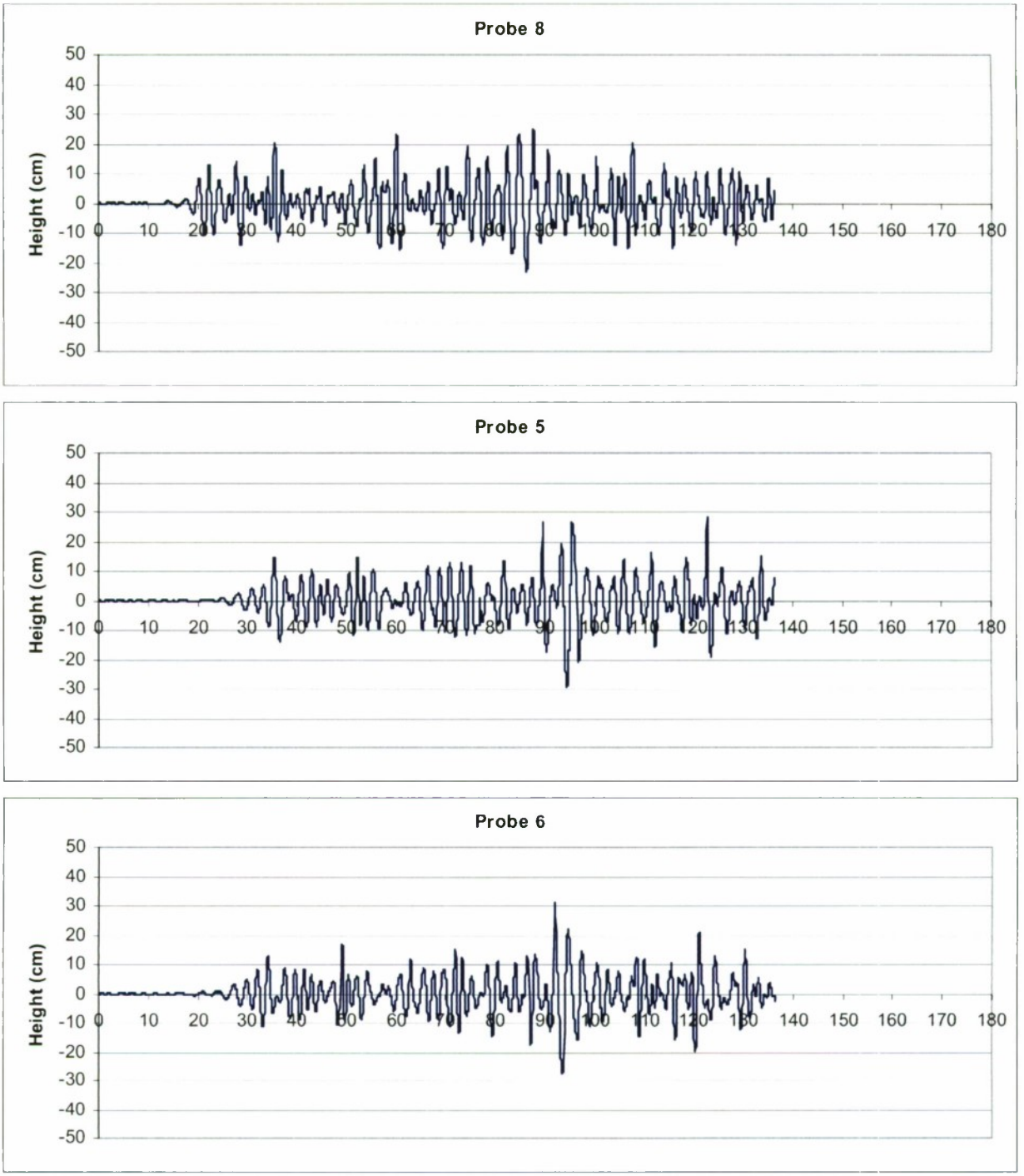

Figure 71. Measured wave time-history of sonic probes 8 (closest to wave-maker) to 1 (closest to the beach), Phase II, Run 43

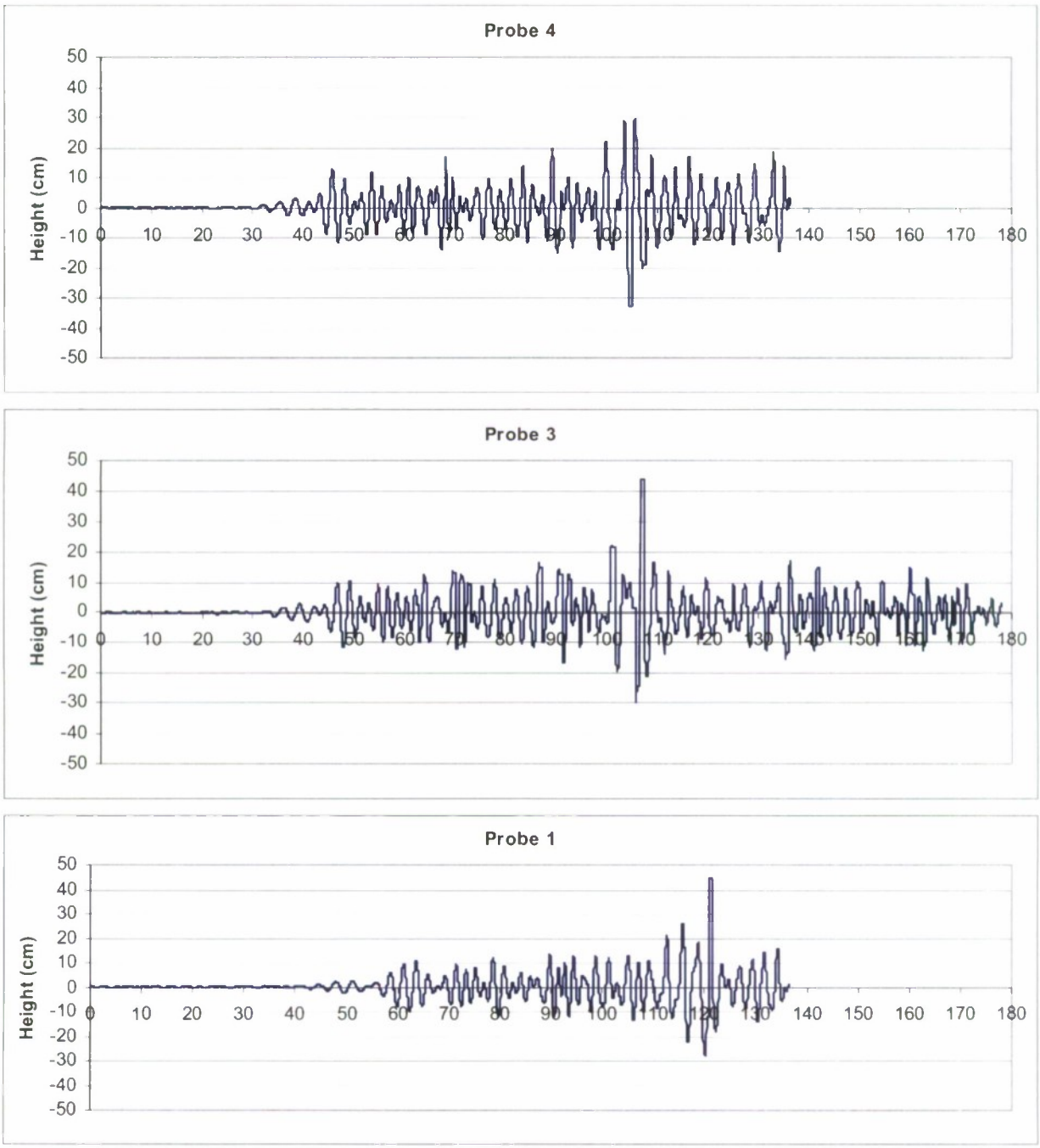

Figure 71 (continued)

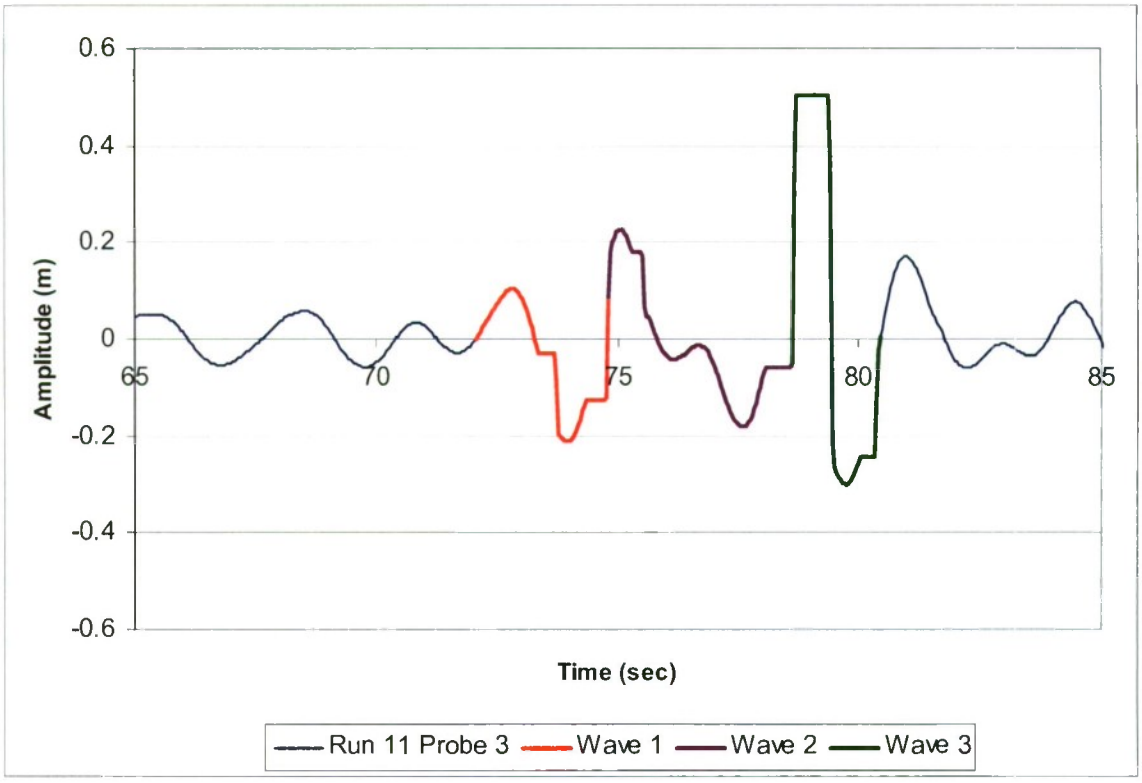

	Wave 1	Wave 2	Wave 3
Max Amplitude (m)	0.103	0.036	0.004
Min Amplitude (m)	-0.210	-0.181	-0.301
Wave Height (m)	0.314	0.218	0.304
Wave Period (sec)	2.8	3.0	1.0
Wave Length (m)	11.8	13.7	1.6
Steepness	1/38	1/68	1/7

Scale ratio:	Scaled wave heights (m):		
10	3.1	4.1	8.0
20.8	6.5	8.5	16.7
30	9.4	12.2	24.1
40	12.5	16.3	32.2
46.6	14.6	19.0	37.5

	Sig. Wave Height (m)	
Scale ratio:	Before wave group	After wave group
1	0.3	0.3
10	3.4	3.2
20.8	7.1	6.6
30	10.2	9.5
40	13.6	12.7
46.6	15.8	14.8

Figure 72. Wave characteristics at sonic probe 3, Phase II, Run 11

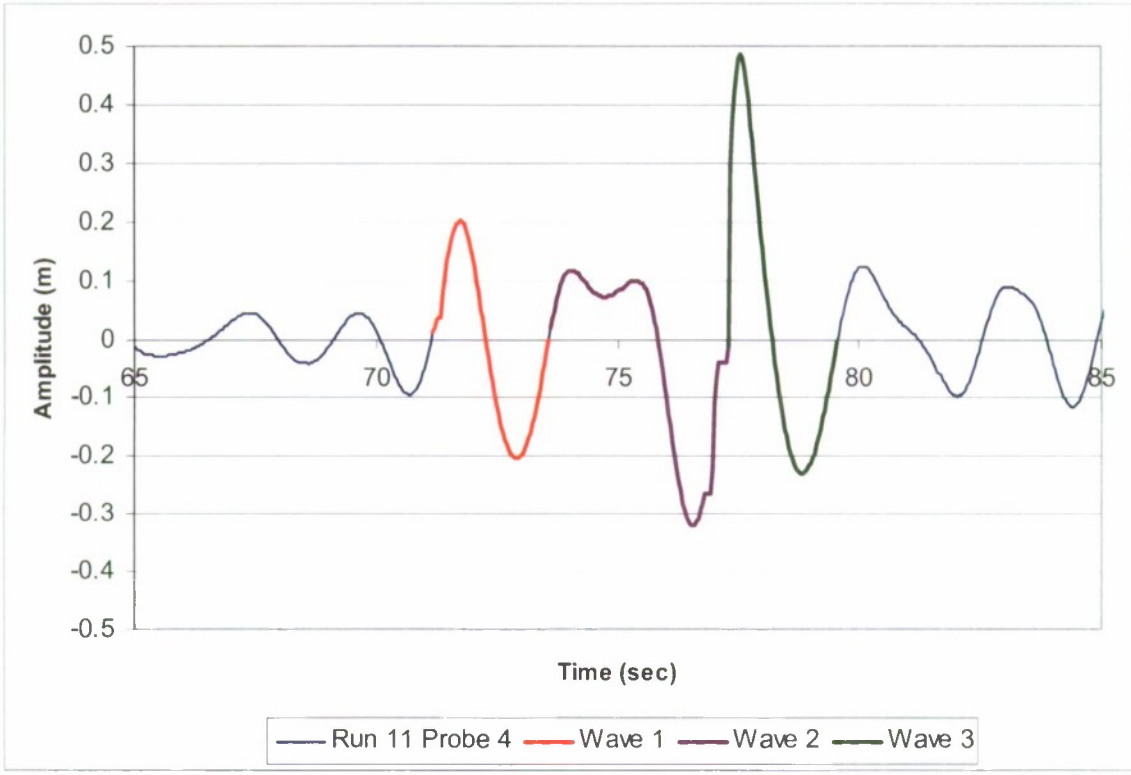

	Wave 1	Wave 2	Wave 3
Max Amplitude (m)	0.202	0.118	0.485
Min Amplitude (m)	-0.204	-0.320	-0.229
Wave Height (m)	0.406	0.437	0.714
Wave Period (sec)	2.4	3.7	2.3
Wave Length (m)	9.1	21.0	7.9
Steepness	1/22	1/48	1/11

Scale ratio:	Scaled wave heights (m):		
10	4.1	4.4	7.1
20.8	8.4	9.1	14.9
30	12.2	13.1	21.4
40	16.2	17.5	28.6
46.6	18.9	20.4	33.3

	Sig. Wave Height (m)	
Scale ratio:	Before wave group	After wave group
1	0.3	0.4
10	3.4	3.5
20.8	7.2	7.3
30	10.3	10.6
40	13.8	14.1
46.6	16.0	16.4

Figure 73. Wave characteristics at sonic probe 4, Phase II, Run 11

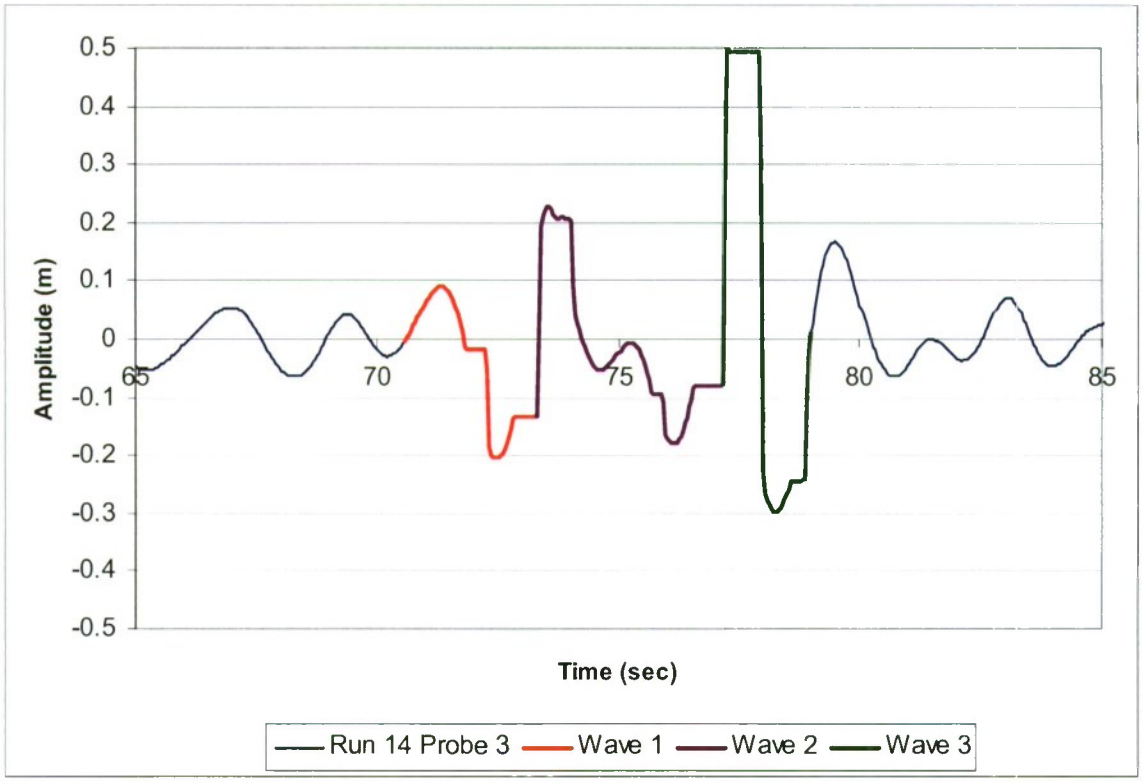

	Wave 1	Wave 2	Wave 3
Max Amplitude (m)	0.090	0.227	0.502
Min Amplitude (m)	-0.204	-0.180	-0.297
Wave Height (m)	0.294	0.406	0.799
Wave Period (sec)	2.8	3.8	1.8
Wave Length (m)	11.8	22.9	5.2
Steepness	1/40	1/56	1/7

Scale ratio:	Scaled wave heights (m):		
10	2.9	4.1	8.0
20.8	6.1	8.5	16.6
30	8.8	12.2	24.0
40	11.8	16.3	32.0
46.6	13.7	18.9	37.2

	Sig. Wave Height (m)	
Scale ratio:	Before wave group	After wave group
1	0.3	0.3
10	3.5	3.0
20.8	7.2	6.3
30	10.4	9.0
40	13.9	12.0
46.6	16.1	14.0

Figure 74. Wave characteristics at sonic probe 3, Phase II, Run 14

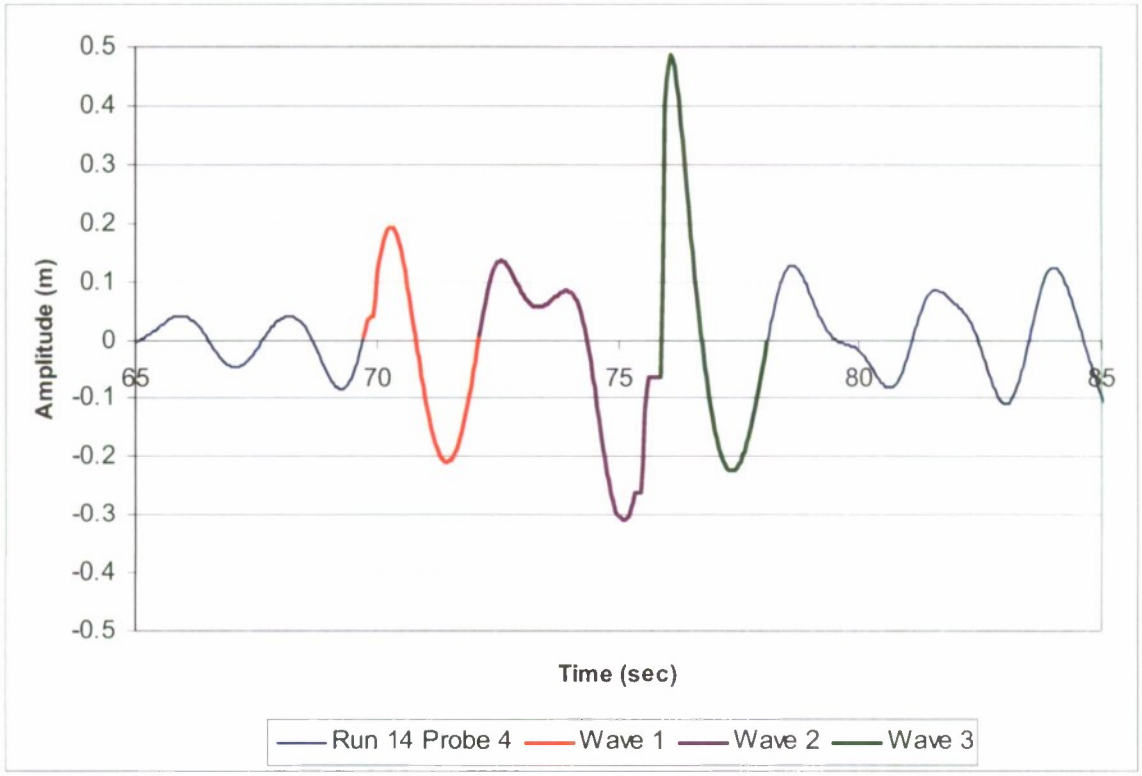

	Wave 1	Wave 2	Wave 3
Max Amplitude (m)	0.193	0.136	0.485
Min Amplitude (m)	-0.209	-0.311	-0.224
Wave Height (m)	0.403	0.447	0.710
Wave Period (sec)	2.4	3.8	2.2
Wave Length (m)	9.1	21.9	7.3
Steepness	1/22	1/49	1/10

Scale ratio:	Scaled wave heights (m):		
10	4.0	4.5	7.1
20.8	8.4	9.3	14.8
30	12.1	13.4	21.3
40	16.1	17.9	28.4
46.6	18.8	20.8	33.1

	Sig. Wave Height (m)	
Scale ratio:	Before wave group	After wave group
1	0.4	0.3
10	3.5	3.4
20.8	7.3	7.2
30	10.6	10.3
40	14.1	13.8
46.6	16.5	16.1

Figure 75. Wave characteristics at sonic probe 4, Phase II, Run 14

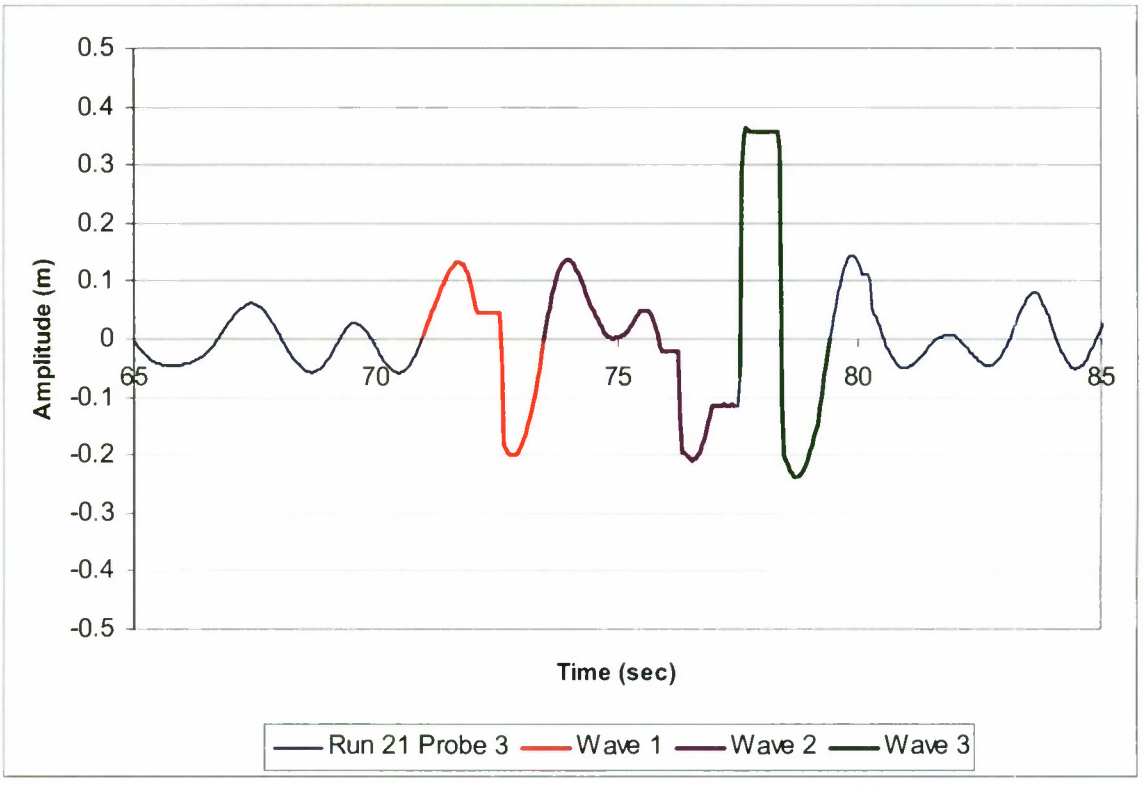

	Wave 1	Wave 2	Wave 3
Max Amplitude (m)	0.133	0.138	0.364
Min Amplitude (m)	-0.200	-0.208	-0.238
Wave Height (m)	0.333	0.346	0.602
Wave Period (sec)	2.5	4.0	1.9
Wave Length (m)	10.1	25.5	5.5
Steepness	1/34	1/74	1/9

Scale ratio:	Scaled wave heights (m):		
10	3.3	3.5	6.0
20.8	6.9	7.2	12.5
30	10.0	10.4	18.1
40	13.3	13.8	24.1
46.6	15.5	16.1	28.1

	Sig. Wave Height (m)	
Scale ratio:	Before wave group	After wave group
1	0.3	0.3
10	3.4	3.1
20.8	7.0	6.5
30	10.2	9.3
40	13.5	12.4
46.6	15.8	14.5

Figure 76. Wave characteristics at sonic probe 3, Phase II, Run 21

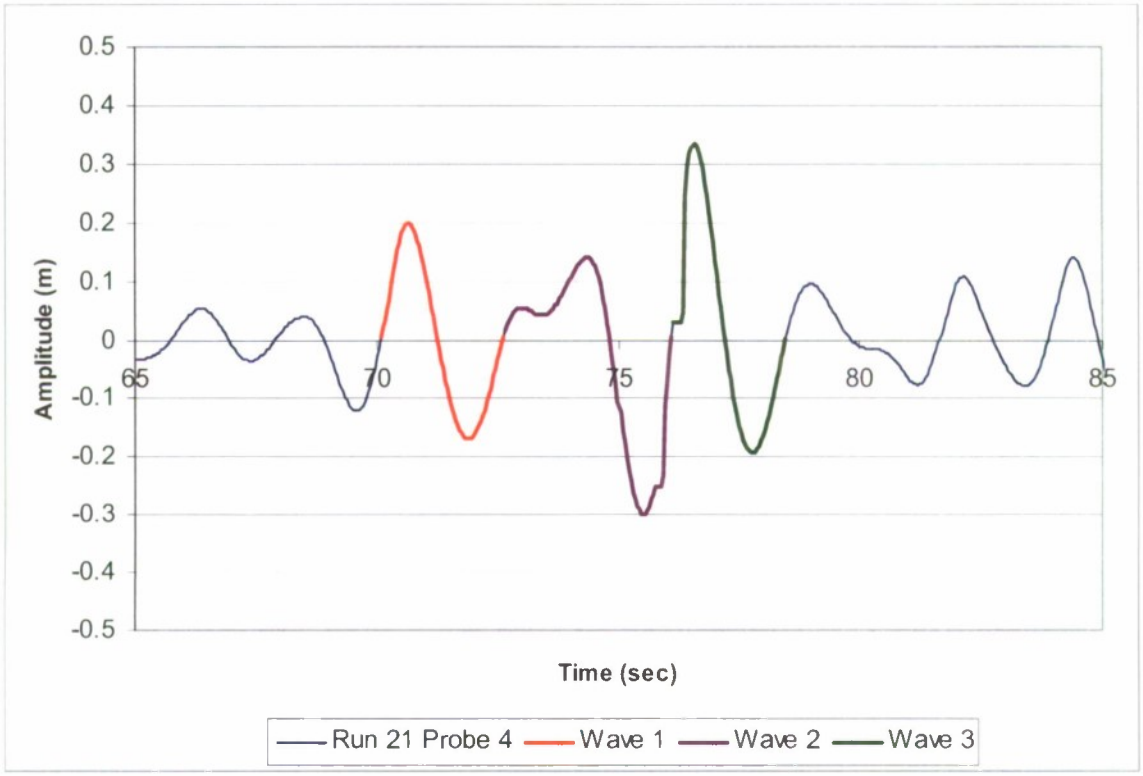

	Wave 1	Wave 2	Wave 3
Max Amplitude (m)	0.198	0.140	0.333
Min Amplitude (m)	-0.169	-0.299	-0.192
Wave Height (m)	0.367	0.439	0.525
Wave Period (sec)	2.5	3.4	2.3
Wave Length (m)	10.1	18.2	8.5
Steepness	1/25	1/41	1/16

Scale ratio:	Scaled wave heights (m):		
10	3.7	4.4	5.3
20.8	7.6	9.1	10.9
30	11.0	13.2	15.8
40	14.7	17.5	21.0
46.6	17.1	20.4	24.5

	Sig. Wave Height (m)	
Scale ratio:	Before wave group	After wave group
1	0.4	0.4
10	3.6	3.5
20.8	7.5	7.3
30	10.9	10.5
40	14.5	14.1
46.6	16.9	16.4

Figure 77. Wave characteristics at sonic probe 4, Phase II, Run 21

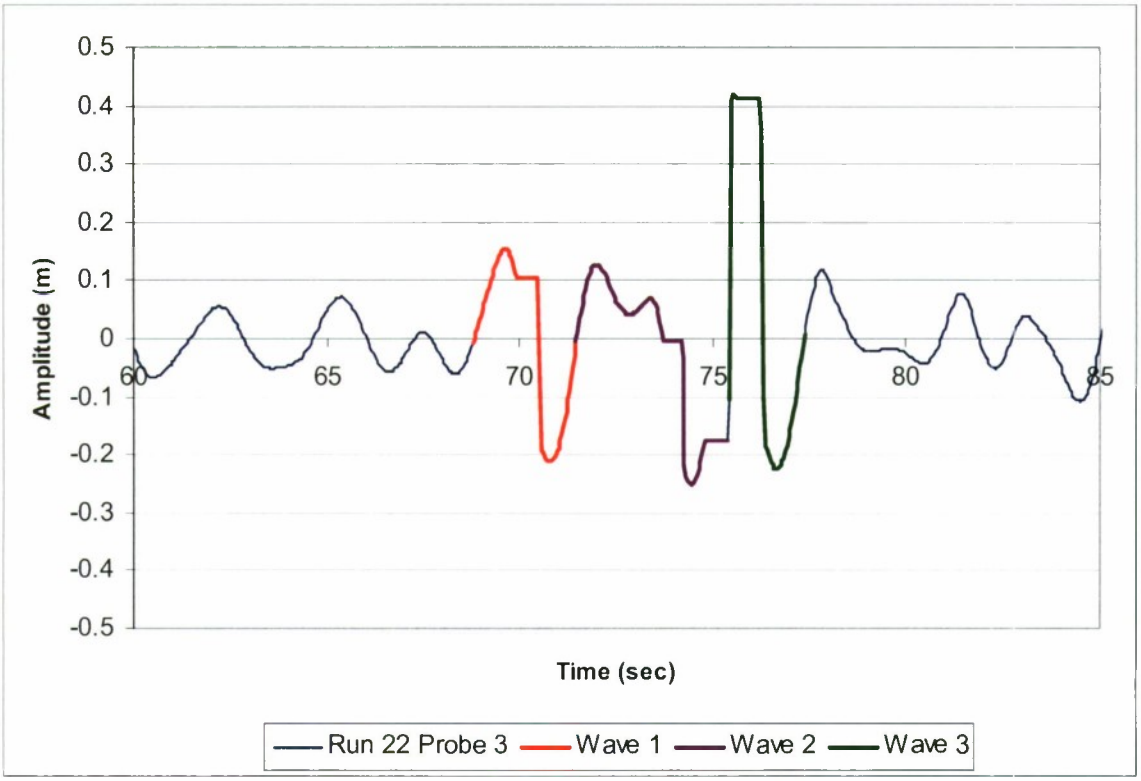

	Wave 1	Wave 2	Wave 3
Max Amplitude (m)	0.155	0.127	0.421
Min Amplitude (m)	-0.211	-0.250	-0.223
Wave Height (m)	0.366	0.377	0.644
Wave Period (sec)	2.7	4.0	2.0
Wave Length (m)	11.4	24.4	6.0
Steepness	1/31	1/65	1/9

Scale ratio:	Scaled wave heights (m):		
10	3.7	3.8	6.4
20.8	7.6	7.8	13.4
30	11.0	11.3	19.3
40	14.7	15.1	25.8
46.6	17.1	17.6	30.0

	Sig. Wave Height (m)	
Scale ratio:	Before wave group	After wave group
1	0.3	0.3
10	3.4	3.1
20.8	7.0	6.4
30	10.1	9.2
40	13.5	12.2
46.6	15.8	14.2

Figure 78. Wave characteristics at sonic probe 3, Phase II, Run 22

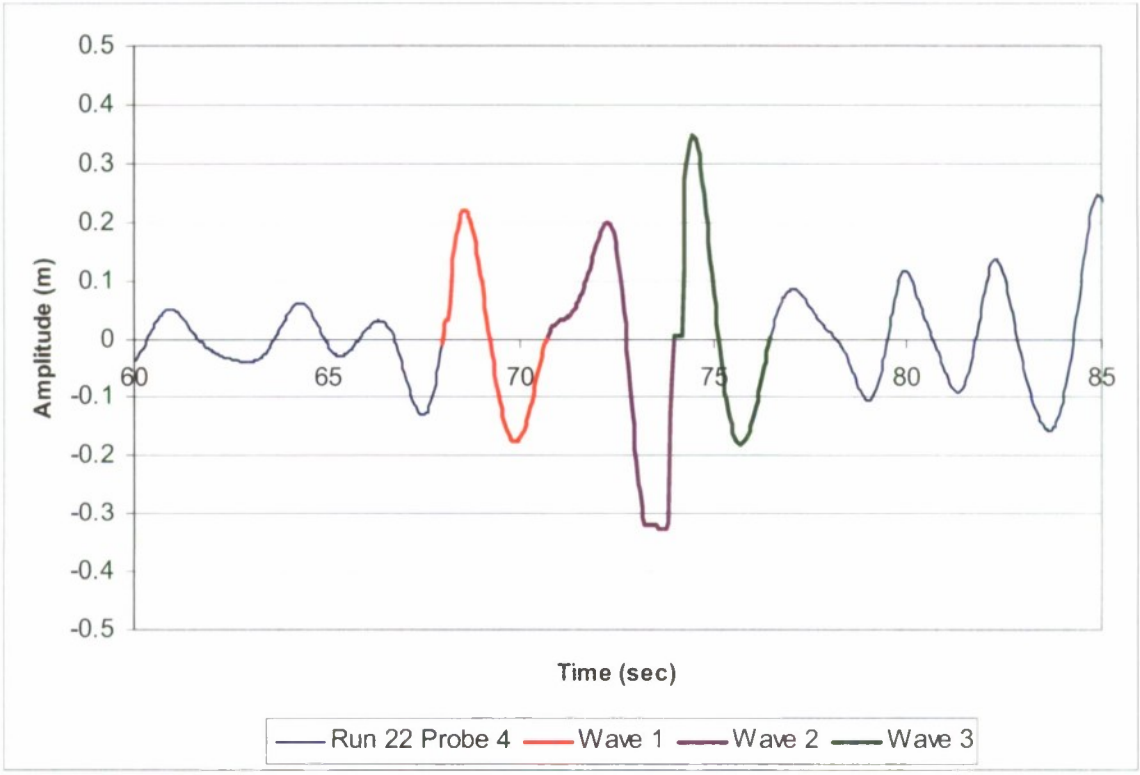

	Wave 1	Wave 2	Wave 3
Max Amplitude (m)	0.221	0.199	0.349
Min Amplitude (m)	-0.176	-0.327	-0.181
Wave Height (m)	0.397	0.526	0.530
Wave Period (sec)	2.8	3.3	2.5
Wave Length (m)	11.8	16.5	9.7
Steepness	1/30	1/33	1/20

Scale ratio:	Scaled wave heights (m):		
10	4.0	5.3	5.3
20.8	8.3	10.9	11.0
30	11.9	15.8	15.9
40	15.9	21.0	21.2
46.6	18.5	24.5	24.7

	Sig. Wave Height (m)	
Scale ratio:	Before wave group	After wave group
1	0.4	0.4
10	3.6	3.9
20.8	7.4	8.1
30	10.7	11.7
40	14.3	15.6
46.6	16.6	18.2

Figure 79. Wave characteristics at sonic probe 4, Phase II, Run 22

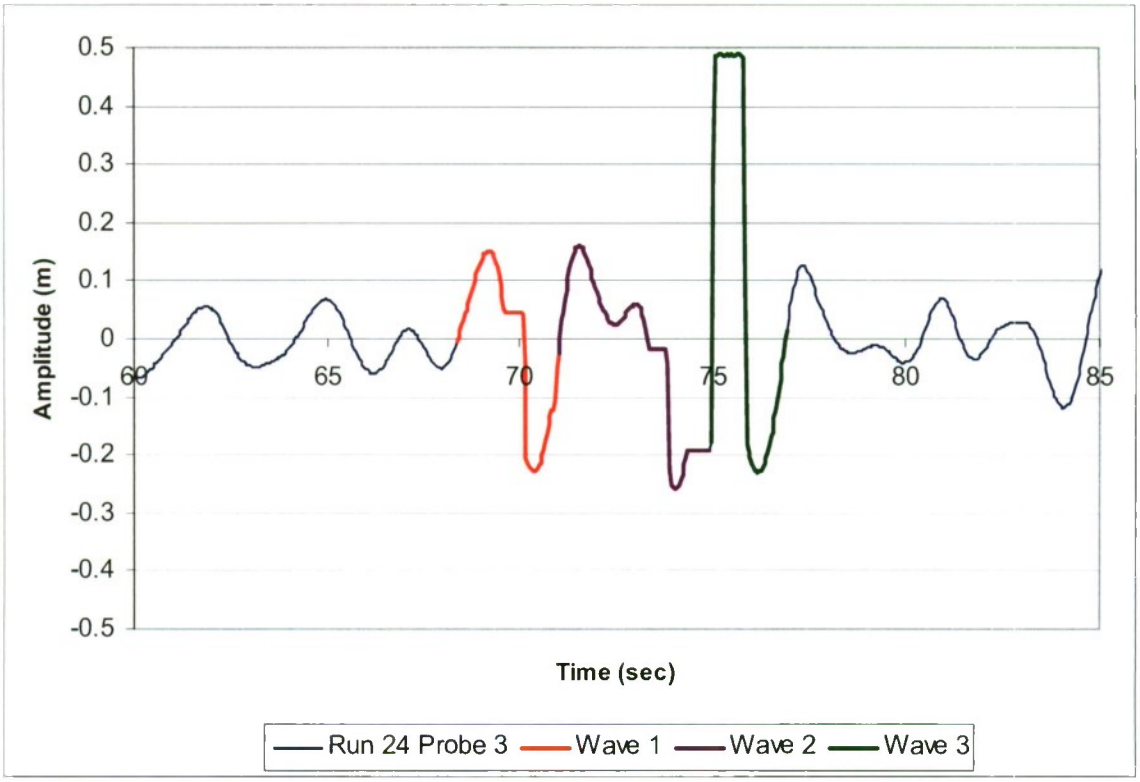

	Wave 1	Wave 2	Wave 3
Max Amplitude (m)	0.151	0.160	0.488
Min Amplitude (m)	-0.228	-0.258	-0.230
Wave Height (m)	0.379	0.418	0.718
Wave Period (sec)	2.6	4.0	2.0
Wave Length (m)	10.7	24.4	6.0
Steepness	1/25	1/58	1/8

Scale ratio:	Scaled wave heights (m):		
10	3.8	4.2	7.2
20.8	7.9	8.7	14.9
30	11.4	12.5	21.5
40	15.2	16.7	28.7
46.6	17.7	19.5	33.4

	Sig. Wave Height (m)	
Scale ratio:	Before wave group	After wave group
1	0.3	0.3
10	3.3	2.8
20.8	6.8	5.9
30	9.8	8.5
40	13.1	11.3
46.6	15.3	13.2

Figure 80. Wave characteristics at sonic probe 3, Phase II, Run 24

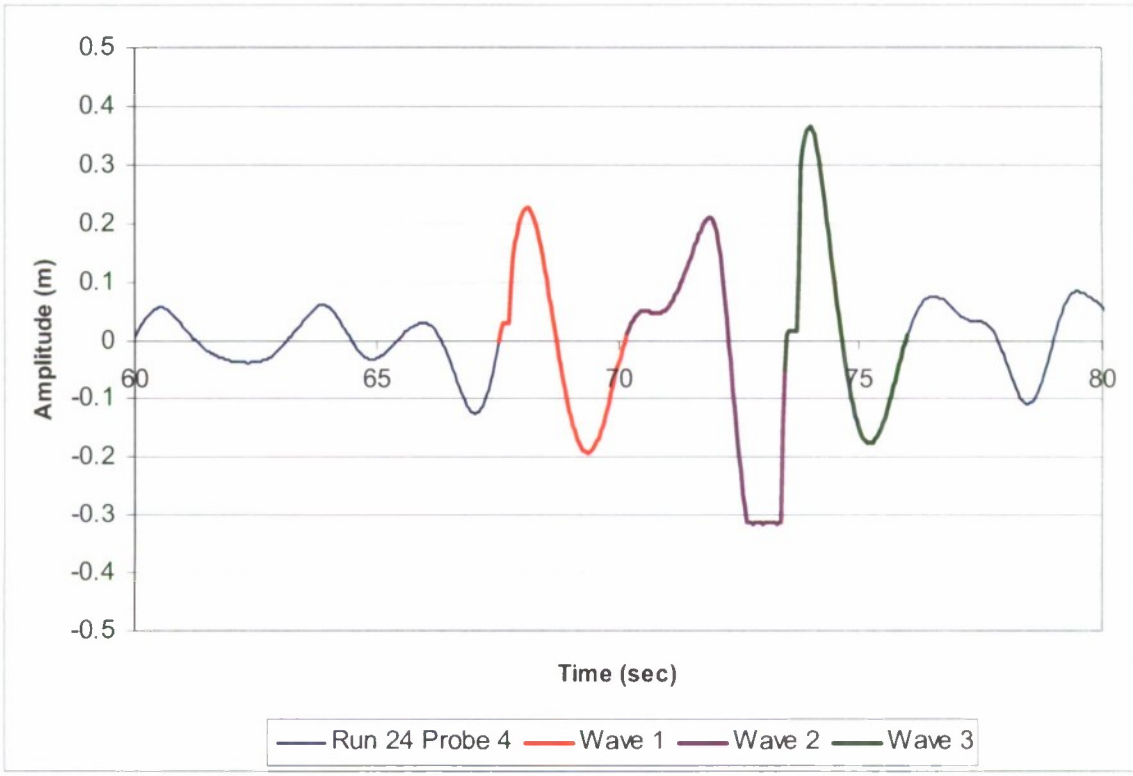

	Wave 1	Wave 2	Wave 3
Max Amplitude (m)	0.226	0.211	0.364
Min Amplitude (m)	-0.192	-0.315	-0.176
Wave Height (m)	0.417	0.526	0.540
Wave Period (sec)	2.6	3.3	2.5
Wave Length (m)	10.7	17.3	10.1
Steepness	1/25	1/35	1/19

Scale ratio:	Scaled wave heights (m):		
10	4.2	5.3	5.4
20.8	8.7	10.9	11.2
30	12.5	15.8	16.2
40	16.7	21.0	21.6
46.6	19.4	24.5	25.2

	Sig. Wave Height (m)	
Scale ratio:	Before wave group	After wave group
1	0.3	0.4
10	3.3	3.5
20.8	6.9	7.3
30	10.0	10.6
40	13.3	14.1
46.6	15.5	16.4

Figure 81. Wave characteristics at sonic probe 4, Phase II, Run 24

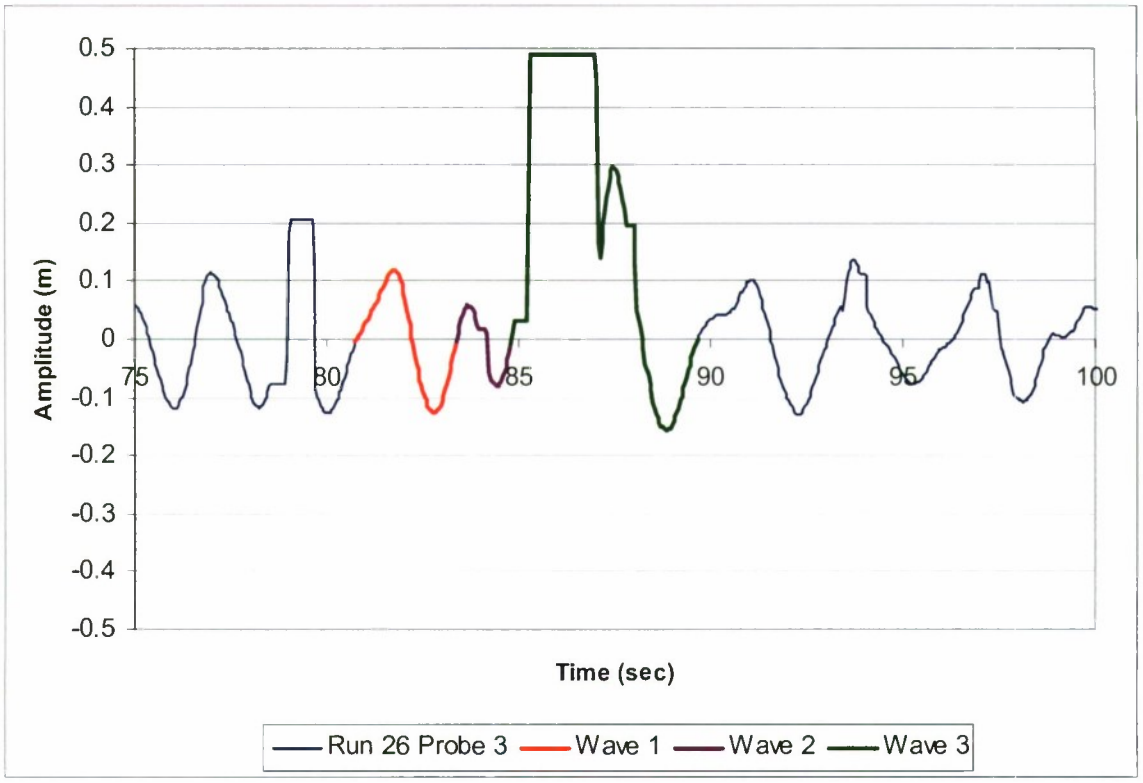

	Wave 1	Wave 2	Wave 3
Max Amplitude (m)	0.120	0.058	0.489
Min Amplitude (m)	-0.126	-0.080	-0.158
Wave Height (m)	0.246	0.137	0.647
Wave Period (sec)	2.7	1.5	4.9
Wave Length (m)	11.1	3.3	37.1
Steepness	1/55	1/33	1/57

Scale ratio:	Scaled wave heights (m):		
10	2.5	1.4	6.5
20.8	5.1	2.9	13.5
30	7.4	4.1	19.4
40	9.8	5.5	25.9
46.6	11.5	6.4	30.2

	Sig. Wave Height (m)	
Scale ratio:	Before wave group	After wave group
1	0.4	0.2
10	3.8	2.5
20.8	7.9	5.2
30	11.4	7.5
40	15.2	10.0
46.6	17.7	11.6

Figure 82. Wave characteristics at sonic probe 3, Phase II, Run 26

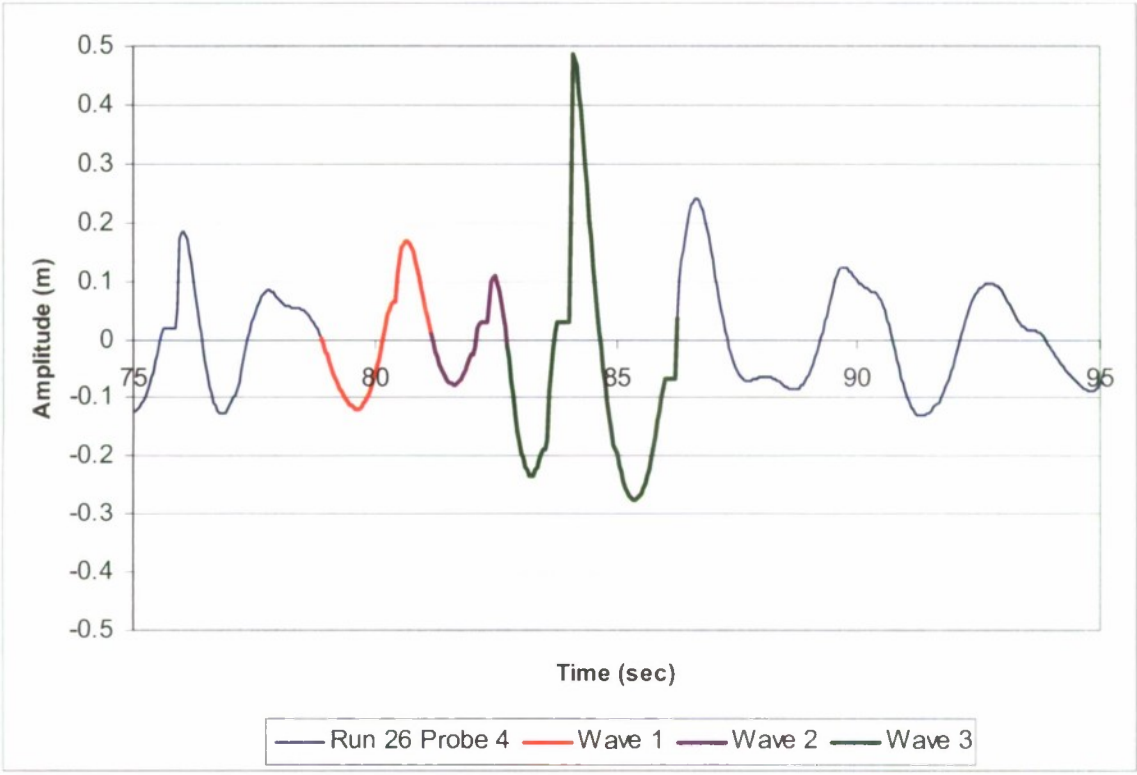

	Wave 1	Wave 2	Wave 3
Max Amplitude (m)	0.168	0.107	0.486
Min Amplitude (m)	-0.120	-0.078	-0.276
Wave Height (m)	0.288	0.185	0.761
Wave Period (sec)	2.3	1.6	3.5
Wave Length (m)	8.5	3.9	19.1
Steepness	1/33	1/21	1/25

Scale ratio:	Scaled wave heights (m):		
10	2.9	1.9	7.6
20.8	6.0	3.9	15.8
30	8.6	5.6	22.8
40	11.5	7.4	30.5
46.6	13.4	8.6	35.5

	Sig. Wave Height (m)	
Scale ratio:	Before wave group	After wave group
1	0.3	0.3
10	3.4	2.6
20.8	7.1	5.5
30	10.2	7.9
40	13.6	10.6
46.6	15.9	12.3

Figure 83. Wave characteristics at sonic probe 4, Phase II, Run 26

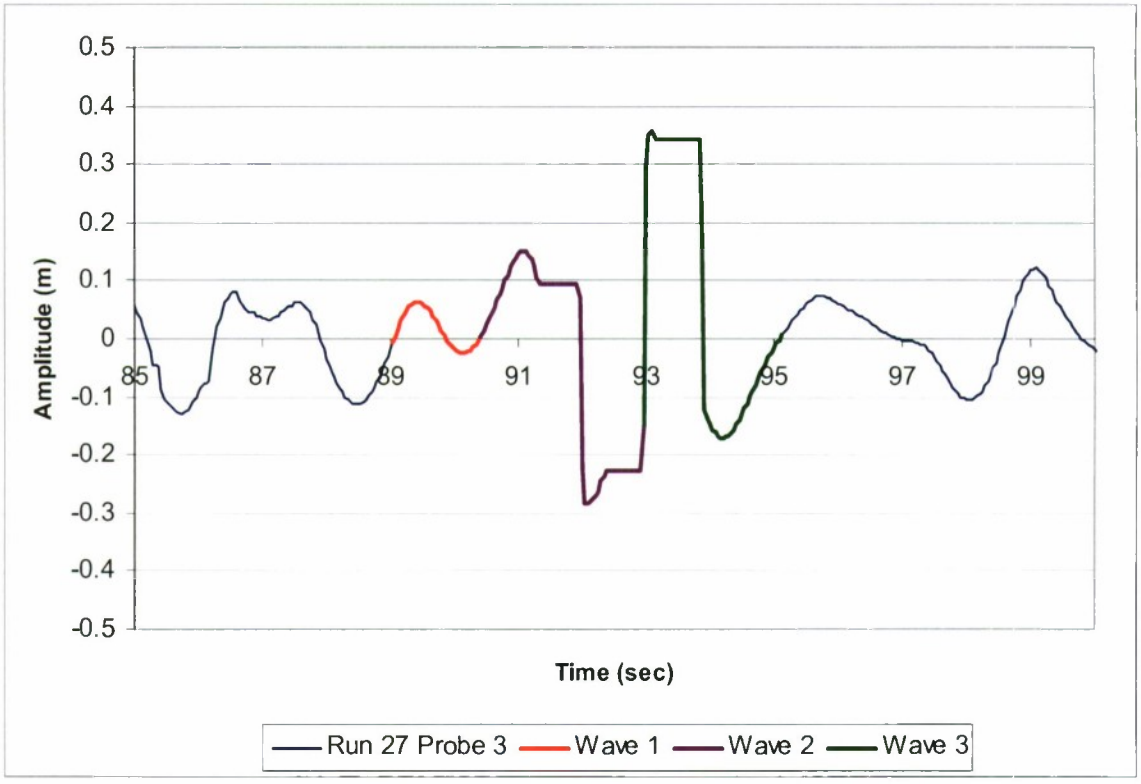

	Wave 1	Wave 2	Wave 3
Max Amplitude (m)	0.064	0.151	0.358
Min Amplitude (m)	-0.024	-0.285	-0.171
Wave Height (m)	0.087	0.435	0.530
Wave Period (sec)	1.4	2.5	2.2
Wave Length (m)	2.9	10.1	7.3
Steepness	1/34	1/23	1/14

Scale ratio:	Scaled wave heights (m):		
10	0.9	4.4	5.3
20.8	1.8	9.1	11.0
30	2.6	13.1	15.9
40	3.5	17.4	21.2
46.6	4.1	20.3	24.7

	Sig. Wave Height (m)	
Scale ratio:	Before wave group	After wave group
1	0.3	0.2
10	2.8	2.1
20.8	5.8	4.3
30	8.4	6.2
40	11.2	8.2
46.6	13.0	9.6

Figure 84. Wave characteristics at sonic probe 3, Phase II, Run 27

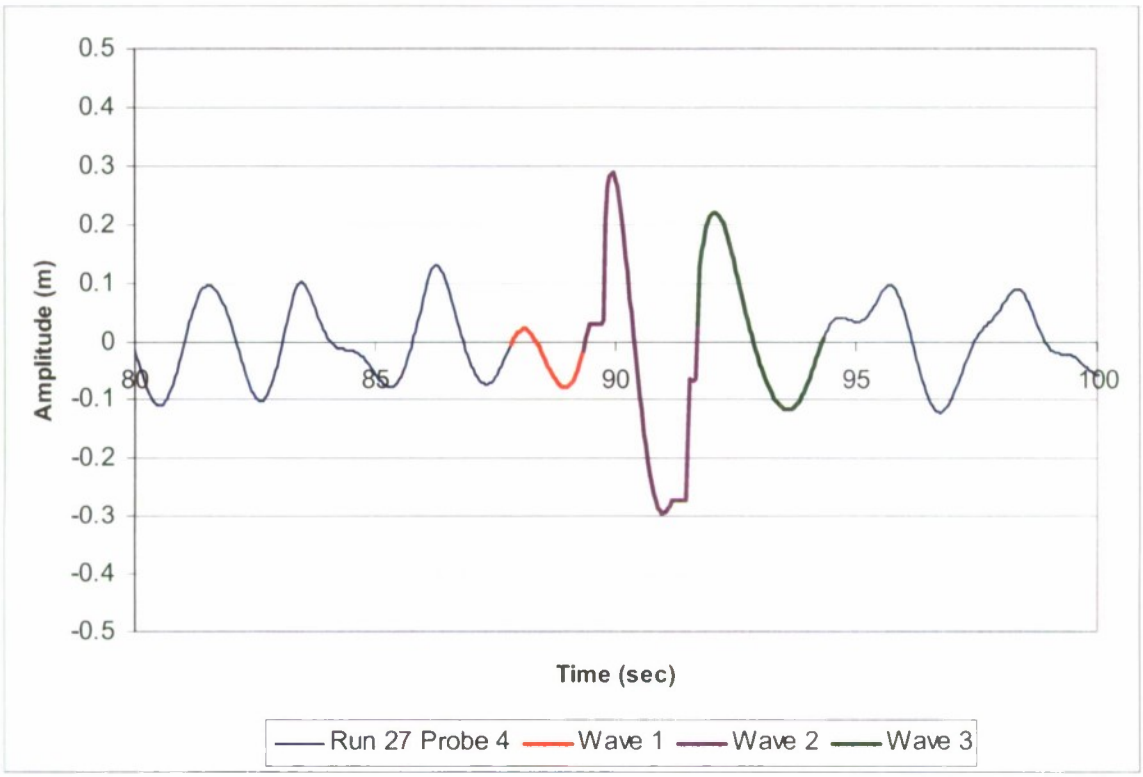

	Wave 1	Wave 2	Wave 3
Max Amplitude (m)	0.021	0.288	0.221
Min Amplitude (m)	-0.078	-0.294	-0.117
Wave Height (m)	0.099	0.582	0.338
Wave Period (sec)	1.5	2.4	2.6
Wave Length (m)	3.7	8.8	10.7
Steepness	1/37	1/15	1/32

Scale ratio:	Scaled wave heights (m):		
10	1.0	5.8	3.4
20.8	2.1	12.1	7.0
30	3.0	17.5	10.1
40	4.0	23.3	13.5
46.6	4.6	27.1	15.8

	Sig. Wave Height (m)	
Scale ratio:	Before wave group	After wave group
1	0.3	0.2
10	2.5	1.8
20.8	5.2	3.8
30	7.5	5.5
40	10.0	7.3
46.6	11.7	8.5

Figure 85. Wave characteristics at sonic probe 4, Phase II, Run 27

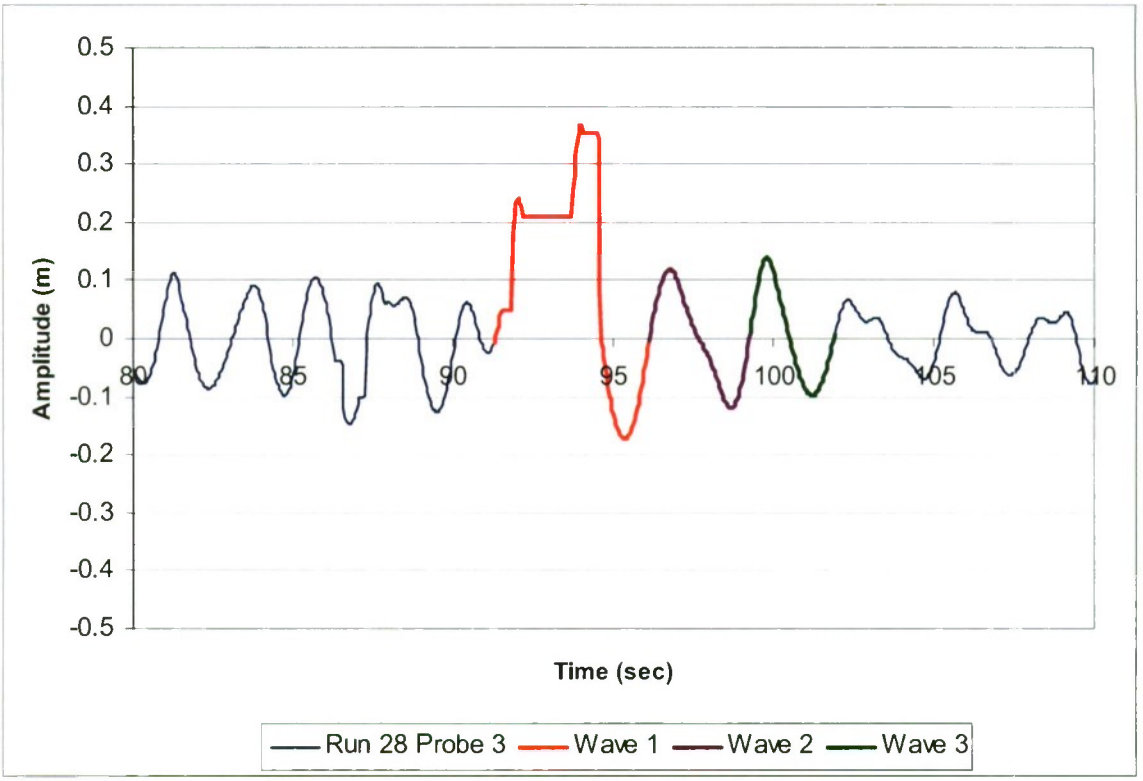

	Wave 1	Wave 2	Wave 3
Max Amplitude (m)	0.366	0.118	0.138
Min Amplitude (m)	-0.171	-0.119	-0.098
Wave Height (m)	0.537	0.237	0.236
Wave Period (sec)	4.9	3.2	2.6
Wave Length (m)	37.1	15.6	10.7
Steepness	1/67	1/66	1/53

Scale ratio:	Scaled wave heights (m):		
10	5.4	2.4	2.4
20.8	11.2	4.9	4.9
30	16.1	7.1	7.1
40	21.5	9.5	9.4
46.6	25.0	11.1	11.0

	Sig. Wave Height (m)	
Scale ratio:	Before wave group	After wave group
1	0.3	0.2
10	2.8	1.8
20.8	5.8	3.8
30	8.4	5.5
40	11.1	7.3
46.6	13.0	8.5

Figure 86. Wave characteristics at sonic probe 3, Phase II, Run 28

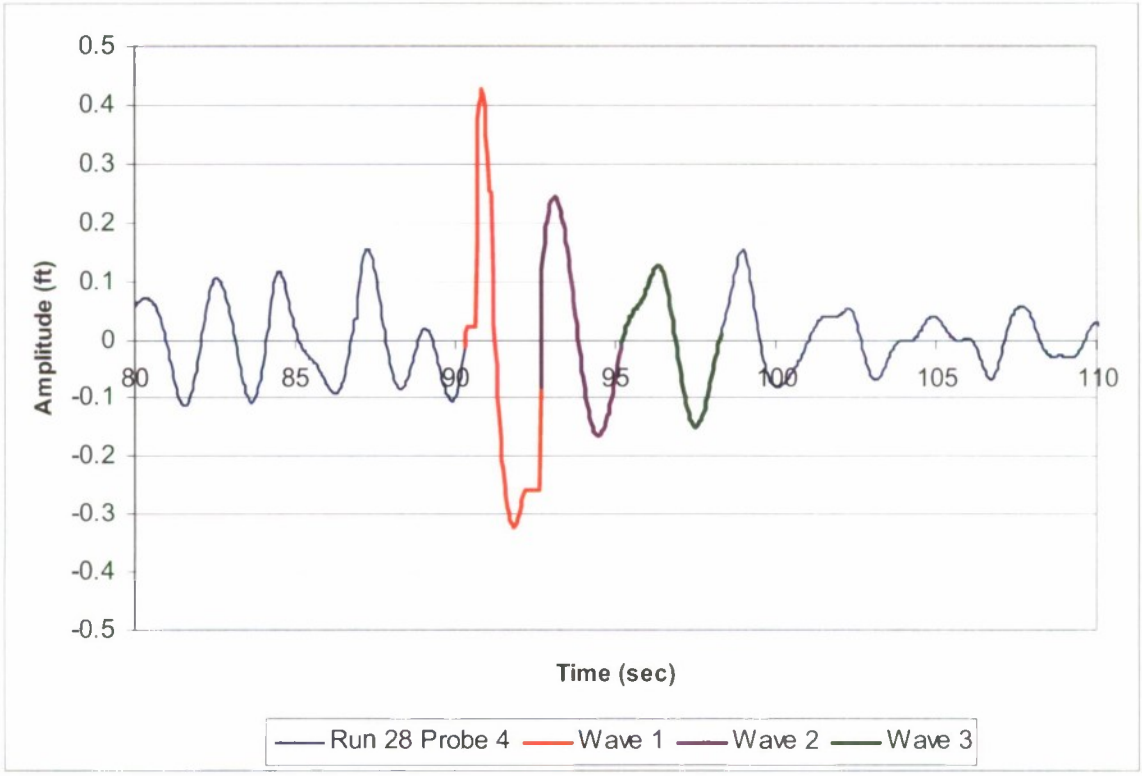

	Wave 1	Wave 2	Wave 3
Max Amplitude (ft)	0.428	0.243	0.127
Min Amplitude (ft)	-0.322	-0.164	-0.149
Wave Height (ft)	0.750	0.407	0.276
Wave Period (sec)	2.4	2.5	3.1
Wave Length (ft)	8.8	10.1	14.8
Steepness	1/11	1/25	1/53

Scale ratio:	Scaled wave heights (m):		
10	7.5	4.1	2.8
20.8	15.6	8.5	5.7
30	22.5	12.2	8.3
40	30.0	16.3	11.1
46.6	35.0	19.0	12.9

	Sig. Wave Height (m)	
Scale ratio:	Before wave group	After wave group
1	0.3	0.2
10	2.7	1.9
20.8	5.6	3.9
30	8.1	5.7
40	10.8	7.6
46.6	12.5	8.8

Figure 87. Wave characteristics at sonic probe 4, Phase II, Run 28

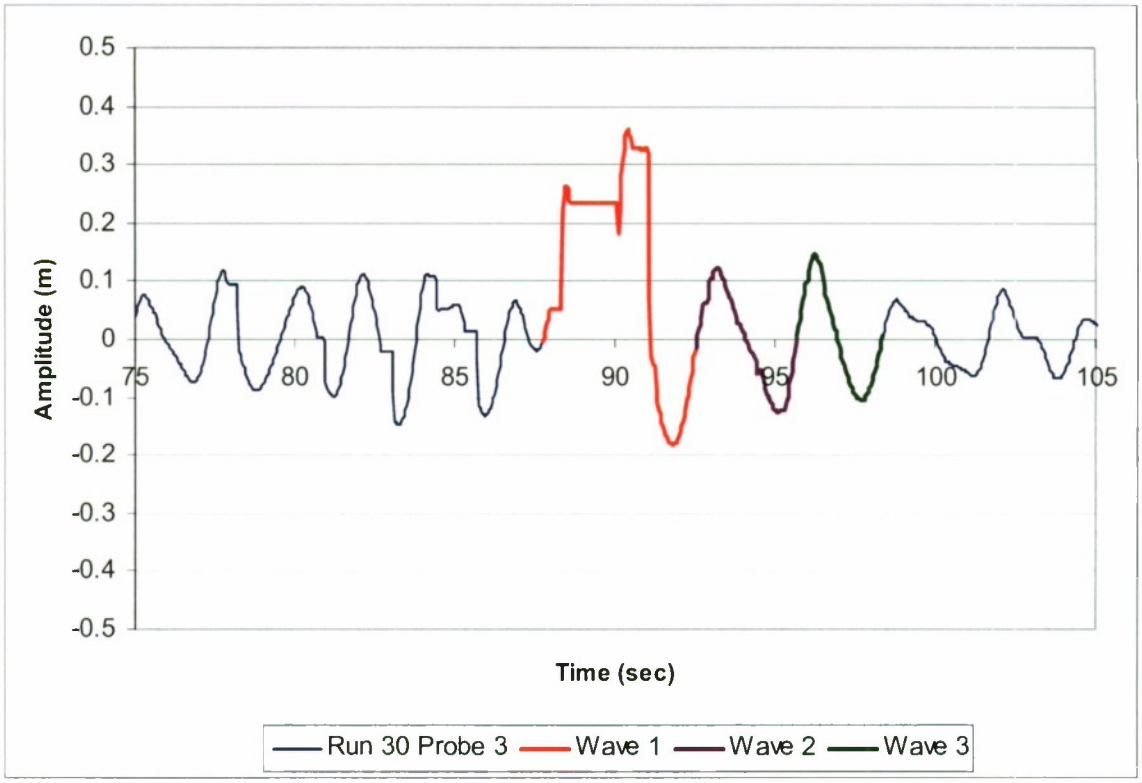

	Wave 1	Wave 2	Wave 3
Max Amplitude (m)	0.360	0.122	0.146
Min Amplitude (m)	-0.182	-0.125	-0.106
Wave Height (m)	0.542	0.247	0.252
Wave Period (sec)	4.8	3.2	2.7
Wave Length (m)	36.4	15.6	11.1
Steepness	1/67	1/63	1/45

Scale ratio:	Scaled wave heights (m):		
10	5.4	2.5	2.5
20.8	11.3	5.1	5.2
30	16.3	7.4	7.6
40	21.7	9.9	10.1
46.6	25.3	11.5	11.8

	Sig. Wave Height (m)	
Scale ratio:	Before wave group	After wave group
1	0.3	0.2
10	2.9	1.9
20.8	6.1	4.0
30	8.8	5.7
40	11.7	7.6
46.6	13.6	8.9

Figure 88. Wave characteristics at sonic probe 3, Phase II, Run 30

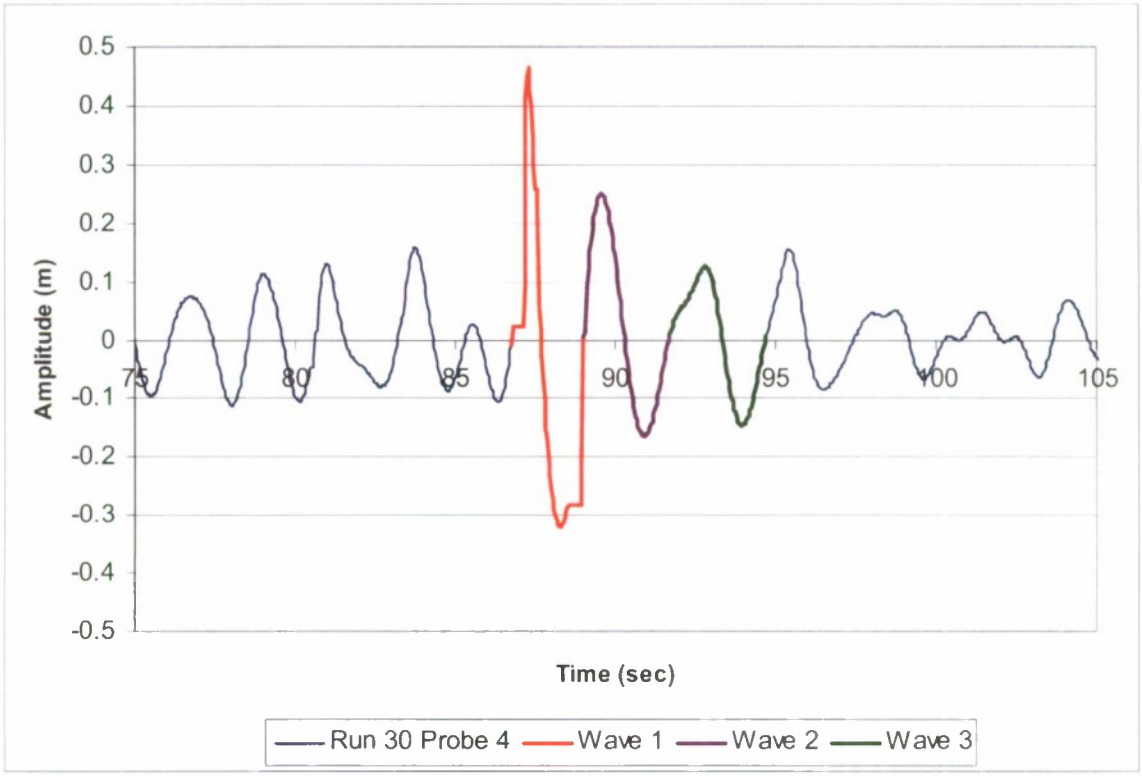

	Wave 1	Wave 2	Wave 3
Max Amplitude (m)	0.465	0.249	0.125
Min Amplitude (m)	-0.321	-0.164	-0.146
Wave Height (m)	0.786	0.413	0.271
Wave Period (sec)	2.3	2.7	3.0
Wave Length (m)	7.9	11.4	14.0
Steepness	1/10	1/28	1/53

Scale ratio:	Scaled wave heights (m):		
10	7.9	4.1	2.7
20.8	16.3	8.6	5.6
30	23.6	12.4	8.1
40	31.4	16.5	10.8
46.6	36.6	19.2	12.6

	Sig. Wave Height (m)	
Scale ratio:	Before wave group	After wave group
1	0.3	0.2
10	2.7	1.9
20.8	5.6	3.9
30	8.0	5.6
40	10.7	7.5
46.6	12.5	8.7

Figure 89. Wave characteristics at sonic probe 4, Phase II, Run 30

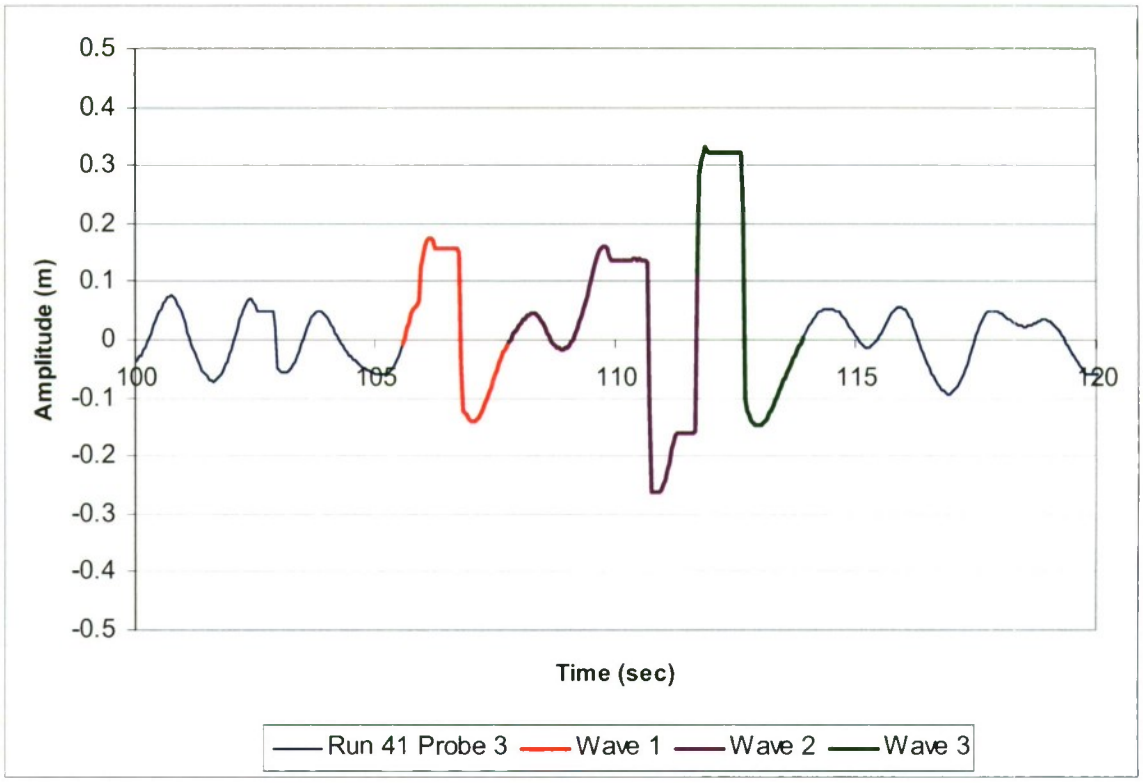

	Wave 1	Wave 2	Wave 3
Max Amplitude (m)	0.176	0.162	0.331
Min Amplitude (m)	-0.140	-0.264	-0.149
Wave Height (m)	0.317	0.425	0.480
Wave Period (sec)	2.3	3.9	2.2
Wave Length (m)	7.9	23.9	7.6
Steepness	1/25	1/56	1/16

Scale ratio:	Scaled wave heights (m):		
10	3.2	4.3	4.8
20.8	6.6	8.8	10.0
30	9.5	12.8	14.4
40	12.7	17.0	19.2
46.6	14.8	19.8	22.4

	Sig. Wave Height (m)	
Scale ratio:	Before wave group	After wave group
1	0.2	0.2
10	2.3	2.2
20.8	4.8	4.6
30	6.9	6.7
40	9.2	8.9
46.6	10.7	10.4

Figure 90. Wave characteristics at sonic probe 3, Phase II, Run 41

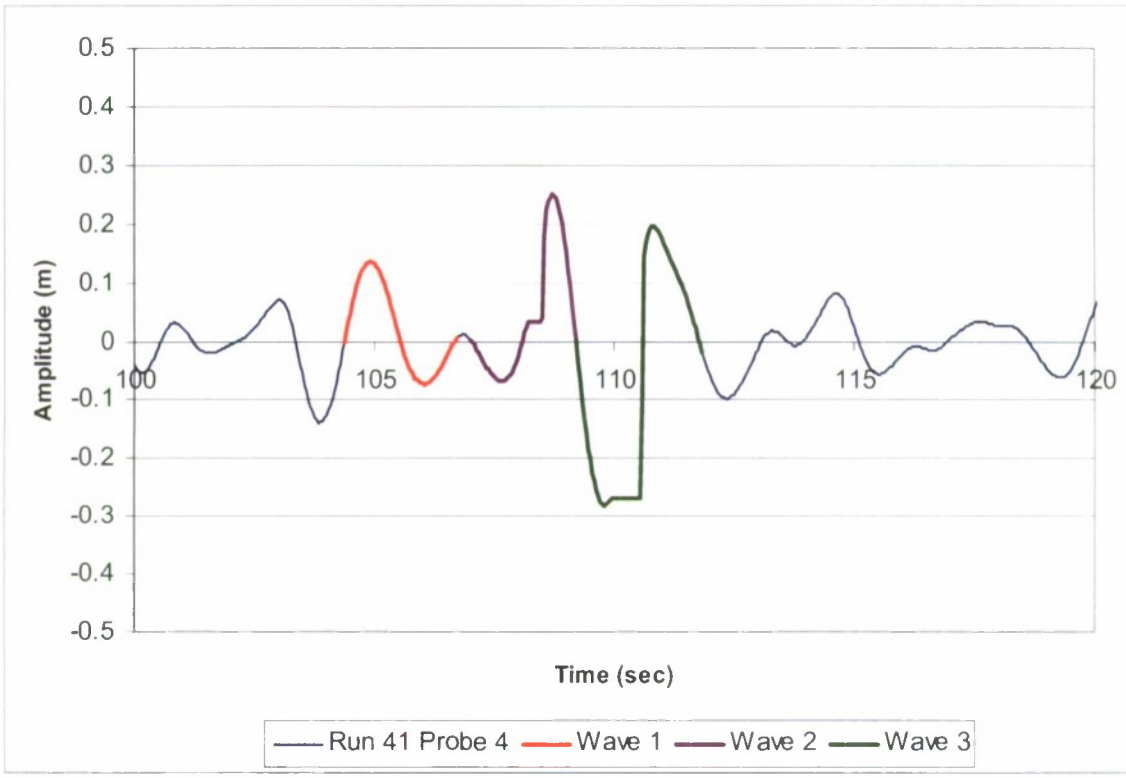

	Wave 1	Wave 2	Wave 3
Max Amplitude (m)	0.136	0.249	0.197
Min Amplitude (m)	-0.073	-0.067	-0.281
Wave Height (m)	0.209	0.316	0.478
Wave Period (sec)	2.3	2.2	2.6
Wave Length (m)	8.5	7.6	10.7
Steepness	1/41	1/25	1/25

Scale ratio:	Scaled wave heights (m):		
10	2.1	3.2	4.8
20.8	4.3	6.6	9.9
30	6.3	9.5	14.3
40	8.4	12.6	19.1
46.6	9.7	14.7	22.3

	Sig. Wave Height (m)	
Scale ratio:	Before wave group	After wave group
1	0.2	0.2
10	2.3	2.1
20.8	4.8	4.4
30	6.9	6.4
40	9.2	8.5
46.6	10.7	9.9

Figure 91. Wave characteristics at sonic probe 4, Phase II, Run 41

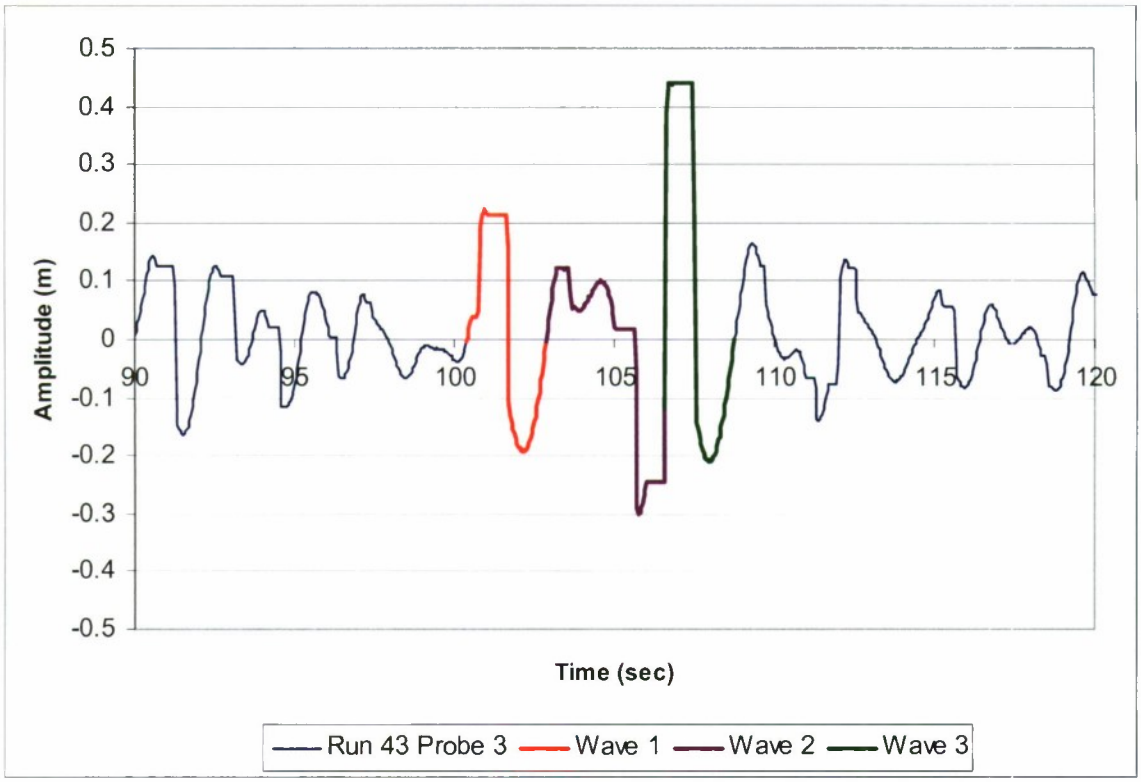

	Wave 1	Wave 2	Wave 3
Max Amplitude (m)	0.223	0.123	0.439
Min Amplitude (m)	-0.191	-0.301	-0.209
Wave Height (m)	0.414	0.424	0.649
Wave Period (sec)	2.5	3.7	2.2
Wave Length (m)	10.1	21.5	7.3
Steepness	1/25	1/51	1/11

Scale ratio:	Scaled wave heights (m):		
10	4.1	4.2	6.5
20.8	8.6	8.8	13.5
30	12.4	12.7	19.5
40	16.6	17.0	25.9
46.6	19.3	19.8	30.2

	Sig. Wave Height (m)	
Scale ratio:	Before wave group	After wave group
1	0.3	0.3
10	2.7	2.5
20.8	5.6	5.2
30	8.1	7.5
40	10.7	10.0
46.6	12.5	11.7

Figure 92. Wave characteristics at sonic probe 3, Phase II, Run 43

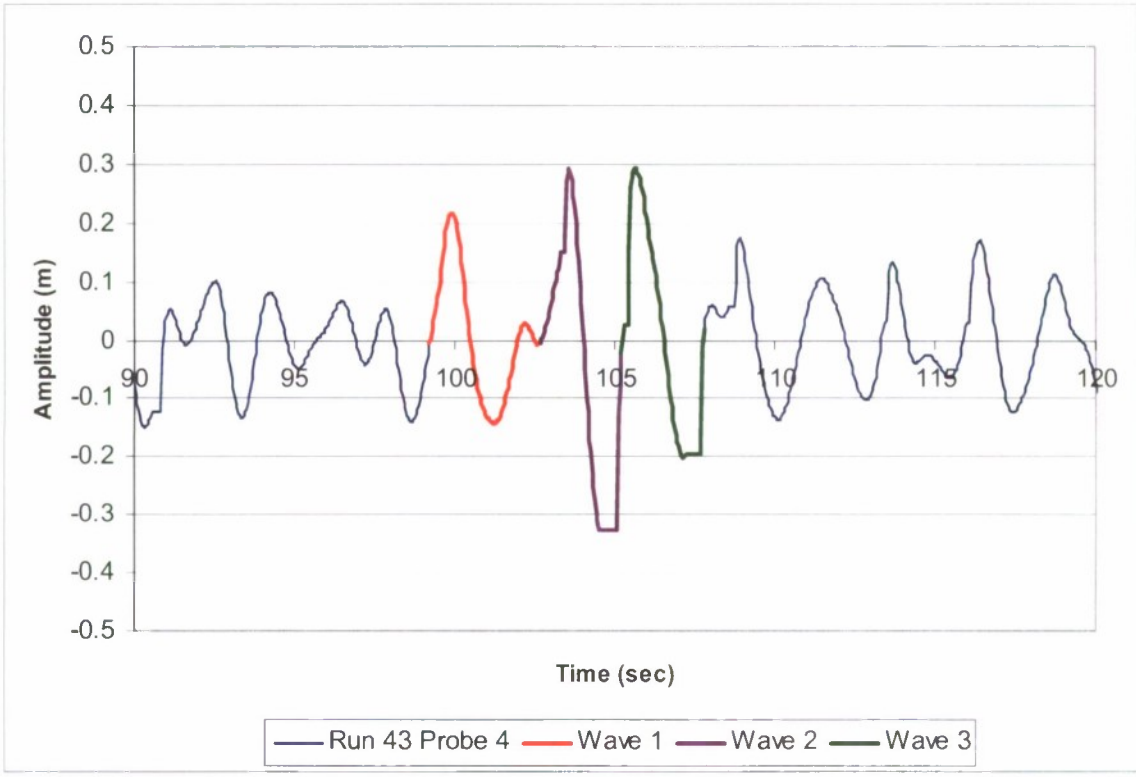

	Wave 1	Wave 2	Wave 3
Max Amplitude (m)	0.218	0.291	0.293
Min Amplitude (m)	-0.142	-0.328	-0.201
Wave Height (m)	0.360	0.619	0.494
Wave Period (sec)	3.5	2.6	2.6
Wave Length (m)	19.1	10.4	10.4
Steepness	1/48	4/67	1/21

Scale ratio:	Scaled wave heights (m):		
10	3.6	6.2	4.9
20.8	7.5	12.9	10.3
30	10.8	18.6	14.8
40	14.4	24.8	19.8
46.6	16.8	28.8	23.0

	Sig. Wave Height (m)	
Scale ratio:	Before wave group	After wave group
1	0.3	0.3
10	2.5	2.6
20.8	5.3	5.4
30	7.6	7.8
40	10.1	10.3
46.6	11.8	12.1

Figure 93. Wave characteristics at sonic probe 4, Phase II, Run 43

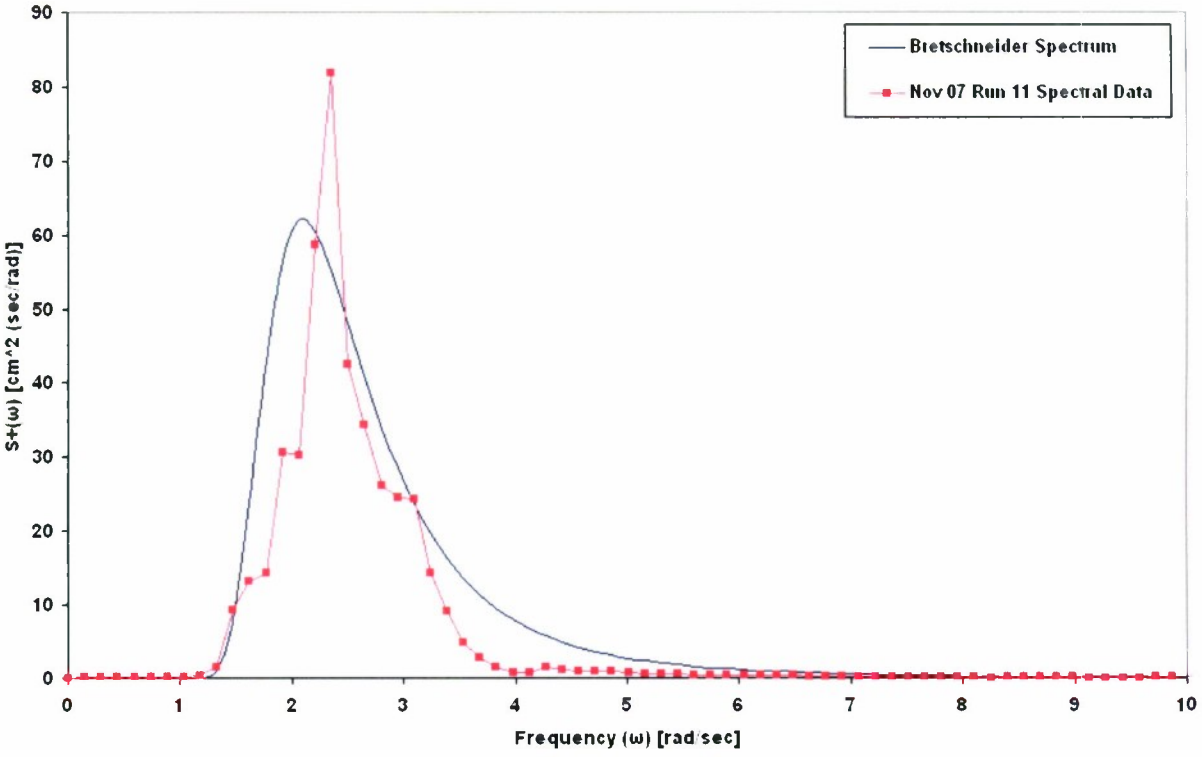

Figure 94. Spectral Analysis of Phase II, Run 11- Bretschneider SS8, λ=30, Hs= 38.1 cm (15.0 in.), Tm= 3.0s with large grouped waves embedded

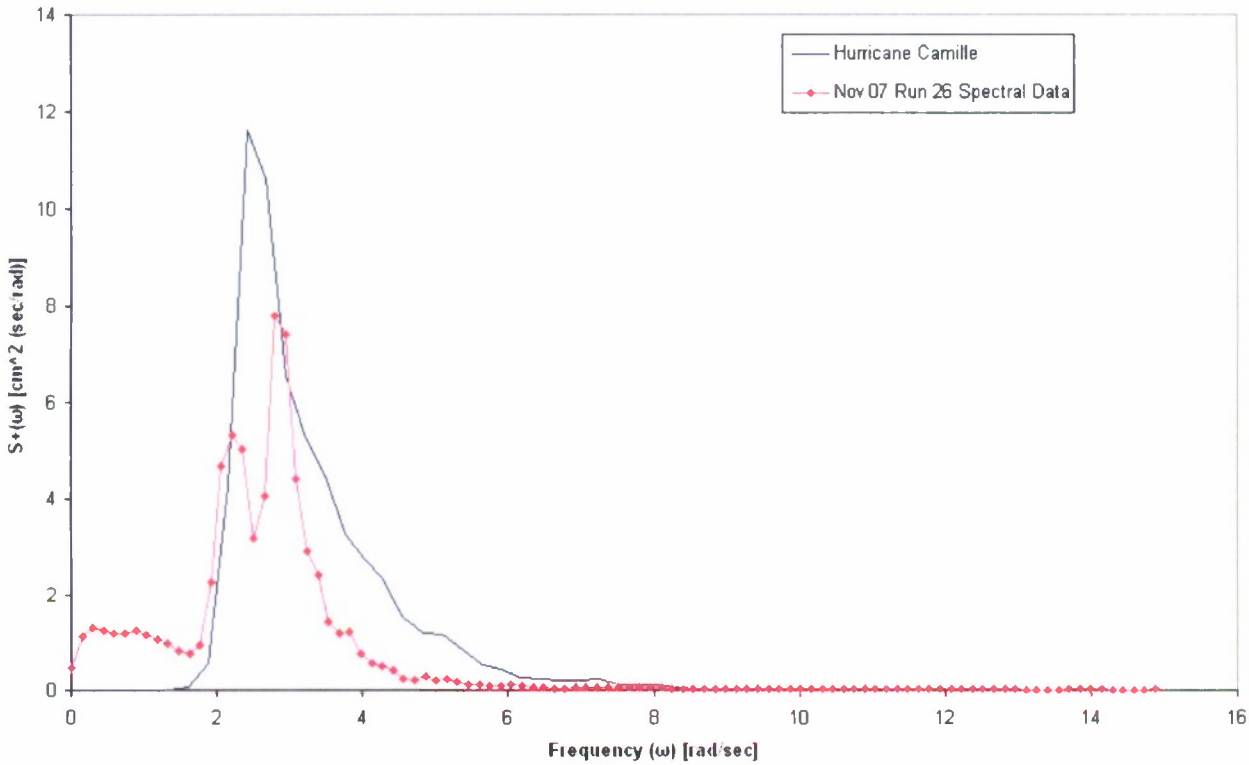

Figure 95. Spectral Analysis of Phase II, Run 26- Hurricane Camille, λ=30, Hs= 40.64 cm (16.0 in.), Tm= 2.45s with wave group embedded

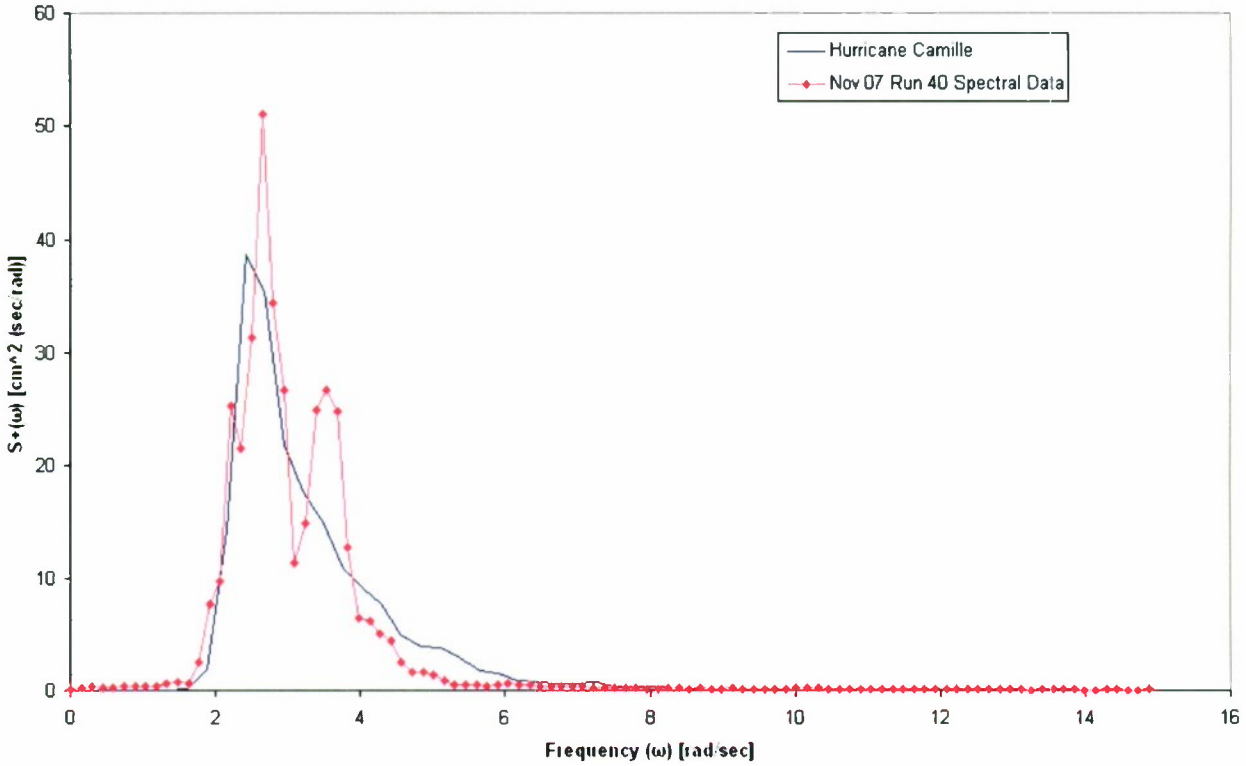

Figure 96. Spectral Analysis of Phase II, Run 40- Hurricane Camille, λ=46.6, Hs= 26.16 cm (10.3 in.), Tm= 1.96s with wave group embedded

Appendix D: GLRP Results

Results from GLRP measurements and comparisons to Senix probe data are shown in this Appendix. Three-dimensional representations of GLRP data are presented every third figure, in Figures 97–121. These representations show several snapshots of the wave group evolution in the measurement region. The first frame shows the water surface before the wave group enters the measurement region. The second frame shows the beginning of the wave group. In the third and fourth frames, the maximum and minimum wave heights encountered in the measurement are shown. The final frame shows the calm water surface at the end of the run.

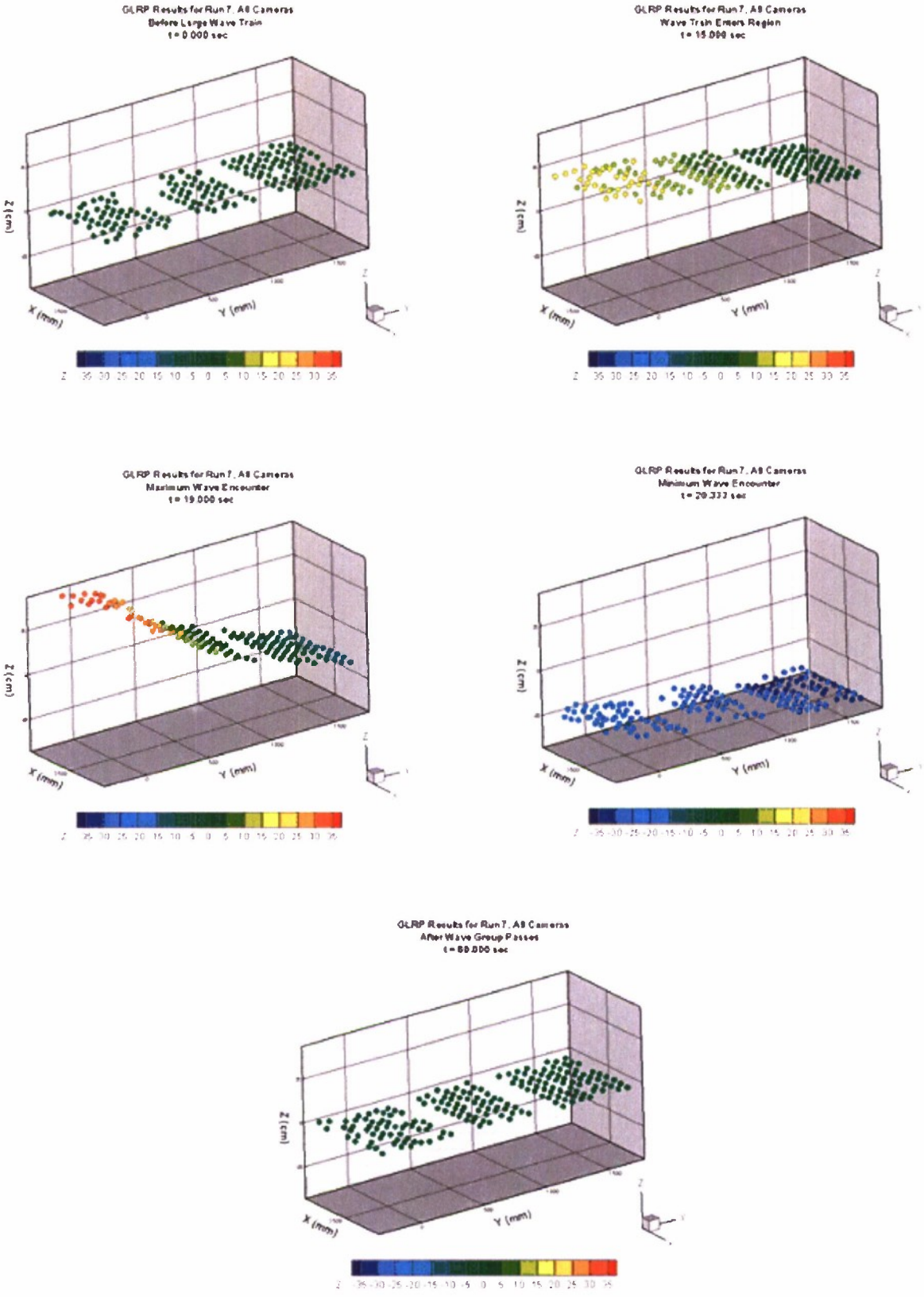

Figure 97. Three-dimensional wave surface plots for Phase II, Run 7

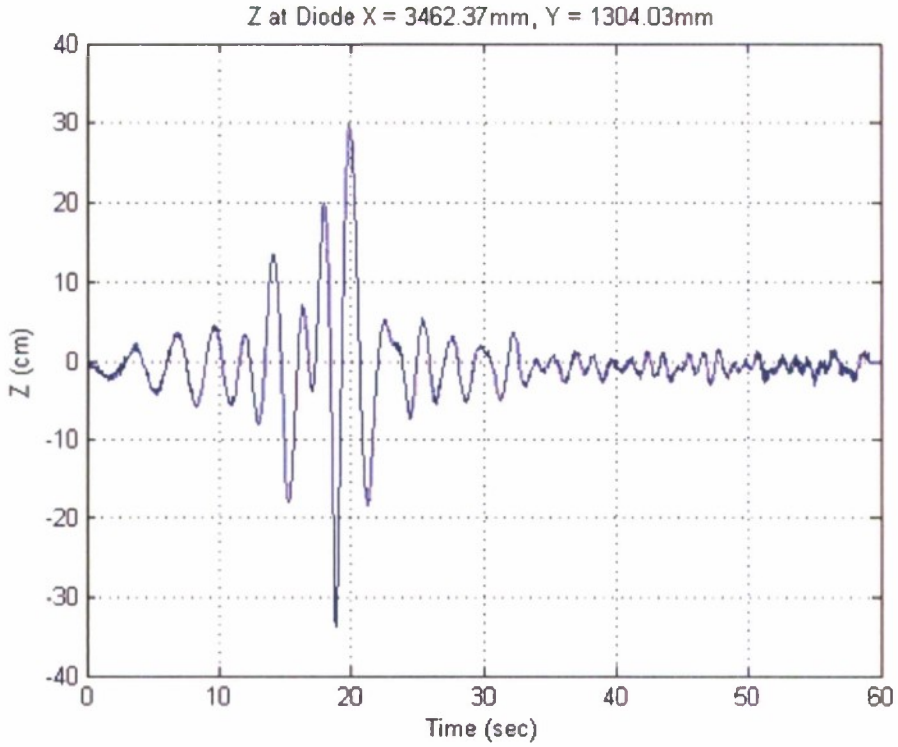

Figure 98. GLRP Single Point Time History for Phase II, Run 7

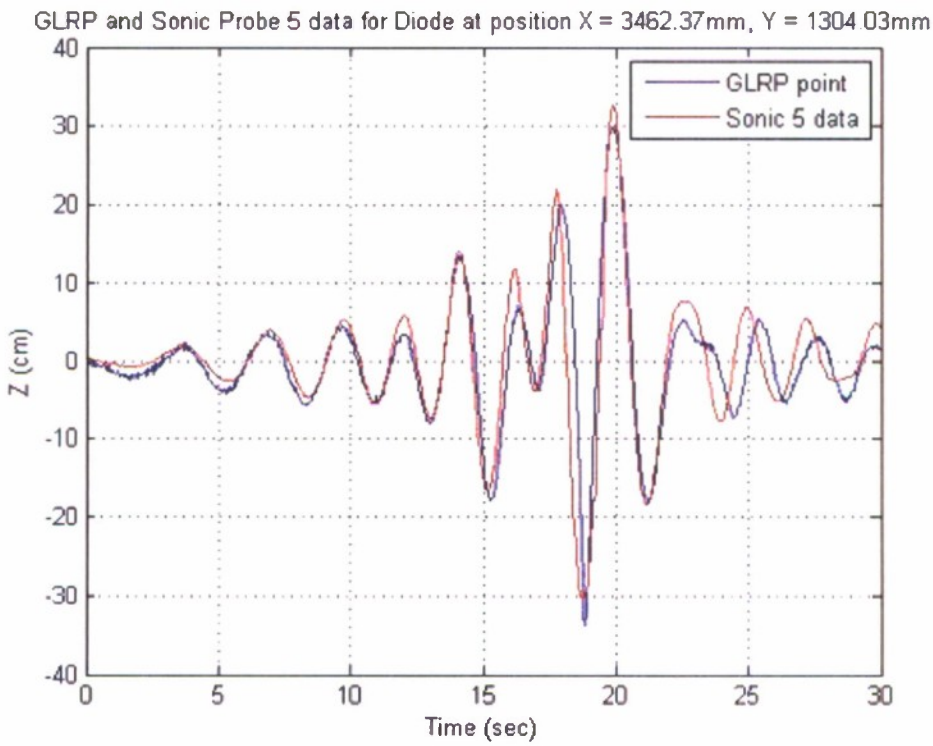

Figure 99. GLRP single point and Sonic data comparison for Phase II, Run 7

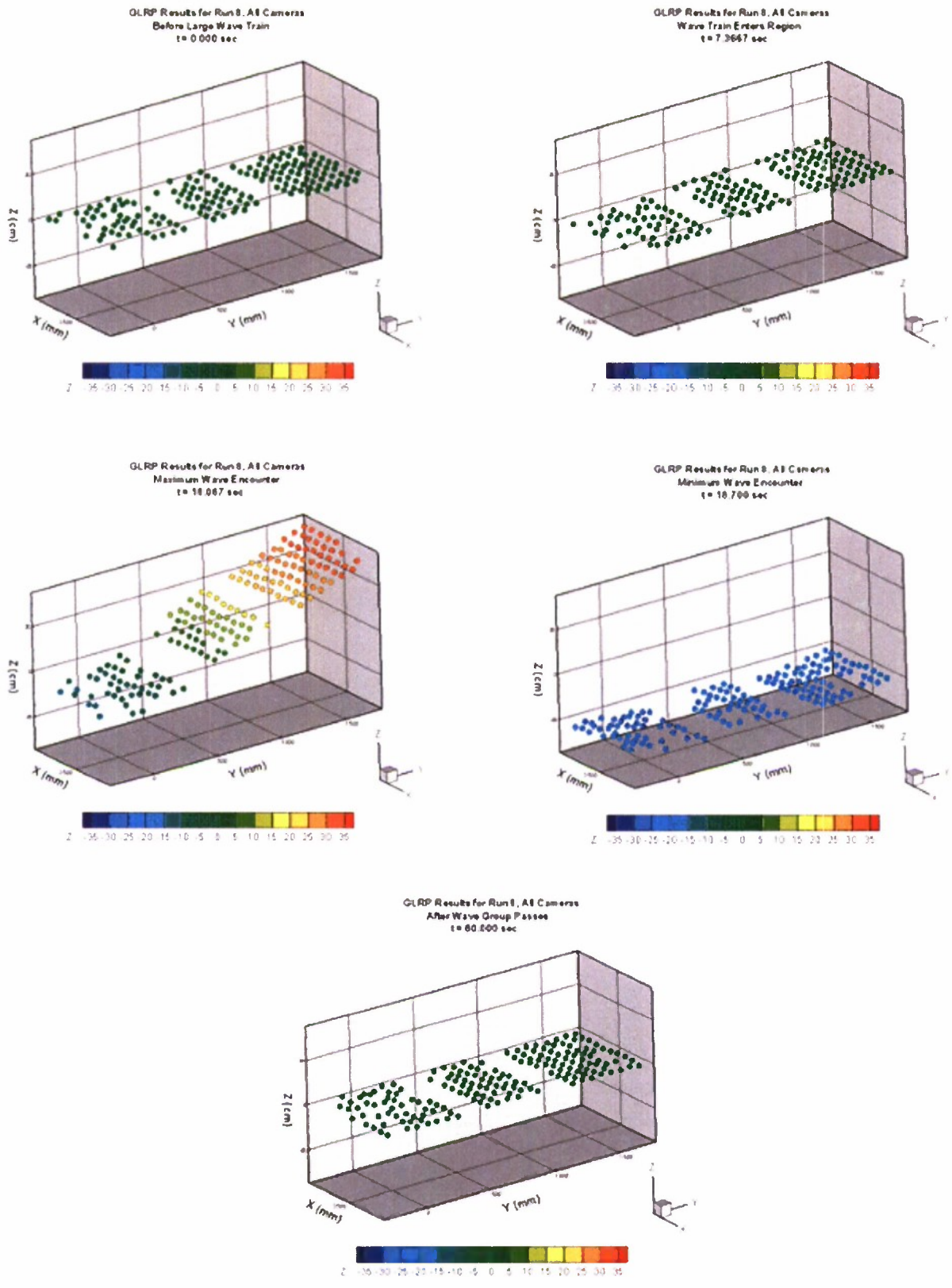

Figure 100. Three-dimensional wave surface plots for Phase II, Run 8

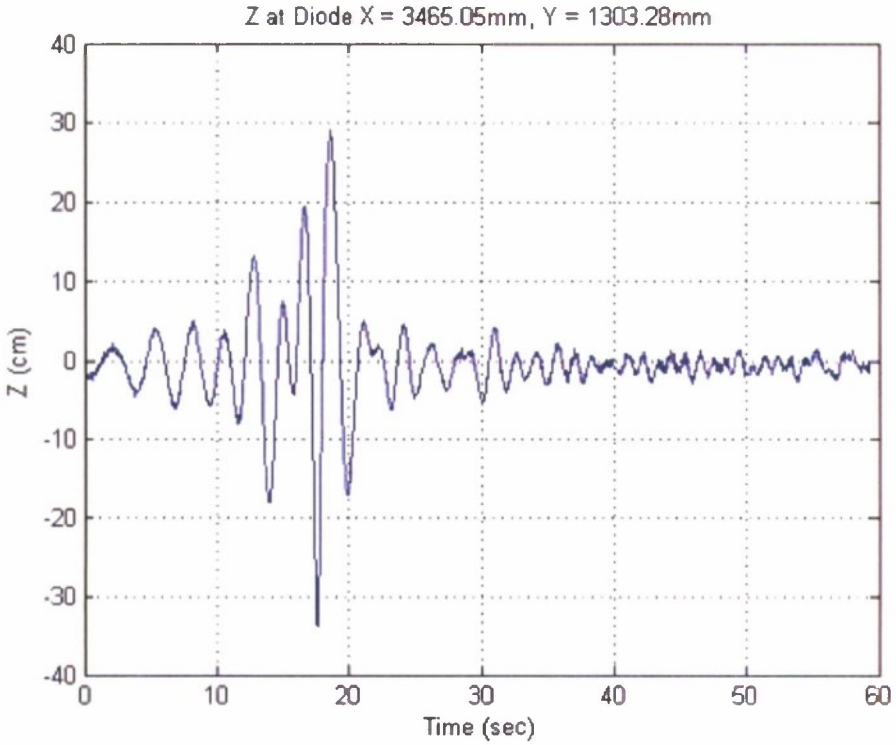

Figure 101. GLRP Single Point Time History for Phase II, Run 8

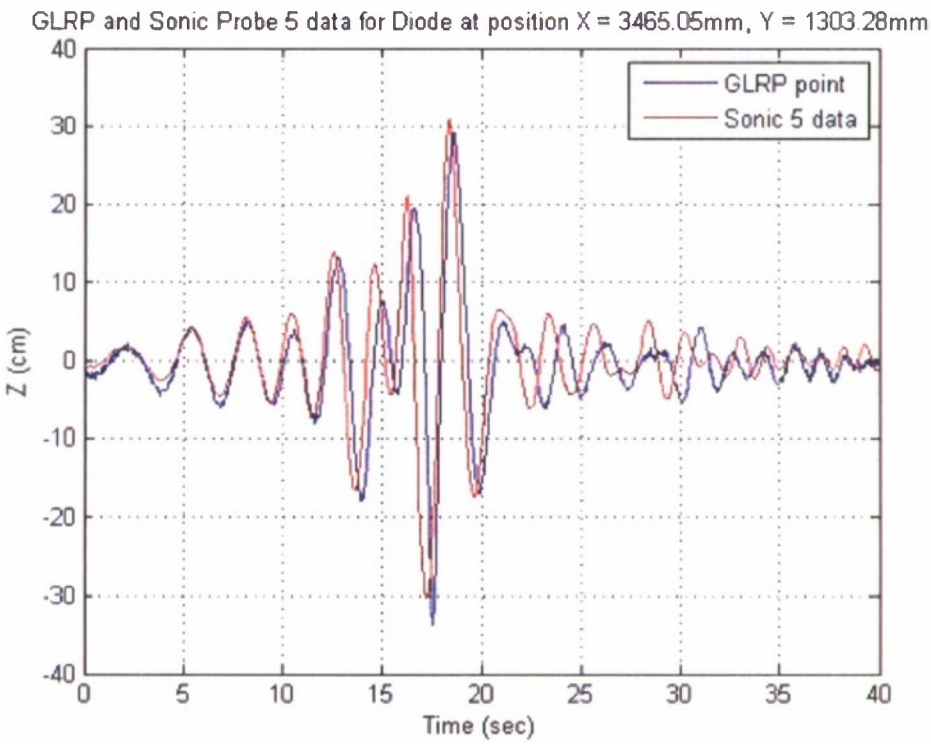

Figure 102. GLRP single point and Sonic data comparison for Phase II, Run 8

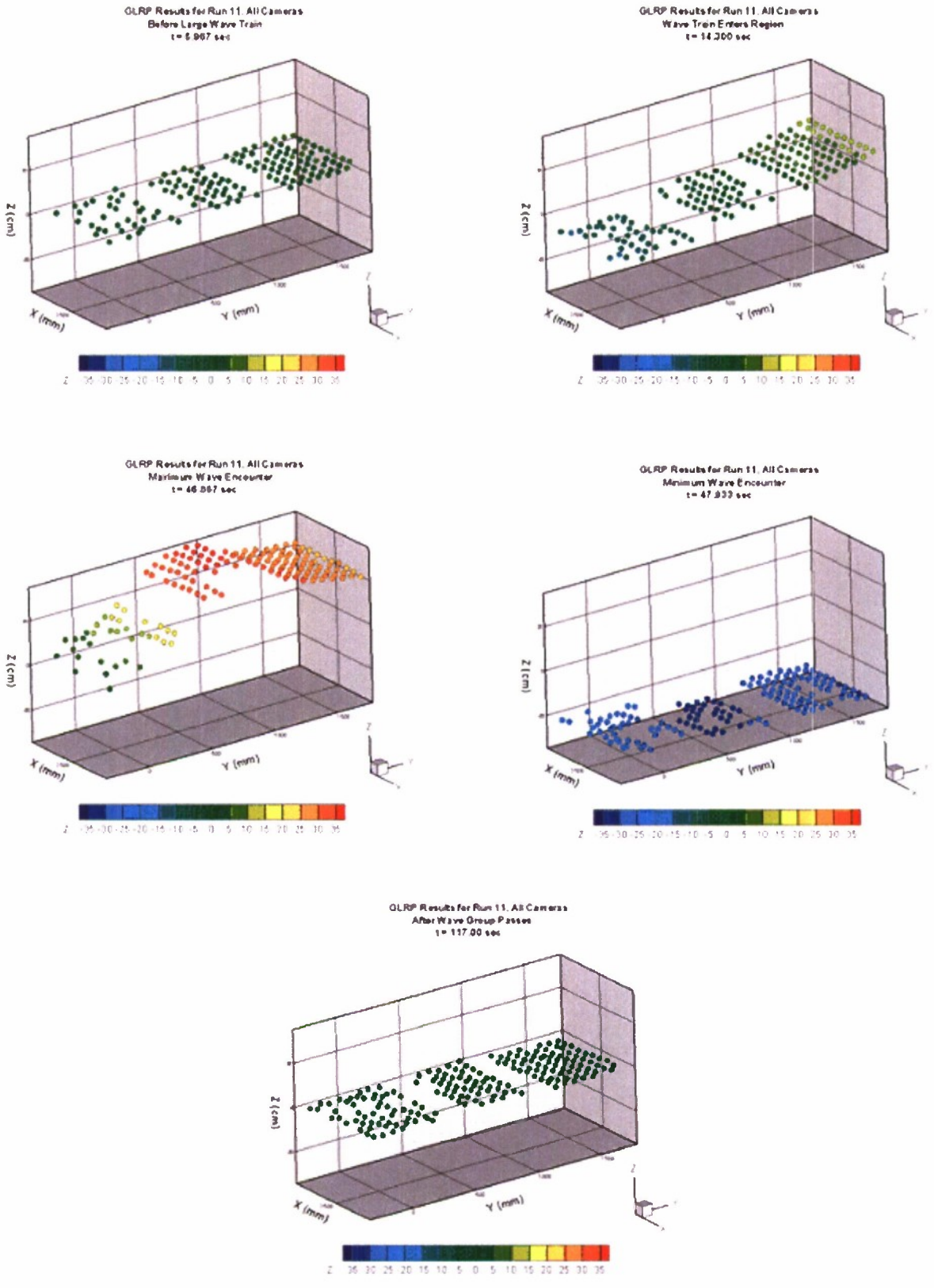

Figure 103. Three-dimensional wave surface plots for Phase II, Run 11

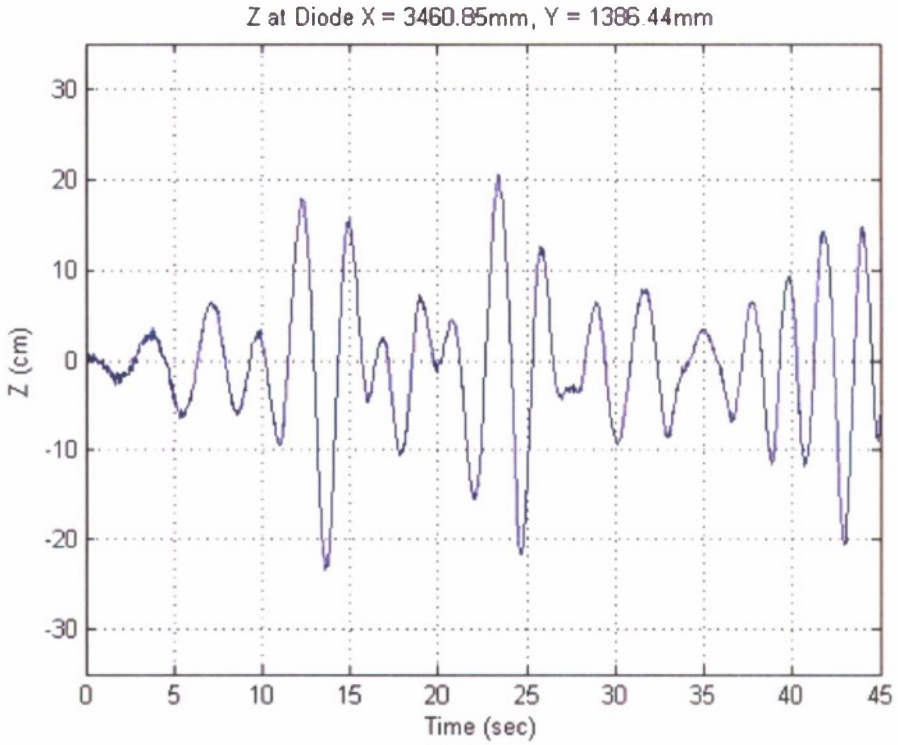

Figure 104. GLRP Single Point Time History for Phase II, Run 11

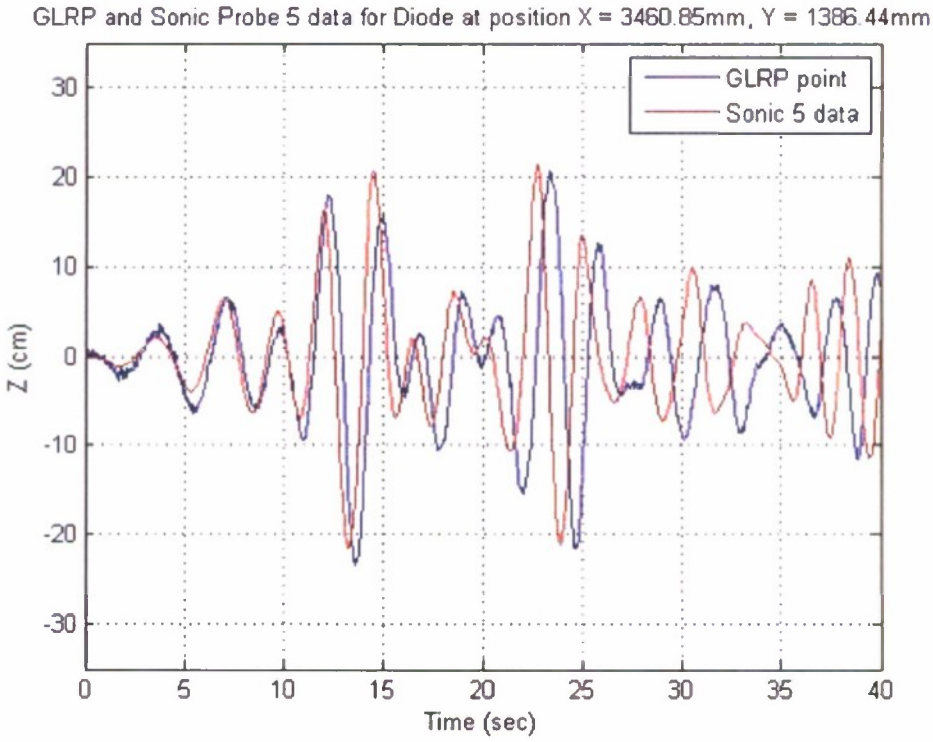

Figure 105. GLRP single point and Sonic data comparison for Phase II, Run 11

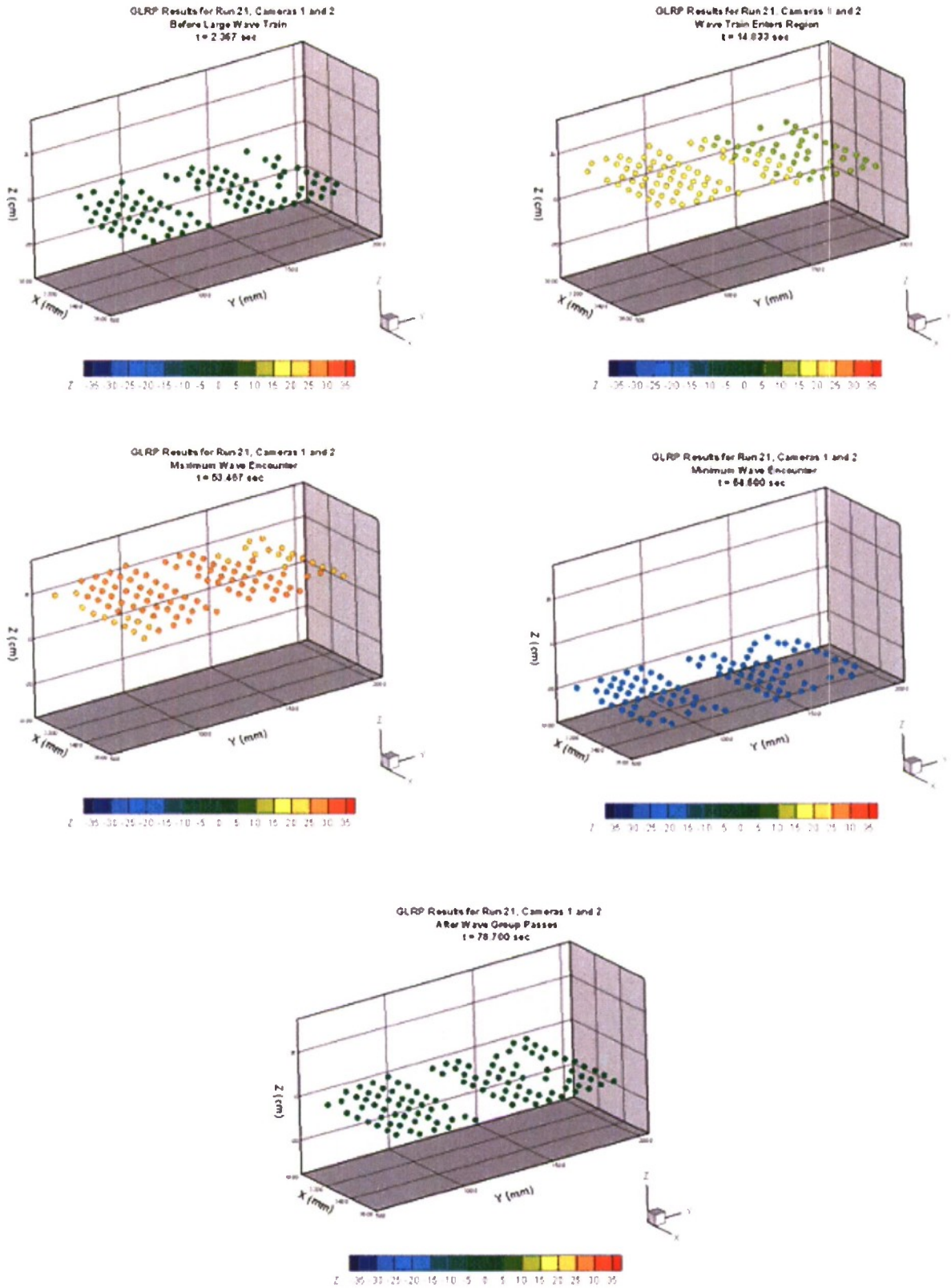

Figure 106. Three-dimensional wave surface plots for Phase II, Run 21

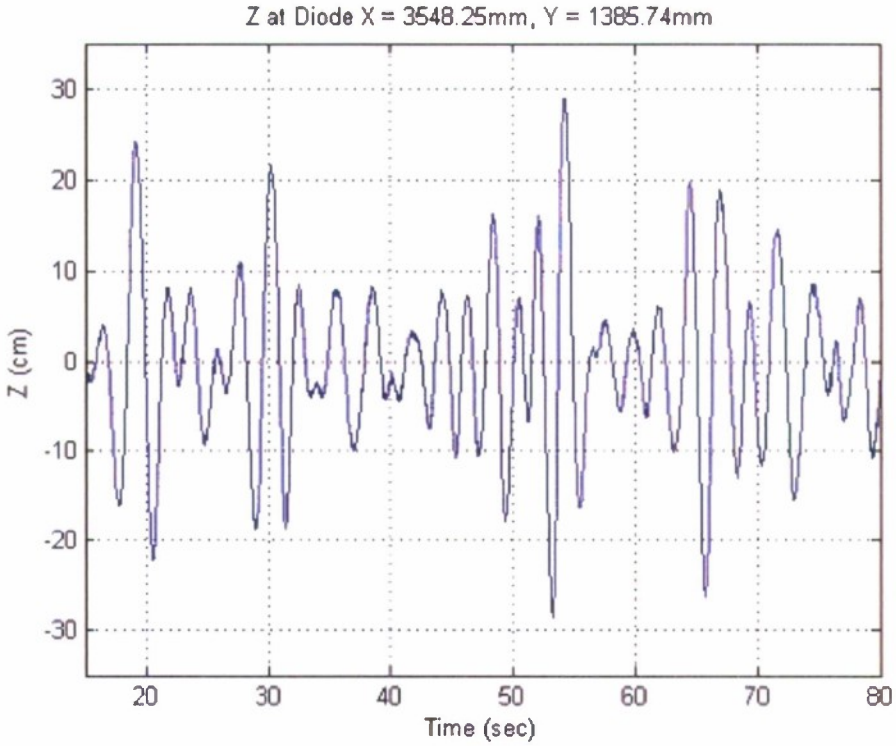

Figure 107. GLRP Single Point Time History for Phase II, Run 21

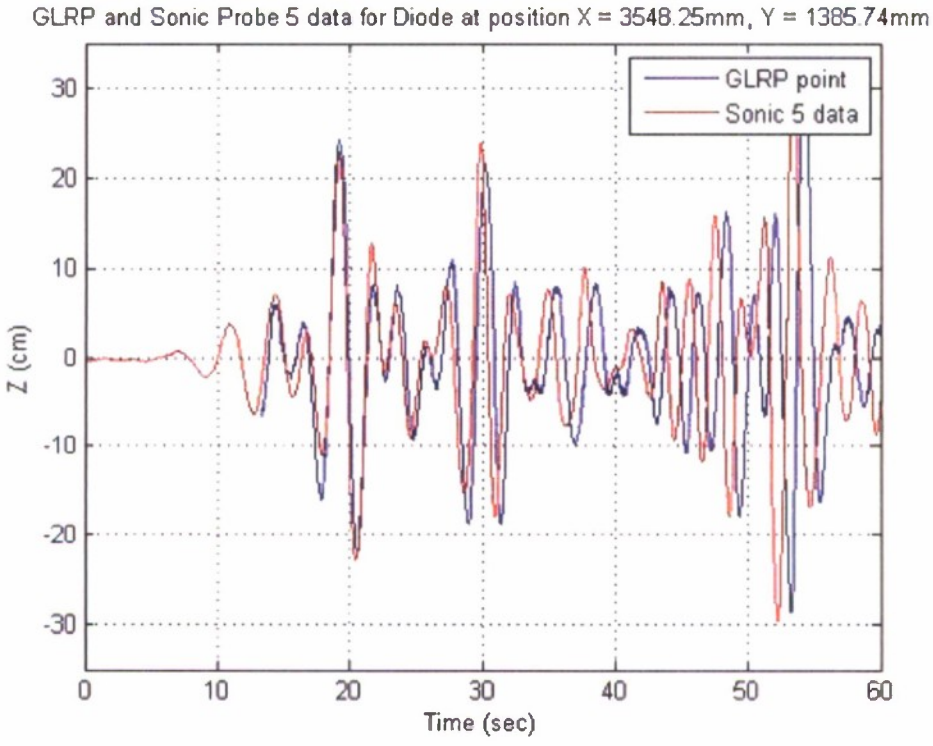

Figure 108. GLRP single point and Sonic data comparison for Phase II, Run 21

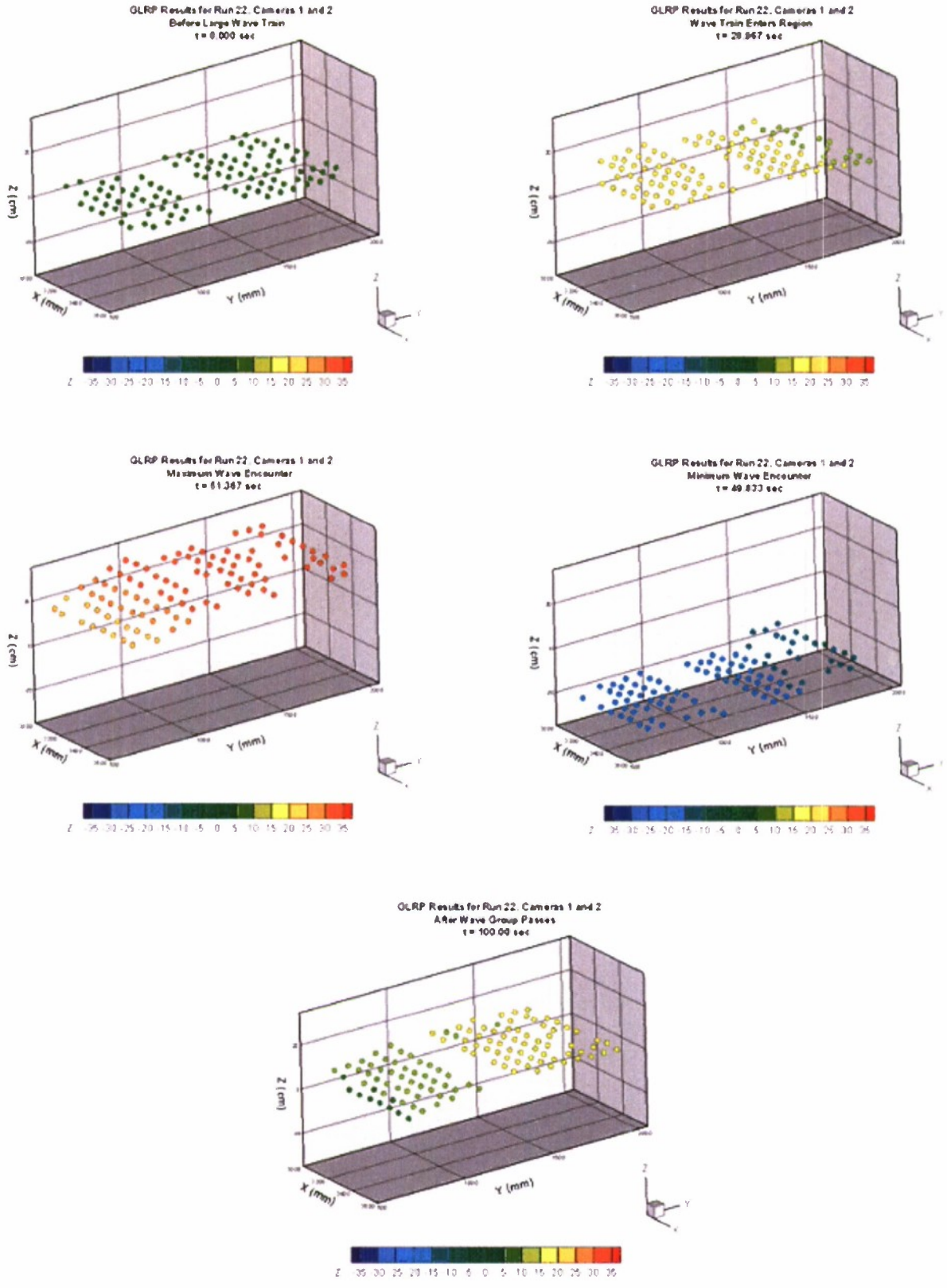

Figure 109. Three-dimensional wave surface plots for Phase II, Run 22

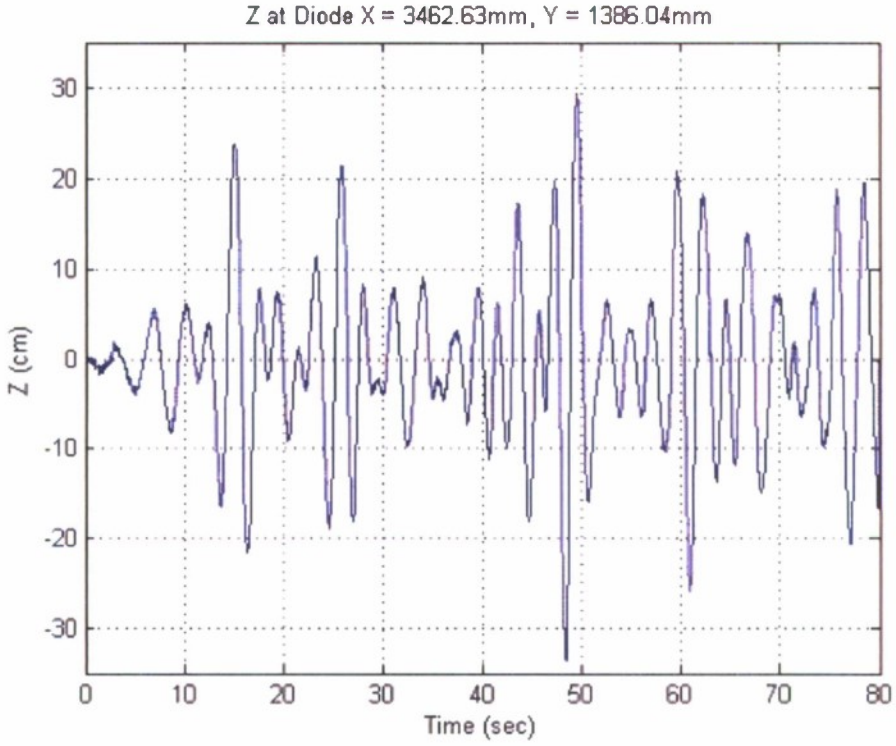

Figure 110. GLRP Single Point Time History for Phase II, Run 22

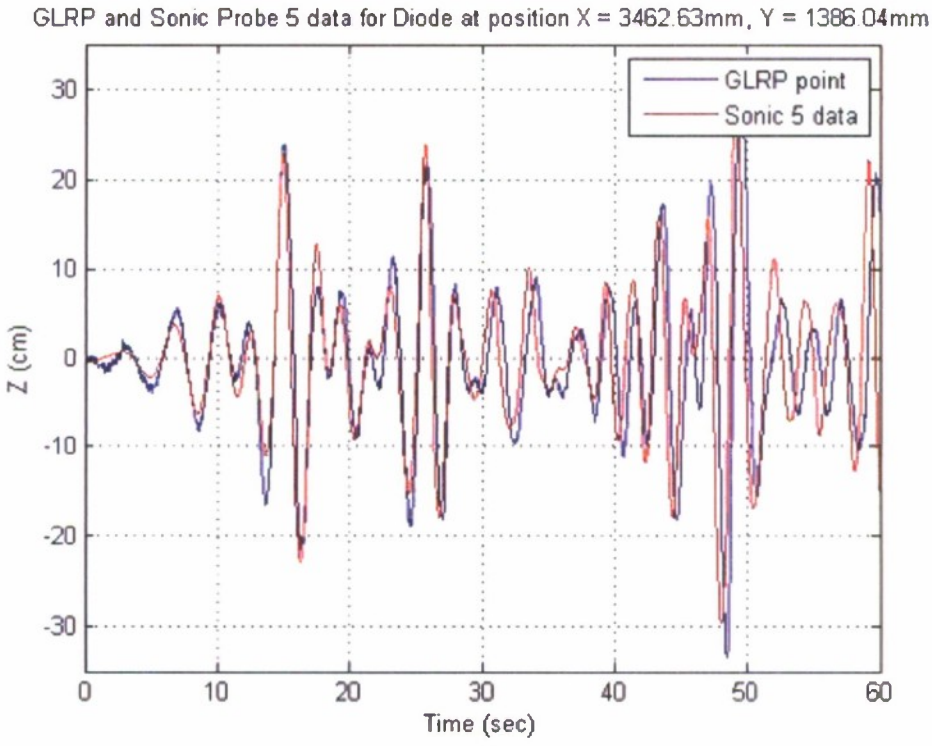

Figure 111. GLRP single point and Sonic data comparison for Phase II, Run 22

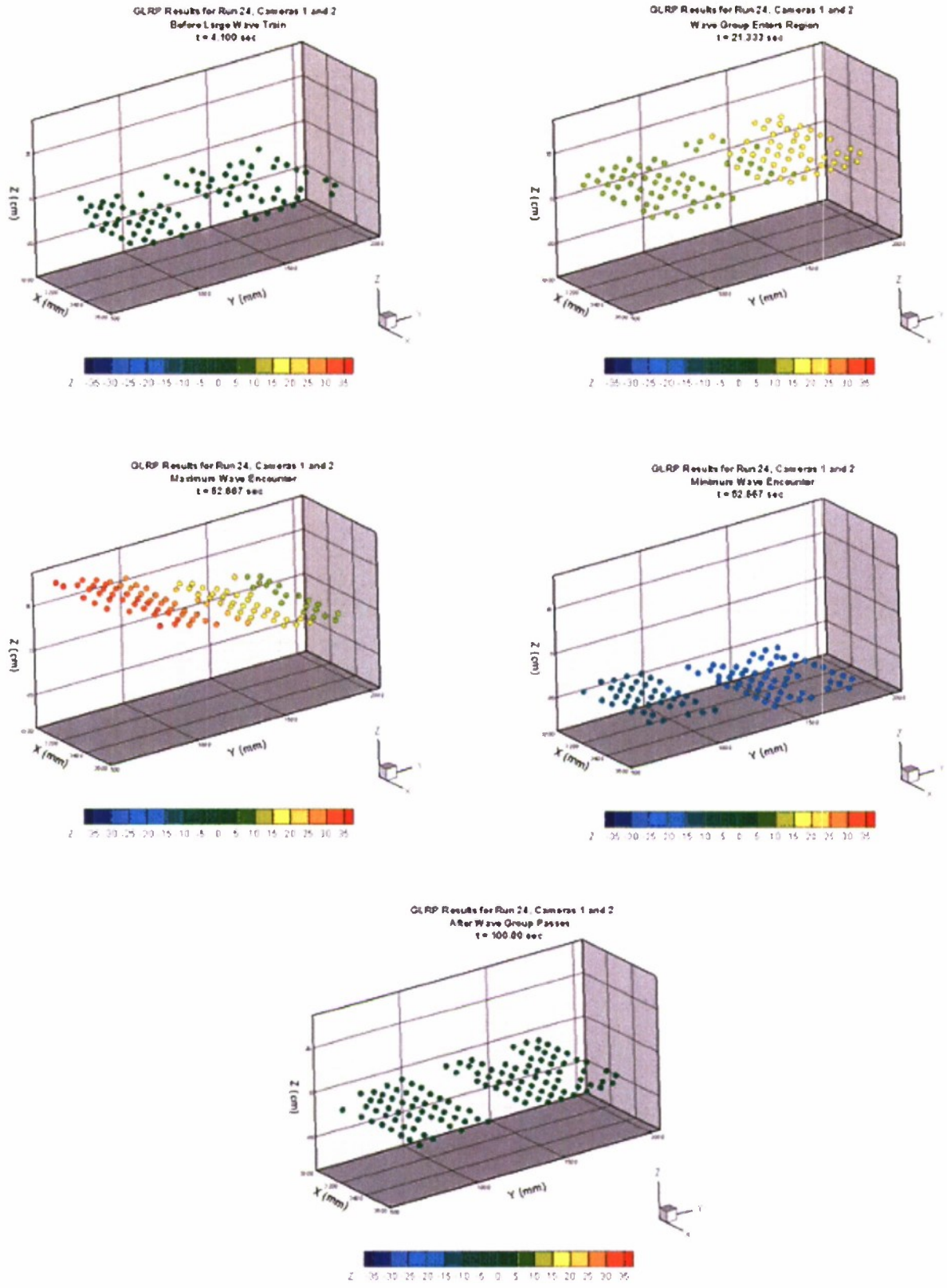

Figure 112. Three-dimensional wave surface plots for Phase II, Run 24

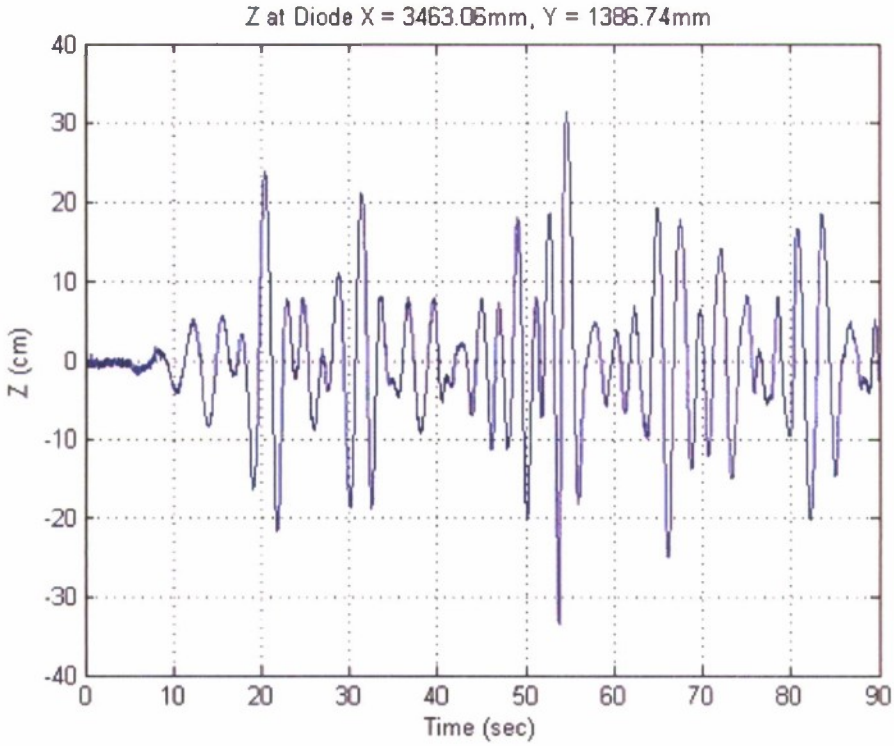

Figure 113. GLRP Single Point Time History for Phase II, Run 24

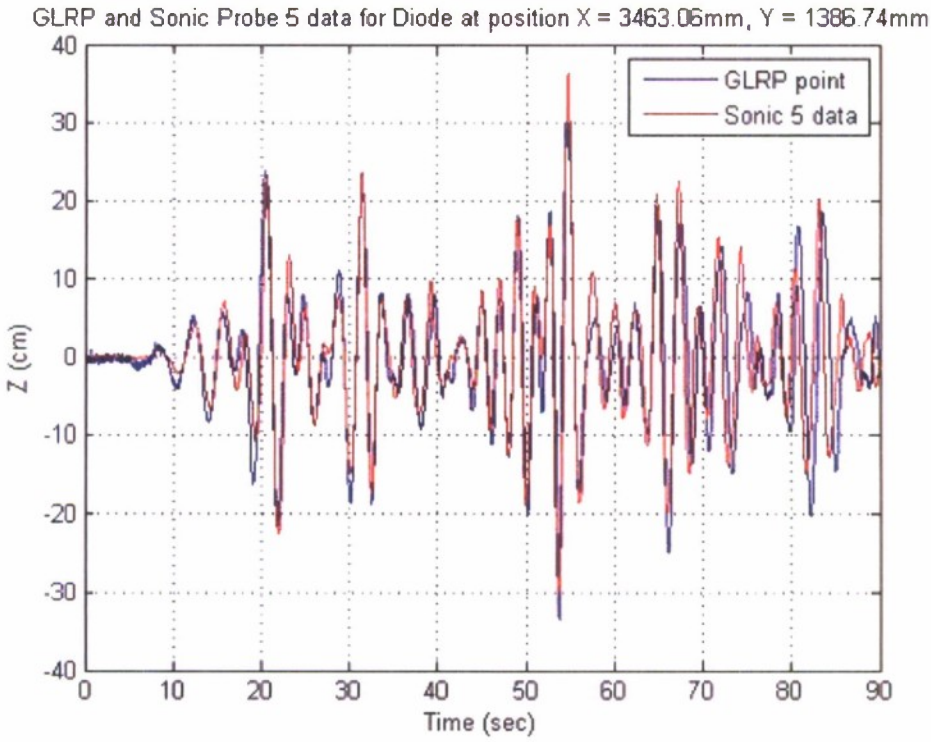

Figure 114. GLRP single point and Sonic data comparison for Phase II, Run 24

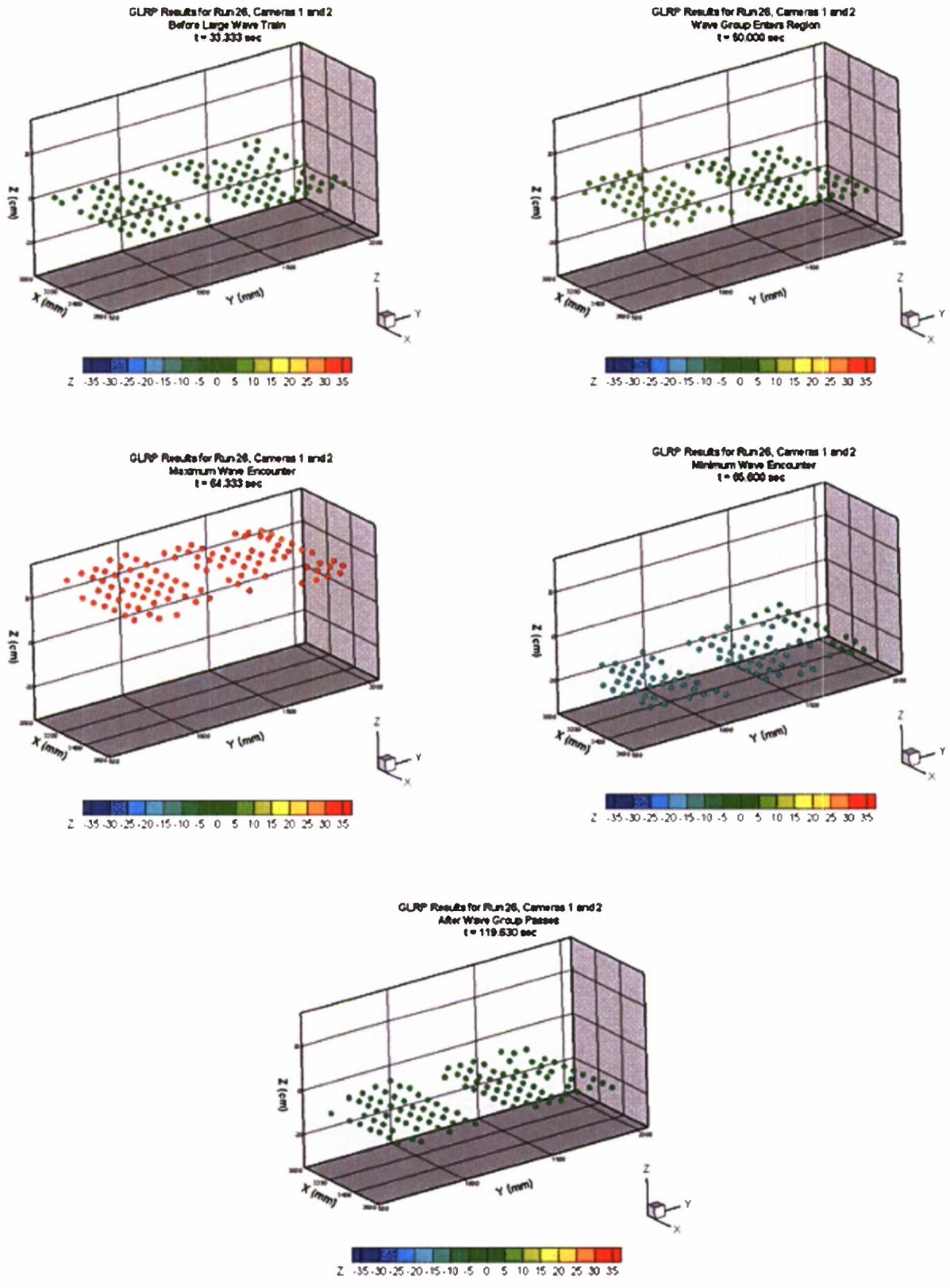

Figure 115. Three-dimensional wave surface plots for Phase II, Run 26

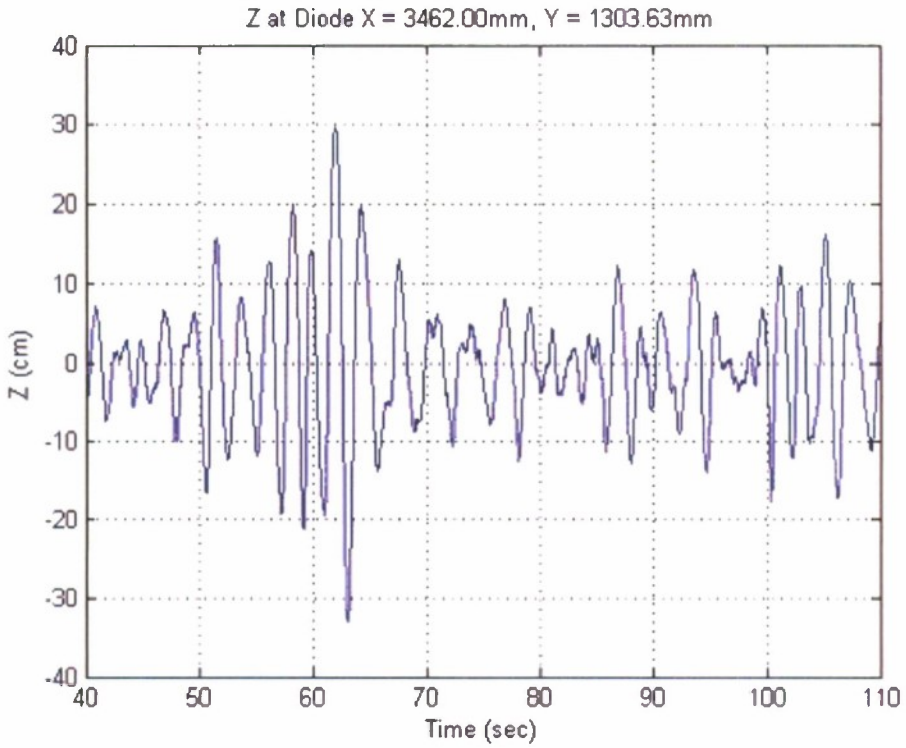

Figure 116. GLRP Single Point Time History for Phase II, Run 26

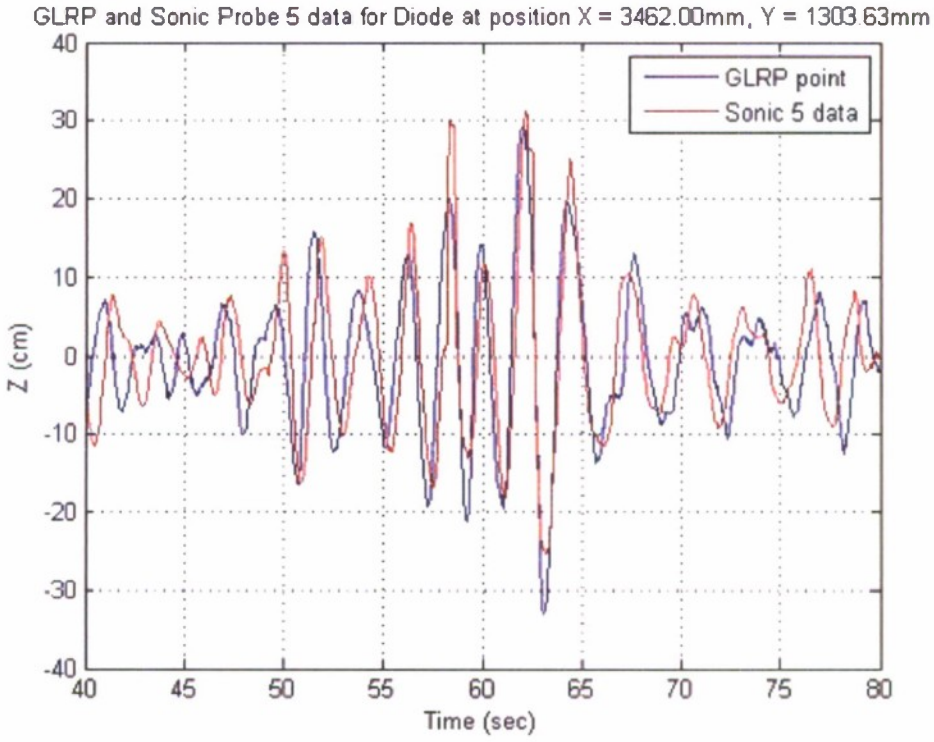

Figure 117. GLRP single point and Sonic data comparison for Phase II, Run 26

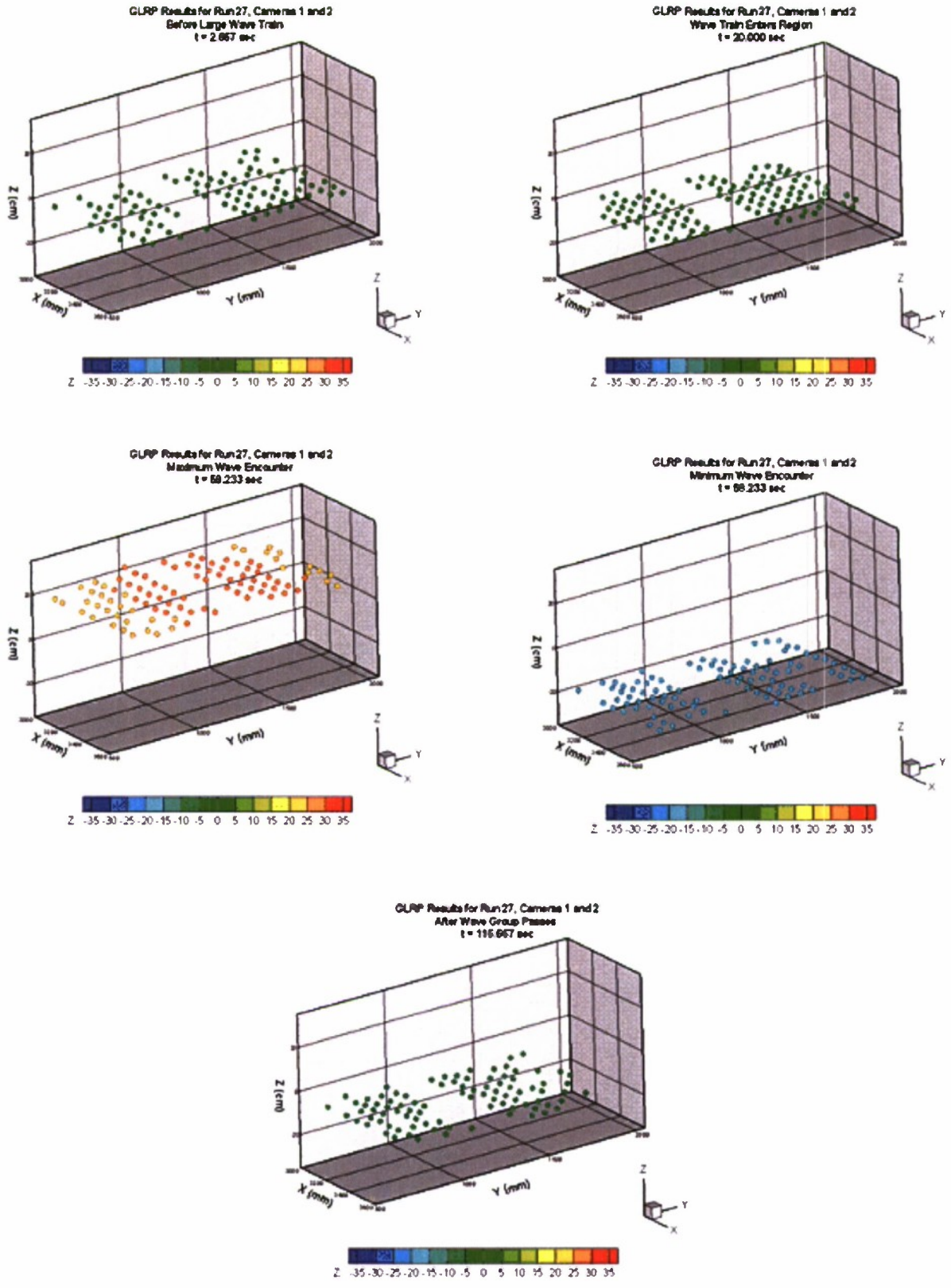

Figure 118. Three-dimensional wave surface plots for Phase II, Run 27

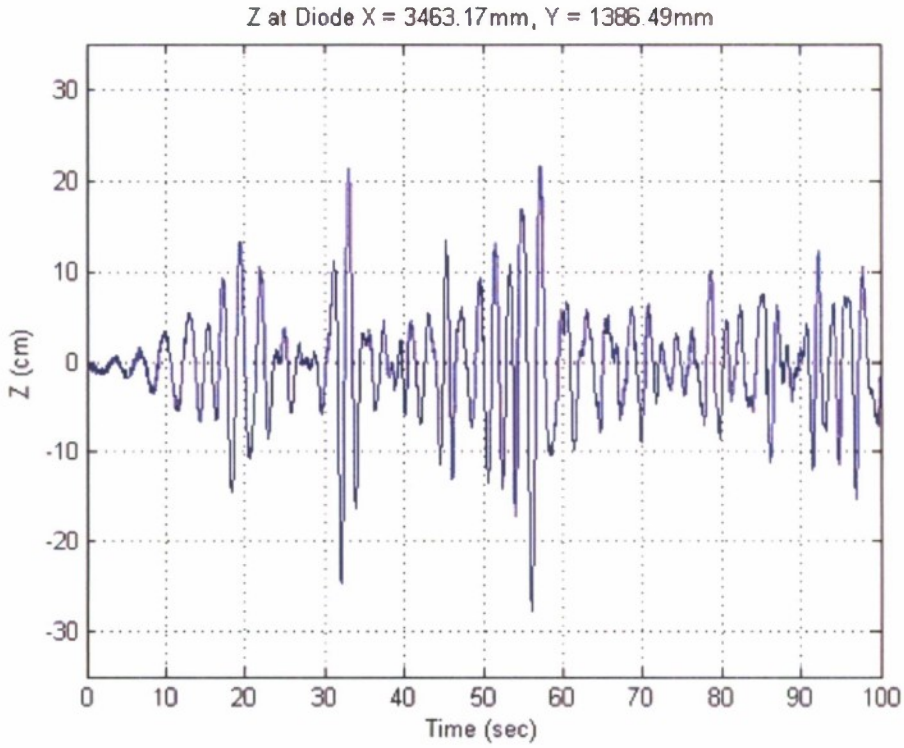

Figure 119. GLRP Single Point Time History for Phase II, Run 27

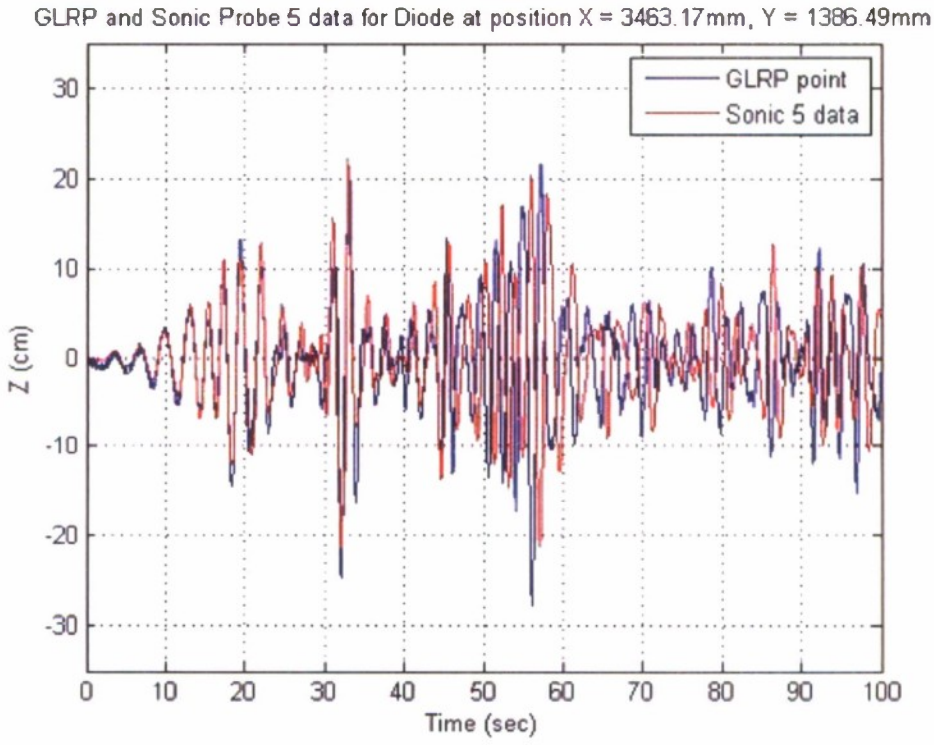

Figure 120. GLRP single point and Sonic data comparison for Phase II, Run 27

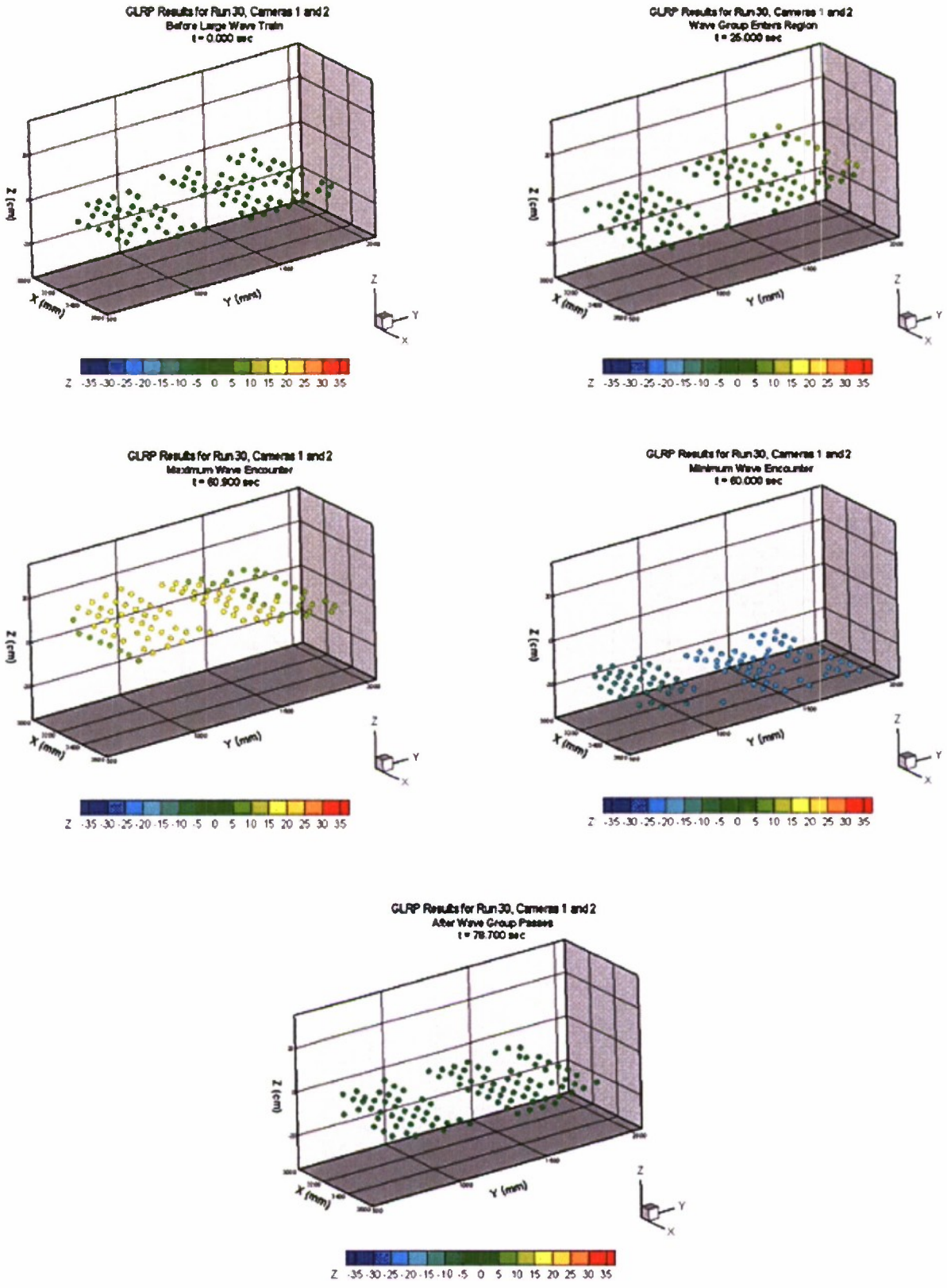

Figure 121. Three-dimensional wave surface plots for Phase II, Run 30

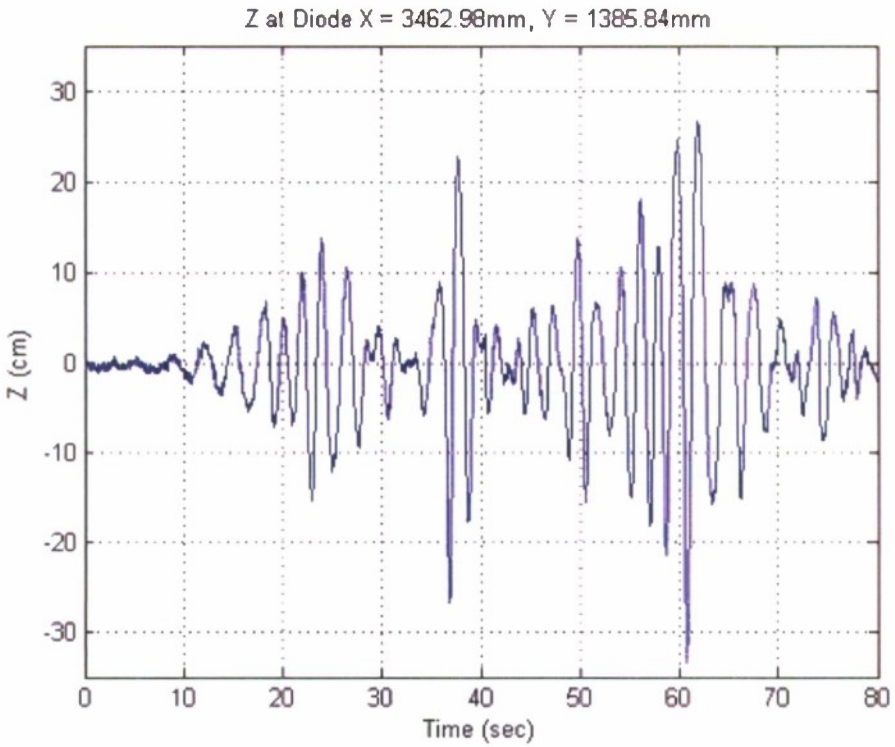

Figure 122. GLRP Single Point Time History for Phase II, Run 30

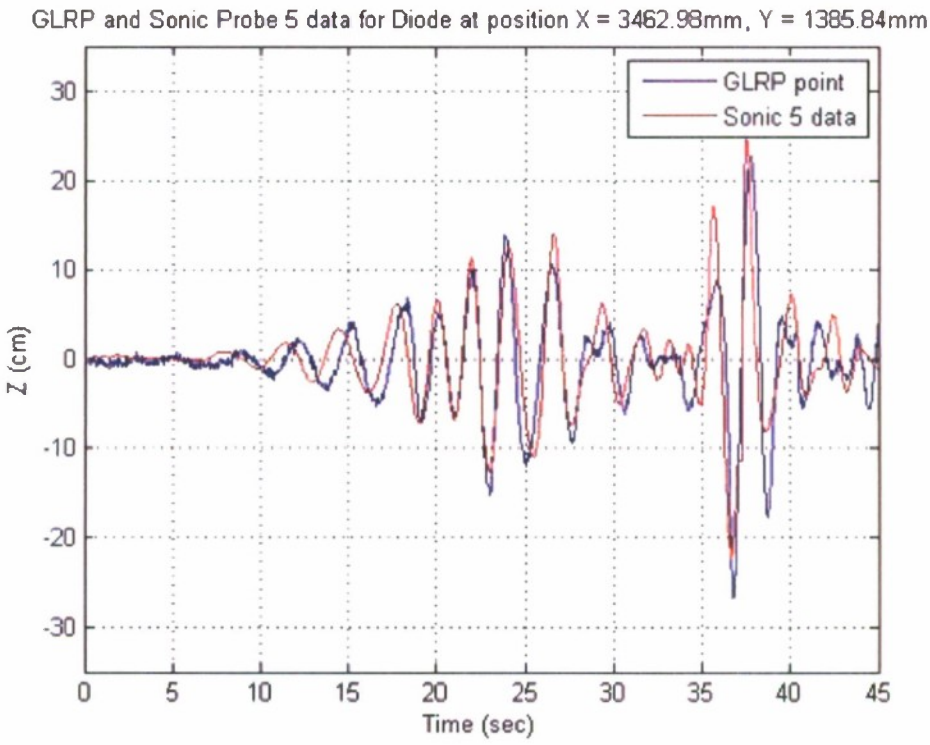

Figure 123. GLRP single point and Sonic data comparison for Phase II, Run 30

This page intentionally left blank

Initial Report Distribution

Number of Copies	Office	Individual	Total Copies
1	Office of Naval Research, 331	L. Patrick Purtell	1
1	NAVSEA 05D1	J. Webster	2
2	NAVSEA 05D1	G. Lang	4
1	DTIC		5

Number of Copies	NSWCCD Code	Individual	Total Copies
1	3452 (Library)	(pdf only)	
1	50	I.-Y. Koh	6
1	505	A. Reed	7
1	5060	D. Walden	8
3	5500	Office Files	11
1	5500	T. Applebee	12
5	5500	M. Dipper	17
1	5500	T. Smith	18
1	5500	J. Hickok	19
1	5500	D. Hayden	20
1	5500	J. Hoyt	21
5	5500	C. Bassler	26
1	5500	S. Lee	27
1	5500	J. Park	28
1	5500	T. Carrico	29
1	5500	W. Belknap	30
1	5500	B. Campbell	31
1	5600	J. Carneal	32
1	5600	E. Ammeen	33
1	5600	P. Atsavapranee	34
1	5800	T. Fu	35
1	653	A. Engle	36

This page intentionally left blank


UNITED STATES NAVY
SURFACE WARFARE CENTER